COMPLETED
264

Y3.N88:10/1265

NUREG-1265

Uncertainty Papers on Severe Accident Source Terms

ORIGINAL

U.S. Nuclear Regulatory Commission

Office of Nuclear Regulatory Research

090

NOTICE

Availability of Reference Materials Cited in NRC Publications

Most documents cited in NRC publications will be available from one of the following sources:

1. The NRC Public Document Room, 1717 H Street, N.W.
   Washington, DC 20555
2. The Superintendent of Documents, U.S. Government Printing Office, Post Office Box 37082,
   Washington, DC 20013-7082
3. The National Technical Information Service, Springfield, VA 22161

Although the listing that follows represents the majority of documents cited in NRC publications, it is not intended to be exhaustive.

Referenced documents available for inspection and copying for a fee from the NRC Public Document Room include NRC correspondence and internal NRC memoranda; NRC Office of Inspection and Enforcement bulletins, circulars, information notices, inspection and investigation notices; Licensee Event Reports; vendor reports and correspondence; Commission papers; and applicant and licensee documents and correspondence.

The following documents in the NUREG series are available for purchase from the GPO Sales Program: formal NRC staff and contractor reports, NRC-sponsored conference proceedings, and NRC booklets and brochures. Also available are Regulatory Guides, NRC regulations in the *Code of Federal Regulations*, and *Nuclear Regulatory Commission Issuances*.

Documents available from the National Technical Information Service include NUREG series reports and technical reports prepared by other federal agencies and reports prepared by the Atomic Energy Commission, forerunner agency to the Nuclear Regulatory Commission.

Documents available from public and special technical libraries include all open literature items, such as books, journal and periodical articles, and transactions. *Federal Register* notices, federal and state legislation, and congressional reports can usually be obtained from these libraries.

Documents such as theses, dissertations, foreign reports and translations, and non-NRC conference proceedings are available for purchase from the organization sponsoring the publication cited.

Single copies of NRC draft reports are available free, to the extent of supply, upon written request to the Division of Information Support Services, Distribution Section, U.S. Nuclear Regulatory Commission, Washington, DC 20555.

Copies of industry codes and standards used in a substantive manner in the NRC regulatory process are maintained at the NRC Library, 7920 Norfolk Avenue, Bethesda, Maryland, and are available there for reference use by the public. Codes and standards are usually copyrighted and may be purchased from the originating organization or, if they are American National Standards, from the American National Standards Institute, 1430 Broadway, New York, NY 10018.

NUREG-1265

Uncertainty Papers on Severe Accident Source Terms

Manuscript Completed: April 1987
Date Published: May 1987

Office of Nuclear Regulatory Research
U.S. Nuclear Regulatory Commission
Washington, DC 20555

BLANK PAGE

ABSTRACT

An assessment of the severe accident source term technology was recently published by the NRC in NUREG-0956. State-of-the-art methods described in NUREG-0956 are now being used in risk assessments and as the basis for implementing the NRC's Severe Accident Policy Statement and its Safety Goal. Notwithstanding major advances in source term technology resulting from recent severe accident research programs, NUREG-0956 identified eight technical areas where uncertainties remain large and where our near-term research efforts should be focused. Individual programs within the severe accident research program are being adjusted to address these eight areas of uncertainty with a concentrated effort. To plan for these program changes, NRC research program managers have reviewed the nature of the uncertainties in their respective subject areas and prepared background papers. These background papers (or uncertainty papers) are presented in this report.

BLANK PAGE

TABLE OF CONTENTS

Page

1. INTRODUCTION 1-1

2. NATURAL CIRCULATION IN REACTOR COOLANT SYSTEM (J. T. Han) .... 2-1 -4

2.1 Introduction 2-1
2.2 Current Technical Uncertainties .... 2-2 -5

2.2.1 Important Subissues 2-2
2.2.2 Calculations and Experiments Completed .... 2-3 -6

2.3 Analytical Results .... 2-5 -8

2.3.1 Summary of Analysis Results 2-5
2.3.2 Discussion of Analytical and Experimental Results .... 2-8 -11
2.3.3 Staff Technical Position .... 2-33 -36

2.4 Future Work 2-33

References for Chapter 2 .... 2-35 -38

3. IN-VESSEL CORE MELT PROGRESSION AND HYDROGEN GENERATION (R. W. Wright) .... 3-1 -41

3.1 Introduction 3-1

3.1.1 Core Melt Progression 3-1
3.1.2 Hydrogen Generation 3-1
3.1.3 Characteristics of Core Debris at Vessel Failure and Mode of Vessel Failure .... 3-2 -42

3.2 Past Research Results and Current Technical Uncertainties ... 3-2

3.2.1 Core Melt Progression Phenomenology 3-2
3.2.2 Core Melt Progression Analysis Codes .... 3-10 -50
3.2.3 Summary of Current Significant Technical Uncertainties .... 3-13 -53

3.3 Comparison of MELPROG 1-D and 2-D Analyses of Surry TMLB' Sequence With MARCH 2.0 1-D Analyses .... 3-15 -55

3.4 Planned Research Program .... 3-17 -57

3.4.1 Current Research Program (FY 1987) 3-17
3.4.2 Future Research Program (FY 1988-1990) .... 3-19 -59

References for Chapter 3 .... 3-21 -61

TABLE OF CONTENTS (Continued)

Page

4. HIGH-PRESSURE MELT EJECTION (DIRECT CONTAINMENT HEATING) (T. M. Lee) 4-1-64

4.1 Introduction 4-1

4.1.1 Definition of Issue 4-1
4.1.2 Important Subissues and Related Uncertainties 4-2-65
4.1.3 Review of Current Modeling 4-6-69

4.2 Description of Past, Present, and Future Research 4-6

4.2.1 Past Research 4-6
4.2.2 Present Research .... 4-11 -74
4.2.3 Program Strategy 4-11
4.2.4 Future Research .... 4-12 -75

4.3 Technical Uncertainty Evaluation .... 4-14 -77

4.3.1 Uncertainties Expected To Be Reduced By Current Program 4-14
4.3.2 Programs Needed to Further Reduce Uncertainties .... 4-15 -78

4.4 Implementation of Research Results 4-15
4.5 Summary .... 4-16 -79

Annex to Chapter 4 .... 4-17 -80

References for Chapter 4 .... 4-23 -86

5. CORE-CONCRETE INTERACTIONS (S. B. Burson) 5-1-88

5.1 Introduction 5-1

5.1.1 Qualitative Characteristics of Core-Concrete Interactions 5-1
5.1.2 Potential Consequences of Core-Concrete Interactions 5-2-89
5.1.3 Core-Concrete-Interaction Analysis Codes--CORCON and VANESA 5-6-93
5.1.4 Sources of Uncertainties Associated With Predictions of Core-Concrete-Interaction Consequences 5-7-94
5.1.5 Subissues Affecting Uncertainties in Calculating Core-Concrete-Interaction Phenomena 5-9-96
5.1.6 IDCOR Modeling 5-10

5.2 Research Program on Molten Core-Concrete Interactions .... 5-11 -98

5.2.1 Sensitivity of Core-Concrete-Interaction Predictions to Modeling and Input Variables 5-11

TABLE OF CONTENTS (Continued)

Page

5.2.2 Comparison of Code Predictions With Experimental Results.. 5-20 -107
5.2.3 Conclusions and Recommendations of CSNI Specialist Meeting on Core-Concrete Interactions............... 5-27 -114

5.3 NRC Molten Core-Concrete-Interaction Research Program and Technical Uncertainty Evaluation............................ 5-30 -117

5.3.1 Principal Sources of Uncertainty in Core-Concrete-Interaction Predictions............................ 5-30
5.3.2 NRC Research Program on Molten Core-Concrete Interaction... 5-30
5.3.3 Relationship Between Core-Concrete-Interaction Research Program and Expected Reduction in Code Prediction Uncertainties............................. 5-35-122

References for Chapter 5.. 5-37-124

Bibliography.. 5-38-125

6. HYDROGEN COMBUSTION (P. Worthington)............................ 6-1 -126

6.1 Introduction.. 6-1
6.2 Description of Past, Present, and Future Research.......... 6-2 -127

6.2.1 Deflagration.. 6-2
6.2.2 Accelerated Flames and Transition from Deflagration to Detonation.. 6-12-137
6.2.3 Detonation.. 6-13-138
6.2.4 Uncertainty in DDT and Detonation....................... 6-14-139

References for Chapter 6.. 6-17-142

7. IODINE CHEMICAL FORM (L. K. Chan)............................... 7-1 -146

7.1 Introduction.. 7-1
7.2 Description of Past, Present, and Future Research.......... 7-2 -147

7.2.1 Past Research... 7-2
7.2.2 Present Research (FY 1987).............................. 7-11-156
7.2.3 Future Research (FY 1988 and Beyond).................... 7-13-158

7.3 Technical Uncertainty Evaluation............................ 7-14-159

7.3.1 RCS Iodine Chemical Form (1987)......................... 7-14
7.3.2 Containment Iodine Chemical Form (1987)................. 7-16-161
7.3.3 RCS Iodine Chemical Form (1988 and Beyond).............. 7-16
7.3.4 Containment Iodine Chemical Form (1988 and Beyond)... 7-17-162

References for Chapter 7.. 7-18-163

TABLE OF CONTENTS (Continued)

Page

8. FISSION PRODUCT REVAPORIZATION (L. K. Chan) 8-1-165

8.1 Introduction 8-1
8.2 Description of Past, Present, and Future Research 8-3-167

8.2.1 Past Research 8-3
8.2.2 Present Research (FY 1987) 8-9-173
8.2.3 Future Research (FY 1988 and Beyond) 8-10-174

8.3 Technical Uncertainty Evaluation 8-11-175

8.3.1 Thermal Hydraulics (FY 1987) 8-11
8.3.2 Revaporization Chemistry (FY 1987) 8-13-177
8.3.3 Integrated Analysis (FY 1988) 8-13
8.3.4 Experimental Validation 8-14-178

References for Chapter 8 8-15-179

LIST OF TABLES

Table — Page

1.1 Major areas of uncertainty affecting current source term analysis 1-2

2.1 A summary of NRC-sponsored code calculations and studies investigating RCS natural circulation under high-pressure TMLB' accident conditions in a PWR 2-6

2.2 Calculated temperature at or near the inner surface of hot leg nozzle under high-pressure TMLB' accident conditions 2-7

2.3 Possible failure locations of RCS pressure boundary during high-pressure TMLB' accident in Westinghouse PWRs before ejection of core melt from reactor vessel lower head to containment 2-8

2.4 MELPROG-calculated TMLB' event sequence 2-10

2.5 Estimated hydrogen generation during TMLB' accident in Surry plant 2-16

2.6 RCS pressure measurements during TMI-2 core uncovery period 2-18

2.7 Estimated critical temperature above which the structure may lose integrity within the rupture time under high-pressure TMLB' accident conditions in Surry plant 2-24

3.1. Conditions at vessel failure 3-15

3.2 State of core debris at vessel failure in MELPROG 2-D analysis 3-16

4.1 Direct containment heating test matrix for Surtsey direct heating facility 4-12

4A.1 Surry direct containment heating (input for statistical analysis of pressure rise versus probability) 4-19

5.1 Potential risk-related consequences of core-concrete interactions 5-3

5.2 Sources of uncertainties associated with predictions of core-concrete-interaction consequences 5-7

5.3 Subissues--significant input variables for CORCON and VANESA 5-10

5.4 Fission product groups used in sensitivity studies 5-12

LIST OF TABLES (Continued)

Table		Page
5.5	Sensitivity of ex-vessel fission product release predictions to debris pool radius (TB1/TB2 sequence, Mark I BWR containment)	5-13
5.6	Sensitivity of ex-vessel fission product release predictions to surface emissivity of debris pool (TB1/TB2 sequence, Mark I BWR containment)	5-14
5.7	Sensitivity of ex-vessel fission product release predictions to ablation temperature of concrete (TB1/TB2 sequence, Mark I BWR containment)	5-14
5.8	Parameter variations used in Peach Bottom and Surry uncertainty studies	5-15
5.9	Refractory fission product release for Peach Bottom plant (total release in % at 10 hours)--AE sequence	5-16
5.10	Refractory fission product release for Surry plant (total release in % at 10 hours)	5-16
5.11	Total amount of gas released for Peach Bottom	5-18
5.12	Comparison of potential BWR Mark I failure mode times	5-19
5.13	BETA experiment features	5-24
5.14	Principal sources of uncertainties associated with thermal-hydraulic aspects of core-concrete-interaction phenomena	5-31
5.15	Principal sources of uncertainties associated with fission product and aerosol release aspects of core-concrete-interaction phenomena	5-32
5.16	Current NRC research program on molten core-concrete interactions	5-33
5.17	Additional planned research	5-34
6.1	Capabilities of HECTR versions 1.0 and 1.5	6-8
6.2	Modeling differences between HECTR and MAAP	6-10
7.1	Atmospheric release of iodine aerosols and vapors (percent of core inventory)	7-9
7.2	Tasks and schedules	7-14
8.1	Tasks and schedules	8-12

LIST OF FIGURES

Figure Page

2.1 MELPROG-calculated hot leg nozzle temperature for TMLB' accident in Surry.......... 2-11

2.2 Temperature distribution in vessel at 6500 s.......... 2-12

2.3 Flow and temperature distributions at 7500 s.......... 2-13

2.4 Flow and temperature distributions at 9525 s.......... 2-14

2.5 Flow and temperature distributions at 11000 s.......... 2-15

2.6 Schematic of hot leg nozzle and hot leg pipe.......... 2-19

2.7 Average wall temperature versus rupture time for hot leg nozzle.......... 2-21

2.8 Average wall temperature versus rupture time for hot leg pipe.......... 2-22

2.9 Average wall temperature versus rupture time for steam generator tube.......... 2-23

2.10 Front view of experimental reactor model.......... 2-25

2.11 Velocity vectors from LDA for natural circulation of SF_6, 0.9 kW heating and hot legs blocked.......... 2-27

2.12 Velocity vectors from LDA for natural circulation of water, 28 kW, with steam generators cooling hot leg flows.......... 2-28

2.13 Temperatures in steam generator model in °C test with water on February 7, 1985, tube number shown.......... 2-29

2.14 CORMLT-calculated upper-plenum internal surface temperature.......... 2-30

2.15 CORMLT-calculated inner surface temperature of surge line.......... 2-31

2.16 MAAP-calculated upper-plenum reactor vessel wall temperature for Zion TMLB' versus no natural circulation case.......... 2-32

3.1 $\alpha(O)$-Zr-UO_2 pseudo binary phase diagram.......... 3-6

4A.1 Surry DHEAT2 calculations.......... 4-18

4A.2 Estimated peak pressure in direct containment heating for Surry.......... 4-22

LIST OF FIGURES (Continued)

Figure		Page
5.1	Erosion data test SWISS-1	5-21
5.2	Erosion data test SWISS-2	5-21
5.3	Core concrete interaction test TURC-ISS: aerosol source	5-21
5.4	Core concrete interaction test TURC-2: aerosol source	5-21
5.5	VANESA TE release predictions	5-21
5.6	BETA facility	5-23
5.7	BETA crucible (V1.8)	5-25
5.8	BETA crucible (V2.3)	5-26

1. INTRODUCTION

After the accident at Three Mile Island, the NRC initiated a severe accident research program to support anticipated changes in the regulatory process. Since then the agency has implemented a TMI Action Plan (Refs. 1.1 and 1.2), issued a Severe Accident Policy Statement (Ref. 1.3) that is now being implemented, and issued a Safety Goal (Ref. 1.4) that is yet to be implemented.

In 1986, after the severe accident research program had reached a point where significant results were emerging, the NRC made a formal assessment of the severe accident source term technology and published its findings in NUREG-0956 (Ref. 1.5). State-of-the-art methods described in NUREG-0956 are now being used in risk assessments (Ref. 1.6) and as the basis for implementing the policy statement and the safety goal. Notwithstanding major advances in source term technology resulting from this recent severe accident research program, NUREG-0956 identified eight technical areas where uncertainties remain large. These eight major areas of uncertainty are listed in Table 1.1 and are areas where our near-term research efforts should be focused.

Individual programs within the severe accident research program are being adjusted to address these eight areas of uncertainty with a concentrated effort. To plan for these program changes, NRC research program managers have reviewed the nature of the uncertainties in their respective subject areas and prepared background papers. These background papers (or uncertainty papers) are presented in the following sections. A major review of steam explosions was recently conducted by the NRC's Steam Explosion Review Group (Ref. 1.7). Since their report, NUREG-1116, addresses the subject and is readily available, a separate section on steam explosions was not included in this report.

The uncertainty papers that follow, along with other information, were provided to expert review groups organized by Brookhaven National Laboratory to facilitate the review of NRC's revised research plans. A report, "Review of Research on Uncertainties in Estimates of Source Terms from Severe Accidents in Nuclear Power Plants," was recently issued by Brookhaven National Laboratory (Ref. 1.8) describing these expert reviews of NRC's severe accident research plans. Final revised severe accident research plans will be developed by the NRC staff based on the above-mentioned information and will be presented to the Commission in the late spring of 1987.

Table 1.1 Major areas of uncertainty affecting current source term analysis.

	Area of Uncertainty
1.	Natural circulation in reactor coolant system
2.	Core melt progression and hydrogen generation
3.	Steam explosions
4.	High-pressure melt ejection
5.	Core-concrete interactions
6.	Hydrogen combustion
7.	Iodine chemical form
8.	Fission product revaporization

REFERENCES FOR CHAPTER 1

1.1 U.S. Nuclear Regulatory Commission (USNRC), "NRC Action Plan Developed as a Result of the TMI-2 Accident," NUREG-0660, Vols. 1 and 2, May 1980.

1.2 USNRC, "Clarification of TMI Action Plan Requirements," NUREG-0737, November 1980.

1.3 USNRC, "NRC Policy on Future Reactor Designs: Decisions on Severe Accident Issues in Nuclear Power Plant Regulation," NUREG-1070, July 1985.

1.4 USNRC, "Policy Statement on Safety Goals for the Operation of Nuclear Power Plants," Federal Register, Vol. 51, p. 28044, August 4, 1986.

1.5 M. Silberberg et al., "Reassessment of the Technical Bases for Estimating Source Terms," NUREG-0956, July 1986.

1.6 USNRC, "Reactor Risk Reference Document," NUREG-1150, Vols. 1-3, Draft Report for Comment, February 1987.

1.7 Steam Explosion Review Group, "A Review of the Current Understanding of the Potential for Containment Failure from In-Vessel Steam Explosions," NUREG-1116, June 1985.

1.8 H. Kouts et al., "Review of Research on Uncertainties in Estimates of Source Terms from Severe Accidents in Nuclear Power Plants," Brookhaven National Laboratory, NUREG/CR-4883, BNL-NUREG-52061, May 1987.

2. NATURAL CIRCULATION IN REACTOR COOLANT SYSTEM

J. T. Han

2.1 Introduction

Reactor coolant system (RCS) natural circulation in a PWR is defined as the buoyancy-driven coolant circulation between the core and the upper-plenum region (in-vessel circulation) with or without a countercurrent flow in the hot leg piping between the vessel and steam generators (ex-vessel circulation). This kind of "multidimensional" buoyancy-driven flow circulation serves as a means of transferring the heat from the core to the structures in the upper plenum, hot legs, and possibly steam generators. As a result, the RCS piping and other pressure boundaries may be heated to high temperatures at which the structural integrity is challenged.

RCS natural circulation is likely to occur during the core uncovery period of the TMLB' accident in a PWR when the vessel upper plenum and hot leg are already drained and filled with steam and possibly other gaseous species. Hot gas rises from the central region of the core to the upper plenum while the relatively cold gas either descends from the outer region of the upper plenum to the outer region of the core below or makes a 90-degree turn (near the upper core plate above the core) toward the central region of the upper plenum. Multidimensional ex-vessel natural circulation may also exist in which relatively hot gas leaves the vessel in the upper portion of the hot leg toward the steam generator, and relatively cold gas flows back in the lower portion of the hot leg toward the vessel after making a 180-degree turn in the steam generator inlet plenum and/or steam generator tubes. Note that the RCS natural circulation defined here is somewhat different from the flow described in thermal-hydraulic data reports as the buoyancy-driven water or water-steam flow in the entire RCS when the steam generators remain as a heat sink.

RCS natural circulation was not analyzed in the Reactor Safety Study (Ref. 2.1) or in the Battelle Columbus Laboratories studies (Refs. 2.2 and 2.3). NRC investigation of this issue was initiated by NRR (Ref. 2.4). An NRR user need letter was received by RES in August 1984 (Ref. 2.5), and a RES response to the NRR need was issued in February 1985 (Ref. 2.6). It should also be pointed out that RCS natural circulation is one of the major areas of uncertainty identified in NUREG-0956 (Ref. 2.7).

RCS natural circulation is being studied for the Surry plant during the TMLB' accident in which station blackout coincides with the loss of auxiliary feedwater and no operator actions. Addressed in this issue are the effects of the multidimensional RCS natural circulation during the TMLB' accident on:

1. RCS structural integrity in terms of the location and size of the induced break, including steam generator tube rupture,

2. Initial conditions and likelihood for high-pressure melt ejection that may lead to direct containment heating,

BEST COPY AVAILABLE

3. Magnitude and rate of in-vessel hydrogen generation and release to the containment, and

4. Fission product retention in the RCS and release to the containment.

2.2 Current Technical Uncertainties

2.2.1 Important Subissues

The potential impact of the multidimensional RCS natural circulation is determined by several important subissues:

1. Determination of whether the vessel lower head will fail before the RCS is depressurized to low pressure (below 200 psig).

This subissue is determined by the timing and size of the induced break during the high-pressure TMLB' accident. If the reactor vessel fails through the lower head at high pressure, molten core debris and structure materials will be ejected into the containment. This high-pressure melt ejection may lead to direct containment heating and containment overpressurization, and, as a result, the containment integrity is challenged. However, if the RCS piping or steam generator tubes fail before molten core materials breach the vessel lower head, the adverse impact of direct containment heating will be reduced or even eliminated, depending on the vessel internal pressure when the lower head fails. This subissue will determine the likelihood and initial conditions for the direct containment heating. Therefore, the outcome of the RCS natural circulation will have a significant impact on the phenomenon of high-pressure melt ejection.

2. Failure location of the RCS pressure boundary.

Failure location of the RCS pressure boundary affects the RCS retention of the radioactive materials and the release of the radioactive materials to the containment. If steam generator tube rupture occurs when the RCS pressure is higher than the steamline pressure, the radioactive materials will be transported to the secondary side of the steam generator and from there to the atmosphere through the atmospheric dump valve or steamline safety valves. As a result, the containment is bypassed for a period of time during the accident.

3. Power-operated relief valve and safety relief valve status and operator actions.

The outcome of this subissue may have significant impact on the course of the accident. Based on our experience with the 1979 Three Mile Island Unit 2 accident (Ref. 2.8), the power-operated relief valve (PORV) can play a critical role in accident progression. Whether it will fail in open position during the TMLB' accident is not certain, but it is possible for the PORV to become stuck open after cycling a few times. The 1982 Ginna event (Ref. 2.9) and the 1985 Davis-Besse event (Ref. 2.10) are two more examples of the stuck-open PORV. The operator can isolate the stuck-open PORV by closing the block valve of the pressurizer and rely on the safety relief valves (SRVs) to prevent system overpressurization.

5

Although we have little experience regarding stuck-open SRVs in PWRs, the spring-loaded SRV could fail to reseat itself properly after cycling a number of times and as a result a leak is formed. However, there is no way for the operator to isolate a stuck-open SRV.

The following questions need to be answered for PWRs:

a. How will a stuck-open PORV or SRV change the course of the TMLB' accident, including the pressure at which the core melt is ejected into the containment?

b. What should and what can the operator do to mitigate the TMLB' accident? Should the operator try to isolate a stuck-open PORV as soon as a leakage is detected?

Under what conditions should the operator depressurize the RCS by opening the PORV?

How far could the RCS be depressurized by opening the PORV before the vessel lower head fails?

c. Are PORVs needed for a PWR? What is the recommended PORV capacity (opening area) for the plant?

Although the resolution of the above questions is beyond the scope of this document, these questions should be addressed for PWRs, including those without PORVs (Ref. 2.11).

4. Hydrogen generation.

Natural circulation flow in the vessel can potentially increase the magnitude of hydrogen generation by circulating upper-plenum steam back into the core to react with the Zircaloy cladding of fuel rods. Because of natural circulation, the upper-plenum structure can reach a higher temperature than the case without circulation; this tends to promote structure oxidation and produce additional hydrogen if steam is available in the region.

5. Fission product retention in the RCS before and after vessel failure.

Because of multidimensional natural circulation in the vessel and in the ex-vessel piping, the upper-plenum structures and ex-vessel piping and components are likely to be heated to a higher temperature than the once-through calculations neglecting the possible presence of natural circulation. A higher surface temperature will certainly affect fission product retention, including revaporization in the RCS.

2.2.2 Calculations and Experiments Completed

Various studies have been performed to address the issue. The following is a list of analytical and experimental studies sponsored by NRC and the industry through the Electric Power Research Institute (EPRI) and the Industry Degraded Core Rulemaking (IDCOR) program.

1. A state-of-the-art review of all studies on RCS natural circulation and relevant subjects (Refs. 2.12 through 2.40), including those performed for NRC, EPRI, and IDCOR.

2. Two-dimensional MELPROG calculations (Refs. 2.15 through 2.17) analyzing in-vessel natural circulation under constant pressure boundary conditions (at the PORV setpoint). Thermal hydraulics is coupled with core melt progression in these calculations; however, decay heating due to fission product deposition on structures, hydrogen generation by upper-plenum steel reaction with steam, PORV cycling, and rod ballooning are not accounted for. Additional calculations are under way to include these phenomena as well as the coolant flow in the ex-vessel piping and steam generators.

3. Initial phase of TMLB' calculations prior to core damage using the best-estimate thermal-hydraulic codes, including TRAC-PF1 (Refs. 2.15 through 2.17) and COBRA-NC (Ref. 2.18) for comparison with the MELPROG calculations above.

4. Structural integrity analysis (Refs. 2.19 through 2.21) estimating how long it will take to fail the RCS pressure boundary due to creep rupture as a function of temperature and RCS pressure. Three piping components were studied: vessel hot leg nozzle (A-508, Class 2 carbon steel), hot leg piping (316 stainless steel for Westinghouse plants), and steam generator tubes (Inconel 600).

5. Scoping calculations analyzing RCS natural circulation flow patterns using the COMMIX code with intact core geometry (Refs. 2.22 and 2.23). Results will be used to guide future calculations in modeling the hot leg and the steam generator.

6. Scoping analysis performed by Theofanous et al. for NRC (Refs. 2.24 and 2.25).

7. EPRI-sponsored 1/7-scale natural circulation experiment (Refs. 2.26 and 2.27) operated by Westinghouse using either water or sulfur hexafluoride gas as coolant. These experiments provide qualitative information such as flow patterns in the hot leg and the steam generator under simulated TMLB' accident conditions.

8. Analyses performed for EPRI using the CORMLT code modeling both in-vessel and ex-vessel RCS natural circulation in the Zion plant under the TMLB' accident conditions (Refs. 2.28 through 2.31).

9. Analyses performed for IDCOR using the MAAP code modeling in-vessel natural circulation (Ref. 2.32) in the Zion plant under TMLB' accident conditions but with pump seal LOCA (leakage of 50 gpm for each of four pumps starting at 45 minutes after accident initiation due to loss of seal cooling).

10. Hand calculations.

11. A RELAP5 calculation assessing whether pump seal leakage will clear the water in the loop seal (the U-shaped piping between the steam generator and pump) during the TMLB' accident in the Seabrook plant (Ref. 2.33).

12. Analysis and data of the TMI-2 accident (Refs. 2.5 and 2.34 through 2.36) used to investigate if multidimensional natural circulation occurred during the TMI-2 accident.

Table 2.1 lists the NRC-sponsored studies and code calculations addressing the issue of RCS natural circulation. Future work is also included.

2.3 Analytical Results

2.3.1 Summary of Analysis Results

This section summarizes and compares the results of analytical studies obtained for NRC, EPRI, and IDCOR. Table 2.2 lists the inner surface temperature at or near the vessel hot nozzle (connecting the vessel to hot leg piping), as calculated by three computer codes including MELPROG (NRC code), CORMLT (EPRI code), and MAAP (IDCOR code). CORMLT-calculated inner surface temperature of the surge line (connecting the pressurizer to hot leg) is also included for reference (Refs. 2.28 and 2.29). However, the current MELPROG (Ref. 2.15) and MAAP (Ref. 2.32) calculations do not model ex-vessel flow and therefore the surge line temperature is not calculated.

Based on the structural integrity analysis performed at the Idaho National Engineering Laboratory (INEL) (Refs. 2.19 through 2.21), at an average wall temperature of 1,000 K or higher, the hot leg nozzle is likely to fail in a few minutes because of creep rupture. However, the initial rupture size is not available. Note that the MELPROG and CORMLT calculations above are respectively more than 200 to 50 K higher than this critical temperature (note that average temperature is around 15 K lower than inner surface temperature). However, the MAAP-calculated value is about 100 K below the critical temperature of 1,000 K. It is important to recognize that the uncertainty in those calculated temperatures is not known and needs to be determined. It should also be recognized that all these computer codes have extremely limited code validation by comparing calculations with data or with other validated code results, and they have not been scrutinized by peer review. Needless to say, uncertainty also exists for the rupture time and critical temperature predicted by the structural integrity analysis and needs to be determined or bounded. Nevertheless, it should be pointed out that code validation for MELPROG is under way and will continue in the future.

Based on the CORMLT calculation above, the surge line reaches 1,530 K at t = 3.1 hours (t = 0 at TMLB' initiation), which is 500 K above the EPRI-estimated threshold of 1,030 K (1,400°F) for the structure to fail. Because the surge line temperature is quite high (higher than hot leg nozzle temperature in the CORMLT calculation), EPRI concludes that RCS structural integrity may be lost during the TMLB' accident before vessel lower-head failure and that the likely failure locations are (1) the surge line, (2) instrumentation lines close to the hot leg nozzle, and (3) PORV and SRVs. However, the IDCOR study (Ref. 2.32) concludes that the temperatures high enough to fail the RCS were not achieved in the MAAP results.

BEST COPY AVAILABLE

Table 2.1 A summary of NRC-sponsored code calculations and studies investigating RCS natural circulation under high-pressure TMLB' accident conditions in a PWR.

Code	Purpose	Completion Date*
COBRA-NC	Calculating in-vessel natural circulation assuming intact core geometry and using MARCH-supplied boundary conditions. Results were compared with MELPROG/TRAC calculations prior to core degradation.	3/85
TRAC-PF1	Calculating in-vessel natural circulation assuming intact core geometry. Results were compared with MELPROG/TRAC calculations prior to core degradation.	2/86
MELPROG	Calculating in-vessel natural circulation up to vessel failure. No fission product release and retention, hydrogen generation calculated.	3/86
MELPROG	Same calculation as above but including fission product release and retention. Calculation will proceed to some point after vessel failure.	12/86
COMMIX	Scoping calculations to investigate multidimensional natural circulation flow in the RCS. Results will be used to provide guidance on how to model flow split in hot leg and steam generator in MELPROG/TRAC and SCDAP/RELAP5.	8/86
MELPROG/TRAC	Analyzing multidimensional RCS natural circulation in the entire RCS during a PWR TMLB' accident. Fission product release and retention included.	7/87
SCDAP/RELAP5	Analyzing the same TMLB' accident as above but prior to vessel failure. This calculation provides a comparison for the above MELPROG/TRAC results and a sensitivity study on the time-temperature history.	7/87
RELAP5	Assessing whether pump seal leakage will clear the water from the loop seal during a TMLB' accident in the Seabrook plant (once-through core flow was assumed in the calculation).	10/84
	Simple scoping calculations using a three lumped-mass model to represent the vessel (Refs. 2.21 and 2.22).	3/84
	RCS structural integrity analysis using pressure and temperature as key parameters (Refs. 2.16 through 2.18).	3/86

*Date shown is for the completion of the first calculation. Additional calculations will follow if needed.

Table 2.2 Calculated temperature at or near the inner surface of hot leg nozzle under high-pressure TMLB' accident conditions.*

Code	Code User (Sponsor)	Plant	Hot Leg Nozzle Temperature	Time from Start of TMLB' Accident
MELPROG (Ref. 2.15)	LANL/SNL (NRC)	In-vessel circulation in Surry	1,240 K (delta T across hot leg pipe = 27 K)	t = 3.6 h, about 50 min before vessel lower-head failure
CORMLT (Refs. 2.28 and 2.29)	SAI (EPRI)	In-vessel & ex-vessel circulation in Zion	1,070 K (Surge line = 1,530 K at t = 3.1 h)	t = 3.1 h
MAAP (Ref. 2.32)	FAI (IDCOR)	In-vessel circulation in Zion	910 K	t = 3.65 h when the vessel lower head fails

*1. The MAAP calculation above is for TMLB' with pump seal LOCA starting at at t = 45 minutes; the leak area per pump is assumed to be 0.28 inch in equivalent diameter, which allows a leakage of 50 gpm of water per pump until the pump seal is uncovered and the leakage is reduced to mainly gas flow.
This MAAP calculation indicates that some water remains in the RCS loop seal, which is not empty until after the vessel lower head fails. No seal LOCA is assumed in either the MELPROG or the CORMLT calculation above.
2. MELPROG calculates flow patterns of in-vessel circulation as a function of time, while both CORMLT and MAAP use the user-input flow patterns. Ex-vessel flow is accounted for in the CORMLT calculation above, but it does not model vessel failure.
3. The MELPROG and CORMLT calculations above do not account for the decay heating of fission products deposited on the upper-plenum structures as in the MAAP calculation.
4. MELPROG results are preliminary in nature. Improved calculations to account for the ex-vessel natural circulation, decay heating due to fission product deposition, PORV cycling, and any rod ballooning will be included in the future work to be discussed in Section 2.4.
5. Differences in the vessel design between Surry and Zion are not expected to affect the results significantly.

Scoping studies by Theofanous et al. (Refs. 2.24 and 2.25) suggest that the RCS piping temperature will lag behind the core temperature for only a few hundred degrees K during the TMLB' accident and, as a result, the RCS pressure boundary may fail before core melting and slumping to the lower plenum. Possible failure locations are not identified in the studies.

Table 2.3 summarizes the possible failure locations of the RCS structural boundary during the PWR high-pressure TMLB' accident before the failure of vessel lower head, as predicted by various studies as of September 1986. (Note that uncertainties in the results are unknown and yet to be estimated.)

Table 2.3 Possible failure locations of RCS pressure boundary during high-pressure TMLB' accident in Westinghouse PWRs before ejection of core melt from reactor vessel lower head to containment.

Studies/Judgments	Failure Locations	Remark
NRC-Sponsored (Refs. 2.12 through 2.25)	Hot leg nozzle and possibly elsewhere.	MELPROG calculation is for in-vessel circulation only.
EPRI-Sponsored (Refs. 2.28 through 2.31)	Surge line to pressurizer, instrumentation lines close to hot leg nozzle, and PORV and SRVs.	Failure of hot leg nozzle was not identified in the studies although the temperature is high.
IDCOR-Sponsored (Ref. 2.32)	None	MAAP calculation is for in-vessel circulation only but including fission product heating on structures.

2.3.2 Discussion of Analytical and Experimental Results

This section will discuss results of in-vessel natural circulation during the TMLB' accident in a PWR as calculated by the MELPROG code (Refs. 2.15 through 2.17), the RCS structural integrity analysis using temperature and pressure loading as two key parameters (Refs. 2.19 and 2.20), the TMI-2 accident (Refs. 2.28 and 2.34 through 2.37), the EPRI-sponsored RCS natural circulation experiments at Westinghouse (Refs. 2.26 and 2.27), the status of the loop seal (Refs. 2.32 and 2.33), and analyses sponsored by EPRI (Refs. 2.28 through 2.31) and IDCOR (Ref. 2.32).

MELPROG Calculations

The MELPROG code is a state-of-the-art computer code being developed at Los Alamos National Laboratories and Sandia National Laboratories. It models two-dimensional thermal hydraulics (in axial and radial directions). In the future,

BEST COPY AVAILABLE

11

core melt progression phenomena, including the release of fission products and hydrogen in a reactor vessel, will be provided. Physical processes are mechanistically modeled and built upon fundamental laws and correlations. MELPROG is being linked with the TRAC thermal-hydraulic system code to become the integrated MELPROG/TRAC code, which will be capable of analyzing the severe accident progression in the entire RCS from accident initiation to core melt and to vessel failure. It should be pointed out that the thermal-hydraulics models in MELPROG were adopted from TRAC-PF1 with modifications to account for high-temperature properties, movement of degraded core materials in the coolant, etc.

Table 2.4 shows the calculated events and timing during the TMLB' accident in a PWR. The initial calculation, from accident initiation at t = 0 to t = 6500 s when boiling begins in the core, is based on a TRAC-PF1 calculation for the Zion plant. From 6500 s and on, MELPROG calculates what happens in the Surry vessel assuming a constant PORV setpoint pressure of 2,360 psia at the vessel hot leg nozzle and zero mass flow at the vessel cold leg inlet. The core begins to uncover and to expose to steam at t = 1 h 58 min (7070 s), and the whole core is dry and exposed to steam at t = 2 h 19 min (8350 s). Hydrogen generation begins at t = 2 h 35 min (9280 s). Molten Zircaloy is assumed to relocate at 2,200 K, and the first relocation occurs around t = 2 h 50 min (10180 s). (It should be pointed out that the temperature may not be the only factor controlling cladding relocation, which may also be affected by the thickness of the zirconium oxide layer outside of unoxidized cladding and by any existing pressure difference across the cladding.) Core slumps around 4 h 8 min (14880 s), and the vessel lower head fails at 4 h 26 min (15930 s) after the TMLB' accident begins.

Figure 2.1 shows the MELPROG-calculated hot leg nozzle temperatures. At around t = 3 h (10800 s), the average hot leg nozzle temperature reaches 1,000 K. Based on the INEL structural integrity analysis (Refs. 2.19 through 2.21), creep rupture will fail the hot leg nozzle in about 10 minutes. The hot leg nozzle temperature reaches 1,200 K around 3.6 h (12900 s), which is about 50 minutes before the failure of the vessel lower head. If the uncertainty in the MELPROG results is within 200 K of this value, the hot leg nozzle could fail long before the failure of the vessel lower head to provide sufficient time for the RCS to depressurize to the accumulator setpoint of around 600 psia.

Figure 2.2 shows the temperature distribution in the vessel at t = 6500 s when the peak water temperature in the vessel reaches saturation. Figures 2.3 through 2.5 show the flow circulation in the upper plenum and the uncovered core region, and core melt progression during the TMLB' accident in the Surry vessel. In these figures, the vessel is divided into five radial rings--three in the core and one each in the core bypass region (baffle-barrel region) and vessel downcomer. Each radial ring is axially divided into 13 computational cells, and there are 65 cells for the entire vessel. The upper number in each cell is the coolant temperature, and the lower number is the surface temperature of the structure and fuel rods (in cells containing fuel rods and structure, fuel rod surface temperature is shown). The solid line with arrow head represents the coolant velocity in the cell with the arrow showing the direction and the length corresponding to the magnitude. Fuel rod volume fraction in the core is represented by the vertical solid lines. The density of dotted lines in each cell indicates the volume fraction of water in that cell (e.g., the density of dotted lines in each cell in Fig. 2.2 indicates that the cell is filled with water, and the dotted lines in the upper-plenum and upper-core region in Fig. 2.3 indicate that no water is present there). The angle of the

12

Table 2.4 MELPROG-calculated TMLB' event sequence (Ref. 2.15).

Time(s)	Event
0	Loss of offsite power, loss of feedwater.
4170	Steam generators dry.
6500	Incipient boiling, begin MELPROG calculation.
7070	Core uncovered.
8350	Core empty.
9280	Hydrogen generation begins at top of core.
9970-10145	Control rods fail in top three levels in Rings 1 & 2; steam temperature > 1,700 K.
10156	Cladding begins to melt in Ring 1, Level 5; cladding temperature > 2,100 K.
10181	Fuel rods disintegrate in Ring 1, Level 5; cladding molten and temperature >2,200 K.
10216-10221	Control rods fail in Ring 3, at top of core.
10241-10303	Cladding melts and fuel disintegrates in center two rings, top four levels of core.
10319-10377	Cladding melts and fuel disintegrates in top four levels of Ring 3.
10377-10403	Fuel rods in Rings 1 and 2 disintegrate in Level 2.
10387	Upper core plate melts in Ring 1.
10808	Fuel rods in Ring 3, Level 2 disintegrate.
11345-10260	"Thin" metal in upper plenum melts.
11522	Control rods fail in Ring 1, Level 1.
11680	Core baffle fails mechanically.
11824	Core baffle begins to melt.
12305	Control rods fail in Ring 2, Level 2.
14877	Debris region crust fails, core slumps.
14878	Level 1 fuel rods disintegrate.
15371-15874	Lower support structures melt.
15928	Lower head fails, end MELPROG calculation.

13

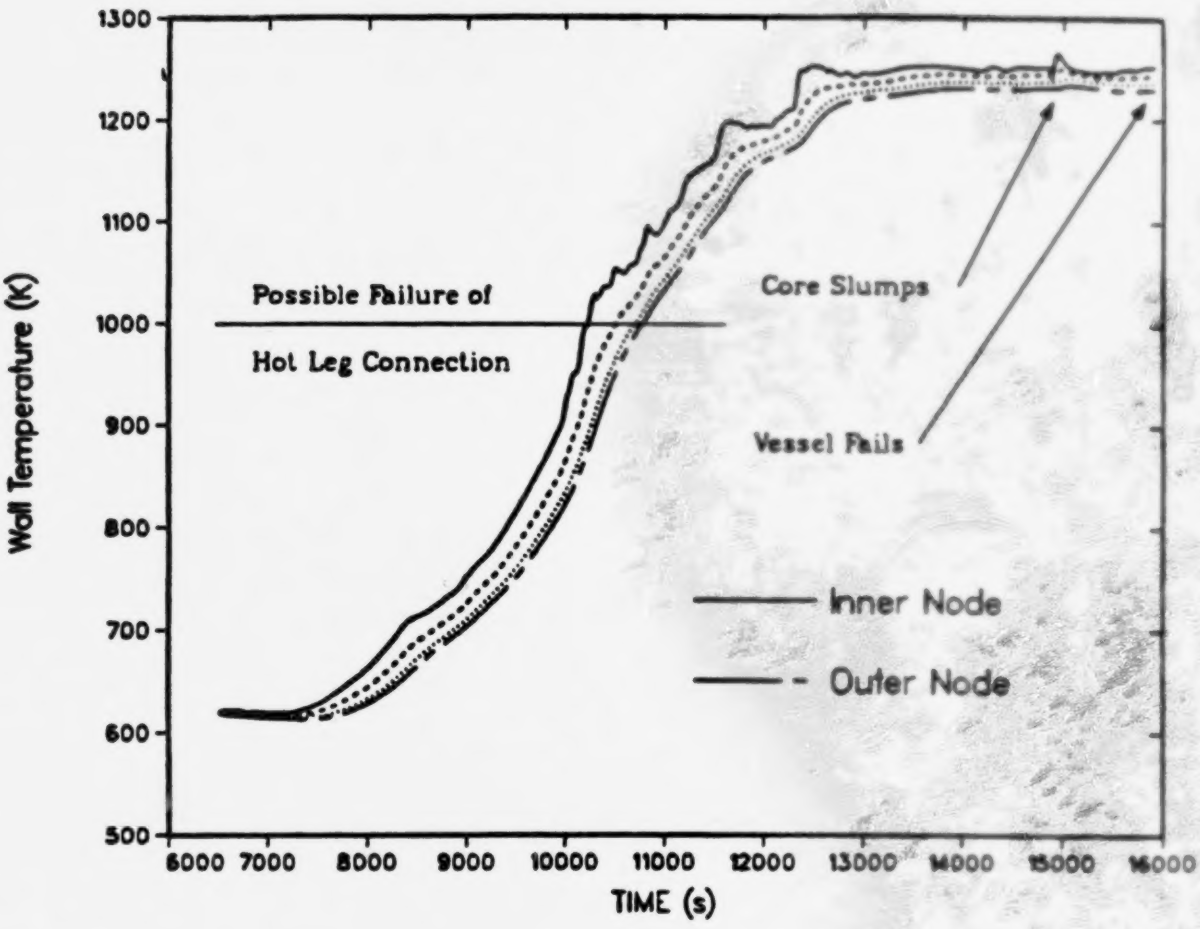

Figure 2.1 MELPROG-calculated hot leg nozzle temperature for TMLB' accident in Surry (Ref. 2.15).

BEST COPY AVAILABLE

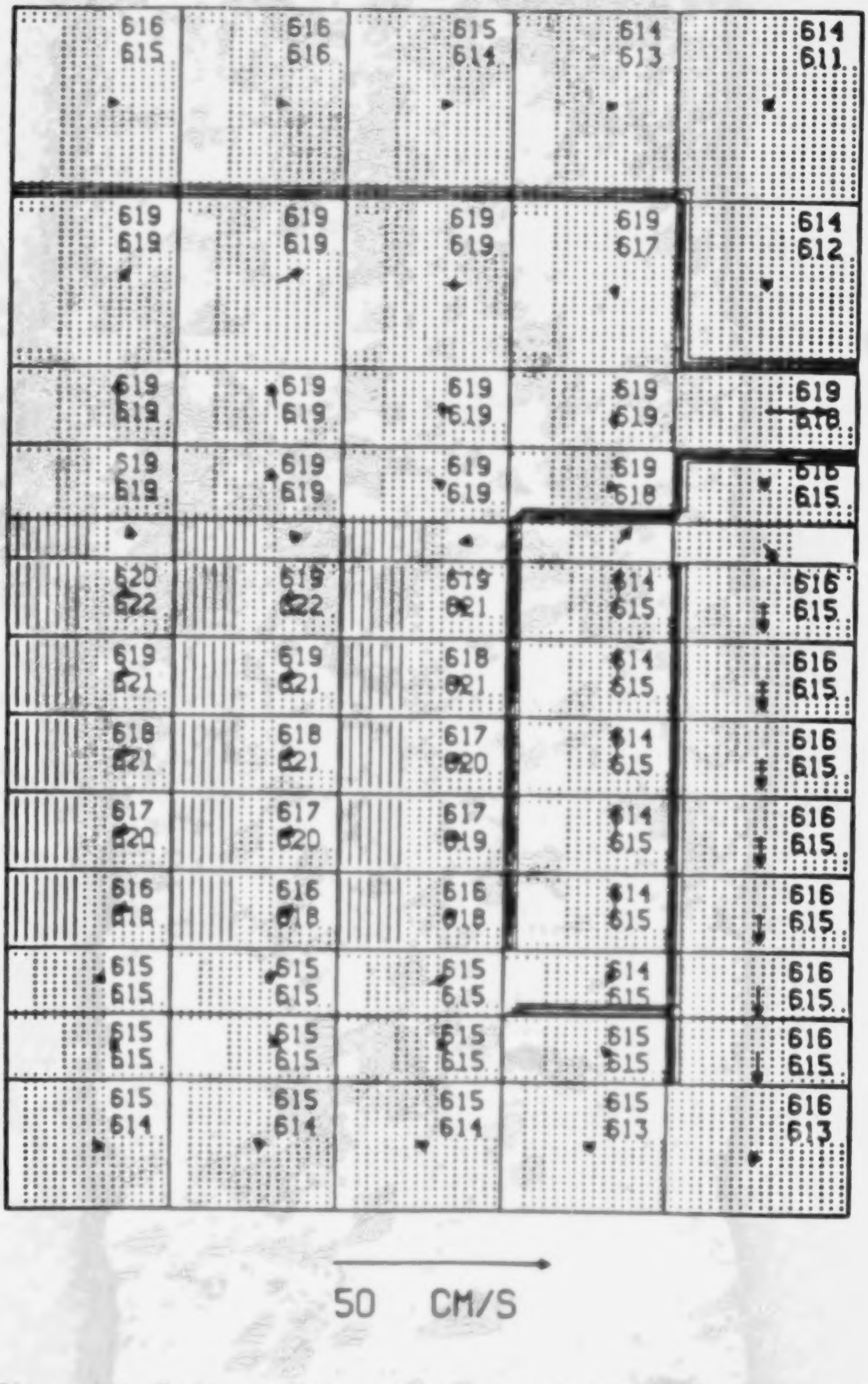

616
615
616
616
615
614
614
613
614
611
619
619
619
619
619
619
619
617
614
612
619
619
619
619
619
619
619
619
619
618
619
619
619
619
619
619
619
618
616
615
620
622
619
622
619
621
614
615
616
615
619
621
619
621
618
621
614
615
616
615
618
621
618
621
617
620
614
615
616
615
617
620
617
620
617
619
614
615
616
615
616
618
616
618
616
618
614
615
616
615
615
615
615
615
615
615
614
615
616
615
615
615
615
615
615
615
615
615
616
615
615
614
615
614
615
614
615
613
616
613
50 CM/S

Figure 2.2 Temperature distribution in vessel at 6500 s (Ref. 2.15).

BEST COPY AVAILABLE

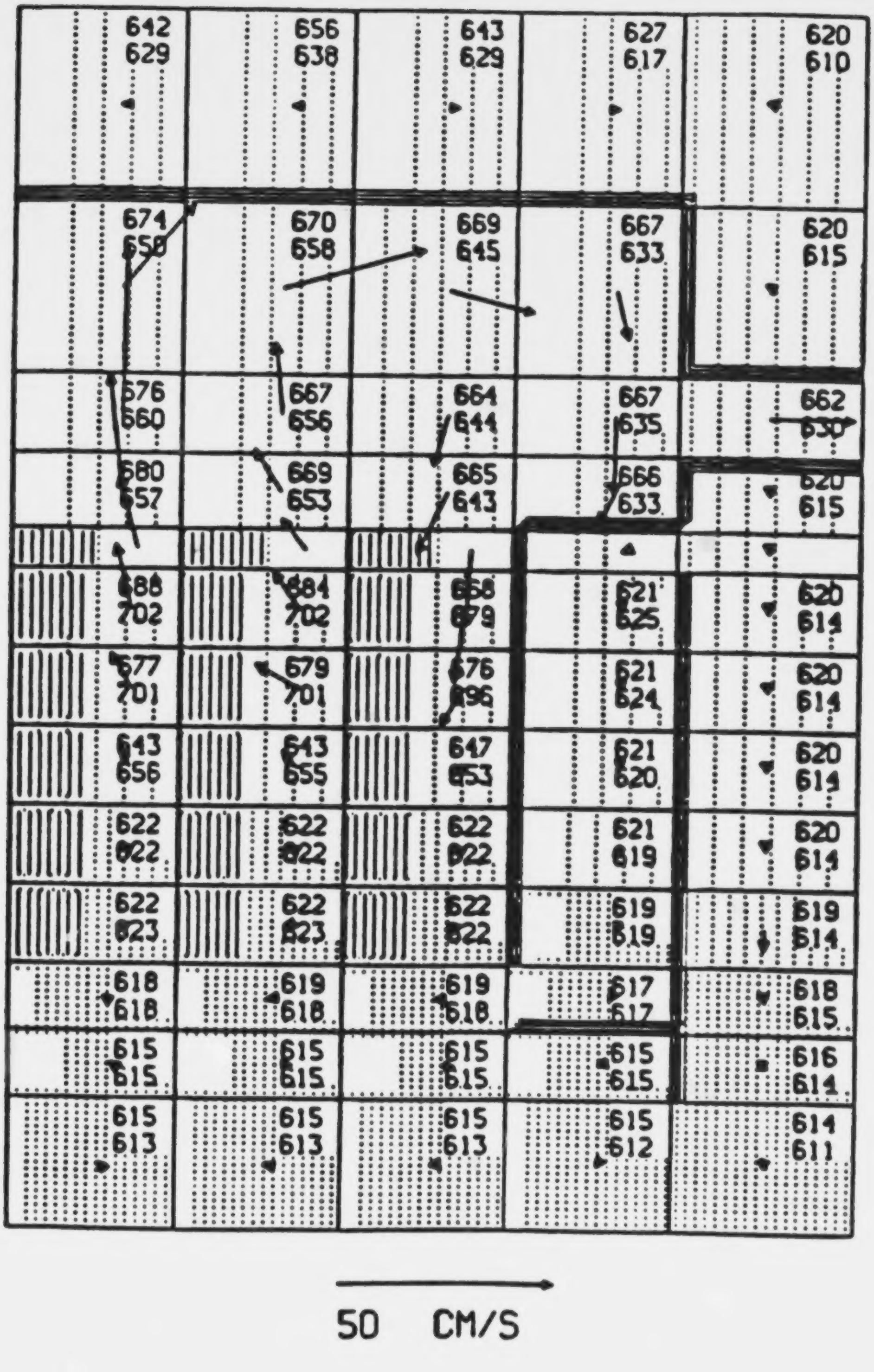
642
629
656
638
643
629
627
617
620
610
674
658
670
658
669
645
667
633
620
615
676
660
667
656
664
644
667
635
662
630
680
657
669
653
665
643
666
633
620
615
688
702
684
702
658
679
621
625
620
614
677
701
679
701
676
696
621
624
620
614
643
656
643
655
647
653
621
620
620
614
622
622
622
622
622
622
621
619
620
614
622
623
622
623
622
622
619
619
619
614
618
618
619
618
619
618
617
617
618
615
615
615
615
615
615
615
615
615
616
614
615
613
615
613
615
613
615
612
614
611
50 CM/S

Figure 2.3 Flow and temperature distributions at 7500 s (Ref. 2.15).

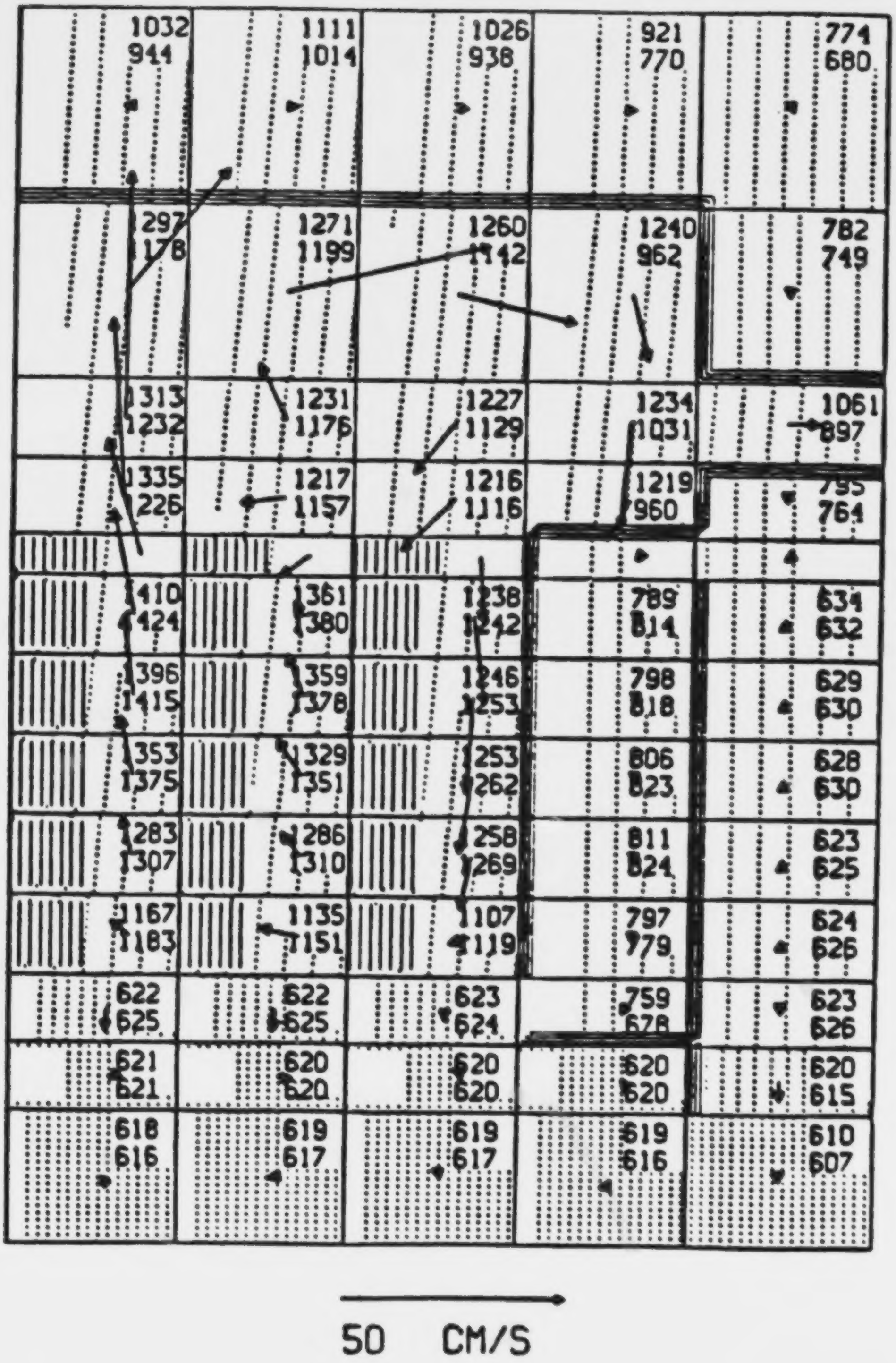
1032
944
1111
1014
1026
938
921
770
774
680
1297
1178
1271
1199
1260
1142
1240
962
782
749
1313
1232
1231
1176
1227
1129
1234
1031
1061
897
1335
1226
1217
1157
1216
1116
1219
960
795
764
1410
1424
1361
1380
1238
1242
789
814
631
632
1396
1415
1359
1378
1246
1253
798
818
629
630
1353
1375
1329
1351
1253
1262
806
823
628
630
1283
1307
1286
1310
1258
1269
811
824
623
625
1167
1183
1135
1151
1107
1119
797
779
624
626
622
625
622
625
623
624
759
678
623
626
621
621
620
620
620
620
620
620
620
615
618
616
619
617
619
617
619
616
610
607
50 CM/S

Figure 2.4 Flow and temperature distributions at 9525 s (Ref. 2.15).

BEST COPY AVAILABLE

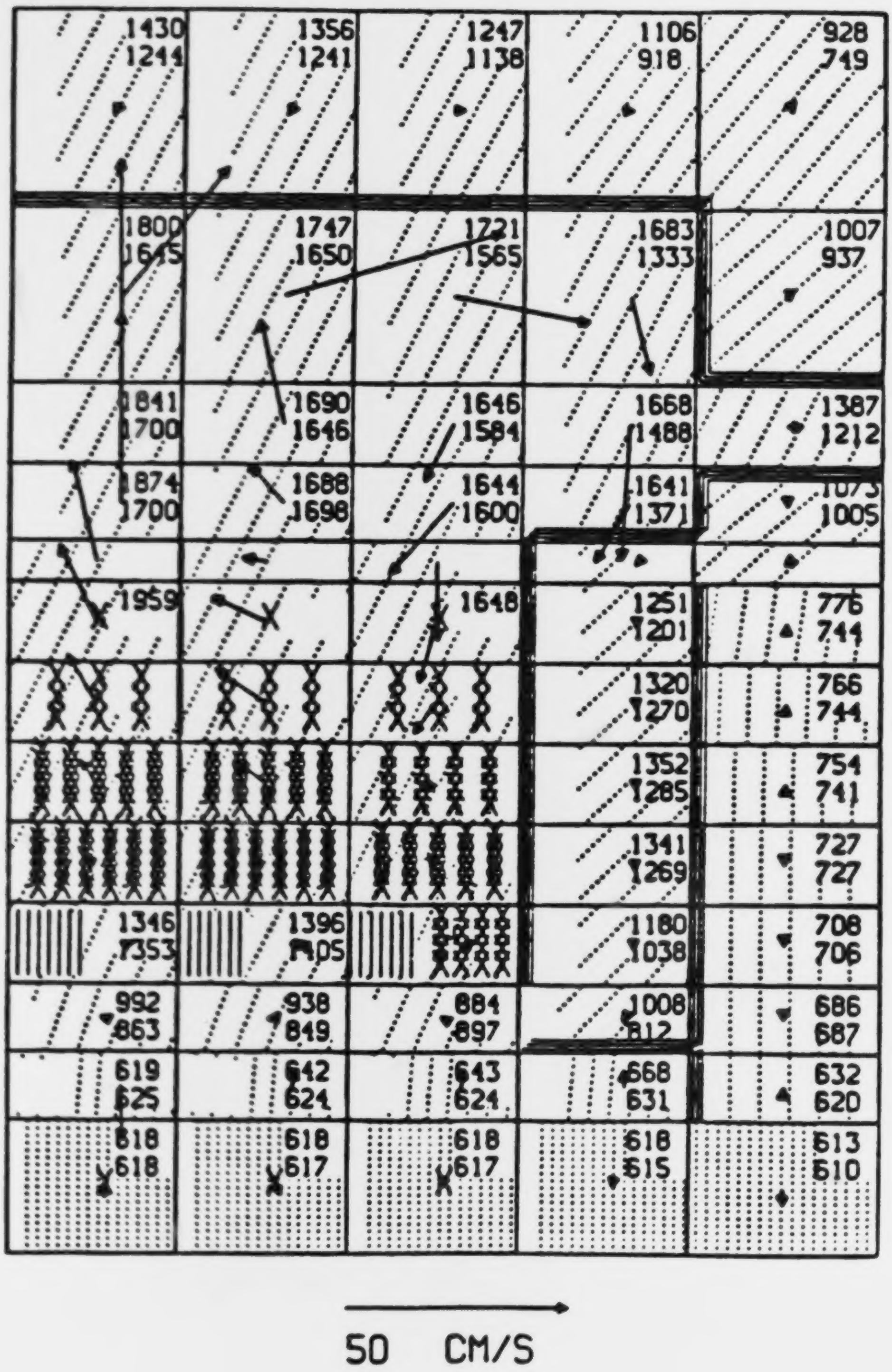
1430
1244
1356
1241
1247
1138
1106
918
928
749
1800
1645
1747
1650
1721
1565
1683
1333
1007
937
1841
1700
1690
1646
1646
1584
1668
1488
1387
1212
1874
1700
1688
1698
1644
1600
1641
1371
1073
1005
1959
1648
1251
1201
776
744
1320
1270
766
744
1352
1285
754
741
1341
1269
727
727
1346
1353
1396
1405
1180
1038
708
706
992
863
938
849
884
897
1008
812
686
687
619
625
642
624
643
624
668
631
632
620
618
618
618
617
618
617
618
615
613
610
50 CM/S

Figure 2.5 Flow and temperature distributions at 11000 s (Ref. 2.15).

dotted lines from the vertical position is proportional to the hydrogen partial pressure in the cell (e.g., vertical dotted lines mean no hydrogen). The density of the "x" in a cell corresponds to the volume fraction of the debris bed in the cell formed after fuel rod failure. An important message from these figures is that coolant circulation exists in the upper plenum and the uncovered core regions before and after core is damaged. Hot coolant rises from the inner region of the core to the upper plenum above, and it circulates to the outer region of the upper plenum with the temperature being reduced by heating up the upper-plenum structures. The coolant in the outer region of the upper plenum either descends to the core below or makes a 90-degree turn above the core and flows back to the inner region of the upper plenum. Flow circulation between the core and upper plenum distributes some of the decay heat to the upper-plenum structures; as a result, structures in the upper plenum (e.g., control rod guide tubes and support columns) are heated up to the steel melting point of around 1,700 K as shown in Figure 2.5.

MELPROG also calculates hydrogen generation due to steam and fuel cladding reaction for two cases: (1) two-dimensional calculations accounting for in-vessel natural circulation and (2) one-dimensional calculations neglecting circulation. However, current calculations do not model possible hydrogen generation due to steam and upper-plenum steel reaction, which will be included in future calculations. Table 2.5 lists the estimated hydrogen generation in the Surry plant during the TMLB' accident. Best-estimate values calculated by MELPROG are equivalent to 40 to 60 percent of the fuel cladding oxidized. A value of 75 percent cladding oxidized is selected to account for additional hydrogen that may be produced by steam-steel reaction in the upper plenum and by other uncertainties. It should be pointed out that the Battelle Columbus study (Ref. 2.2) using the one-dimensional MARCH code obtains 59 percent of cladding oxidation for the TMLB' accident in Surry, and this value is within the range of the best-estimate values in Table 2.5. It is also worth noting that the TMI-2 accident produced an amount of hydrogen equivalent to about 45 to 50 percent of cladding oxidized (Refs. 2.8 and 2.34).

Table 2.5 Estimated hydrogen generation during TMLB' accident in Surry plant

	Low Estimate	Best Estimate	High Estimate
Maximum Hydrogen Generation Rate	0.5 kg/s	1 kg/s	3 kg/s
Total Hydrogen Generation	220 kg	290-440 kg	540 kg
Fraction of Fuel Cladding Oxidized	30%	40%-60%	75%

Calculations using the detailed mechanistic thermal-hydraulic codes such as TRAC-PF1 (Refs. 2.15 through 2.17) and COBRA-NC (Ref. 2.18) were also performed. The purpose is to compare these calculations with the MELPROG calculations before the core is damaged. Reasonable agreement exists for the comparisons and this

BEST COPY AVAILABLE

tends to support the soundness of the thermal-hydraulic modeling in MELPROG because both TRAC and COBRA-NC have gone through extensive code assessment and model validation.

TMI-2 Accident

It is appropriate to discuss here what happened in the TMI-2 vessel during the 1979 accident (Refs. 2.8 and 2.34 through 2.36). Based on the postaccident examination (Ref. 2.35), the peak surface temperatures registered on the two control rod leadscrews in the TMI vessel upper plenum do not indicate characteristics of natural circulation as shown in Figures 2.3 through 2.5. The leadscrew near the center of the upper plenum revealed a peak surface temperature around 1,255 K (1,800°F) at the lower end (near the upper core plate) and a peak surface temperature of around 666 K (740°F) at its upper end, which is about 9 feet above; the axial temperature difference is about 589 K (1,060°F) on the center leadscrew. The leadscrew in the outer upper-plenum region had a peak surface temperature of around 1,030 K (1,400°F) at the lower end and a temperature of around 723 K (840°F) at the upper end; the axial temperature difference is about 310 K (558°F). No melting occurred on the upper-plenum steel structures, but there were localized meltings of the upper core plate above the core. To the contrary, the axial temperature differences for structures in the inner region (1st and 2nd radial rings) of the upper plenum are less than 60 K (108°F) as shown in Figures 2.4 and 2.5. Therefore, the large axial surface temperature difference on the TMI central leadscrew seems to indicate the absence of in-vessel natural circulation in the TMI-2 accident. In addition, because the peak structure surface temperature in the TMI upper plenum was more than 400 K below the stainless steel melting point and the upper-plenum structures remained unmelted, natural circulation flow was not evident in the TMI-2 accident. However, the above indications do not necessarily rule out any brief presence of in-vessel natural circulation during the course of the TMI-2 accident. (It is worth noting that the MELPROG calculation shown in Figures 2.4 and 2.5 does not account for fission product heating on the upper-plenum structure surface.)

This leads to the question as to why in-vessel natural circulation did not seem to exist, at least not long enough to register its presence, during the TMI-2 accident. A plausible answer to this question is that the TMI-2 accident was a combination of a small-break LOCA (when the PORV was stuck open until it was isolated by the operator), pump on and off, and emergency core cooling system water injection on and off. It is different from the TMLB' accident, which occurs at an approximately constant pressure (perturbed by PORV cycling open and closed) without the disturbance of either RCS pump operation or emergency core cooling system injection. In other words, the flow environment inside the TMI-2 vessel is expected to be much more dynamic than what would happen in the TMLB' accident. During the TMI-2 core uncovery period from about 100 to 210 minutes after the accident began, the RCS pressure varied significantly and did not oscillate near a constant value as in the TMLB' accident. Table 2.6 presents the pressure variations during the TMI-2 core uncovery period from about 100 minutes to 210 minutes from the accident initiation.

Table 2.6 RCS pressure measurements during TMI-2 core uncovery period (Refs. 2.8 and 2.34).

Time (min)	Pressure (psia)	dP/dt* (psi/min)
100	890	
		- 9.4
130	607	
		5.7
142	675	
		30.
190	2,110	
		-34.
210	1,425	

*dP/dt is the linear pressure gradient between two instants in time. For example, the linear pressure gradient between 100 and 130 minutes is calculated as (607-890)/(130-100) = - 9.4 psia/min. Negative value indicates that the RCS is depressurized during this period.

The above rates of pressure change could have impeded the in-vessel natural circulation. Furthermore, rod ballooning might also hinder natural circulation. It is worth noting that a preliminary RELAP5 calculation using multiple-channel modeling to approximate in-vessel natural circulation indicates that under the high-pressure TMLB' conditions in-vessel natural circulation could exist in the TMI-2 vessel (Ref. 2.37).

The TMI-2 office of the Department of Energy has planned to provide TMI data as an international standard problem for code validation. The integrated MELPROG/TRAC and SCDAP/RELAP5 codes will be used to participate in this exercise. It is expected that additional insight, regarding whether in-vessel natural circulation ever existed in the TMI-2 vessel, will come out as a result of this exercise scheduled to be completed in 1989.

Structural Integrity Analysis

In parallel with the in-vessel natural circulation studies using MELPROG and other codes, a structural integrity analysis has been obtained by INEL (Refs. 2.19 through 2.21) for three RCS components--vessel hot leg nozzle (A-508, Class 2 carbon steel), hot leg piping (316 stainless steel), and steam generator tubes (Inconel 600), as existed in the Surry plant and probably in other Westinghouse plants as well. Figure 2.6 shows a sketch of the hot leg nozzle, hot leg piping, and the weld connecting the hot leg piping to the nozzle. As pointed out in the analysis, the weld is a potentially weak point of the RCS because of possible loss of ductility. Unfortunately, analysis cannot be made for the weld due to lack of creep rupture data of the material.

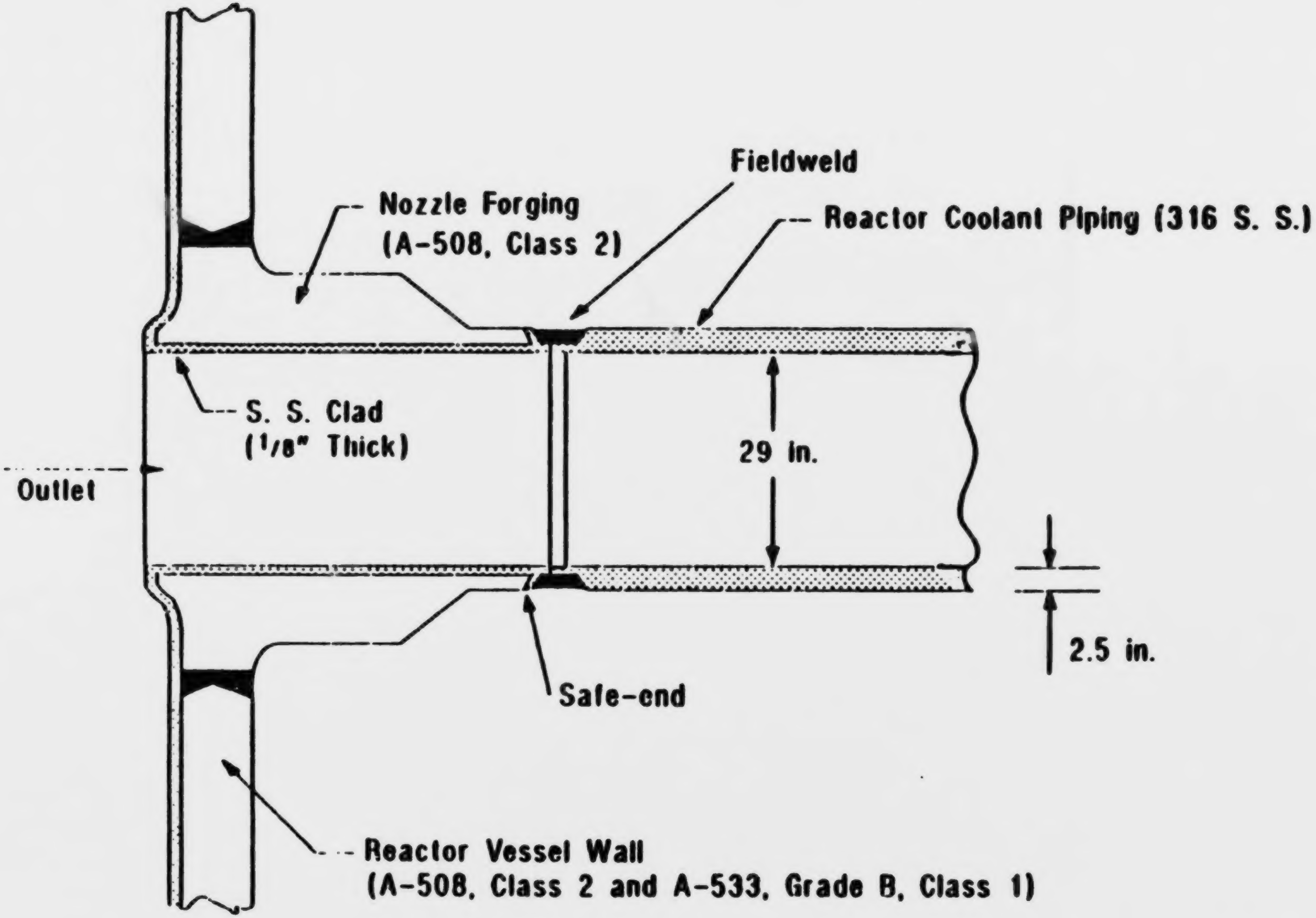
Fieldweld
Nozzle Forging
(A-508, Class 2)
Reactor Coolant Piping (316 S. S.)
S. S. Clad
($^1/_8$" Thick)
Outlet
29 in.
2.5 in.
Safe-end
Reactor Vessel Wall
(A-508, Class 2 and A-533, Grade B, Class 1)

Figure 2.6 Schematic of hot leg nozzle and hot leg pipe (Ref. 2.20).

Figure 2.7 shows how long a hot leg nozzle can maintain its integrity (rupture time) before it is failed by creep rupture using the average wall temperature and the pressure difference between the pipe inside and outside pressures as two independent parameters. Similarly, the rupture time curves for hot leg piping and steam generator tubes are shown in Figures 2.8 and 2.9, respectively. Based on these figures, the rupture temperature above which the structure may rupture in a short time is obtained and listed in Table 2.7. The temperature below which the rupture time is more than an hour is listed in Table 2.7 for comparison. At this latter temperature, the reactor coolant system is likely to remain pressurized until failure of the vessel lower head.

Status of Loop Seal

The loop seal is formed in the U-shaped piping connecting the lower end of a steam generator to the inlet of an RCS pump. The concern here is whether the loop seal will lose all the water in it during the TMLB' accident because of pump seal LOCA (due to loss of seal cooling) or other mechanisms. If the loop seal is cleared of water due to pump seal LOCA, the coolant will leak to the containment through the failed pump seal. As a result, more flow may go through the steam generator tubes, and the flow patterns in the hot leg may be affected. On the other hand, if pump seal LOCA does not lead to the total clearing of loop seal water, the flow in the hot leg and in the steam generator may not be noticeably affected by the seal LOCA. It is worth noting that if the loop seal is empty and if the vessel downcomer is also empty so that a pathway is established for the gas in the downcomer to flow to the core, the possibility may exist for the gas flow to circulate in the entire RCS, including the cold leg.

Studies regarding the status of the loop seal during TMLB' accidents are rather limited. There are only two analyses--one by INEL using the RELAP5 code (Ref. 2.33) and the other by FAI using the MAAP code (Ref. 2.32). In the INEL analysis (Ref. 2.33), a one-dimensional RELAP5 calculation was obtained for analyzing the RCS response during the TMLB' accident with pump seal LOCA in the Seabrook plant. The calculation is terminated at around 8600 s (2 h 23 min) when the peak steam temperature reaches 1,500 K (close to RELAP5 limitations). The pump seal LOCA is specified as: at t = 0 to 2700 s (45 min), a leakage of 20 gpm of water (at 2,250 psia and 557°F) occurs for each of four pumps; at t = 2700 s, a larger seal leak area is assumed so that the leakage is increased to 475 gpm (until the pump seal is uncovered and gas leakage is established) for each of four pumps. Note that the 475-gpm leakage for each pump is considered to be the maximum value expected for the pumps used in the existing Westinghouse plants (Refs. 2.33 and 2.40). The RELAP5 calculation predicts that some temperature reaches 1,500 K (close to RELAP5 limitations). The pump seal LOCA is specified as: at t = 0 to 2700 s (45 min), a leakage of 20 gpm of water (at 2,250 psia and 557°F) occurs for each of four pumps; at t = 2700 s, a larger seal leak area is assumed so that the leakage is increased to 475 gpm (until the pump seal is uncovered and gas leakage is established) for each of four pumps. Note that the 475-gpm leakage for each pump is considered to be the maximum value expected for the pumps used in the existing the Westinghouse plants (Refs. 2.33 and 2.40). The RELAP5 calculation predicts that some water will remain in the loop seal at 8600 s (2 h 23 min) after the initiation of the TMLB' accident assumed in the Seabrook plant. Although the calculation assumes one-dimensional flow in the vessel and in-vessel natural circulation during the core uncovery period is not accounted for, the conclusion regarding the water in the loop seal may still be valid. Nevertheless, additional calculations

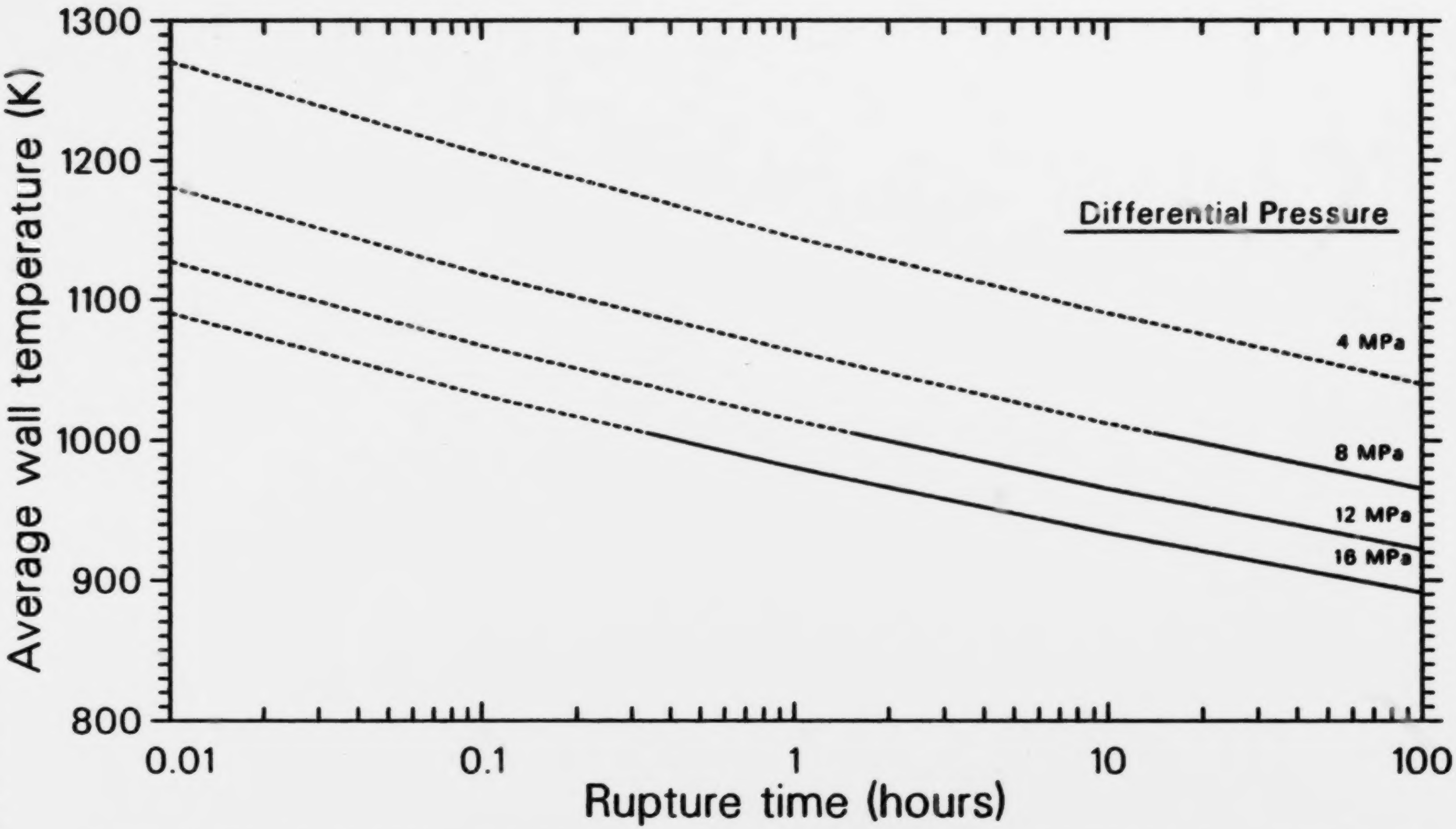

Note: Phase change occurs at about 1005 K (1350 °F). Calculated rupture times above this temperature (indicated by dashed lines) may not be valid.

Figure 2.7 Average wall temperature versus rupture time for hot leg nozzle (A-508, Class 2 carbon steel) (Ref. 2.20).

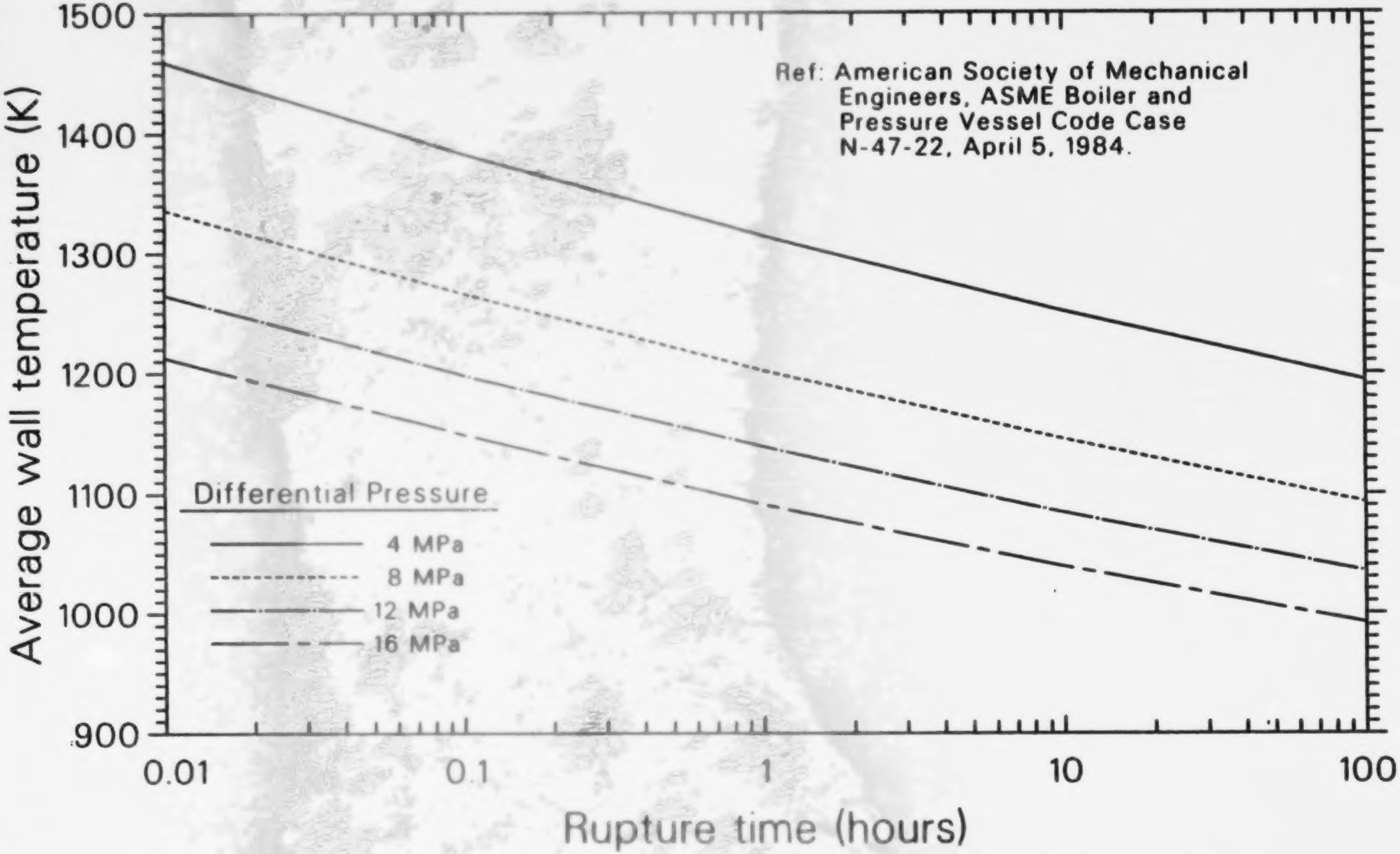

Ref: American Society of Mechanical Engineers, ASME Boiler and Pressure Vessel Code Case N-47-22, April 5, 1984.

Figure 2.8 Average wall temperature versus rupture time for hot leg pipe (316 stainless steel) (Ref. 2.20).

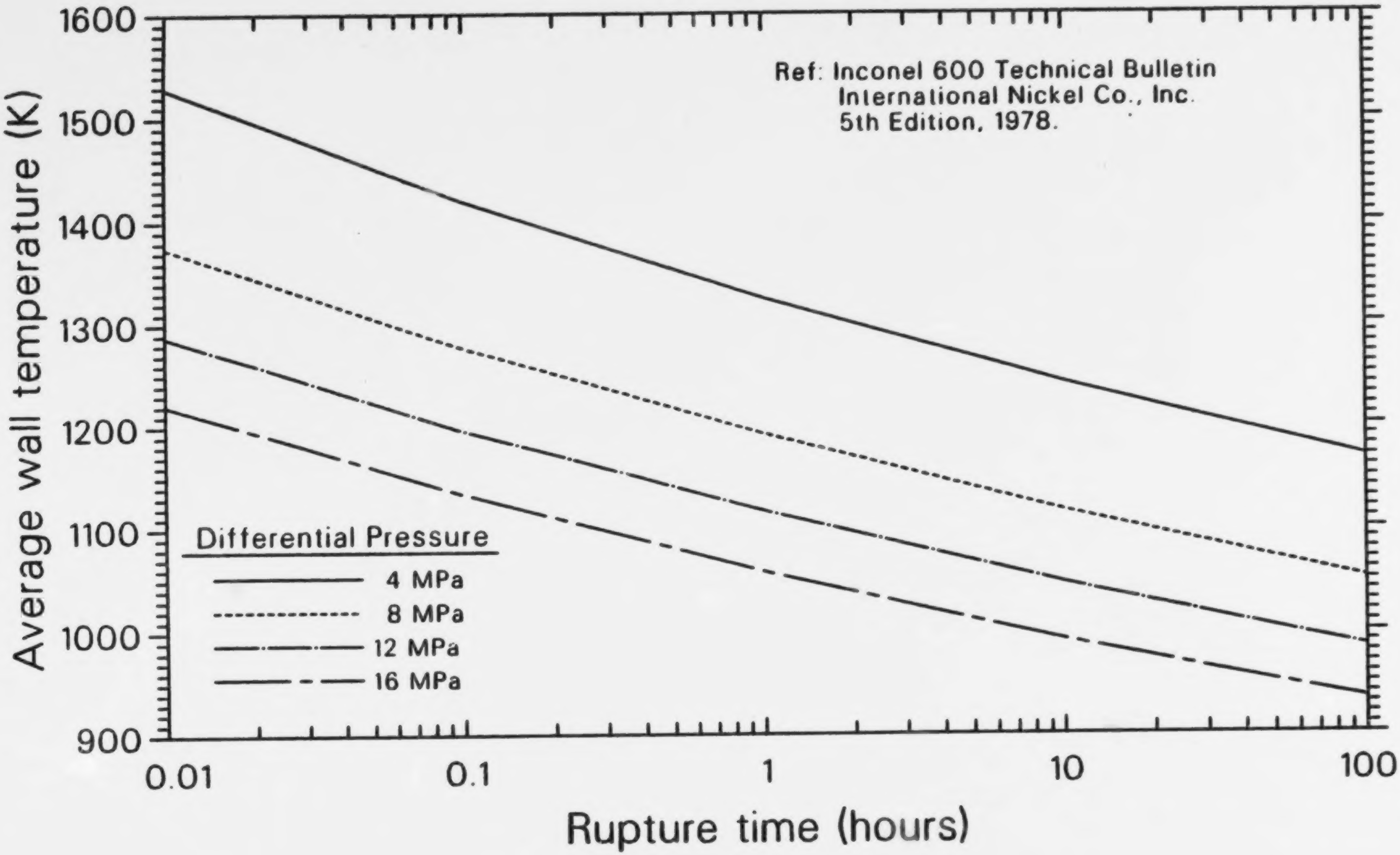

Ref: Inconel 600 Technical Bulletin
International Nickel Co., Inc.
5th Edition, 1978.

Figure 2.9 Average wall temperature versus rupture time for steam generator tube (Inconel 600) (Ref. 2.20).

26

Table 2.7 Estimated critical temperature above which structure may lose integrity within rupture time under high-pressure TMLB' accident conditions in Surry plant.*

RCS Pressure Boundary	Rupture Temperature	Rupture Time	Temperature with 1-hour Rupture Time
Vessel Hot Leg Nozzle (A-508, Class 2 carbon steel)	1,000 K (1,340°F)	20 minutes	980 K
Hot Leg Piping (316 stainless steel)	1,150 K (1,610°F)	6 minutes	990 K
Steam Generator Tubes (Inconel 600)	1,280 K (1,840°F)	6 minutes	1,170 K

*Pressure difference across the wall = PORV setpoint - outside pressure, where the outside pressure is the containment pressure for both hot leg nozzle and piping, and for steam generator tubes it is selected as the atmospheric dump valve setpoint at 1,050 psia (pressure difference = 9 MPa in Fig. 2.9).

using either the integrated MELPROG/TRAC code or the SCDAP/RELAP5 code are needed to proceed beyond 8600 s with in-vessel natural circulation modeled.

The MAAP calculation obtained by FAI for IDCOR (Ref. 2.32) as listed in Table 2.2, also predicts that some water will remain in the loop seal during the TMLB' accident with pump seal LOCA in Zion until the failure of vessel lower head at 3 h 40 min. However, the seal leakage specified in this MAAP calculation is much less than the value used in RELAP5. A seal leakage of 50 gpm is specified for each of four RCS pumps starting at t = 2700 s (45 min) until the seal is uncovered and the leak flow changes to gas.

These two calculations give us some idea regarding the status of loop seal during the TMLB' accident with pump seal LOCA. However, more studies are needed.

Experimental Results

Data on the RCS natural circulation are rather limited. A 1/7-linear-scale test facility is operated by Westinghouse under EPRI sponsorship (Refs. 2.26 and 2.27). The facility consists of a half cylindrical vessel with electrically heated rods in the simulated core and with upper-plenum structures above the core, a hot leg connecting to a simulated pressurizer and steam generator, and another hot leg connecting to a steam generator. It is designed to simulate one-half of a Westinghouse 4-loop plant such as Zion but without cold legs and pumps. Experiments were performed using water around 14.7 psia for flow visualization and also using sulfur hexafluoride (SF_6) at pressures up to 600 psia for simulating steam heat transfer. Figure 2.10 shows the simulated reactor vessel of the Westinghouse facility in which each fuel assembly is represented by a heated rod.

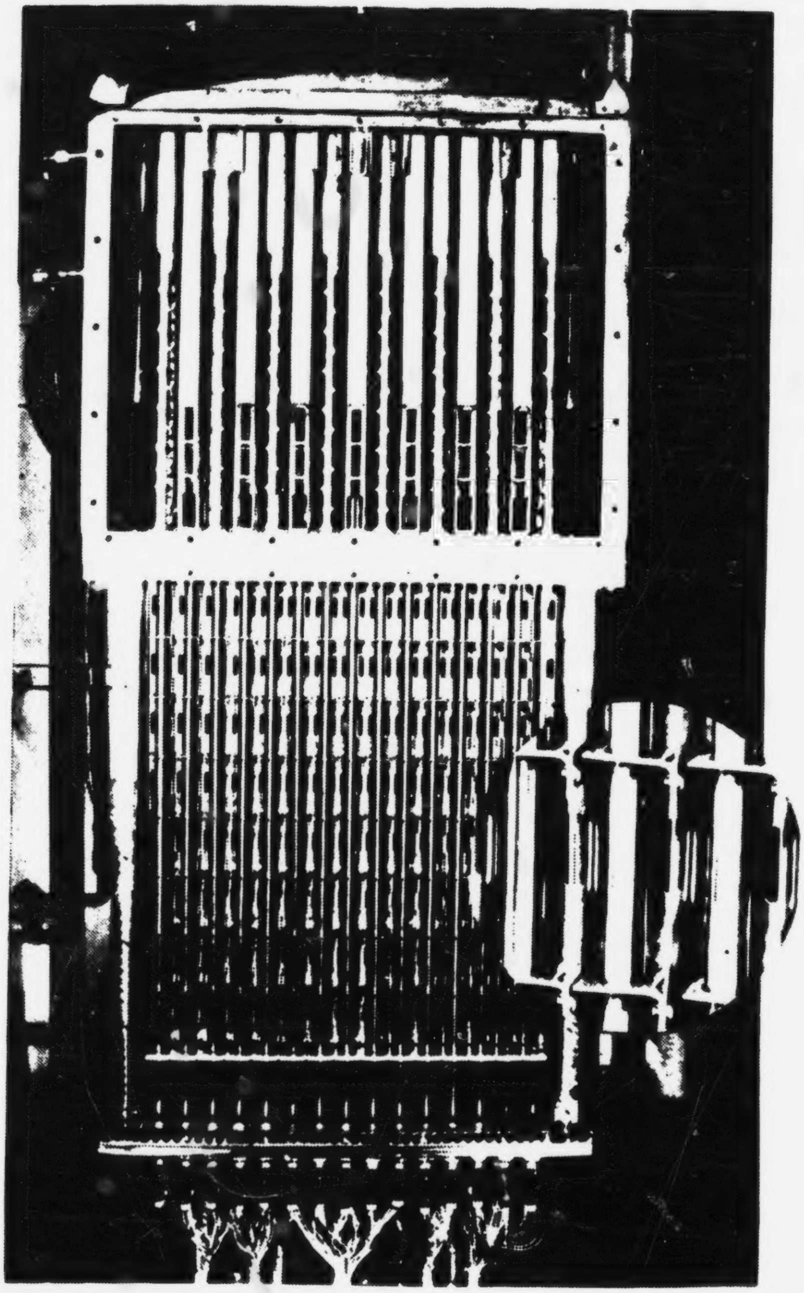

Figure 2.10 Front view of experimental reactor model. Inset shows core construction (Ref. 2.26).

Westinghouse experiments have provided some qualitative insight on natural circulation flow patterns that may exist in the vessel and in the hot leg and steam generator during the TMLB' accident. Figure 2.11 shows in-vessel natural circulation flow using SF_6 as coolant and with hot legs blocked. Figure 2.12 shows in-vessel natural circulation flow in water when coolant flow was allowed in both hot legs and steam generators. Flow patterns in these experiments are qualitatively similar to the MELPROG results as shown earlier in Figures 2.3 through 2.5. Flow visualization in water for countercurrent flow in the hot leg with or without PORV cycling was also obtained in the experiments. An important point is that the countercurrent flow indeed exists in the experiments in which relatively hot coolant flows in the upper section of the hot leg pipe toward the steam generator, while the lower section of the hot leg pipe is occupied by cooler coolant flowing in the reverse direction toward the vessel. Cross-sectional areas occupied by these two streams of flow are not constant and change along the hot leg. However, no figures are available at this time to be presented here. Figure 2.13 shows the preliminary temperature measurements inside steam generator tubes with water as the coolant. The vertical temperature gradient is evident in the hot leg pipe at the entrance to the steam generator (e.g., top point is at 37.9°C and is 8.9°C higher than the lowest point at 29°C); it should be pointed out that temperatures shown in a steam generator tube may also include measurements in other tubes at the same projected position as seen by a viewer looking at the steam generator (e.g., 4.6°C at tube number 39 in the second tube from the left is not in the same tube as for 28.7°C at tube number 47).

EPRI has also sponsored code calculations to support these experiments by using the COMMIX code at the Argonne National Laboratory (Ref. 2.39).

Analyses by EPRI and IDCOR

Basically, two computer codes have been used by the industry: the CORMLT code for EPRI analyses and the MAAP code for IDCOR analyses. Compared with the MELPROG code, CORMLT and MAAP are less mechanistic. For example, flow patterns for natural circulation in the vessel have to be provided to CORMLT and MAAP as user input, while MELPROG calculates flow patterns based on the fundamental laws of thermal hydraulics. Nevertheless, all these codes have provided insight to help us understand the very complex issue in which RCS natural circulation is coupled with core degradation and melt.

Figures 2.14 and 2.15 show respectively the CORMLT-calculated surface temperatures of the upper-plenum internals and the surge line connecting the pressurizer to a hot leg. The temperature beyond which the structure will lose its strength is estimated by EPRI to be 1,030 K (1,400°F), and 2.7 hours after the accident initiation the surge line has reached this temperature.

Figure 2.16 shows the MAAP-calculated reactor wall surface temperatures in the upper-plenum region. Two cases are compared: a base case where in-vessel natural circulation is modeled, and the case assuming once-through flow without accounting for circulation. By the time the vessel lower head fails at 3.65 hours, the inner surface of the vessel wall close to the hot leg nozzle has reached 910 K (1,180°F), but it not hot enough to fail the hot leg nozzle.

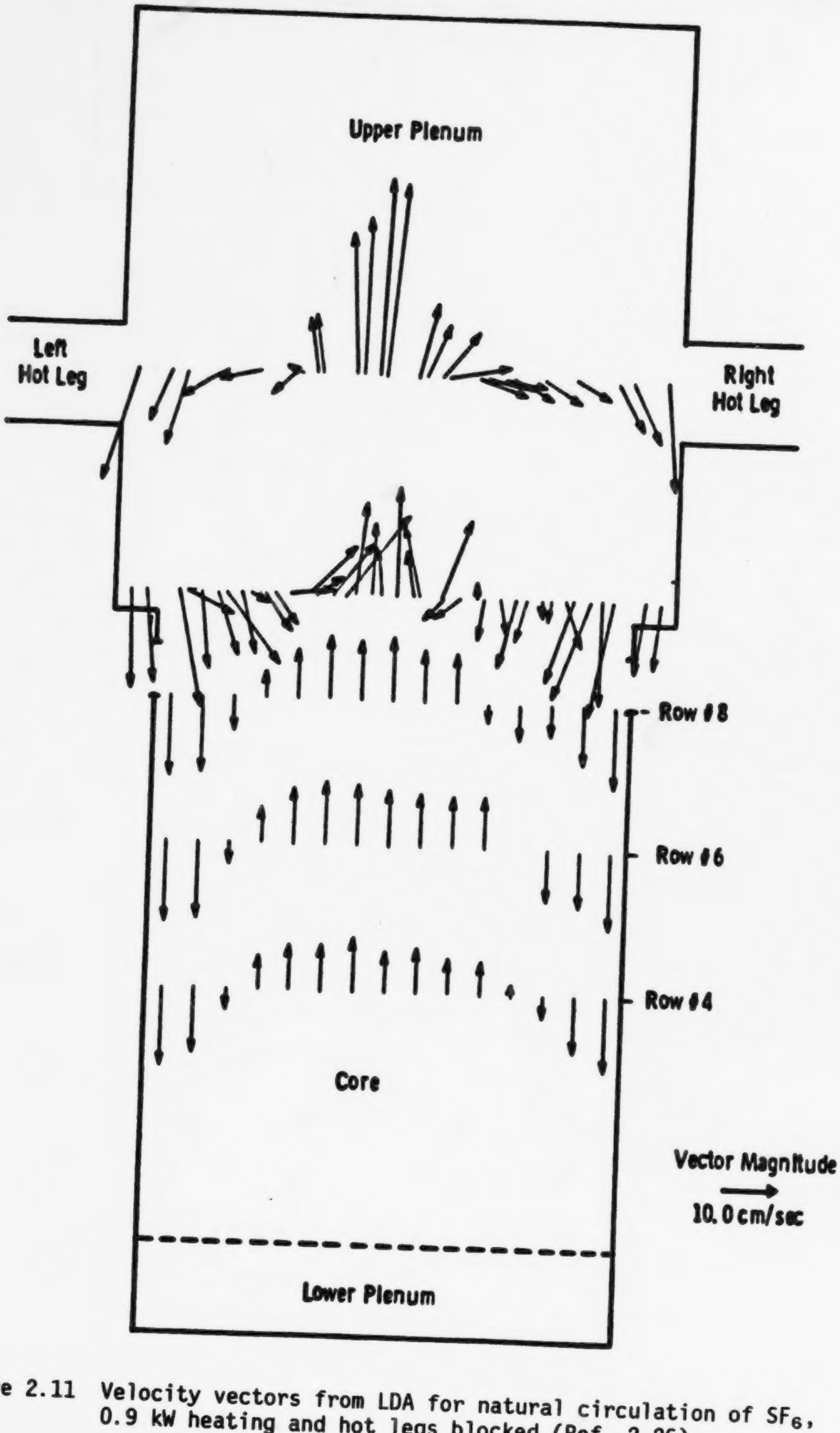
Upper Plenum
Left Hot Leg
Right Hot Leg
Row #8
Row #6
Row #4
Core
Vector Magnitude
10.0 cm/sec
Lower Plenum

Figure 2.11 Velocity vectors from LDA for natural circulation of SF_6, 0.9 kW heating and hot legs blocked (Ref. 2.26).

BEST COPY AVAILABLE

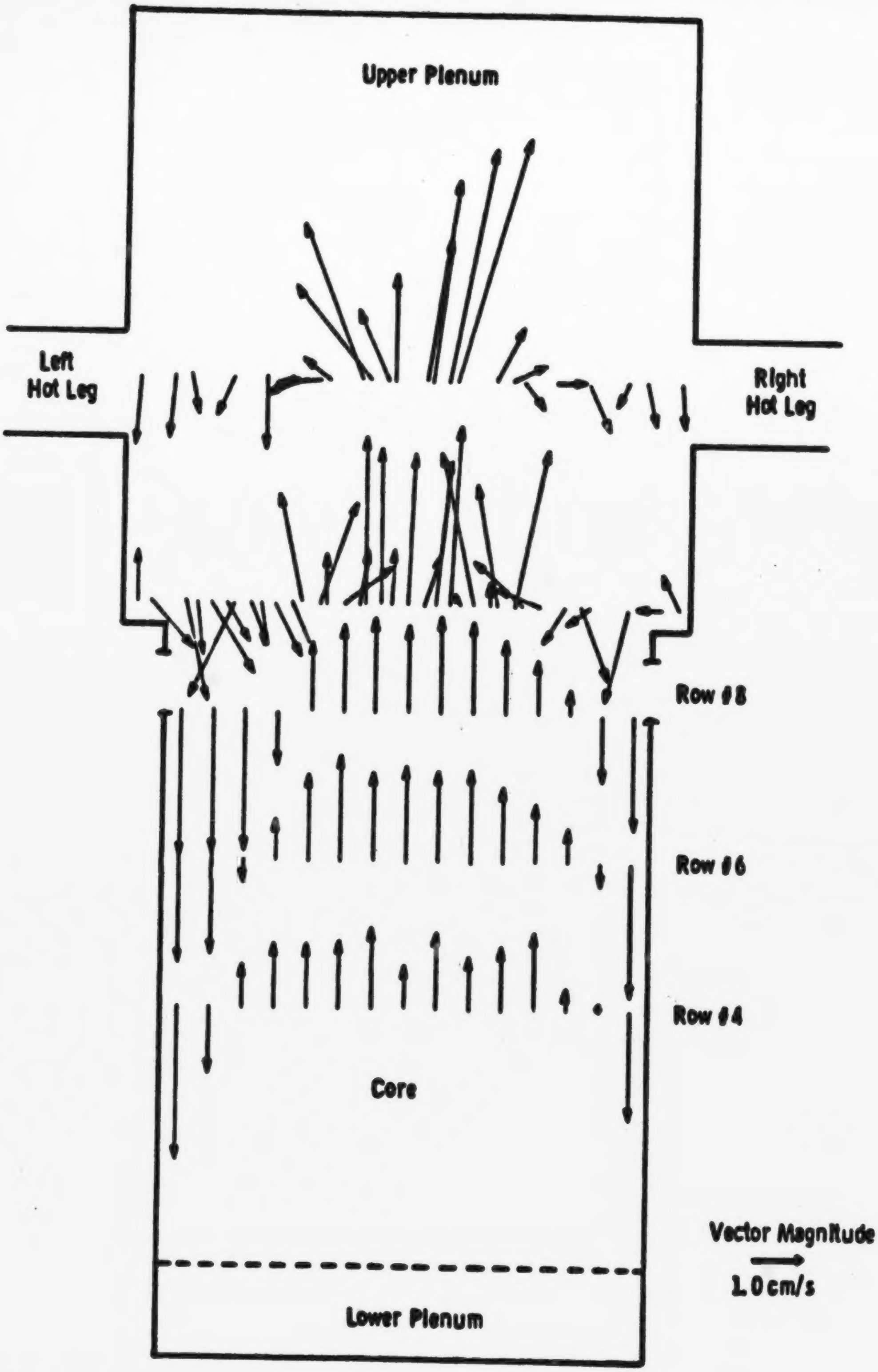
Upper Plenum
Left Hot Leg
Right Hot Leg
Row #8
Row #6
Row #4
Core
Vector Magnitude
1.0 cm/s
Lower Plenum

Figure 2.12 Velocity vectors from LDA for natural circulation of water, 28 kW, with steam generators cooling hot leg flows (Ref. 2.26).

BEST COPY AVAILABLE

31

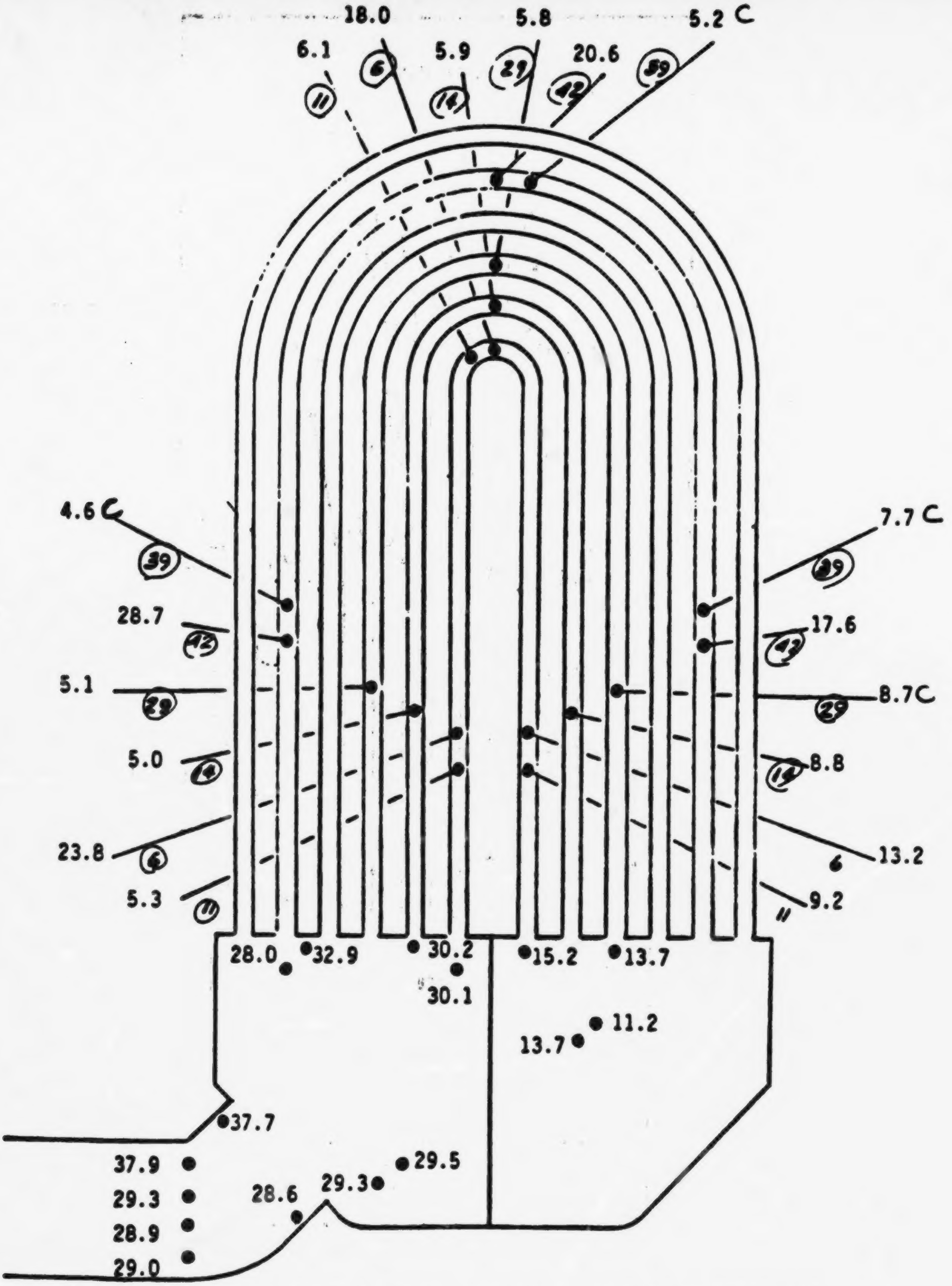
18.0
5.8
5.2 C
6.1
5.9
20.6
11
6
14
29
42
39
4.6 C
39
28.7
42
5.1
29
5.0
14
23.8
6
5.3
11
7.7 C
29
17.6
42
8.7C
29
8.8
14
13.2
6
9.2
11
28.0
32.9
30.2
30.1
15.2
13.7
11.2
13.7
37.7
37.9
29.3
28.9
29.0
28.6
29.3
29.5

Figure 2.13 Temperatures in steam generator model in °C test with water on February 7, 1985, tube number shown (Ref. 2.26). (Note that the circled number indicated steam generator tube number where the measurement was obtained.)

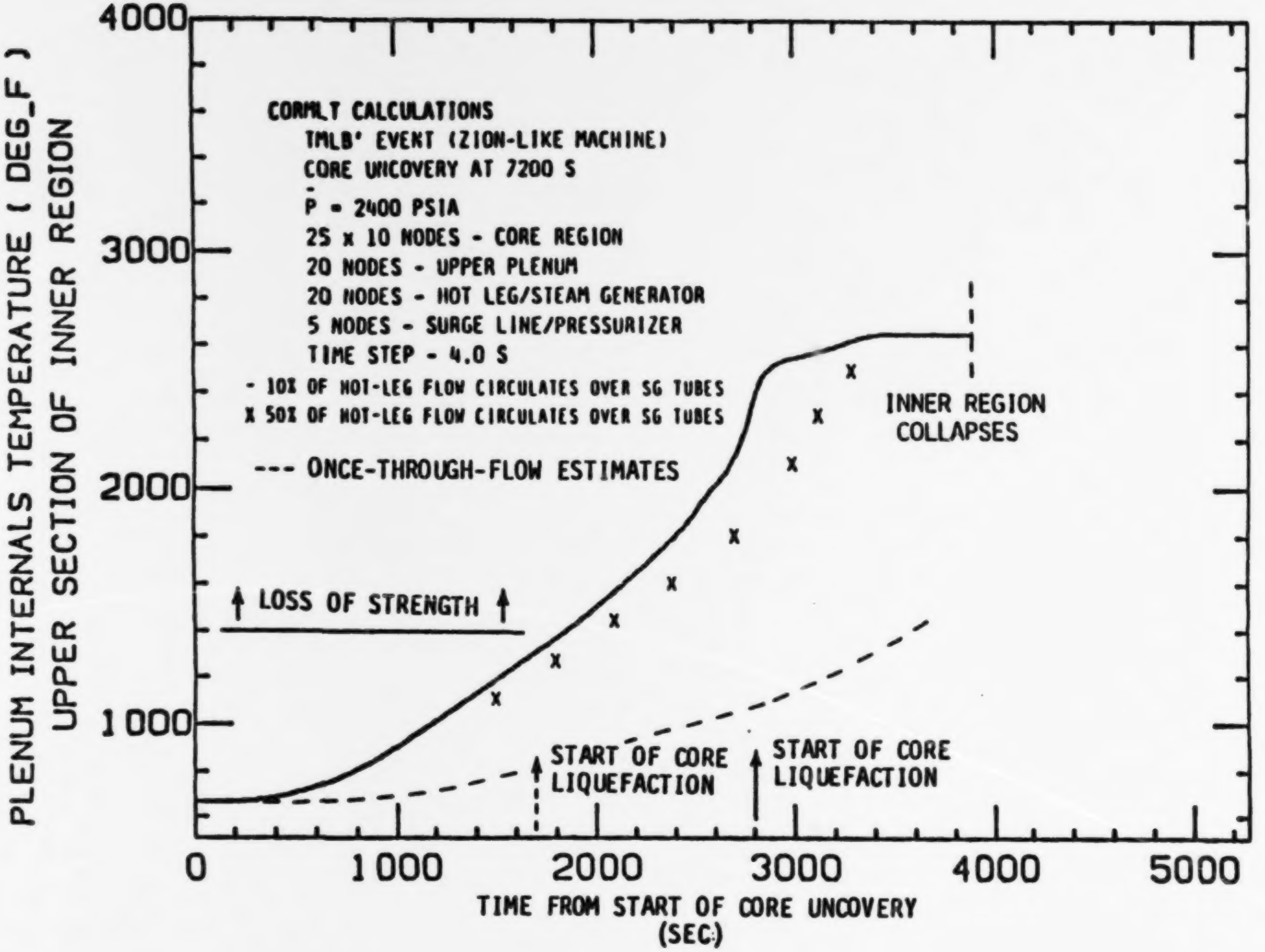

Figure 2.14 CORMLT-calculated upper-plenum internal surface temperature (Ref. 2.28).

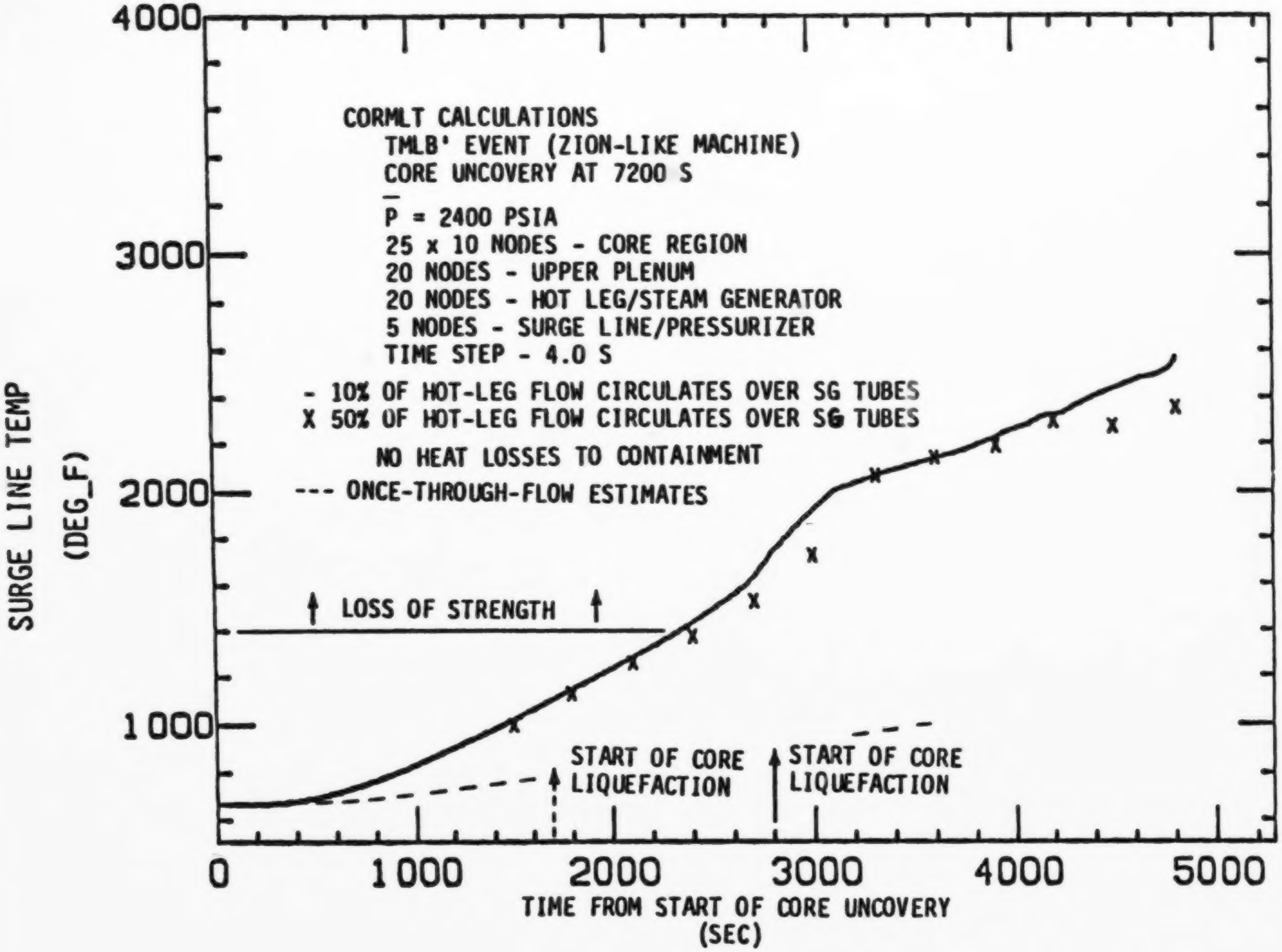

Figure 2.15 CORMLT-calculated inner surface temperature of surge line (Ref. 2.28).

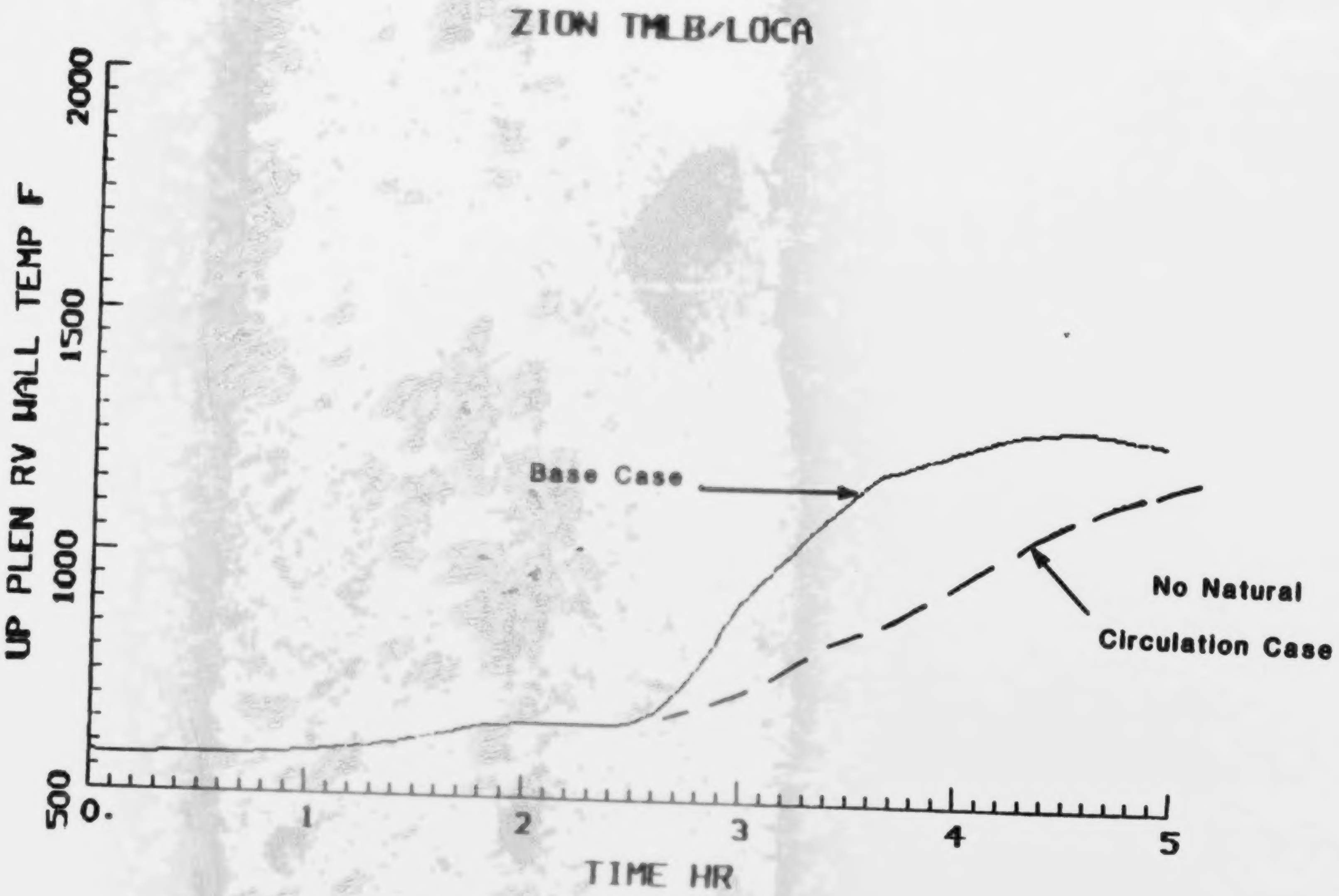

Figure 2.16 MAAP-calculated upper-plenum reactor vessel wall temperature for Zion TMLB' versus no natural circulation case (Ref. 2.32).

2.3.3 Staff Technical Position

Based on the existing but rather limited studies, the staff has reached the following conclusions:

1. During the high-pressure TMLB' accident in the Surry plant, the vessel hot leg nozzle or the weld adjacent to it or the surge line may fail before the failure of vessel lower head. As a result, the RCS may be depressurized to a low pressure (less than 200 psig) before vessel lower head failure. A value of 0.7 is selected for the likelihood of this event.
2. A value of 0.3 is selected as the likelihood for high-pressure (above 200 psia) melt ejection to the containment that may lead to direct heating of the containment.
3. Size of the induced break of the RCS is also of importance in evaluating the outcome of the high-pressure sequence.
4. RCS natural circulation is likely to increase the hydrogen generation in the vessel as compared with one-dimensional calculation, but not significantly.
5. Further analytical and experimental studies are needed to increase our understanding of the issue and to give the staff more solid evidence in supporting the NRC position. Recommended future work will be discussed in Section 2.4.

2.4 Future Work

Additional analytical and experimental studies are needed to provide sufficient evidence for the staff to resolve the issue. The following are staff recommendations for future work in priority order. Note that funding does not exist for some of the work.

1. Completion of a MELPROG/TRAC calculation modeling the vessel, the hot legs, the pressurizer, and the steam generators. Important phenomena such as fission product transport and deposition, fission product decay heating on the structure surface, and potential hydrogen generation due to steam-steel reaction in the upper plenum should be included. The calculation is expected to be completed by July 1987.
2. As a comparison check of the MELPROG/TRAC calculation above, completion of the SCDAP/RELAP5 calculation and sensitivity study up to core slump by July 1987. (Note that the hot leg and surge line could become very hot before core slump and the code has been validated against severe fuel damage experiments in the Power Burst Facility and LOFT.)
3. Completion of a MELPROG/TRAC calculation similar to the one above but either with small pump seal LOCA or with stuck-open PORV.
4. Sensitivity studies by varying some important parameters in these codes (e.g., relocation temperature of molten cladding of fuel rods).

5. Completion of a structural integrity analysis for the weld between the hot leg nozzle and piping, the surge line, and instrumentation penetrations on the hot leg.

6. Estimation of the size of induced break due to creep rupture.

7. Validation of the MELPROG/TRAC code against Westinghouse 1/7-scale natural circulation data.

8. Completion of detailed flow pattern calculations using the COMMIX code, in supporting Items 1 and 2 above.

9. Experiments from other test facilities may be needed.

REFERENCES FOR CHAPTER 2

2.1 U.S. Nuclear Regulatory Commission (USNRC), "Reactor Safety Study--An Assessment of Accident Risks in U.S. Commercial Nuclear Power Plants," WASH-1400 (NUREG-75/014), October 1975.

2.2 J. A. Gieseke et al., "Radionuclide Release Under Specific LWR Accident Conditions: PWR-Large, Dry Containment Design (Surry Plant Recalculations)," Battelle Columbus Laboratories, BMI-2104, Vol. V, Draft, July 1984.

2.3 R. S. Denning et al., "Radionuclide Release Calculations for Selected Severe Accident Scenarios: PWR, Subatmospheric Containment Design," Battelle Columbus Laboratories, NUREG/CR-4624, Vol. 3, BMI-2139, July 1986.

2.4 W. L. Lyon, NRC, memorandum to Distribution, "Meeting: RCS Pressure Boundary Heating During Severe Accidents," dated May 4, 1984.*

2.5 R. M. Bernero, NRR, memorandum to D. F. Ross, RES, Subject: Need for Multidimensional Modeling of RCS Behavior in Support of Severe Accident Investigations, dated August 30, 1984.*

2.6 D. F. Ross, RES, memorandum to R. M. Bernero, NRR, Subject: RES Response to NRR Need For Multidimensional Modeling of RCS Behavior Under Severe Accident Conditions, dated February 11, 1985.*

2.7 M. Silberberg et al., "Reassessment of the Technical Bases for Estimating Source Terms," NUREG-0956, July 1986.

2.8 M. Rogovin et al., "Three Mile Island--A Report to the Commission and to the Public," NUREG/CR-1250, Vols. 1 and 2, Parts 1, 2, and 3, January 1980.

2.9 T. T. Martin, "NRC Report on the January 25, 1982 Steam Generator Tube Rupture at R. E. Ginna Nuclear Power Plant," NUREG-0909, April 1982.

2.10 USNRC, "Loss of Main and Auxiliary Feedwater Event at the Davis-Besse Plant on June 9, 1985," NUREG-1154, July 1985.

2.11 L. Marsh and C. Liang, "Evaluation of the Need for a Rapid Depressurization Capability for Combustion Engineering Plants," NUREG-1044, December 1984.

2.12 J. T. Han, RES, memorandum to M. Silberberg, RES, Subject: A Summary of March 17, 1986 Meeting on RCS Natural Circulation Studies, dated May 1, 1986.*

2.13 J. E. Kelly, SNL, letter to J. T. Han, USNRC, "Comments from the MELPROG Staff on Natural Circulation Issue Paper," dated January 24, 1986.*

---

*Available in the NRC Public Document Room, 1717 H Street NW., Washington, DC.

2.14 C. M. Allison, INEL, letter to J. T. Han, USNRC, "Comments from the SCDAP Staff on Natural Circulation Issue Paper," dated February 13, 1986.*

2.15 J. E. Kelly, R. J. Henninger, and J. F. Dearing, "MELPROG-PWR/MOD1 Analysis of a TMLB' Accident Sequence," Sandia National Laboratories, NUREG/CR-4742, SAND86-2175, January 1987.

2.16 R. J. Henninger, J. E. Kelly, and J. F. Dearing, "Preliminary 2-D MELPROG Calculation for the TMLB' Accident in Surry," presented at the March 17, 1986 Meeting on RCS Natural Circulation Studies, Bethesda, MD.*

2.17 J. F. Dearing, "Flow-Pattern Results for a TMLB' Accident Sequence in the Surry Plant Using MELPROG," Los Alamos Scientific Laboratory, LA-UR-85-3668, November 1985.

2.18 M. J. Thurgood, T. E. Guidotti, and C. L. Wheeler, "COBRA-NC Analysis of a Station Blackout Transient (TMLB') for the Surry Plant," Draft Report FATE-85-103, PNL, March 1985.

2.19 V. N. Shah, "Structural Failure Studies of RCS," presented at the April 23, 1986 Meeting on Direct Containment Heating, Bethesda, MD.*

2.20 B. L. Harris, V. N. Shah, and G. E. Korth, "Creep Rupture of Three Components of the Reactor Primary Coolant System During the TMLB' Accident," Idaho National Engineering Laboratory, EGG-EA-7431, November 1986.

2.21 G. A. Berna, INEL, letter to J. T. Han, USNRC, "Failure of Hot Leg Nozzle During A PWR TMLB'," dated February 10, 1986.*

2.22 H. M. Domanus et al., "COMMIX PWR Calculations for Postulated TMLB' Accident," presented by W. T. Sha to the NRC staff on August 21, 1986, Rockville, MD.*

2.23 V. L. Shah, "COMMIX Application in TMLB' Accident Scenario Simulation," presented at the March 17, 1986 Meeting on RCS Natural Circulation Studies, Bethesda, MD.*

2.24 H. P. Nourbakhsh, C. H. Lee, and T. G. Theofanous, "Natural Circulation Phenomena and Primary System Failure in Station Blackout Accidents," Proceedings of Sixth Information Exchange Meeting on Debris Coolability, University of California at Los Angeles, pp. 24-1 through 24-10, November 1984.

2.25 USNRC, "Estimates of Early Containment Loads from Core Melt Accidents," NUREG-1079, Draft Report for Comment, December 1985.

2.26 W. A. Stewart, "Determine the Flow Patterns and Velocities in a PWR System During a Postulated Severe Accident," presented at the NRC/EPRI Meeting (Pittsburgh, PA), April 4, 1985.*

---

*Available in the NRC Public Document Room, 1717 H Street NW., Washington, DC.

2.27 W. A. Stewart, A. T. Pieczynski, and V. Srinivas, "Experiments on Natural Circulation Flow in a Scale Model PWR Reactor System During Postulated Degraded Core Accidents," Proceedings of Third International Topical Meeting on Reactor Thermal Hydraulics (Newport, RI), American Nuclear Society, Vol. I, p. 10.C-1, October 1985.

2.28 B. R. Sehgal, "Natural Convection/Relation to Containment Heat-Up Issue," presented at April 23, 1986 Meeting on Direct Containment Heating, Bethesda, MD.*

2.29 B. R. Sehgal et al., "Effects of Natural Convection Flows on PWR High Pressure Severe Accidents," Proceedings of a Symposium on Source Term Evaluation for Accident Conditions (Columbus, OH), International Atomic Energy Agency, STI/PUB/700, p. 293, March 1986.

2.30 B. R. Sehgal et al., "Effects of Natural Convection Flows on PWR System Temperatures During Severe Accidents," Proceedings of 23rd ASME/AICHE/ANS National Heat Transfer Conference (Denver, CO), American Nuclear Society, August 1985.

2.31 V. E. Denny and B. R. Sehgal, "PWR Primary System Temperature During Postulated Severe Accidents," Trans. ANS, Vol. 47, pp. 317-319, November 1984.

2.32 Fauske and Associates, Inc., "IDCOR Technical Report 85.2: Technical Support for Issue Resolution," Atomic Industrial Forum, pp. 3-1 to 3-64, July 1985.

2.33 P. D. Bayless, "Analysis of a Station Blackout Transient with Reactor Coolant Pump Seal Leakage for the Seabrook Nuclear Plant," EG&G Idaho Letter Report, June 6, 1985.*

2.34 Nuclear Safety Analysis Center, "Analysis of Three Mile Island-Unit 2 Accident," NSAC-1, July 1979.

2.35 K. Vinjamuri, D. W. Akers, and R. R. Hobbins, "Examination of H8 and B8 Leadscrews from Three Mile Island Unit 2 (TMI-2)," EG&G Idaho, Inc., GEND-INF052, September 1985.

2.36 C. M. Allison, INEL, letter to J. T. Han, USNRC "Comments on In-Vessel Hydrogen Generation and Case Melt Progression," dated July 24, 1986.*

2.37 R. J. Dallman, "TMI-2 Natural Circulation Study," EG&G Idaho Inter-office Correspondence, dated September 27, 1985.*

2.38 USNRC, "Estimates of Early Containment Loads from Core Melt Accidents," NUREG-1079, Draft Report for Comment, pp. 8-1, 9-1, 9-2, A-1, and A-13, December 1985.

2.39 B. C-J Chen et al., "Degraded Core Study Using the Multidimensional COMMIX Code," Trans. ANS, Vol. 49, pp. 453-454, June 1985.

2.40 Private Communications with J. Jackson and R. Riggs of NRR, "Generic Issue 23 - Reactor Coolant Pump Seal Failures," July 28-29, 1986.*

---

*Available in the NRC Public Document Room, 1717 H Street NW., Washington, DC.

40

3. IN-VESSEL CORE MELT PROGRESSION AND HYDROGEN GENERATION

R. W. Wright

3.1 Introduction

3.1.1 Core Melt Progression

In-vessel core melt progression concerns the state of the reactor core from the start of core uncovery to reactor vessel failure. Included are the thermal attack by the core debris upon the reactor structure and the reactor vessel and in-vessel hydrogen generation. Related phenomena are in-vessel natural convection and heat transfer, in-vessel fission product and aerosol transport, and explosive and nonexplosive in-vessel rapid steam generation. The significant output information from core melt progression includes hydrogen generation and its time dependence; the mode of vessel failure; and the state of the core debris at the time of vessel failure, including the debris mass, the debris temperature, spatial, and composition distributions, and the melt distribution within the debris.

The state of the core during in-vessel core melt progression is a primary determinant of in-vessel hydrogen generation, in-vessel fission product and aerosol release, and much of the fission product and aerosol transport (and retention) in the reactor coolant system. These processes occur throughout the development of core melt progression up to vessel failure, so information on the state of the core as a function of time is needed. This time-dependent information is also needed to evaluate the threat to the reactor vessel and the containment from an in-vessel steam explosion, the thermal attack of the core debris upon the core-support structure and the vessel lower head, the time and mode of vessel failure, and the characteristics of the core debris released into the reactor cavity at vessel failure.

Recently attention has been focused on in-vessel natural circulation and heat transfer and the resultant effects on in-vessel core melt progression and other severe accident behavior. There is some indication that wall heating from in-vessel natural circulation may cause early failure of the primary system boundary and reactor coolant system depressurization before meltthrough of the vessel in high-pressure sequences like the TMLB' station blackout. This might prevent high-pressure melt ejection (direct containment heating) at vessel meltthrough in high-pressure sequences, depending in part on the effect of the release of accumulator water upon system depressurization.

3.1.2 Hydrogen Generation

During a core uncovery accident, hydrogen is generated by high-temperature steam oxidation of the core Zircaloy, of the reactor vessel steel, and, even to a lesser extent, of the UO_2 fuel itself. Of interest are the total amount and the rate of hydrogen generated during the in-vessel core melt progression sequence. At steam boiloff velocities, significant oxidation starts at about 1,500 K, limited by parabolic-rate-law oxygen diffusion through the accumulating ZrO_2 layer, and rapid autocatalytic oxidation starts at about 1,700 K (Ref. 3.1).

41

The rapid local temperature rise (of the order of 10 K per second) is limited by steam starvation and by relocation of molten cladding material into lower, colder regions of the core. In-vessel natural circulation would decrease the effect of the steam-starvation limitation. A previously hypothesized "hydrogen blanketing" rate limitation from steam diffusion through a hydrogen surface boundary layer has been found not to be operative under reactor accident conditions (Ref. 3.2).

A major issue and difference between NRC and the Industry Degraded Core Rulemaking (IDCOR) analyses has been the IDCOR assumption that blockages form at the onset of cladding melting. IDCOR assumes that such blockages block steam flow in intact individual BWR subassemblies to permanently cut off hydrogen generation and that blockages divert steam flow in PWRs to substantially reduce the hydrogen generation (Ref. 3.3). This position has not been accepted by NRC, and a significant difference exists between the IDCOR and NRC staffs on hydrogen generation. In the severe fuel damage tests in the Power Burst Facility (PBF) test reactor, substantial partial blockages were formed by the relocated molten unoxidized metallic Zircaloy (and dissolved UO_2), but neither complete blockage nor significant flow interference occurred. (Refs. 3.1 and 3.4 through 3.6). Most of the hydrogen generation in these tests occurred after the onset of Zircaloy relocation (Ref. 3.7). In the recent FLHT-4 test in the National Reactor Universal (NRU) at Chalk River, Canada, hydrogen generation continued throughout a 30-minute high-temperature hold during which there was no steam blockage from Zircaloy relocation.

3.1.3 Characteristics of Core Debris at Vessel Failure and Mode of Vessel Failure

The information on the characteristics of the core debris at vessel failure and on the mode of that failure provides the initial conditions for analysis of the ex-vessel core melt loads to the containment, including core melt-concrete interactions and high-pressure melt ejection. Significant are the debris mass; the distributions of temperature, melt fraction, and material composition; and the mode of debris ejection into the reactor cavity that is itself highly dependent upon the mode of vessel failure. In the nonmechanistic MARCH module of the Source Term Code Package, these are input parameters. For the analyses reported in BMI-2104, it is assumed that 100 percent of the core is deposited in the reactor cavity when 75 percent of the core has reached an assumed $Zr-UO_2$ "liquidus" temperature of 2,550 K, to cite the numbers used in BMI-2104 (Refs. 3.8 and 3.9). Somewhat different treatment has been given to in-vessel core melt progression in analyses with the industry MAAP and CORMLT codes (Refs. 3.10 and 3.11). The most comprehensive analysis, however, is contained in the new NRC mechanistic MELPROG code (Ref. 3.12). Currently, there are only limited data available for validation of the more mechanistic codes, particularly for the later stages of core melt progression. More data will be forthcoming from the severe accident research program.

3.2 Past Research Results and Current Technical Uncertainties

3.2.1 Core Melt Progression Phenomenology

The general in-vessel accident sequence and core-melt-progression phenomenology in a PWR severe accident as determined by past research are given below. Starting with an initially intact core and reactor vessel, the initiating event is a break in the coolant system or loss of heat removal capability, both with reactor scram. In either case, coolant loss from the system occurs. As the coolant level drops below the top of the core, the fission product decay heat generated in the fuel rods and the degraded cooling cause the core to heat up. During the heatup stage, natural circulation in the uncovered part of the core and in the upper-plenum region may transfer a significant fraction of the heat from the core to the upper-plenum structure and to the primary system pressure boundary. During the later stages of core heatup, radiation becomes important and ultimately becomes a a dominant heat transfer mechanism. As the temperature increases above about 1,500 K, oxidation of the Zircaloy cladding by steam becomes important. This reaction is exothermic, providing additional heating of the fuel rods, and it also generates hydrogen. As the temperature increases, the rate of oxidation increases rapidly. As the temperature passes about 1,700 K, rapid autocatalytic oxidation occurs, except where limited locally in the core by conversion of all the steam into hydrogen, a process called "steam starvation." A "burn front" may develop in the upper regions of the core at the steam-starvation boundary and may move downward as autocatalytic oxidation progresses. Except during high-pressure sequences, internal fission gas and fill gas in the fuel may balloon the cladding away from the fuel as the heatup proceeds. This significantly reduces the clad-fuel heat transfer and can increase the rate of cladding oxidation and hydrogen generation. Experiments have shown that cladding ballooning does not block the steam flow, but it might significantly divert steam flow in the open-lattice PWR core and might reduce natural circulation flow through the core (Ref. 3.13). Rates of fuel temperature that increase by tens of degrees Kelvin per second can occur during the autocatalytic oxidation of the fuel rod cladding, and much of the hydrogen generation in the accident occurs during this initial transient. Heat is transported during core heatup to the reactor vessel structure and walls by natural circulation and by radiation heat transfer, reducing the rate of core heatup.

Under core-uncovery accident conditions, significant hydrogen generation from steam oxidation of the Zircaloy cladding starts at about 1,500 K, and the temperature transients from rapid autocatalytic oxidation start at about 1,700 K. The oxidation transient is rate limited by the diffusion of oxygen through the ZrO_2 surface sheath that builds up on the surface of the Zircaloy cladding, and it may also be limited by steam starvation. The rate limitation from oxygen diffusion through the growing oxide layer gives parabolic rate kinetics. This is used for the earlier intact-geometry Zircaloy oxidation and hydrogen generation in the MARCH and MAAP codes, as well as in the more mechanistic MELPROG and SCDAP codes. The best data on the parabolic rate constants come from the newer experiments by Prater and Courtright at Pacific Northwest Laboratories, and these rate constants are used in MELPROG and in the mechanistic SCDAP fuel damage code (Ref. 3.14). MARCH and MAAP use rate constants from the older data of Cathcart below the ZrO_2 tetragonal-to-cubic phase transition at 1,800 K, and of Baker and Just above it (MAAP), or rate constants from the data of Urbanic and Heidrick (MARCH) (Refs. 3.15 through 3.17). The Urbanic and Heidrick data are suspect, but use of these data or the Cathcart and the Baker-Just rate constants rather than the newer Prater ones does not significantly affect the overall hydrogen generation.

On the basis of earlier experiments by Chung and Thomas, a hydrogen-blanketing model was developed for an hypothesized gas-phase rate limitation by oxygen diffusion through a surface boundary layer of hydrogen (Ref. 3.18). (This is different from the real steam-starvation cutoff to oxidation that occurs when the

43

entire incoming steam flow has been converted into hydrogen.) Recent experimental work by Prater has shown that, under LWR core-uncovery accident conditions, such a rate limitation from gas-phase hydrogen-blanketing is negligible in comparison with the solid-phase rate limitation from oxygen diffusion through the ZrO_2 layer (Ref. 3.2). The hydrogen-blanketing models have now been removed from MELPROG and SCDAP to simplify the codes. These models are included as an option in MARCH, but because they are used in series with the rate limitation from oxygen diffusion through the ZrO_2 surface layer on the cladding, which is governing, the impact of using the hydrogen-blanketing option is negligible.

The uncertainties in hydrogen generation become large with the onset of Zircaloy melting, relocation and fuel dissolution, and the loss of the initial intact and well-characterized core geometry. There are significant uncertainties involving (1) the effects of the relocation of the molten unoxidized metallic Zircaloy accompanied by the dissolution (liquefaction) of some of the UO_2 fuel; (2) the surface area available for further oxidation of the relocated Zircaloy and questions about the presence of oxidation-limiting ZrO_2 films on the surface of the relocating molten cladding; (3) questions of steam flow blockage (BWR) or diversion (PWR) by the relocated material; and (4) hydrogen generation following slumping of the molten core debris into the water in the lower plenum. As indicated previously, these effects are treated in MARCH and in the original version of MAAP as input parameters, with the relocation of all the material, including the Zircaloy, occurring as a single, assumed core slump. (A later version of MAAP has a separate Zircaloy relocation model.) MAAP puts strong emphasis on steam flow blockage (BWR) and flow diversion in the open-lattice PWR core to significantly reduce hydrogen generation. MARCH has a user option for high-surface-area oxidation of the unoxidized molten Zircaloy following core slump into the lower-plenum water that, based on the QUEST uncertainty study, could increase the total hydrogen generation by about 40 percent (Ref. 3.19). The Zircaloy relocation and continued oxidation are mechanistically modeled in SCDAP and MELPROG, and hydrogen and steam generation following core slump are being modeled mechanistically in MELPROG. There are few data currently available to support this mechanistic modeling, however.

During the heatup process, the first failures in the core typically occur in the control rods. For PWR silver-indium-cadmium control rods, failure occurs near the 1,700 K melting point of the stainless steel control rod cladding. The cadmium rapidly vaporizes at rod failure and condenses into an aerosol when cooled outside the core. The molten silver and indium relocate downward with no interaction with the stainless steel control rod cladding and little interaction with the Zircaloy control rod guide tubes, eventually to freeze in the colder regions of the core. If it falls into the water, this relocated hot control rod material can cause significant additional steam generation and may temporarily overcome steam starvation. There is, however, a strong interaction of Zircaloy with stainless steel and with Inconel (rod spacer grids), with eutectics at about 1,500 K. The Al_2O_3 in Zircaloy-clad B_4C-Al_2O_3 burnable poison rods forms eutectics with Zircaloy at 1,750 K and with both ZrO_2 and UO_2 at about 2,200 K. There are indications from recent work at KfK that these strong interactions may open flow paths through the degrading core. There are indications that this may have happened in the TMI-2 accident. In BWRs, the stainless steel clad cruciform B_4C control blades between the Zircaloy fuel assembly channel-box walls fail at lower temperatures than the Zircaloy fuel cladding. There are recent indications from KfK that a eutectic alloy forms between B_4C and stainless steel that liquefies the cladding and may fail the

BWR control blades at temperatures as low as 1,500 K, with subsequent relocation and possible blockage formation by the liquefied material. It has also been found that the B_4C-stainless-steel alloy can liquefy the Zircaloy channel box and that it can also inhibit steam oxidation of the boron.

The fuel rods normally fail when molten unoxidized metallic Zircaloy fails the ZrO_2 surface sheath that oxidation is producing on the cladding. The molten metallic Zircaloy then relocates downward along the individual rods in a "candling" process. This process removes the supply of metallic Zircaloy for oxidation from the high-temperature region of the core where oxidation can occur, effectively limiting the rapid temperature rise and the rapid hydrogen generation from autocatalytic oxidation of the initially intact fuel rods. This limitation is represented nonmechanistically in the current mechanistic accident analysis codes as a temperature threshold for relocation downward of the molten unoxidized Zircaloy in a given axial node. The relocation of the molten unoxidized metallic Zircaloy is the first of three significant and distinct material relocation processes that occur during in-vessel core melt progression. In the simplified MARCH code, these three separate and distinct processes, which actually occur at different times and at different temperatures, are lumped into a single assumed "core slump" (Ref. 3.8). This assumption significantly affects the MARCH results, particularly with regard to hydrogen generation.

Near its 2,100 K melting point, molten metallic zirconium can dissolve up to 10 percent of its mass of solid UO_2 in a liquefaction process and up to 20 mass percent as the temperature increases to the 2,700 K liquid monotectic point, at which temperature this fraction increases to over 80 percent (Fig. 3.1) (Ref. 3.20). It has been observed (PBF, ACRR, KfK, TMI-2) that the material that relocates downward following Zircaloy melting and fuel rod failure is this UO_2-containing molten Zircaloy, which has been called liquefied fuel. This material relocates downward and freezes on colder portions of the fuel rods and the rod spacer grids. As water boils off and core melt progression proceeds, this solidified material may remelt and relocate downward again in a repetitive process. Only the initial stages of this process were observed in the Power Burst Facility (PBF) and Annular Core Research Reactor (ACRR) in-pile tests and in Hagen's out-of-pile tests at KfK, but it is known to have occurred in the TMI-2 accident and to have formed the tough "hard pan" across the mid-region of the core (Refs. 3.1, 3.4 through 3.6, and 3.21 through 3.23).

An important question is the extent to which blockages are formed by this relocated material and whether they significantly affect the boiloff steam flow and further Zircaloy oxidation and hydrogen generation. IDCOR has maintained that such blockages will form and that they will cut off (BWR) or significantly reduce (PWR) further oxidation and hydrogen generation (Ref. 3.3). The Zircaloy melting point was taken by IDCOR in the original modeling in the MAAP code as the threshold for the formation of those blockages and as a permanent cutoff or significant reduction of further oxidation heating and hydrogen generation (Ref. 3.10). This MAAP modeling was modified in later IDCOR analyses with a molten Zircaloy relocation model that gave similar results on blockage formation (Ref. 3.3). The question of blockage formation is a major area of disagreement between NRC and IDCOR, and differences of over a factor of two exist in the assessment of hydrogen generation between NRC and IDCOR (Refs. 3.3 and 3.9). There is strong experimental evidence from the PBF and the NRU tests, which are effectively in the intact BWR channel-box geometry, that the hypothesized temperature cutoff of oxidation heating and hydrogen generation upon Zircaloy melting and fuel failure is not

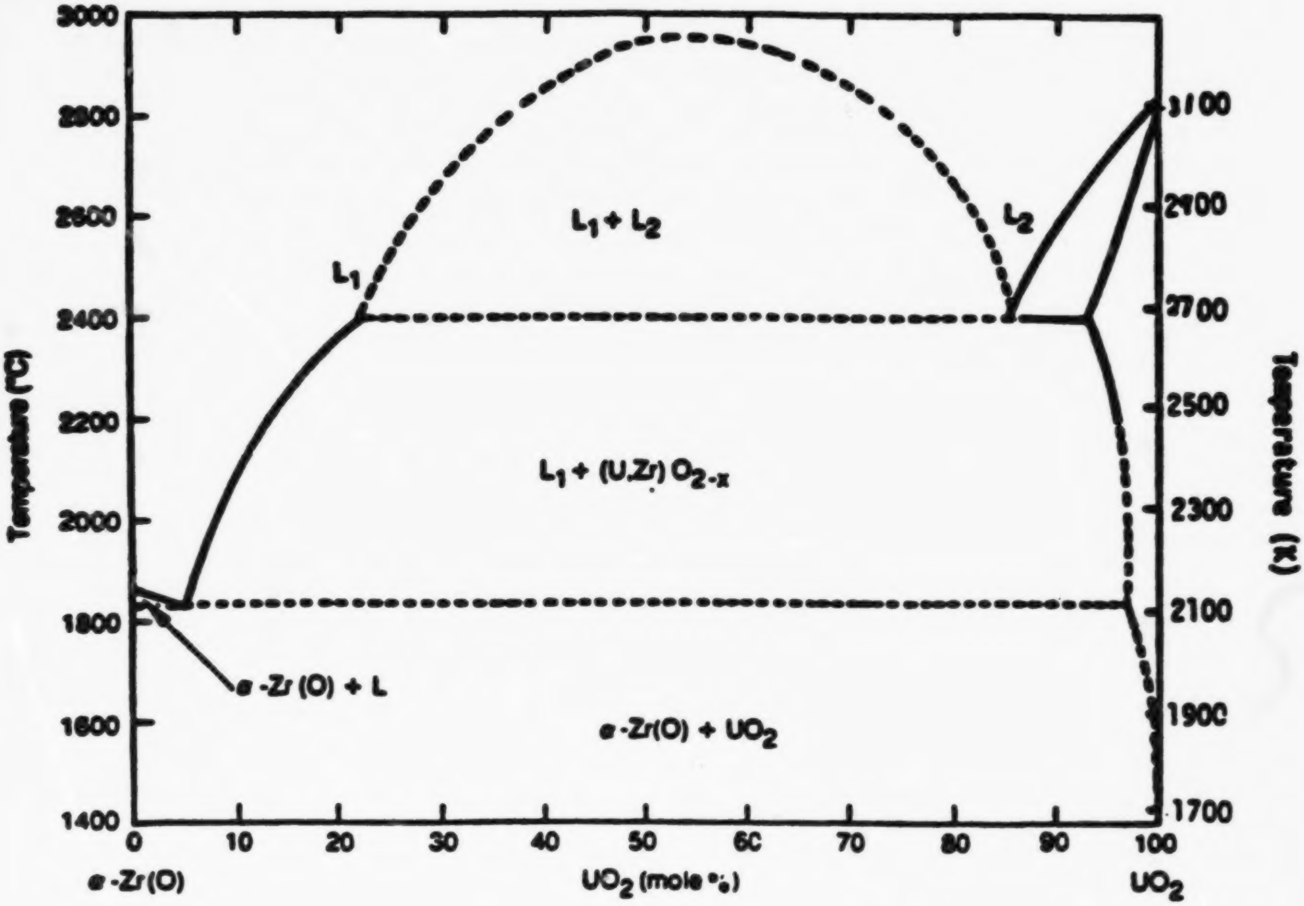

Figure 3.1 α(O)-Zr-UO$_2$ pseudo binary phase diagram (Ref. 3.20).

46

valid (Ref. 3.7). The partial blockages in the PBF tests (up to 90 percent of the flow area) had a negligible effect upon the boiloff steam flow and apparently on hydrogen generation (Ref. 3.7). In the PBF Severe Fuel Damage 1-1 test at boiloff steam flow rates, 85 percent of the hydrogen was generated after the start of Zircaloy melting at 2,150 K, the original IDCOR threshold for cutting off hydrogen generation. About 65 percent of the hydrogen was generated after this hypothesized cutoff in the SFD Scoping Test at higher steam flow rates (Ref. 3.7). The fuel temperature increase from oxidation also continued well beyond the hypothesized temperature threshold. In the recent NRU FLHT-4 test, hydrogen generation at the steam boiloff rate continued throughout a 30-minute high-temperature hold without steam blockage from Zircaloy relocation while 80 percent of the uncovered Zircaloy was oxidized. Posttest metallographic measurement of local (not averaged) peak temperatures of the PBF debris up to the 3,100 K UO_2 melting point indicated continued oxidation and hydrogen generation to higher temperatures (Refs. 3.1 and 3.4). Such very high local temperatures were also measured from metallographic examination of TMI-2 particulate debris from the upper regions of the core (Ref. 3.23). The fact that complete blockages did not occur in the PBF or the NRU tests or at TMI-2, however, does not prove that steam flow-significant blockages can never occur, particularly in the enclosed BWR channel boxes before they lose flow integrity. The case has not been made, however, that such complete blockages do occur in BWRs, or that they always occur, as assumed in the IDCOR analyses.

The PBF tests have shown that essentially freestanding columns of declad, stacked, cracked ceramic (UO_2, ZrO_2) fuel "pellets" in essentially the original rod geometry exist following the initial autocatalytic oxidation transient and relocation of the molten metallic Zircaloy (and dissolved UO_2) (Refs. 3.1 and 3.4 through 3.6). The later collapse of the ceramic-pellet columns is the second major material relocation process involved in core melt progression. This collapse forms a rubble bed on top of the layer of frozen relocated Zircaloy and liquefied fuel and substantially changes the thermal characteristics of the debris, including its flow resistance. The natural circulation flow from the upper plenum into the damaged core is virtually eliminated by this collapse. The conditions under which this collapse occurs are not currently known. No collapse occurred in the four PBF 32-rod tests, even with the water quenching in the initial scoping test. It is not currently known whether or not the collapse of the pellet stacks in the TMI-2 accident occurred before the restart of the B coolant pump that quenched the damaged core.

As steam boiloff continues, the debris region, which consists of frozen relocated Zircaloy and liquefied fuel in the fuel rod stubs at the bottom and mostly ceramic particulate rubble above, is heated by fission product decay and probably by some continued oxidation of the relocated Zircaloy. Because of surface heat removal, melting starts near the center of the debris region, and increasing thermal loads are imposed upon the lower crust and the core support structure. The third major material relocation comes with failure of the lower support crust, or possibly first the core support plate, with slumping of the corium melt into the lower plenum and quenching of the surface of the melt mass by the lower-plenum water. This occurred at TMI-2, where about 20 percent of the core mass was found in the lower plenum as solidified molten corium (not fine particulate debris) (Ref. 3.23). During the quenching process, copious quantities of steam are generated producing a steam pressure spike, and oxidation of the molten unoxidized Zircaloy can generate considerable additional hydrogen. This hydrogen generation is dependent on the surface area of metallic Zircaloy that becomes available, and at TMI-2 this available area appears to have been small. A steam explosion might occur when the corium mass slumps into the lower-plenum water in lower-pressure accident sequences below about 500 psi. (The pressure at TMI-2 was too high at slumping (1,800 psi) for a steam explosion to have been triggered.) An energetic steam explosion can deliver significant impulsive shock loads, possibly failing the vessel lower head, and can significantly redistribute the core debris. It is noted that fragmented unoxidized metallic Zircaloy that participates in a steam explosion (becoming quenched) will be too cold to generate hydrogen at the same time. There is also potential for failure of the containment by a missile generated by an energetic in-vessel steam explosion, but this is outside the scope of this report. Following quenching of the melt surface, which occurs relatively rapidly because of the low thermal conductivity of the ceramic corium, the melt boils the lower plenum dry, reheats, and attacks the vessel lower head and the penetrations. The ejection rate of the melt and solid debris into the reactor cavity upon vessel failure is dependent upon the mode of vessel failure.

Natural circulation and the resultant heat transfer between the uncovered region of the intact core (before collapse) and the upper plenum and even the steam generator can have a significant effect upon in-vessel severe accident behavior. This has been shown by analysis with the detailed COMMIX thermal-hydraulics code, the two-dimensional MELPROG/TRAC code, the SCDAP/RELAP5 code, the Electric Power Research Institute (EPRI) CORMLT code, and the IDCOR MAAP code (Refs. 3.10 through 3.12 and 3.24). EPRI-sponsored 1/7-scale experiments at Westinghouse have demonstrated these phenomena and have provided basic data to support the analysis. The analysis indicates that steam and hydrogen convection velocities in the intact core geometry are about an order of magnitude greater than the steam boiloff velocities used in the traditional one-dimensional analysis in the Source Term Code Package and in the in-pile fuel damage experiments in PBF, ACRR, and NRU (Ref. 3.25). Preliminary analysis indicates that in-vessel natural circulation produces more uniform core temperatures and also transfers more of the core heat to the upper-plenum structure and walls, the hot leg nozzles, and even, by countercurrent flow in the hot leg, to the steam generator tubes. There is some indication that this wall heating may cause early failure of the primary system pressure boundary and reactor coolant system depressurization before the meltthrough of the reactor vessel in high-pressure sequences like the TMLB' station blackout. This depressurization would lead to discharge of the accumulator water to the core as the pressure falls below about 600 psi, and the melt progression would be arrested until the accumulator water inventory was boiled off. If the primary system pressure has fallen sufficiently at the time of corium meltthrough of the vessel lower head, pressurized ejection and dispersion of the melt will not occur, eliminating the threat of pressurized melt ejection (direct containment heating) to the integrity of the containment. Current indications are that this threshold pressure is about 200 psi. In the period before possible natural circulation failure of the primary system and discharge of the accumulator water, in-vessel natural circulation delays the onset of core melt progression, hydrogen generation, and fission product and aerosol release and would appear to change these processes significantly. The relatively high-velocity circulating convective gas stream is a steam-hydrogen mixture, and the phenomena of steam starvation as a limit on oxidation and hydrogen generation in the upper region of the core during the early rapid autocatalytic oxidation transient would be modified. In-vessel natural circulation and heat transfer and their effects are treated in a separate chapter.

The sequence of events that follows discharge of the accumulator water into a severely damaged core has not been well investigated. The water inlet flow rate and the time to boil off the accumulator water and to resume core heatup and melt progression are important, and both are a function of the primary system break size. Little information exists on the governing phenomena in reflooding a hot, severely damaged core. In the PBF Scoping Test, the slow bottom reflooding did not fragment and collapse the standing columns (rods) of declad, hot, cracked ceramic fuel pellets, but did produce significant hydrogen generation (possibly from UO_2 oxidation by steam) and high fission product release (Ref. 3.1). At TMI-2, however, the standing declad ceramic fuel rods did collapse upon the lower metallo-ceramic hard pan to form a debris bed, and this is presumed to have occurred upon the restart of main coolant pump B (Ref. 3.23). Experiments at Brookhaven National Laboratory have shown that the reflood quenching of hot debris from the bottom occurs at essentially the inlet flow rate at moderate flow rates, but that, with top reflooding, the quenching is very slow because the upward steam flow interferes with the incoming water (Refs. 3.26 and 3.27). Following boiloff of the water discharged by the accumulators, core melt progression will be resumed unless additional corrective action has been taken.

In-vessel core melt progression in BWRs involves the same general phenomena as in PWRs, but with some significant differences. A most significant difference between BWRs and PWRs is the distributed core support from below the core by the control rod guide tubes. The core plate carries no load, but its restricted openings do provide a possibility for the formation of blockages. This distributed support makes for a major difference from PWRs in the core melt attack on the core support structure, in the mode of vessel failure, and in the mass and rate of melt ejection from the vessel. For the BWRs, local failure of the vessel at the control rod guide tube penetrations is to be expected, rather than massive failure of the lower head that may be the failure mode in some PWR accident sequences.

There are also significant differences in the BWR core design that affect core melt progression. The 62-rod fuel assemblies are enclosed in Zircaloy channel boxes that prevent crossflow. This prevents any upper-plenum natural circulation loop from penetrating into the reactor core. It also provides the potential for complete blockage to cut off the steam flow within a channel box so long as the channel-box walls remain intact. In the IDCOR analysis of BWR accidents with the MAAP code, modeling of the relocation of molten Zircaloy produces channel-box blockage that is assumed to cut off permanently the steam flow and further oxidation and hydrogen generation (Refs. 3.3 and 3.10). Such blockages did not occur in the PBF tests that used 28- or 32-rod test assemblies, 1 meter long, or in the NRU tests with full-length 4-meter-long, 12-rod test assemblies, all under core uncovery accident conditions (Refs. 3.1 and 3.4 through 3.7).

In the BWR core, a cruciform B_4C control blade is installed in the gap between each set of four channel boxes. These gaps furnish parallel flow paths between the channel boxes. The temperature in the control blades, which lack fission product decay heat, will lag behind the fuel rod temperatures during the core heatup, but analysis indicates that the gap and control blades will lead the fuel rod temperatures during the autocatalytic oxidation transient. The stainless-steel-clad B_4C blades fail at a lower temperature than the Zircaloy-clad fuel rods. It had been thought that failure occurs near the 1,700 K stainless steel melting point, but recent KfK results have indicated that failure is produced at about 1,500 K by formation of a B_4C-stainless-steel-alloy eutectic. The resultant liquefied alloy relocates downward and has the potential to form blockages in the gaps between the channel boxes that contain the control blades. The liquefied alloy also attacks Zircaloy and may penetrate and fail the BWR channel-box walls and further alter the accident sequence. (Experiments currently under way at KfK and in the ACRR should provide information on these questions.) Steam oxidation of the B_4C may furnish an additional thermal-energy source, but recent KfK results indicate that B_4C alloying with the stainless steel may prevent B_4C oxidation by the steam. The boron can also affect the fission product chemistry.

3.2.2 Core Melt Progression Analysis Codes

The older MARCH 2.0 code used in the BMI-2104 analysis and its more recent MARCH 3.0 update used in the Source Term Code Package have a much simplified nonmechanistic treatment of in-vessel core melt progression (Ref. 3.8). MARCH calculates the coolant boildown and initial core heatup with the one-dimensional steam boiloff velocities. The rate of oxidation of the intact Zircaloy cladding by steam is limited by the steam supply and by oxygen diffusion through the thickening ZrO_2 surface layer on the cladding that is treated by parabolic rate kinetics.

As noted earlier, there are three significant and distinct material relocation processes involved in in-vessel core melt progression. First, molten unoxidized metallic Zircaloy and liquefied fuel (UO_2 dissolved in molten metallic Zircaloy) relocate downward upon failure of the ZrO_2 cladding sheath formed by cladding oxidation and freeze to form a possibly permeable metallo-ceramic hard pan across the fuel rods. Secondly, the remaining freestanding declad fuel rods collapse upon the hard pan to form a rubble bed. Thirdly, molten corium from melting of the rubble bed melts through the lower hard pan crust and slumps onto the PWR lower core support plate or onto the BWR core plate and distributed core support structure and onto the vessel lower head. These three separate and distinct material relocation processes occur at different times during in-vessel core melt progression, and the mechanisms of relocation are different for each of the three.

Only the new mechanistic MELPROG core melt progression code models all three of these processes (Ref. 3.12). Fundamental data on these relocation processes, however, are only now being acquired in the severe accident research program. Under these circumstances, current accident analysis codes generally use a nonmechanistic temperature threshold for the start of relocation. In addition, two or even all three of these relocation processes are usually lumped together nonmechanistically. In MARCH, all three are lumped into one "core slumping" model. It is assumed in MARCH that fuel heating in each node is stopped at an assumed 2,550 K "corium melting" or eutectic temperature, and that no material relocation downward occurs until the bottom node in an axial column of nodes becomes molten corium at 2,550 K (Ref. 3.8). At this time, all the fully molten nodes in the column above slump onto the first support grid and very soon onto the vessel lower head. It has been observed experimentally (PBF, ACRR, KfK) that downward relocation of molten unoxidized Zircaloy limits the autocatalytic oxidation temperature rise and the hydrogen generation by removing unoxidized Zircaloy from the hotter regions of the core. (This unoxidized Zircaloy, however, may become available for oxidation and hydrogen generation later in the

BEST COPY AVAILABLE

accident, either in-vessel or ex-vessel.) Calculations (MELPROG, for example) have shown that increasing an assumed temperature threshold for relocation of molten Zircaloy from 2,200 K to 2,500 K can increase the hydrogen generation by as much as 100 percent. Thus, the MARCH modeling that allows no relocation of unoxidized Zircaloy before an assumed slump of the entire core at 2,550 K can give substantially greater hydrogen release in the autocatalytic oxidation transient than actually occurs. It is assumed in MARCH that the fuel temperature in a node does not exceed the 2,550 K assumed corium melting and slumping temperature, even though oxidation heating and hydrogen generation in the node continue. Any heat generated by oxidation or by fission product decay above that required to maintain the node at the defined eutectic temperature is transferred to the next lower node in simulation of downward melt progression. When the bottom axial node in a column of nodes reaches this temperature and slumping of the column onto the lower grid does occur, oxidation and hydrogen generation are cut off. An exception is that an arbitrary "DROP" model allows oxidation and hydrogen generation to continue for one time step to give some accounting for oxidation during the slumping process. MARCH models in a parametric fashion the interaction of the molten corium that slumps into the lower-plenum water to generate steam and hydrogen. An arbitrary particle size is assumed for the slumped melt, and an arbitrary fraction of the metallic melt is assumed to be in the center of ceramic particles where it cannot generate hydrogen because of isolation from the steam. Varying this parameter from 1.0 to 0.0 increased the fraction of cladding oxidation in the Surry TMLB' base case in the QUEST study by about 40 percent (Ref. 3.19). The BWR version of MARCH does include the Zircaloy in the channel-box walls in the analysis.

The integrated MAAP code has been developed by the industry IDCOR program for severe accident analysis (Ref. 3.10). Detailed descriptions of the MAAP code and its revisions have not been available for review so the descriptions of the MAAP modeling given here may be inaccurate and incomplete. In addition, the MAAP code has been modified and upgraded with new information that has become available so that previous model assessments become dated (Ref. 3.3). For core melt progression, the original version of MAAP, rather like MARCH, assumed a single relocation or slumping of corium "eutectic" at 2,500 K (Ref. 3.10). Comparison calculations were made for slumping at the full 3,100 K UO_2 melting temperature. In MAAP, the corium melt slumps node-to-node as a film until frozen by colder preexisting material in a node. This simulates the candling process somewhat but ignores rivulet flow. The process is used to calculate blockage formation. As previously mentioned, IDCOR has argued that this melt slump blocks the steam flow in BWR channel boxes to cut off hydrogen generation and diverts the steam flow in the open-lattice PWR core to substantially reduce the hydrogen generation. IDCOR cites the PBF results in support of this modeling, although formation of complete blockage and cutoff of Zircaloy oxidation and hydrogen generation did not occur in the PBF or the NRU tests (Ref. 3.3). IDCOR has added a treatment of in-vessel natural circulation and heat transfer to MAAP, using assumed one-dimensional convective flow patterns (tubes) as in the EPRI CORMLT model. MAAP allows for the addition of a user-specified mass of molten steel from the upper-plenum structure to the core melt inventory. It assumes that in all cases the failure of the vessel lower head occurs at head penetrations, giving a small initial flow area that opens rapidly by ablation.

The new mechanistic MELPROG core melt progression code is the most comprehensive of all the tools currently available for the analysis of in-vessel core melt progression (Ref. 3.12). MELPROG incorporates mechanistic modeling of the key melt progression processes, but detailed mechanistic models of some phenomena are just now being incorporated in the code to replace earlier simplified models. Currently available results are from preliminary simplified versions of the code. MELPROG is still in the early stages of validation against data and of checking against existing codes. Data are not yet available for assessing several of the models in MELPROG, particularly for the latter stages of core melt progression that follow the initial autocatalytic oxidation transient and the beginning of the relocation of ceramic debris. The new MELPROG core model CORE uses a four-field fluid treatment in addition to solid structure, which provides separate treatment and relocation for solid and liquid core debris. The four fluid fields are liquid debris, solid debris, liquid coolant, and gas. MELPROG uses a two-dimensional (r,z) version of TRAC thermal hydraulics to provide treatment of in-vessel natural circulation and heat transfer that continues through fuel damage development and core melt progression. MELPROG has been linked with a one-dimensional TRAC version of the primary system thermal hydraulics for treatment of the primary system outside the reactor vessel. The first-principles mechanistic VICTORIA fission product behavior module, which can also be used as a stand-alone code, has recently been incorporated in MELPROG. Fission product effects, including the substantial depletion of the decay heat source in the fuel and the fission product transport of this heat source to the walls, have not yet been included in any MELPROG calculations.

MELPROG separately models all three of the important material relocation processes, the molten Zircaloy and liquefied fuel relocation from the initial rod geometry, the collapse of the standing declad rods of cracked ceramic pellets (remaining after initial cladding oxidation and relocation) to form a rubble bed on the underlying metallo-ceramic layer of solidified relocated Zircaloy and liquefied fuel, and the slumping of the corium pool mass through the lower supporting crust onto the core support plate and the lower head. Currently the data base for modeling these three relocation processes is inadequate for the first of these and nearly nonexistent for the latter two. Current models of these processes, particularly the latter two, are therefore based primarily on analysis. Significant research information on these relocation processes will soon be forthcoming, however, from new out-of-pile MELPROG validation experiments at Sandia National Laboratories, in-pile melt progression experiments in ACRR, and the CORA fuel damage tests at KfK in the Federal Republic of Germany. A promising new model for the process of fuel failure and subsequent relocation of the molten Zircaloy and liquefied fuel is under development. This model treats fuel failure as the result of dissolution of the ZrO_2 cladding sheath by molten Zircaloy, in analogy to the dissolution of UO_2, to form liquefied fuel. In this situation, assumed temperature thresholds for the three separate relocation processes are often currently used for sensitivity studies. Unique and valuable data on the later stages of in-vessel core melt progression are being obtained from the TMI-2 core examination and should be obtained in the Post-Irradiation Examination (PIE) of the LOFT FP-2 test.

MELPROG includes analysis of the thermal and mechanical attack of the core debris upon the reactor structure, the vessel head, and the head penetrations (Ref. 3.12). Treatment of the head penetrations is particularly important for analyzing BWR vessel failure that is complicated by the BWR distributed core support structure of the control rod guide tubes. The MELPROG analysis includes the mode of vessel failure and the characteristics of the core debris at vessel failure. These characteristics include the melt fraction, the temperature distribution, the composition distribution, and the debris spatial distribution. If failure of the reactor vessel occurs at high pressure so that pressurized melt ejection can occur to produce direct containment heating, MELPROG calculates the characteristics of the jet of fragmented melt ejected into the reactor cavity.

The older and more mature mechanistic SCDAP fuel damage code is used for analyzing the earlier stages of the accident up through the relocation of molten Zircaloy cladding and liquefied fuel, including hydrogen generation (Ref. 3.14). SCDAP is used for analysis of terminated accidents with recovery by reflooding and includes core debris coolability models. SCDAP has a somewhat more detailed treatment than MELPROG of the early stages of fuel damage, including fuel failure and the relocation of molten Zircaloy and liquefied fuel and potential blockage formation. SCDAP has been particularly useful for the detailed analysis and interpretation of the PBF, ACRR, NRU, and KfK fuel damage experiments and the LOFT FP-2 test. A new mechanistic model for fuel (cladding) failure based on the dissolution of the ZrO_2 cladding sheath by molten metallic Zircaloy is being specifically developed for SCDAP but will also be used in MELPROG. SCDAP also has the capability of analyzing in-vessel natural circulation and heat transfer using RELAP5 thermal hydraulics and crossflow mixing coefficients. SCDAP has been linked with the RELAP5 thermal-hydraulic systems code for analysis of the primary coolant system. Along with supplementary analysis of the later phase of the accident, SCDAP is being used by the Department of Energy for its analysis of the TMI-2 accident in conjunction with the TMI-2 core examination.

Development of the BWR version of MELPROG has not yet been completed, and the BWR version of SCDAP has just recently become operational. BWR-specific features that have a significant effect upon in-vessel core melt progression are the individual channel boxes, the B_4C control blades, the core plate, and the distributed core support structure. Somewhat more mechanistic models of BWR in-vessel core melt progression than those currently available with MARCH 3.0 can now be obtained with the Oak Ridge National Laboratory MARCON 2.2B version of MARCH (Ref. 3.28). In addition, development is nearing completion on an advanced simplified integral code, MELCOR, for the analysis of severe accident consequences and risk. MELCOR is designed to eventually replace the Source Term Code Package, and, although a simplified integral code, it has a considerably more mechanistic treatment of in-vessel core melt progression than does the MARCH 3.0 element of the Source Term Code Package (Ref. 3.29).

The mechanistic MELPROG core melt progression code (and its BWR version when available) will be used to benchmark the MARCH 3.0 code and also the new simplified MELCOR integrated risk code. MELPROG and SCDAP provide mechanistic tools for evaluating the effects of in-vessel natural circulation and for uncertainty assessment. The mechanistic codes, including MELPROG for in-vessel core melt progression, also provide the most precise analysis available for accident sequences and plants where the uncertainties are particularly significant and for evaluating specific plant or parameter changes.

3.2.3 Summary of Current Significant Technical Uncertainties

The areas of current significant technical uncertainty involving in-vessel core melt progression can be summarized as follows:

53

1. The threshold and mechanisms of molten Zircaloy relocation, including blockage formation.

2. The effects of stainless-steel-clad PWR Ag-In-Cd and the BWR B_4C control rods and of B_4C-Al_2O_3 burnable poison rods upon melt progression, aerosol formation, and system chemistry. Included are the effects of alloying melting-point reduction (eutectics) and liquefaction on relocation and blockage formation and on the potential for opening vertical pathways through the core.

3. The time in the melt progression sequence of the loss of flow integrity of the BWR channel boxes and location of the failure.

4. Longer-term hydrogen generation with molten Zircaloy relocation and potential blockage formation.

5. Potential failure of the primary system pressure boundary from in-vessel natural circulation and heat transfer and the effects of such failure.*

6. The effects of the release of accumulator water, including questions of core cooling and accident arrest by core reflood, duration of the arrest, and the effect upon the subsequent accident sequence, including in-vessel core melt progression.

7. Formation of an across-core metallo-ceramic hard pan in the fuel rod stubs by the relocated material and characterization of the hard pan with respect to permeability (for steam flow and hydrogen generation), thickness, and strength.

8. Collapse of the array of freestanding declad rods of cracked ceramic fuel pellets onto the metallo-ceramic hard pan to form a debris bed and characterization of the debris bed.

9. Characterization of the growing corium pool, the surface crusts, and the surrounding debris.

10. Meltout failure of the lower pool crust and relocation of the melt, including the mode of the meltout and chracterization of the debris at meltout.

11. The effects of explosive and nonexplosive rapid steam generation from melt interaction with the lower-plenum water, including potential direct consequences (alpha mode containment failure and lower-plenum failure), hydrogen generation, fission product and aerosol release, and the effects upon further core melt progression.*

12. Failure of the reactor structure and the vessel lower head by core melt thermal-mechanical attack. Included are the mode of vessel failure, failure of vessel penetrations, the particular failure mode of the BWR distributed core support structure, the characteristics of the core debris

---

*Uncertainty also addressed in other NRC research programs.

BEST COPY AVAILABLE

and the melt at the time of vessel failure, and the characteristics of the melt and debris ejected into the reactor cavity or of the melt jet (for pressurized ejection).

3.3 Comparison of MELPROG 1-D and 2-D Analyses of Surry TMLB' Sequence With March 2.0 1-D Analyses

Analyses of the Surry TMLB' (station blackout) sequence were made with the new 2-D version of MELPROG, which includes in-vessel natural circulation, and with the older 1-D version. Comparisons were made with the MARCH 2.0 analysis. MARCH 2.0 is similar in its treatment of core melt progression to the upgraded MARCH 3.0 used in the Source Term Code Package. In the simplified PINS fuel damage model used in these MELPROG calculations, the important molten Zircaloy relocation temperature is an input parameter, as in MARCH.

Three MELPROG calculations were made in the analysis of the Surry TMLB' sequence. Two were with the one-dimensional version of MELPROG and one with the new two-dimensional version. The calculated conditions at vessel failure are shown in Table 3.1 (Ref. 3.25) along with the results of Surry TMLB' calculations with MARCH 2.0 from BMI-2104 (Ref. 3.9). The important Zircaloy relocation temperature (assumed input) was varied in the two MELPROG one-dimensional calculations, and modeling of the downcomer water was included in the second calculation at the higher relocation temperature.

Table 3.1 Conditions at vessel failure.*

	MARCH	MELPROG 1-D		MELPROG 2-D
		Case 1	Case 2	
$T_{relocate}$ (K)	2,550**	2,200**	2,500**	2,200**
Time from Saturation to Vessel Failure (min)	90	115	105	157
Zr Oxidized (%)	59%	31%	60%	40%
Hydrogen Mass (kg)	430	230	440	300
T_{mean} (K)	2,380	2,600	2,120	2,400
Debris Melt Fraction (%)	***	34%	16%	30%
Debris Zr Mass (kg)	6,700	11,400	6,500	9,000
Debris Steel Mass (kg)	35,000	900	10,300	19,300

*Core mass is 116,600 kg.

**Parameter assumed.

***Not modeled in MARCH.

55

As seen from the results in Table 3.1, the assumed Zircaloy relocation temperature has a major effect upon the fraction of Zircaloy oxidized (and the hydrogen generation) as well as upon the core debris average temperature and melt fraction (the fraction of the debris molten) at vessel failure. At similar (high) assumed Zircaloy relocation temperature thresholds, MARCH 2.0 and MELPROG 1-D gave similar results for the fraction of the Zircaloy oxidized (hydrogen generation), but MELPROG gave a somewhat higher average debris temperature. Increasing the Zircaloy relocation temperature threshold from 2,200 K to 2,500 K increased the oxidized Zircaloy (hydrogen generation) by a factor of two. Assuming the higher relocation temperature, this reduced the debris melt fraction at vessel failure by a factor of two and also significantly reduced the mean debris temperature at failure because the hotter relocated molten Zircaloy and liquefied fuel decreased the time to vessel failure.

In the past, none of the attempted mechanistic Zircaloy relocation models has fitted the available data, so the Zircaloy relocation temperature has been normally used as an input parameter. A promising new relocation model is under development that treats fuel failure and molten Zircaloy relocation as the result of dissolution of the high-melting-point ZrO_2 cladding sheath by the molten metallic Zircaloy. New experimental data, primarily from the KfK CORA experiments, will be used to check this model, which has been included in preliminary form in the new CORE fuel damage model in MELPROG that replaces PINS.

The in-vessel natural circulation (assuming the same Zircaloy relocation temperature) in the MELPROG 2-D calculation increased the time from saturation to vessel failure by about an hour because of core heat loss to vessel structures. The Zircaloy oxidation (hydrogen generation) was increased by about 30 percent, and the debris melt fraction was decreased by about 15 percent. A major effect of natural circulation was to increase the mass of molten steel in the debris by a factor of 20 because of the increased heat transfer to the vessel internals and the vessel wall. The hotter vessel structure and vessel wall from in-vessel natural circulation will inhibit the plateout of fission products upon the vessel wall and will also increase fission product revaporization.

The state of the core debris at vessel failure from the MELPROG 2-D calculations is given in Table 3.2. This table gives the mass distribution of the chemical compounds in the core and the melt fraction for each.

Table 3.2 State of core debris at vessel failure in MELPROG 2-D analysis.*

	Mass (kg)	Melt Fraction (%)
UO_2	96,000	14
Zr	9,600	100
ZrO_2	9,250	0
Steel	19,300	78
Control Rod Matl.	2,850	100
Total	137,000	30

*Core mass is 116,600 kg.

BEST COPY AVAILABLE

56

In the MELPROG 2-D analysis, 52 percent of the mass of core debris exited the reactor vessel at vessel failure. This included all the molten debris and some of the solid debris. The remaining debris melted by decay heat and drained from the vessel in about 30 minutes. These results are in contrast with the MARCH analysis that assumed that 100 percent of the core debris exits the vessel at failure.

A very significant result of the MELPROG 2-D analysis is that, with in-vessel natural circulation and heat transfer, the hot leg nozzles should reach about 1,250 K tens of minutes before failure of the vessel by melt attack. Indications are that with the high pressures in the TMLB' sequence, the nozzles would fail rapidly at temperatures above about 1,000 K. This failure would depressurize the reactor coolant system so that the accumulators could discharge water to the damaged core. After boiloff of the accumulator water and without further corrective actions, core heatup and melt progression would be resumed, eventually leading to lower-head meltthrough. At this time and depending on the break size, the vessel pressure might be too low to provide pressure-dispersed melt ejection with direct containment heating. It should be noted that such a high-pressure failure of the pressure boundary did not occur in the TMI-2 accident, although this accident did progress to substantial core (ceramic) melting and relocation but not to the point of vessel meltthrough.

3.4 Planned Research Program

3.4.1 Current Research Program (FY 1987)

The current research program on in-vessel core melt progression and hydrogen generation splits into two parts: (1) the early phase of the accident up through metallic but not ceramic material relocation and (2) the later phase through failure of the vessel lower head and melt relocation into the concrete reactor cavity. FY 1987 research on the initial phase of the accident includes: (1) completion of the Post-Irradiation Examination (PIE) and the analysis of results of the last two of the PBF Severe Fuel Damage (SFD) tests that used high-burnup fuel; (2) performance of the NRU Full-Length High Temperature test FLHT-5 on hydrogen generation with Zircaloy relocation during a 30-minute hold at high temperature, and analysis of the results and very limited PIE on the previous FLHT-4 test; and (3) performance of the BWR Damaged Fuel DF-4 test in ACRR on the effects of the BWR Zircaloy channel boxes and B_4C control blades on the early phase of core melt progression and hydrogen generation, PIE, analysis of results, and reporting on the previous PWR DF tests. In addition, important information on the thresholds and mechanisms of Zircaloy relocation and on control rod material interaction effects will be obtained from tests in the new CORA facility and in laboratory work at KfK in the Federal Republic of Germany. The early-phase core melt progression research is coordinated with assessment, improvements, and application of the mechanistic SCDAP and MELPROG codes, with particular emphasis on Zircaloy relocation modeling and on BWR-specific effects.

Very little information is available on the later stages of in-vessel core melt progression except for that from the TMI-2 core examination, which deals with the conditions of a recovered accident. Under those circumstances, the modeling of the later stage in the mechanistic MELPROG melt progression code has had to be based primarily on analysis of the governing processes rather than on data. Major emphasis in the current and future melt progression research is upon furnishing needed data for assessing the modeling in MELPROG and for improving that modeling where appropriate. A new program of analysis and out-of-pile experiments for assessment of the key models in MELPROG was begun in FY 1986, and this should provide much of the data needed for assessment of the MELPROG models. In addition, a new series of integral in-pile tests in ACRR on the later stages of in-vessel core melt progression will be performed starting in late FY 1988, with planning in FY 1987. These tests will provide important data with continuous prototypic heating of the fuel debris on such later stage phenomena as the molten corium attack on the lower crust and the collapse of freestanding declad cracked ceramic fuel rods. The MELPROG validation program also includes comparisons of MELPROG analysis with the available experimental data base and comparison with the TMI-2 results of the international TMI-2 standard problem exercise. Assessment and validation of the simplified integrated codes will include some comparisons with data, comparisons with more mechanistic codes, and participation in the TMI-2 standard problem exercise.

The basic information source on in-vessel severe accident behavior has been the series of four SFD tests performed in the PBF test reactor. Final reports of the first two tests have been issued, the latter of the two in early FY 1987. These reports include the PIE results. The PIE and analysis of the results of the last two tests have not yet been completed. These last two tests used high-burnup fuel in the 28-rod fuel bundle tests, and SFD 1-4 also had four PWR silver-indium-cadmium control rods, while SFD 1-3 did not have control rods. The final PIE and analysis of the results of these last two tests will be completed in FY 1987 and the results reported in FY 1988. An integrated summary report on hydrogen generation in the four PBF SFD tests will also be issued in FY 1987.

The NRU tests with full-length test fuel bundles provide our most prototypic conditions for fuel damage during coolant boildown, with particular emphasis on hydrogen generation and Zircaloy relocation. The FLHT-4 test demonstrated continuous hydrogen generation throughout a 30-minute hold at high temperature with no blockage of the steam flow and hydrogen generation by Zircaloy relocation. FLHT-4 also contained one PWR high-burnup fuel rod, and measurements were made of fission product release and deposition. In FY 1987, analysis of the results and the very limited PIE of FLHT-4 will be completed and reported. Test FLHT-5 with power compensation for the bundle heat losses at high temperature will also be performed in FY 1987.

The BWR DF-4 test in ACRR was performed in early FY 1987. The purpose of DF-4 was to investigate the effects of the BWR channel boxes and the B_4C control blades upon fuel damage, early core melt progression, hydrogen generation, and system chemistry. The 14-rod test assembly contained a simulated BWR stainless-steel-clad B_4C control blade in the gap between two channel-box walls and prototypic flow division between the gap and the fueled, simulated channel boxes. Analysis of the results and limited PIE of DF-4 will be completed and reported in FY 1987. Final experiment reports will be issued on the earlier DF-3 test with a PWR stainless-steel-clad silver-indium-cadmium control rod and DF-2 with no control rod and on the PIE of DF-3. Planning will be performed for the new melt progression test series on the later stages of core melt progression, and design work will be performed for the initial test, MP-1, on the failure of the lower metallo-ceramic crust between the fuel rod stubs under molten corium attack. MP-1 will be performed in late FY 1988.

In the MELPROG assessment and validation program, comparisons will be made of the results of MELPROG analysis and the ACRR and PBF results. Comparisons will also be made between analyses with the first-principles VICTORIA fission product behavior module in MELPROG and results of the old and the new Oak Ridge National Laboratory fission product release experiments and other fission product release data. SCDAP and MELPROG analyses will be performed in support of experiments in the new German CORA facility at KfK on Zircaloy relocation and hydrogen generation and to interpret the CORA results. The CORA results will be the primary data source for the development of mechanistic models for the fuel failure threshold and for molten Zircaloy relocation and potential blockage formation. MELPROG analysis of the TMI-2 accident will be started as part of the Department of Energy TMI-2 standard problem exercise.

In the MELPROG validation program in FY 1987, intermediate-scale experiments will be performed on the attack of molten Zircaloy on thin ZrO_2 shells (for modeling fuel-failure thresholds) and on Inconel grid spacers. The technology for forming pre-cast metallo-ceramic crusts in an array of fuel pin stubs for experiments or crust failure under molten corium attack will be developed and used in intermediate-scale (50 kg) experiments with thermite melts. With these results, preparations will be made for large-scale experiments in the Large Melt Facility (LMF) with 200-kg ceramic melts and susceptor-sustained heating. The initial LMF test is scheduled for mid-FY 1988.

In parallel with this work, improvement and development of the mechanistic MELPROG melt progression code and the mechanistic SCDAP fuel damage code and recovered-accident code will be continued. BWR versions of both MELPROG and SCDAP will be available in FY 1987. Work is actively under way on development of a mechanistic model for the fuel-failure threshold on the basis of dissolution by molten Zircaloy of the ZrO_2 shell on the cladding. The amount of hydrogen generated is highly sensitive to this threshold, which also significantly affects the later stages of core melt progression. Results of the KfK CORA experiments and the MELPROG validation separate-effect experiments will provide input data for this model development.

3.4.2 Future Research Program (FY 1988-1990)

Emphasis in the planned research for the FY 1988 to FY 1990 period is upon reducing the most important uncertainties in the later stages in in-vessel core melt progression where very little information beyond the TMI-2 core examination currently exists. Research results will be used for assessment of the models in the mechanistic MELPROG melt progression code and improvement of the models where indicated. Planned are two melt progression tests per year in ACRR to furnish integral data with prototypic heating of the UO_2 in the debris on late-phase phenomena, including collapse of freestanding declad cracked ceramic fuel rods and molten corium pool growth and melt attack on the lower metallo-ceramic crust. These results will be supplemented by large-scale experiments in the MELPROG validation program on the effects of core melt attack with up-to-200-kg ceramic melts and susceptor-sustained heating. Smaller-scale out-of-pile separate-effect experiments will continue with emphasis on the mechanisms of melt relocation and the collapse of declad fuel rods. With knowledge of melt relocation and of the temperature distributions in the debris, assessment of the heating and failure of the reactor structure and the lower head can be handled analytically, as currently done in MELPROG. Detailed MELPROG analysis of the TMI-2 accident as part of the international TMI-2 standard problem exercise

59

will be completed and reported in FY 1988. Although not funded as part of the research program, MELPROG will be used increasingly for detailed analysis of the in-vessel component of risk-significant accident sequences and for benchmarking simplified risk analysis codes. MELPROG will be linked with the mechanistic TRAC (system thermal hydraulics) and CONTAIN (containment) codes to furnish a complete mechanistic package as a tool for the analysis of the more important risk-significant accident sequences in specific plants.

The research on the earlier phase of core melt progression should be completed in this time period. The final reports on the last two PBF severe fuel damage tests will be issued in FY 1988. Full-length fuel bundle tests in NRU on hydrogen generation and Zircaloy relocation will continue at a one-per-year rate through FY 1989. The currently planned 15-test matrix of out-of-pile tests in the CORA facility at KfK on Zircaloy relocation thresholds and mechanisms should be completed in FY 1988. The CORA results should be reported and incorporated in improved Zircaloy relocation models in MELPROG and SCDAP in FY 1989.

REFERENCES FOR CHAPTER 3

3.1 Z. R. Martinson, D. A. Petti, and B. A. Cook, "PBF Severe Fuel Damage Test 1-1, Test Results Report," EG&G Idaho, Inc., NUREG/CR-4684, Vol. 1, EGG-2463, November 1986.

3.2 J. T. Prater and E. L. Courtright, "High-Temperature Oxidation of Zircaloy-4 in Steam and Steam-Hydrogen Environments," Pacific Northwest Laboratories, NUREG/CR-4476, PNL-5558, February 1986.

3.3 Fauske and Associates, Inc., "IDCOR Technical Report 85.2: Technical Support for Issue Resolution," Atomic Industrial Forum, July 1985.

3.4 A. D. Knipe, S. A. Ploger, and D. T. Osetek, "PBF Severe Fuel Damage Scoping Test--Test Results Report," EG&G Idaho, Inc., NUREG/CR-4683, EGG-2413, August 1986.

3.5 R. W. Miller, R. K. McCardell, and P. Kugon, "Severe Fuel Damage Test 1-3 in the Power Burst Facility," Trans. Am. Nucl. Soc., Vol. 49, p. 249, June 1985.

3.6 Z. R. Martinson and R. W. Miller, "SFD 1-4 Test Results with Irradiated Fuel and Control Rods," Trans. Am. Nucl. Soc., Vol. 50, p. 319, November 1985.

3.7 A. W. Cronenberg, R. W. Miller, and D. J. Osetek, "Zircaloy Oxidation/Hydrogen Generation Behavior During Severe Accident Conditions," Transactions of the 24th National Heat Transfer Conference (Pittsburgh, PA), August 10-15, 1987, to be published.*

3.8 R. O. Wooton, P. Cybulskis, and S. F. Quayle, "MARCH 2 (Meltdown Accident Response Characteristics) Code Description and User's Manual," Battelle Columbus Laboratories, NUREG/CR-3988, BMI-2115, September 1984.

3.9 J. A. Gieseke et al., "Radionuclide Release under Specific LWR Accident Conditions," Battelle Columbus Laboratories, BMI-2104, Vol. 1, Vols. II-VII, Draft, July 1983-July 1986.

3.10 Fauske and Associates, Inc., "MAAP, Modular Accident Analysis Program User's Manual," IDCOR Technical Report 16.2-3, August 1983.

3.11 Electric Power Research Institute, "The CORMLT Code for the Analysis of Degraded Core Accidents," EPRI-NP-3767-CCM, December 1984.

3.12 W. J. Camp et al., "MELPROG-PWR/MOD0: A Mechanistic Code for Analysis of Reactor Core Melt Progression and Vessel Attack Under Severe Accident Conditions," Sandia National Laboratories, NUREG/CR-4909, SAND85-0237, Draft.*

---

*Available in the NRC Public Document Room, 1717 H Street N.W., Washington, DC.

3.13 F. J. Erbacher, "LWR Fuel Cladding Deformation in a LOCA and Its Interaction with Emergency Core Cooling," Proceedings of the ANS/ENS Topical Meeting of the Reactor Safety Aspects of Fuel Behavior (Sun Valley, ID), August 2-6, 1981.

3.14 C. M. Allison, F. R. Carlson, and R. H. Smith, "SCDAP: A Computer Code for Analyzing Light Water Reactor Severe Core Damage," Proceedings of International Meeting on Light Water Reactor Severe Accident Evaluation (Cambridge, MA), American Nuclear Society, August 28-September 1, 1983.

3.15 J. V. Cathcart, "Quarterly Progress Report on the Zirconium Metal-Water Oxidation Kinetics Program Sponsored by the NRC Division of Reactor Safety Research for October-December 1976," Oak Ridge National Laboratory, ORNL/NUREG/TM-87, January 1977.

3.16 L. Baker, Jr., and C. Just, "Studies of Metal-Water Reactions at High Temperatures III, Experimental and Theoretical Studies of the Zirconium-Water Reaction," Argonne National Laboratory, ANL-6548, May 1962.

3.17 V. F. Urbanic and T. R. Heidrick, "High Temperature Oxidation of Zircaloy-2 and Zircaloy-4 in Steam," J. Nuc. Matls., Vol. 75, pp. 251-261, 1978.

3.18 H. M. Chung and G. R. Thomas, "The Retarding Effect of Hydrogen on Zircaloy Oxidation," NSAC-29, Interim Report, July 1981.

3.19 R. J. Lipinski et al., "Uncertainty in Radionuclide Release Under Specific LWR Accident Conditions," Sandia National Laboratories, SAND84-0410, Vols. 1-4, February 1985-December 1985.

3.20 P. Hofmann and C. Politis, "Chemical Interaction Between Uranium Oxide and Zircaloy-4 in the Temperature Range Between 900 and 1500°C," Proceedings of the Fourth International Conference in Zirconium in the Nuclear Industry, Stratford-on-Avon, England, June 26-29, 1978, ASTM STP 681, pp. 537-560, September 1979.

3.21 K. O. Reil et al., "Results of the ACRR DFR Experiments," Proceedings of the International ANS/ENS Topical Meeting on Thermal Reactor Safety (San Diego, CA), February 2-6, 1986.

3.22 S. Hagan and P. Hofmann, "PWR Fuel Element Behavior at Temperatures up to 2350°C," Proceedings of the IAEA Specialists Meeting on Water Reactor Fuel Behavior and Fission Product Release in Off-Normal and Accident Conditions, Vienna, Austria, November 10-13, 1986, to be published.*

3.23 P. Grant, "Overview of the TMI-2 Program," Proceedings of the U.S. Nuclear Regulatory Commission Fourteenth Water Reactor Safety Information Meeting (Gaithersburg, MD), October 27-31, 1986, NUREG/CP-0082, Vol. 6, February 1987.

---

*Available in the NRC Public Document Room, 1717 H Street N.W., Washington, DC.

3.24 V. L. Shah et al., "COMMIX-1B: A Three-Dimensional Transient Single-Phase Computer Program for Thermal Hydraulic Analysis of Single and Multicomponent Systems," Argonne National Laboratory, NUREG/CR-4348, Vols. 1 and 2, ANL-85-42, September 1985.

3.25 J. E. Kelly, R. J. Henninger, and J. F. Dearing, "MELPROG-PWR/MOD1 Analysis of a TMLB' Accident Sequence," Sandia National Laboratories, NUREG/CR-4742, SAND86-2175, January 1987.

3.26 N. K. Tutu et al., "Debris Bed Quenching Under Bottom Flood Conditions (In-Vessel Degraded Core Cooling Phenomenology)," Brookhaven National Laboratory, NUREG/CR-3850, BNL-NUREG-51788, October 1984.

3.27 T. Ginsberg et al., "An Experimental and Analytical Investigation of Quenching of Superheated Debris Beds Under Top-Reflood Conditions--Final Report," Brookhaven National Laboratory, NUREG/CR-4493, BNL-NUREG-51951, January 1986.

3.28 C. R. Hyman and L. J. Ott, "Effects of Improved Modeling of Best-Estimate BWR Severe-Accident Analysis," Proceedings of the U.S. Nuclear Regulatory Commission Twelfth Water Reactor Safety Research Information Meeting (Gaithersburg, MD), October 22-26, 1984, NUREG/CP-0058, Vol. 3, January 1985.

3.29 F. E. Haskin et al., "Development and Status of MELCOR," Proceedings of the U.S. Nuclear Regulatory Commission Fourteenth Water Reactor Safety Information Meeting (Gaithersburg, MD), October 27-31, 1986, NUREG/CP-0082, Vol. 1, February 1987.

4. HIGH-PRESSURE MELT EJECTION
(Direct Containment Heating)

T. M. Lee

4.1 Introduction

4.1.1 Definition of Issue

In certain reactor accidents, such as those initiated by station blackout or a small-break loss-of-coolant accident (LOCA), degradation of the reactor core can take place while the reactor coolant system remains pressurized. Left unmitigated, core melt will slump and collect at the bottom of the reactor vessel. After boiling off the remaining water in the vessel, molten core materials will start attacking the bottom head of the reactor. When the bottom head of the reactor vessel is breached in such accidents, the core melt will be ejected under pressure. The ejected materials are likely to be dispersed out of the reactor cavity into surrounding containment volumes as fine particles, quickly transferring thermal energy to the containment atmosphere. In addition, metallic components of the sprayed core debris, mostly zirconium and steel, can react with oxygen and steam in the atmosphere to generate a large quantity of chemical energy, heating and pressurizing the containment still further. The term "direct containment heating" (DCH) is used in the present discussion to describe this complicated physical and chemical process.

Simple analyses of the containment heat balance indicate that even a large, dry containment of a PWR plant can be pressurized beyond its ultimate strength if a significant fraction of the core materials participate in DCH (Ref. 4.1). The peak containment pressure is normally attained within seconds after the melt ejection. A large amount of aerosols, including refractory fission products, could be generated in a high-pressure melt ejection (Ref. 4.2). If the containment should fail from the DCH loading, a massive release of radioactive materials could result.

Dispersing core debris could induce other hazards. If hydrogen existed in the containment atmosphere, dispersing hot debris particles could serve as a catalyst to promote recombination of the hydrogen with free oxygen even though the H_2 concentration may be below the conventional flammable limit. Hydrogen recombination will generate more energy to raise the pressure and the temperature in the containment. The issue would be further complicated if the reactor cavity is filled with water at the time of the reactor pressure vessel failure. The pressurized stream of molten core materials is likely to cause a steam explosion that may contribute to debris fragmentation and promote debris dispersion, at the same time generating dynamic loading on the containment.

Recently, both Brookhaven National Laboratory (Ref. 4.3) and Sandia National Laboratories (Ref. 4.4) predicted in their analyses that metallic components in the melt will be completely oxidized by steam in the reactor cavity region during high-pressure melt ejection (HPME). Such reactions would generate a large quantity of hydrogen that can readily mix in the containment atmosphere regardless of debris transport. Burning of this hydrogen could challenge the containment integrity (Ref. 4.5).

Other potential hazards associated with HPME/DCH that merit further investigation are containment liner abrasion, effects of high temperature on containment structure and equipment, and possible missile generation.

The risk of DCH is likely to be significantly different for BWR plants (Appendix J.5 of Ref. 4.6) because the automatic depressurization system may be used to depressurize the reactor coolant system. A large body of water in the suppression pool is believed by many to be able to moderate the effect of DCH. On the other hand, the containment volume is much smaller for the BWR plants so that much less corium is needed to pressurize and fail the containment. A BWR generally has a larger core and a higher zirconium content that favor DCH.

The containment of ice condenser plants has a smaller volume and a lower design pressure than a typical large, dry containment of PWR plants. Although it is generally recognized that ice chambers in the ice condenser plants are likely to trap and quench the bulk of the dispersing debris, hydrogen generated in the metal-steam reactions discussed above should be able to migrate through the ice chambers easily. Burning of such hydrogen in the ice chambers or in the upper compartment fail the containment (Ref. 4.7).

4.1.2 Important Subissues and Related Uncertainties

The ultimate concern of the DCH issue is whether the containment could fail and, if it could, what is the amount of airborne radioactive materials at the time of the containment failure. The consequences of DCH depend on a host of subissues that are discussed below.

4.1.2.1 Initial Conditions

The severity of DCH is highly dependent on the conditions inside the reactor vessel at the time of the vessel failure. These conditions are determined by the sequence and progression of the accident and must be provided by sources outside of HPME/DCH programs (such as Severe Accident Sequence Analysis and core melt progression programs).

1. Reactor Coolant System Pressure

   The reactor coolant system pressure provides the motive force for melt ejection and debris dispersion and affects the extent of disintegration and atomization of the melt jet. The reactor coolant system at a higher pressure generally stores more mass and energy that will be released to pressurize the containment in the event of a vessel failure. A higher reactor coolant system pressure will result in higher DCH. The reactor coolant system pressure is likely to remain near the PORV (power-operated relief valve) setpoint for a station blackout accident in a PWR but should be at a lower level that is determined by the break size in a small-break LOCA. The accumulator setpoint is the likely lower bound for this parameter. Once the reactor coolant system can be depressurized below this point, at which a large volume of water is available for flashing, the reactor pressure should fall very rapidly. The range of this parameter is therefore 600-2400 psig.

Recently, the possibility that natural circulation inside the reactor coolant system may induce a failure elsewhere on the primary boundary is being investigated (Appendix J.3 of Ref. 4.6). If the failure size is sufficient to depressurize the reactor coolant system before the core melt breaches the reactor vessel, HPME, and consequently DCH, will not take place. Preliminary findings of the investigation indicate that such failure is possible. These works, however, have not been subjected to an intensive peer review. It may be of interest to note that natural circulation was not in evidence during the core melt accident at Three Mile Island.

2. Melt Temperature

The melt temperature will determine the amount of thermal energy carried into the containment by core debris. It also affects transport properties of the melt, such as surface tension, viscosity, etc., that control the size of debris particles. Finer particles favor heat transfer and chemical reactions because of a higher surface-to-volume ratio. The melt temperature could range from the melting point of steel (1,800 K) to that of uranium oxide (3,100 K). A higher melt temperature will result in higher DCH.

3. Fraction of Core Melted and Ejected

The larger the amount of ejected core materials, the more severe DCH will be. A large uncertainty exists regarding the fraction of the core that would become molten at the time of the meltthrough. It is believed that this fraction is in the range of 20-80 percent of the reactor core (Appendix J.2 of Ref. 4.6).

4. Metallic Components in Melt

Portions of metals (zirconium and iron) in the melt are likely to have reacted with steam inside the vessel prior to the ejection. But a substantial amount of them could remain in metallic forms and be oxidized in the containment atmosphere. The higher the metal contents in the melt, the more chemical energy is available for DCH. At this moment, it is believed that anywhere between 20-80 percent of the zirconium and iron in the melt could remain unoxidized at the time of the vessel meltthrough (Appendix J.2 of Ref. 4.6).

Results of recent National Reactor Universal (NRU) tests seem to suggest that in-vessel metal oxidation may be very extensive for some accident conditions.

5. Dissolved Gas and Steam

Hydrogen and steam can be dissolved in the core melt as the accident progresses (Ref. 4.2). When the melt is ejected, the dissolved gas and steam will boil out, contributing to disintegration of the liquid jet and atomization of the melt. A higher content of dissolved gas and steam tends to break up the melt into finer particles that favor DCH and contribute to aerosol generation. Test data are scarce in the range of the reactor accident conditions.

6. Mode of Vessel Failure

It is assumed in most DCH studies that an instrument tube will fail at its weld to initiate the high-pressure melt ejection. There is, however, a controversy as to the possibility of multiple instrument tube failure. Even a circumferential break of the reactor pressure vessel is not ruled out. Results of High Pressure Melt Streaming (HIPS) tests at Sandia also confirmed the Zion Probabilistic Safety Study's prediction that the aperture will ablate and grow in size during the melt ejection (Ref. 4.8). The rate of hole ablation can be predicted fairly accurately, but the effect of such ablation on debris dispersal and DCH is difficult to quantify. Generally, a larger flow area will increase melt and gas discharge rates, and that tends to favor core debris dispersion and DCH.

4.1.2.2 Effect of Water

It is generally believed that core melt ejected from the reactor vessel can be quenched to moderate or mitigate DCH if water is available. Results of HIPS tests at Sandia seem to indicate that water in the reactor cavity may not be as effective in quenching the melt as was previously believed. In the two HIPS tests (HIPS-4W and -6W) conducted with a water-filled test cavity, a sharp pressure spike was produced in both tests immediately following the melt ejection (Ref. 4.9).

High-speed movies clearly showed that water was pushed out of the cavity by the pressure spike ahead of the dispersing core debris. The level of water in the reactor cavity can be determined by the analysis of a specific accident sequence for a given plant so that uncertainties regarding the availability of water are small; but the effect of the water on DCH is difficult to determine with the present state of understanding. Another effect of the water that merits further investigation is the possibility that ex-vessel steam explosions may promote fragmentation and dispersion of the core debris, thereby enhancing DCH.

4.1.2.3 Debris Transport

1. Mechanism of Debris Dispersal

Results of HIPS tests (Ref. 4.10) at Sandia suggest that entrainment of melt particles in a high velocity gas flow may be the dominant mechanism to disperse core debris out of the reactor cavity region. The situation, however, is very much different from the film entrainment in which liquid particles are stripped from the surface of a liquid pool or film. Disintegration and splashing on the cavity boundary of the melt jet could have created airborne melt particles that are ready to be carried forward in a gas stream.

2. Melt-Structure Interaction

Trapping of core debris particles by structures in and around the reactor cavity is generally considered to have a mitigating effect on DCH. Recent tests at Sandia (HIPS-7C and -8C) (Ref. 4.11), however, raised doubts about the effectiveness of shielding against debris dispersal provided by the structure. In HIPS-7C, the addition of a semienclosure at the exit of the cavity keyway that simulates the instrument shaft at the Zion plant did not seem to appreciably reduce dispersal of core debris out of the test cavity. In HIPS-8C, 25 to 30 percent of ejected materials was found dis-ersed up through a gap that simulates the annular gap around the reactor pressure vessel of the Zion plant. It is believed that melt particles impacted on a concrete surface will splash and bounce right back into the stream and be carried away if the local flow velocity is sufficiently high. When high-temperature, high-speed melt particles impact on a thin steel surface, the steel surface is likely to be ablated or even penetrated. Melt particles that are intercepted by a heavy steel structure could freeze on the surface of the steel. Thickness of the frozen layer is likely to be limited by the heat transfer at the interface. Frozen debris particles may behave differently.

3. Mixing of Debris Particles in Containment Atmosphere

   The extent of containment pressurization by DCH depends on how well the ejected core materials mix with the containment atmosphere. The better the mixing, the more complete the thermal and chemical interactions will be. The chemical reaction and heat transfer are most active when the debris particles are suspended in the air. Interaction with structure and equipment inside containment may affect the airborne time of the debris particles, thereby affecting the extent of DCH.

4. Ex-Vessel Metal-Steam Reactions

   Hydrogen generated in the ex-vessel metal-steam reactions discussed earlier can migrate relatively freely in the containment. Analyses showed that burning of such hydrogen could fail the containment under certain conditions. If confirmed by experiments, this consideration could change the perception regarding the mitigating effect of the structure.

4.1.2.4 Containment Atmosphere Composition

The atmospheric composition in the containment dictates the chemical reactions that the debris particles will be undergoing.

If the atmosphere is inerted by nitrogen (such as BWR Mark I containments), oxidation of metals will not take place. Only the thermal energy of the melt will contribute to DCH.

In the presence of steam, metal-water (steam) reactions will take place. Metal-water reactions take place at higher temperatures than oxidation in air and generate less energy, although hydrogen generated in metal-water reactions can later recombine to generate additional heat if oxygen is available. Steam concentration could range from that in the containment atmosphere during normal operation to 100 percent steam, which may be expected in the lower compartment of an ice condenser when it is completely purged by blowdown steam in certain accident conditions.

Possible recombination of pre-existing hydrogen by hot core debris sprayed into the containment atmosphere was discussed earlier. Hydrogen accumulated in the reactor coolant system will be added to the containment atmosphere when the reactor pressure vessel fails. Heat generated in burning such hydrogen will further pressurize the containment.

4.1.2.5 Aerosol Generation

In Sandia's System Pressure Injection Tests (SPIT) and HIPS tests, an intense cloud of aerosols was observed following each high-pressure melt ejection (Ref. 4.2). Data collected from SPIT-18 and -19 suggest that aerosols generated in a pressurized melt ejection could amount to 1 to 5 percent of the ejected mass. SPIT test samples indicate that aerosol sizes are bimodal: a fraction of a micron and several microns. It is believed that these aerosols are formed by two different mechanisms--condensation of vaporized materials and mechanical breakup of melt particles. Consequently, radioactive materials contained in these aerosols could include refractory as well as volatile fission products.

4.1.3 Review of Current Modeling

The Source Term Code Package does not include a containment code that calculates DCH. The Industry Degraded Core Rulemaking (IDCOR) program has been taking a position (Ref. 4.12) that DCH will not take place because they think structures around the reactor cavity would confine dispersal of core debris. Any debris dispersed out of the reactor cavity was assumed to be quenched by water. It is not known whether IDCOR has a containment code that can calculate DCH. Although they were invited to participate in DCH test calculations, they did not do so.

In the Containment Load Working Group's standard problem exercises (Ref. 4.13), all participants used a single node assumption and calculated mass and energy balances. Chemical reactions were assumed to be complete, thermal equilibrium was attained, and heat losses were neglected. When quenching of the core debris by water was considered, it was simply assumed that thermal energy of a portion of the core melt was expended in generating steam. Chemical energy in the quenched portion of the core melt was ignored.

Recently, several containment codes have adopted rate equations in what is otherwise a lumped-parameter approach to calculate chemical reaction and heat transfer more realistically. However, there is no existing code that can calculate core debris transport. The prospect for these codes to acquire capabilities to calculate rates of debris entrainment and dispersal, particle sizes, airborne time, etc., does not appear promising. However, the metal-steam reactions discussed above may moderate the need for such modeling.

4.2 Description of Past, Present, and Future Research

4.2.1 Past Research

The possibility that core debris could be swept out of the reactor cavity in a high-pressure ejection of core melt from the reactor vessel was first recognized in the Zion Probabilistic Safety Study (Ref. 4.8). While conducting System Pressure Injection Tests (SPIT, 1/20th linear scale) to confirm the debris dispersal, Sandia realized the possibility that thermal and chemical energy of the dispersed core debris may quickly heat and pressurize the containment

BEST COPY AVAILABLE

atmosphere. Sandia continued with larger scaled High Pressure Streaming tests (HIPS, 1/10th linear scale) (Ref. 4.10) to characterize core debris dispersal. SPIT-18 and -19 (Ref. 4.2) were conducted with an interaction chamber while all other tests were conducted outdoors. The Argonne National Laboratory has conducted 1/30th-scale tests (Ref. 4.12) under an Electric Power Research Institute (EPRI) contract independent of Sandia's activities. Argonne test results were included in the IDCOR Technical Report 85.2 and form the basis for IDCOR's position.

4.2.1.1 System Pressure Injection Tests (SPIT)

Nineteen tests were conducted in this series; but only the last two provided useful quantitative data. In SPIT-18 and -19 (Ref. 4.2), iron-aluminum thermite was used to simulate the core melt. A concrete cavity simulating 1/20th linear scale of the Zion reactor cavity was used in SPIT-19 while an alumina cavity was used as the test cavity in SPIT-18. The test apparatus was placed in a makeshift interaction chamber made of sheet metal construction with an estimated pressure rating of 3 psig. The melt generator was pressurized to 1,500 psig by nitrogen gas in both tests.

In SPIT-19, 95 percent of the ejected melt was dispersed out of the test cavity, while only 58 percent was dispersed in SPIT-18. The lower dispersal in SPIT-18 was attributable to higher heat loss, and consequently higher freezeup of the debris, in the alumina cavity. Measured pressure rises of 3.5 and 2 psi were not considered meaningful because the interaction chamber suffered substantial damages in both tests that resulted in large leakage. In SPIT-18, several anchor bolts were "pulled" through a 5-millimeter-thick steel plate causing gaps of 4 to 8 centimeters between the shell of the interaction chamber and its foundation. It was estimated that 1 to 5 percent of the ejected melt was aerosolized.

4.2.1.2 High Pressure Melt Streaming (HIPS) Test (Ref. 4.10)

The HIPS apparatus consists of a melt generator, a concrete test article that is a 1/10th linear scale model of the Zion reactor cavity. The experiment used a mixture of iron oxide and aluminum power to produce a melt by thermitic reaction to simulate molten corium in a core melt accident.

The melt generator was pressurized to a level ranging from 3.3 MPa (480 psia) to 11 MPa (1,600 psia) by either nitrogen or carbon dioxide. The HIPS tests concentrated on investigation of factors contributing to the mechanism of debris dispersal over a range of conditions.

A total of eight tests were conducted in the HIPS series. HIPS-4W and -6W (Ref. 4.9) were conducted with a water-filled test cavity while, in HIPS-7C (Ref. 4.11), structure was added at the exit of the test cavity to simulate the instrument shaft and the seal table areas of the Zion plant. In HIPS-8C (Ref. 4.11), the annular gap around the reactor vessel of Zion Unit 1 was simulated to investigate the potential for core debris dispersal directly into the upper containment dome via this gap.

In all tests, practically all molten materials ejected from the melt generator were dispersed out of the test cavity even at a pressure as low as 3.3 MPa (480 psia). The presence of water in the test cavity did not appreciably affect the fraction of dispersal. High-speed movies showed that a slug of water was expelled ahead of dispersing debris in both HIPS-4W and -6W. A pressure spike on the order of a thousand psi was measured in the cavity following the melt ejection. The reinforced concrete test cavity was destroyed in both tests, and in HIPS-6W the whole test facility was lifted 6 feet in the air.

No appreciable retention of debris was observed in HIPS-7C where the additional structure was expected to trap dispersing debris. In HIPS-8C, approximately one-third of the dispersed debris escaped through the annular gap. This fraction is roughly equal to the ratio of the flow area through the gap to the total outflow area, supporting the theory that the predominant mechanism for debris dispersal is entrainment by high-velocity gas flows. A large cloud of aerosols was observed in each HIPS test.

4.2.1.3 Argonne National Laboratory Experiments (Ref. 4.12)

The Argonne apparatus includes a thermite vessel representing the reactor pressure vessel, an interaction chamber to represent a reactor cavity, a pipeway simulating an instrument tunnel, and an expansion vessel simulating the containment. The interaction chamber, the pipeway, and the expansion chamber are all of steel construction. The experiment used materials composed of uranium dioxide, zirconium dioxide, and stainless steel to simulate the core melt. The molten materials were ejected into the interaction chamber by gas that was pressurized to a level ranging from 0.21 MPa (30.5 psia) to 5.7 MPa (826.5 psia). The scale of this facility is approximately 1/30th linear scale of the Zion plant configuration, but no attempt was made to maintain geometric similarity.

Argonne also conducted a separate series of tests using Wood's metal as the melt simulant to investigate the influence of the containment configuration outside the reactor cavity on the core debris dispersion. Wood's metal has a melting point of 73°C. The injection pressure used in this series of tests ranged from 0.25 MPa (36 psia) to 1.4 MPa (200 psia).

The corium tests showed a sweepout fraction of 1 to 60 percent and a peak pressure rise from 0.12 MPa (17.5 psi) to 0.38 MPa (55 psi). The temperature rise ranged from -4 to 50°C. These results do not include a contribution from oxidation of metallic components since the tests were conducted in an inerted expansion chamber atmosphere. The Wood's metal tests showed that the fraction dispersed out of the test cavity ranged from 10 to 90 percent.

4.2.1.4 Discussion of Experimental Results

Several considerations pertinent to the application of the test results are discussed below.

1. Scaling

   Generally speaking, any test results are valid only for the conditions under which the test is conducted. Extrapolation of test results is possible only to cases with physical similarities. It is imperative to conduct a scaling study if such extrapolation is contemplated. Sandia has provided a scaling study in their HIPS program plan, supplemented by calculations matching the Kutateladze number with postulated accident conditions in the Zion plant to preserve similarity in entrainment and

BEST COPY AVAILABLE

dispersion of core debris. IDCOR Technical Report 85.2 provided no scaling study that could provide guidance for the application of Argonne test results to reactor accident test conditions.

Recently Brookhaven National Laboratory conducted a scaling study and grouped variables that affect core debris dispersal into six dimensionless parameters. Theoretically, if a test can be designed that matches values of all six parameters to the reactor accident conditions, results of the test should be directly applicable to the reactor accident evaluation. In practice, matching more than one dimensionless parameter in a test is very difficult, if it is possible at all. Moreover, Brookhaven's scaling concerned only hydrodynamics of the debris dispersal; it did not consider chemical reactions and heat transfer. It did not even include the thermal effect on a compressible fluid flow.

2. Scale of Test Facility

HIPS attempted to simulate 1/10th linear scale of the Zion plant configuration and SPIT, 1/20th linear scale. Argonne's facility is approximately 1/30th linear scale of Zion. It is generally recognized that the surface-to-volume ratio increases as the scale of the test facility decreases (in 1/10th scale, ten times higher; 1/30th scale, 30 times higher, etc.). This increases the heat loss that promotes freezeup of melt particles. Debris retention in a small-scale test facility will, therefore, be increased and the fraction of dispersal decreased. The effect of disproportionately higher heat loss and debris retention should have been intensified by the all-steel construction of Argonne's test facility, which is not prototypical of commercial reactor plants. The increased surface-to-volume ratio in the small-scale facility also increases the flow resistance and decreases the duration of the blowdown from the reactor pressure vessel, both contributing to further reduce the debris dispersal. For the same reason, Sandia's test results are also believed to underpredict, albeit to a lesser degree, the core debris dispersal.

It should be noted that, in a small-scale facility, the dispersing debris will have a shorter "mean flight path." Airborne time, during which the debris undergoes vigorous chemical and thermal interactions with the atmosphere, is reduced accordingly.

3. Test Pressure

Entrainment of debris particles in a high-velocity gas stream appears to be the predominant mechanism for the dispersal of core debris out of the reactor cavity. The extent of core debris dispersion, therefore, depends on the momentum flux of the gas flow which, in turn, depends on the pressure in the melt vessel. From the above discussion on the scale of the test facility, it is apparent that the test pressure should be slightly more than that in the reactor pressure vessel that the test is simulating to provide an equivalent condition for entrainment and debris dispersion. Test pressures for SPIT and earlier HIPS tests at Sandia are in the range of the reactor coolant system pressure discussed in Section 4.1.2.1. Later HIPS test pressures skirted the lower end of this range. All the Argonne tests, except two corium tests, were conducted with injection pressures substantially below the lower bound (600 psig) of the above-mentioned reactor coolant system pressure range; some were conducted at a pressure as low as 1 bar above atmospheric pressure.

4. Effect of Structure

It is recognized that structures around the reactor cavity could affect the core debris dispersal; the question is "how?" In addition to the smaller scale and lower test pressures discussed above, the Argonne test configuration also lacks geometric similarity with any operating commercial reactor plant. The flow field in and around the interaction chamber and pipeway in the Argonne tests, therefore, is not similar to that expected around the reactor cavity of a nuclear plant during the postulated reactor accident. Consequently, it is difficult to relate these test results to a reactor accident. Sandia has conducted HIPS-7C with a scaled concrete structure simulating the instrument shaft and the seal table at the exit of the Zion reactor cavity. HIPS-7C yielded no measurable difference in the fraction of debris dispersal. The situation could be significantly different in the presence of heavy metal pieces such as structural steel or equipment. Substantial freezeup of the melt particles may be possible on the surfaces of these pieces, especially if they are located in areas of considerable flow deceleration. It must be cautioned that the problem associated with the higher surface-to-volume ratio that is inherent in a small-scale facility will be worsened with additional structures. Some provision to compensate for this effect is needed in the design of tests to investigate the trapping effect of the structure.

5. Effect of Water

In both the tests at Sandia and the corium tests at Argonne that were conducted with a water-filled test cavity, the water was observed to be ejected out of the cavity as a slug ahead of the dispersing debris. Complete mixing of debris with water, therefore, was not observed in the test cavity and in flight. Quenching of debris by the water in the test cavity appeared much less than that assumed in many analyses. The Sandia HIPS tests were conducted outdoors so that no observation was made on the possible interaction with the structure of the water slug and debris swept out of the reactor cavity. Corium test results at Argonne showed that a pool of water on the floor of the expansion chamber (simulating reactor containment) can mitigate direct heating of the expansion chamber atmosphere. The nonprototypical arrangement in the Argonne test configuration where the stream of debris is directed horizontally and downward toward the water pool has not yet been satisfactorily explained. Wood's metal tests are of little value in the assessment of the effect of water.

6. Chemical Reactions

The atmosphere of the expansion chamber was inerted in the Argonne corium tests. This excluded the chemical energy of metal oxidation from heating the containment.

4.2.2 Present Research

Two experimental programs are ongoing; the Surtsey direct containment heating test program at Sandia and the separate-effect test program at Brookhaven National Laboratory.

4.2.2.1 Surtsey Direct Containment Heating Tests

Surtsey is a steel vessel that is approximately 33 feet high and 12 feet in diameter. Its designed maximum working pressure is 150 psig. The vessel has an internal volume of approximately 3,600 cubic feet that is adequate to simulate the volume of a 1/10th linear scaled large, dry PWR containment. Eleven tests are currently scheduled for the Surtsey/DCH series (Table 4.1). The first two of the eleven tests have been completed (DCH-1 in June 1986 and DCH-2 in October 1986). Preliminary observations of these test results confirmed substantial pressurization and aerosol generation in the vessel. Analyses of the test results are continuing.

4.2.2.2 Separate-Effect Tests

The program at Brookhaven will investigate subissues that are important to DCH but are either too difficult or too expensive to be studied in the Surtsey facility. An example of such a subissue is the core debris dispersal. The high-temperature (2,500 K) melt simulant used in Surtsey tests makes it difficult to observe trajectories of dispersing debris. Many tests will be needed to study sensitivities of the debris dispersal to various conditions predicted for different accident scenarios. The relatively high cost of Surtsey tests makes it impractical for such studies. The initial phase of the Brookhaven program includes construction of 1/40th-scale transparent models, using Plexiglass, of Zion, Surry, and Watts Bar reactor cavities and major structures around the cavities.

Water and Wood's metal will be used as melt simulants to study debris transport. It is expected that the Brookhaven tests can identify physics important to analytical modeling of the debris transport and provide a data base for such modeling.

4.2.3 Program Strategy

In view of the complexity of the DCH process, it is highly unlikely that a small-scale experiment can be designed that preserves geometrical, physical, and chemical similarities with postulated commercial reactor accident conditions. Small-scale integrated tests, therefore, are not very meaningful because the results cannot be related to the reactor accidents. Full-scale mockup tests, of course, are not feasible.

The plan to resolve the issue of DCH is to build up, from the Sandia and Brookhaven experimental programs, data bases that are needed for developing analytical models simulating physical and chemical phenomena important to DCH. These models will be incorporated in existing containment codes to analyze the consequences of HPME/DCH in operating reactor plants. These models will be validated against new test data from time to time to reduce uncertainties. Refinement of the models will be brought about as necessary.

74

Table 4.1 Direct containment heating test matrix for Surtsey direct heating facility.

Test	Characteristic
1	Small mass (20 kg)
2	Large mass (80 kg)
3	Surry cavity
4	In-containment structures
5	Defined flow paths
6	Inert atmosphere
7	Air, steam, and H_2
8	Water sprays
9	Corium melt
10	Water-filled cavity
11	Shallow water pool

4.2.4 Future Research

4.2.4.1 Phenomenological Research

As our understanding of the process improves, additional subissues that could have a major impact on the outcome of DCH begin to surface. Additional research will be needed to investigate these subissues. A few such subissues have already been identified.

1. Ex-Vessel Metal-Steam Reactions

   Both Brookhaven and Sandia calculated that metal contents in dispersing core debris could be completely oxidized by steam blown down from the reactor pressure vessel before the debris leaves the reactor cavity region. Hydrogen generated in such reactions can readily be transported, regardless of the debris dispersal, and burn in other parts of the containment.

Because this finding could change the belief that DCH can be moderated or mitigated by containment structures that intercept and trap the melt particles, it is recommended that tests be conducted to confirm and quantify these reactions.

Related subissues include the burning of hydrogen in a high-temperature atmosphere and the catalytic effect of hot debris particles in promoting hydrogen recombination.

2. Ex-Vessel Steam Explosion

In both HIPS-4W and -6W tests, where the melt was ejected into a water-filled cavity, violent steam explosions took place that destroyed the test cavities. Steam explosions associated with high-pressure melt ejection are believed to be more intense than when the melt is ejected under gravity because, in the HPME, ejected melt is likely to be atomized, increasing the surface area available for heat transfer. In addition to generating dynamic loading and possibly missiles, the steam explosion could further fragment the debris and enhance its dispersal. It is planned that measurements for steam explosions will be added to those Surtsey tests with a water-filled cavity. Additional tests will be proposed if the measurements clearly indicate the need for additional and more comprehensive tests.

3. Melt Simulants

Neither iron-aluminum thermite used in the Sandia tests nor corium thermite used in the Argonne tests are representative of molten core materials expected in a severe accident. The use of different melt simulants has an impact on (1) the melt temperature that affects aerosol generations and transport, (2) thermal and chemical energy contents, and (3) transport properties of the melt that affect mixing and interactions of debris in the containment atmosphere.

4.2.4.2 Analyses

The CONTAIN code, together with DHEAT and IDHM (Ref. 4.5), has been used to conduct extensive sensitivity studies of DCH in Surry and in Sequoyah. Results of these studies were referenced in formulating staff positions in NUREG-1150 (Ref. 4.6). DHEAT is an abbreviated version of CONTAIN, while IDHM is an addition that enables CONTAIN, a lumped-parameter code, to analyze the rate-sensitive DCH process. The University of Wisconsin is using the HMC code to analyze DCH. HMC is a union of three existing codes--HECTR, M1, and CORCON. Other participants in DCH test calculations include DHCVIM by Brookhaven and a still unnamed code by Argonne.

All the above discussed codes are lumped-parameter in nature. Each code includes rate equations for chemical reactions and heat transfer, but assumptions had to be made regarding the core debris transport in order to analyze DCH. Among others, each code requires user input for the mean flight path, the debris airborne time, or some other equivalent parameter that is highly dependent on plant geometries and configurations. It is worth noting that the value of this quantity calibrated on one facility is not likely to be applicable to another facility. Debris transport is one problem that lumped-parameter codes are not likely to be able to solve. Additional research is needed in this area.

4.3 Technical Uncertainty Evaluation

The RES staff's best estimate of uncertainties regarding this issue is provided in the annex to this chapter. This estimate represents our present state of understanding. Ongoing research is expected to provide additional insights that could narrow these uncertainties. We understand that the NRR staff has a different view on the range and the degree of belief of some parameters. Their view is presented in Position Paper J.5 of Appendix J to NUREG-1150 (Ref. 4.6).

4.3.1 Uncertainties Expected To Be Reduced by Current Program

Uncertainties associated with initial conditions of HPME will be addressed by other research programs such as Severe Accident Sequence Analysis, core melt progression, and natural circulation inside the reactor coolant system. Technical uncertainties that this program will seek to reduce include those associated with containment heating and pressurization, aerosol generation, and airborne aerosol concentration as a function of time. Experimental programs at Sandia and Brookhaven are expected to provide data bases needed for such exercises.

4.3.1.1 DCH tests in Surtsey Facility

The experiments in the Surtsey facility at Sandia are the mainstay of the DCH research program. By the end of FY 1988, all tests included in Table 4.1 are expected to be completed. Results of these tests will contribute to substantially reduce uncertainties regarding:

1. Rates of chemical reactions and heat transfer,

2. Effect of water, both from the pool water and from suspended water droplets in the containment atmosphere,

3. Effect of structures on core debris dispersal and DCH, and

4. Aerosol generation and transport.

4.3.1.2 Separate-Effect Tests at Brookhaven

Currently, activity at Brookhaven is concentrated on the study of the effect of three different plant configurations (Zion, Surry, and Watts Bar) on the debris dispersal. Results of Brookhaven tests are expected to reduce uncertainties in the following areas:

1. Influence of different reactor cavity designs on core debris dispersal,

2. Effects of structures outside the reactor cavity on core debris dispersal,

3. Sensitivities of debris dispersal to the ejection pressure,

4. Flow fields of the gas-debris mixture in various scaled containment configurations, and

5. Scaling to extrapolate results of small-scale tests for assessment of risk associated with debris dispersal in commercial plants.

4.3.2 Programs Needed To Further Reduce Uncertainties

Areas in which significant uncertainties may still remain at the end of the current program were discussed in Section 4.2.4. The following programs are recommended to reduce these uncertainties.

4.3.2.1 Ex-Vessel Metal-Steam Reactions

An experimental program is needed to confirm oxidation of zirconium and iron in a steam-inerted containment atmosphere and to quantify the rate of hydrogen generation. An additional program is needed to investigate burning of hydrogen at elevated temperatures and in the presence of hot debris. It is believed that hydrogen could behave very differently under these extreme conditions. Chemical reactions are also likely to be more vigorous.

4.3.2.2 Ex-Vessel Steam Explosions

Programs are needed to quantify the intensity of steam explosions initiated by HPME and their effects on fragmentation and dispersal of core debris. If the results of the above programs indicate that the effects of ex-vessel steam explosions could be substantial, additional programs will be needed to quantify these effects--especially the dynamic effect on the containment structure and the possible impact on DCH.

4.3.2.3 Analysis

No computer code currently available for DCH analyses can calculate debris transport, and the prospect that a lumped-parameter code may acquire such capability is not very promising. This is because the debris transport is basically a three-dimensional, two-phase flow problem while the lumped-parameter code is essentially one dimensional. A program is needed to develop additional sophistication in the analytical tool to handle this subissue.

4.3.2.4 Melt Simulants

A couple of tests will be needed to resolve this issue using a melt, generated by induction heating, of the composition predicted by the best available core melt progression analysis. This is a state-of-the-art undertaking that will require a certain lead time to develop the technology. Either relocation of the existing Large Melt Facility or installation of a new melt furnace will be needed.

4.4 Implementation of Research Results

It appears premature at this moment to discuss implementation of research results because the issue is highly controversial and uncertainties are large. Many people are still debating whether the high-pressure melt ejection could take place at all. Even granted that high-pressure melt ejection could take place, considerable uncertainties still exist regarding potential mitigating effects of the containment structures and of the water on the floor or suspended in the containment atmosphere. Until such time when the technical community agrees on these considerations, it may not be appropriate to consider implementation of the research results in the regulatory sense. Regardless of the regulatory decision, results of the research will be incorporated in analytical tools such as CONTAIN as new knowledge becomes available. Such tools can then be used to calculate subsequent tests and, when needed, to analyze the hazard of DCH at operating plants.

4.5 Summary

The issue of HPME/DCH is highly controversial. It has the potential to significantly change the risk profile of operating reactor plants. At the extreme conditions, the containment could fail at a time when a large concentration of radionuclides is airborne. This relatively new issue has large uncertainties regarding the possible consequences, mainly because of the lack of data bases needed to quantify the effect of complicated, interacting variables.

The biggest uncertainty concerns the initial conditions of high-pressure melt ejection. There is a belief, supported by some code calculations, that natural circulation inside the reactor coolant system could induce a failure elsewhere in the reactor coolant system boundary to depressurize the system before the core melt breaches the bottom head of the reactor vessel (Appendix J.3 to Ref. 4.6). HPME, therefore, would not take place in this scenario. There is considerable uncertainty in this concept also, and evidence is not conclusive at this moment to obviate the concern for DCH. In any event, it may be a questionable proposition to depend on an uncontrollable failure of a safety-related system to mitigate an accident of this magnitude. Other initial conditions, such as the melt temperature, fraction of the core melted, and unoxidized zirconium content in the melt are also highly uncertain. It is hoped that further investigation in the area of core melt progression (Appendix J.2 to Ref. 4.6) can help narrow these uncertainties.

Trapping the melt particles by containment structures and quenching the core debris by water are believed to be the two most promising means of mitigating DCH, given HPME. They remain to be confirmed by experiments. Major uncertainties are debris transport, ex-vessel metal-steam reactions, and ex-vessel steam explosions. A broad data base is needed to develop analytical tools for best-estimate analyses.

Annex

ISSUE UNCERTAINTIES

Figure 4A.1 is the result of DHEAT code analyses (Ref. 4.14) for the Containment Load Working Group (CLWG) Standard Problem #2. It will be used as the basis for our estimation of uncertainties in the pressure rise in Surry containment due to DCH. Sensitivities of the pressure rise to changes in the value of various parameters suggested in Table 4A.1 are an approximation from results of later DHEAT analyses. Ranges, degrees-of-belief, and sensitivities provided in Table 4A.1 (Appendix J.5 to Ref. 4.6) were then sampled by a Latin hypercube procedure (Refs. 4.15, 4.16, and 4.17) to compile a composite total pressure versus probability curve that is shown on Figure 4A.2.

80

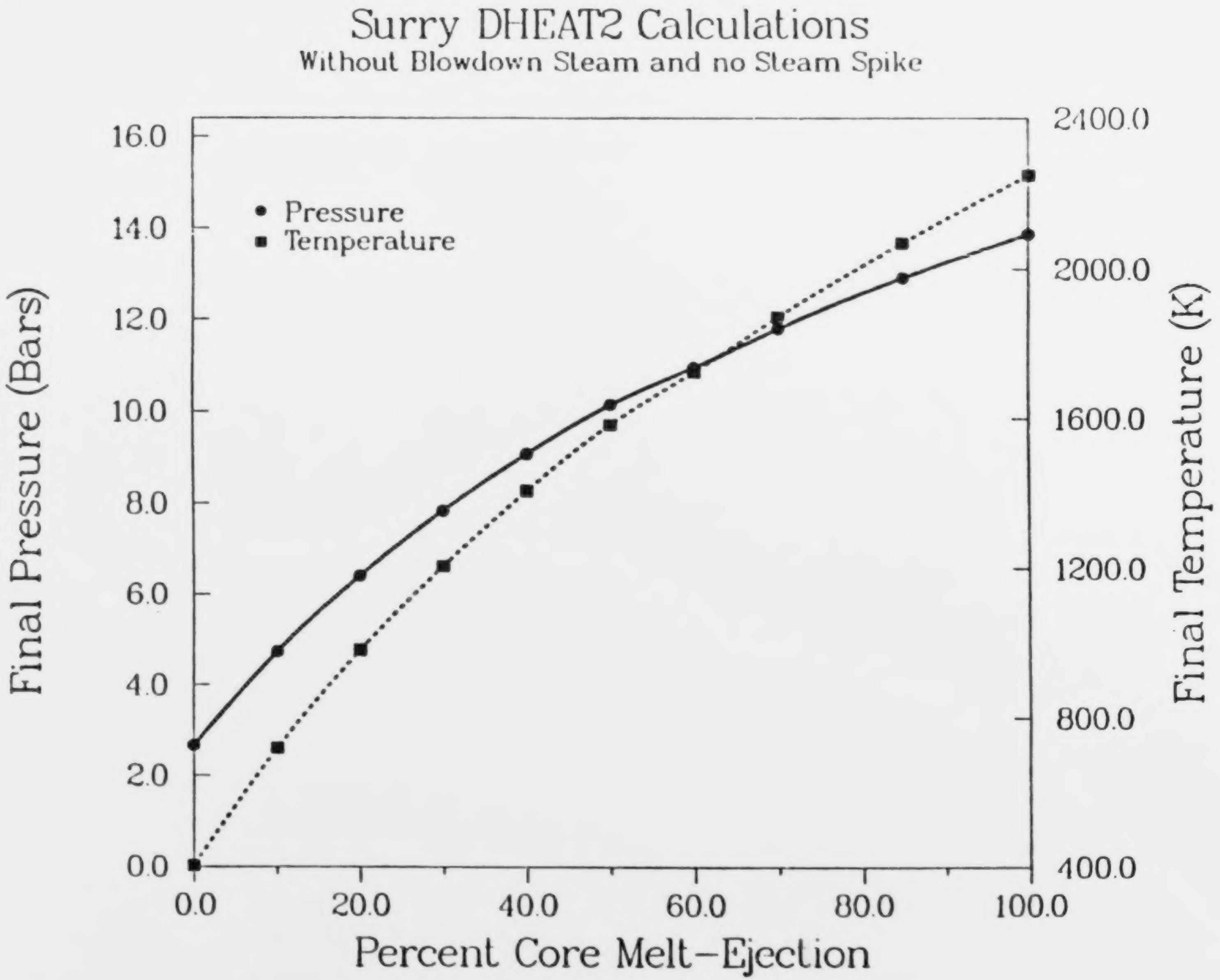

Figure 4A.1 Surry DHEAT2 calculations.

Table 4A.1 Surry direct containment heating (input for statistical analysis of pressure rise versus probability).

1. Reactor Coolant System Pressure (0-2400 psig)

Range	Degree-of-Belief (DOB)
1,000 psig and up	0.1
600 - 1,000 psig	0.2
below 600 psig	0.7

Sensitivity: Considered here is only the effect of the reactor coolant system steam inventory on containment pressurization. Linear interpolation has been used for intermediate values.

Add (+) 18 - 25 psi $= F_1$
for the range 0 - 2,400 psig

2. Melt Temperature (1,800 - 3,100 K)

Range	DOB
2,500 - 3,100 K	0.2
2,300 - 2,500 K	0.65
1,800 - 2,300 K	0.15

Sensitivity

Multiply (x) 0.85 - 1.10 $= F_2$
for the range 1,800 - 3,100 K

3. Fraction of Core Melted and Ejected (20 - 80%)

Range	DOB
60 - 80%	0.3
50 - 60%	0.5
20 - 50%	0.2

Sensitivity

No correction from Figure 4A.1. Value read from Figure 4A.1 = P_3

Table 4A.1 (continued)

4. Unoxidized Metal Contents in Melt (20 - 70%)

Range	DOB
55 - 70%	0.25
40 - 55%	0.5
20 - 40%	0.25

Sensitivity

Multiply (x) 0.8 - 1.0 = F_4
for the range 20 - 70%

5. Effect of Water (0 - 50% quenched)

Range	DOB
0 - 15%	0.3
15 - 30%	0.4
30 - 50%	0.3

Sensitivity

Multiply (x) 1.0 - 0.85 = F_5
for the range 0 - 50%

6. Effect of Structure (75 - 100% dispersed)

Range	DOB
90% and up	0.85
75 - 90%	0.1
below 75%	0.05

Sensitivity

Multiply (x) 0.85 - 1.00 = F_6
for the range 75 - 100%

7. Completeness of Thermal and Chemical Interactions (50 - 95%)

Range	DOB
85 - 95%	0.25
70 - 85%	0.6
50 - 70%	0.15

Table 4A.1 (continued)

Sensitivity

Multiply (x) 0.63 - 0.97 $= F_7$
50 - 95%

8. Hydrogen Recombination (0 - 6% H_2 by volume)

Range	DOB
5 - 6%	0.2
2 - 5%	0.6
0 - 2%	0.2

Sensitivity

Multiply for the range (x) 1.0 - 1.23 $= F_8$
0 - 6% H_2

Estimated Peak Pressure

$P_{max} = P_3 \times F_2 \times F_4 \times F_5 \times F_6 \times F_7 = F_1 = P_o (F_8 - 1)$

$P_o = P_3$ at 0% core fraction = 2.67 bars (Fig. 4A.1)

BLANK
PAGE

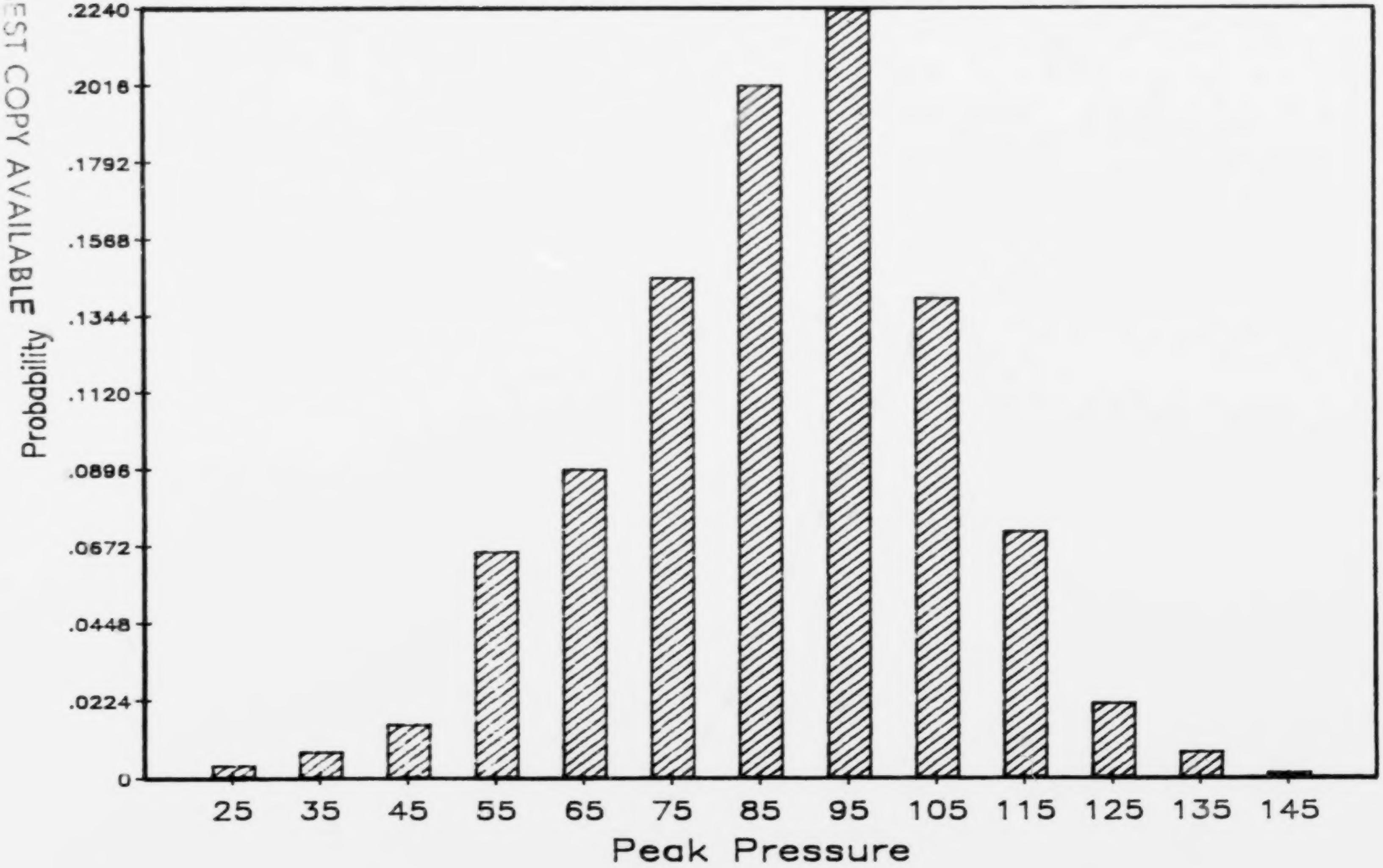

Figure 4A.2 Estimated peak pressure in direct containment heating for Surry.

85

REFERENCES FOR CHAPTER 4

4.1 K. D. Bergeron and D. C. Williams, "CONTAIN Calculation of Containment Loading of Dry PWRs," Nuclear Engineering and Design 90, 1985.

4.2 W. W. Tarbell et al., "Pressurized Melt Ejection Into Scaled Reactor Cavities," Sandia National Laboratories, NUREG/CR-4512, SAND86-0153, October 1986.

4.3 Brookhaven National Laboratory, "Safety Research Programs Sponsored by Office of Nuclear Regulatory Research," Quarterly Progress Report, July - September 1985, NUREG/CR-2331, Vol. 5, No. 3, BNL-NUREG-51454, March 1986.

4.4 D. C. Williams et al., "Impact of Chemical Phenomena in Direct Containment Heating," Proceedings of American Chemical Society Severe Accident Chemistry Symposium (Anaheim, CA), September 8-12, 1986.*

4.5 K. D. Bergeron et al., "Development and Application of the Interim Direct Heating Model for the CONTAIN Computer Code," Proceedings of the U.S. Nuclear Regulatory Commission Fourteenth Water Reactor Safety Information Meeting, NUREG/CP-0082, Vol. 6, February 1987.

4.6 U. S. Nuclear Regulatory Commission (USNRC), "Reactor Risk Reference Document," NUREG-1150, Vol. 3, Draft Report for Comment, February 1987.

4.7 K. Bergeron, Sandia, letter to M. Silberberg, USNRC, dated September 2, 1986.*

4.8 Commonwealth Edison Company of Chicago, "Zion Probabilistic Safety Study," September 1981.*

4.9 W. W. Tarbell et al., "Behavior of Core Debris Ejected From a Pressurized Vessel Into Scaled Reactor Cavities," Proceedings of the U.S. Nuclear Regulatory Commission Twelfth Water Reactor Safety Research Information Meeting, NUREG/CP-0058, Vol. 3, January 1985.

4.10 W. W. Tarbell et al., "High-Pressure Melt Streaming (HIPS) Program Plan," Sandia National Laboratories, NUREG/CR-3025, December 1984.

4.11 W. W. Tarbell et al., "Melt Expulsion and Direct Containment Heating in Realistic Plant Geometries," Proceedings of the International ANS/ENS Topical Meeting on Thermal Reactor Safety (San Diego, CA), American Nuclear Society, February 1986.

4.12 Fauske and Associates, Inc., "IDCOR Technical Report 85.2: Technical Support for Issue Resolution," Atomic Industrial Forum, July 1985.

4.13 USNRC, "Estimates of Early Containment Loads from Core Melt Accidents," NUREG-1079, Draft Report for Comment, December 1985.

---

*Available in the NRC Public Document Room, 1717 H Street, NW., Washington, DC.

86

4.14 K. Bergeron, Sandia, letter to T. Lee, USNRC, "DHEAT2, Parametric Calculations," dated June 23, 1986.*

4.15 R. Iman and W. Conover, "Sensitivity Analysis Techniques: Self-Teaching Curriculum," Sandia National Laboratories, NUREG/CR-2350, SAND81-1978, June 1982.

4.16 M. McKay, W. Conover, and R. Beckman, "A Comparison of Three Methods for Selecting Values of Input Variables on the Analysis of Output From a Computer Code," *Technometrics*, Vol. 21, pp. 239-245, 1975.

4.17 R. Iman and W. Conover, "The Use of the Rank Transform in Regression," *Technometrics*, Vol. 21, No. 4, pp. 499-509, 1979.

---

*Available in the NRC Public Document Room, 1717 H Street, NW., Washington, DC.

5. CORE-CONCRETE INTERACTIONS

S.B. Burson

5.1 Introduction

In those accident scenarios in which the reactor vessel fails, high-temperature core debris may fall into the reactor cavity where it interacts with structural concrete. The consequences of these thermal and chemical core-concrete interactions may significantly impact containment loading, the mode of containment failure, and the radiological source term. This chapter is concerned with the prediction of potential risk-related consequences of core-concrete interactions and quantification of the uncertainties associated with them.

5.1.1 Qualitative Characteristics of Core-Concrete Interactions

5.1.1.1 Composition of Reactants

Neither of the reactants, core debris or concrete, has unique compositions; both depend on the structural details of each particular power plant. The initial debris composition depends on the details of the accident scenario leading to the core meltdown and on the particular reactor design, e.g., BWRs typically have a significantly higher inventory of zirconium than do PWRs. The fission product inventory depends on the power history of the plant and the details of the in-vessel core-degrading events that precede vessel failure. The composition of concrete varies widely; the chemical composition of any particular concrete as well as certain material properties, such as specific heat, ablation temperature, and enthalpy of ablation, must be known.

5.1.1.2 Sources and Sinks of Heat

There are three major sources of energy that heat the debris pool: (1) sensible and latent heat brought down by the debris when it exits the vessel, (2) decay power from the fission products in the debris, and (3) heat from exothermic chemical reactions (such as oxidation of liquid metallic iron and zirconium by water vapor) that accompany the core-concrete interactions. The initial fission product inventory present in the intact core can be computed from various burnup codes such as ORIGEN. The fraction of the inventory released during core degradation, prior to vessel failure, depends on the accident scenario. When exposed to water vapor, carbon dioxide, and other oxidants released from the decomposing concrete, molten metallic constituents may contribute significant chemical heat of reaction to the pool. On the other hand, the thermal decomposition of concrete is highly endothermic and constitutes a major sink for the energy being released by the decay power of the fuel. In addition, certain chemical reactions that occur in the debris pool are also endothermic. Finally, in addition to the inherent heat capacity of the concrete and other structural materials, there are massive components (pumps, motors, valves, overhead cranes, etc.) present in the containment that absorb heat and tend to reduce the rate at which the temperature of the system can be elevated.

5.1.1.3 Significant Phenomena

At high temperatures (approximately 1,300-1,500°C), concrete decomposes; the ablation products commonly include water vapor and carbon dioxide as well as refractory oxides such as CaO and SiO_2. The liquefied oxidic components of the concrete mix with the uranium oxide fuel and metallic oxides of the debris. Typically, the core debris is initially all or partially molten; gases released at the debris-concrete interface bubble through the debris pool. Some of the gaseous components, e.g., H_2O and CO_2, may react chemically with the debris while others escape from the pool surface and enter the containment atmosphere directly. Some of the gases (H_2 and CO) are highly combustible and, when burned, contribute to containment loading. As the bubbles break at the surface, aerosols are formed due to vapor condensation and film rupture. These aerosols contain nonradioactive components as well as radioactive fission products that contribute to the radiological source term.

The major issue under consideration here is the nature and magnitude of containment loading, as well as characterization of the ex-vessel radiological source term attributable to refractory fission products released from the core debris during core-concrete interactions. In the analysis of core-concrete interactions, quasi-steady-state conditions are assumed; transient phenomena are not treated. In particular, thermal detonation phenomena (steam explosions) are disregarded. It has long been acknowledged that such energetic events may occur either at the time core debris flows into a flooded cavity or during later flooding. However, in the event of such interactions, the phenomenological modeling treated in this chapter clearly becomes inapplicable. In addition to the magnitudes of these variables (containment loads and source terms), a knowledge of the uncertainty bands associated with them is necessary to formulate credible evaluations of the potential risk consequences in terms of reactor regulation.

In the following sections, the significance of the phenomena briefly outlined in the foregoing paragraphs is analyzed with respect to a variety of hypothetical accident scenarios. The most significant possible consequences of core-concrete interactions are described in Section 5.1.2. The computer codes that describe the core-concrete interactions are described in Section 5.1.3. The nature of possible sources of uncertainty in code predictions of core-concrete interaction phenomena are discussed in Section 5.1.4.

5.1.2 Potential Consequences of Core-Concrete Interactions

The potential consequences of core-concrete interactions that may impact containment loading and/or the radiological source term are classified into five categories in Table 5.1.

The possible relevance of each category must be determined for each case being analyzed. In all cases, the degree of relevance will depend on the structural design of the particular plant and the accident scenario under consideration. For each plant-scenario combination, all the potential consequences should be examined for possible significance with respect to the ultimate risk.

5.1.2.1 Radioactive and Inert Aerosol Release from Core Debris

The debris pool comprises large amounts (many tons) of nonradioactive materials, e.g., steel and other metals from the reactor vessel and core support structures,

BEST COPY AVAILABLE

Table 5.1 Potential risk-related consequences of core-concrete interactions.

---

1. Radioactive and Inert (nonradioactive) Aerosol Release from Core Debris
    - Ex-vessel radiological source term
    - Plugging of filters and vents
    - Containment atmosphere heating
2. Combustible Gas Generation (H_2 and CO)
    - Containment overpressurization from burning
3. Noncondensible Gas Generation (H_2, CO, and CO_2)
    - Containment overpressurization
4. Convective and Radiative Heat from Debris Pool Surface
    - Containment atmosphere heating
    - Thermal attack on structures
    - Thermal attack on engineered safety features
5. Erosion of Concrete and Other Structures
    - Basemat penetration (radiological source term)
    - Direct attack on structures (e.g., reactor pedestal)
    - Direct attack on engineered safety features (e.g., drywell liner)

---

control rod materials, and refractory byproducts of concrete decomposition. The radioactive species, neutron-activated structural materials, and fission products that were accumulated in the fuel contribute much less material to the total pool mass. The generation of aerosols at the debris pool surface is augmented by the concrete-decomposition gases that bubble through it. At these high temperatures, an equilibrium mixture of the vapor phases of all the components present in the pool is quickly reached within any individual bubble. These vapors include contributions from the inert bulk materials of the pool as well as radioactive fission products that are dissolved in it. The character of these nonradioactive aerosols is also extremely important. Their presence in the bulk aerosol cloud strongly impacts the rate of agglomeration, gravitational settling, etc., which in turn directly influence the properties of the time-dependent source term.

When the bubbles break at the surface, the trapped vapors are convected away into the atmosphere where they cool and condense to form aerosols. These condensation aerosols are very small, typically of submicron size. In addition, as the bubbles penetrate the surface, a thin film of the bulk pool material forms and fragments into fine droplets when the bubbles rupture. Upon cooling, these droplets freeze into particles that are also swept away as aerosols. These mechanically formed aerosols are typically larger in size, approximately 10 microns in mean diameter. Both forms of aerosols must be characterized as to chemical composition, shape, and particle-mass distribution. The ultimate behavior of these aerosols as they are transported away from the debris pool can then be analyzed by various containment and aerosol behavior codes such as CONTAIN, NAUA, QUICK-M, and a number of other similar codes being used in other countries.

If there is an overlying layer of water above the core debris, aerosol release to the containment atmosphere may be significantly attenuated. This effect has been demonstrated in a number of experiments. The decontamination factor (the factor by which the aerosol concentration leaving the debris is reduced by the water) depends on the depth of the pool, temperature, and a number of other variables. The decontamination factor also depends on the aerosol properties, i.e., particle size distribution, shape, density, etc. This decontamination process accentuates the degree to which source term predictions are dependent upon the accident scenario. In most cases where contributions to the ex-vessel radiological source term are attributable to core-concrete interactions, the processes described in this section are dominant.

5.1.2.2 Potential Consequences of Combustible Gas Generation

As gases (largely H_2O and CO_2) from the decomposing concrete pass through the debris pool, they react chemically with metallic constituents to form combustible gases (H_2 and CO). If not ignited, the combustible gases contribute to pressure loading as described in Section 5.1.2.3 below. If burning occurs, the exothermic reactions elevate the containment atmosphere temperature, which creates a pressure pulse. However, examination of the chemical reactions that govern the combustion shows that the total gas volume (at the same temperature as the original mixture) is reduced by the burning. The transport, mixing, and combustion of flammable gases are not considered in this chapter. Only the generation of combustible gases as a result of core-concrete interactions is treated.

5.1.2.3 Pressure Loading of Containment by Noncondensible Gases

The fraction of concrete mass that is converted into gas by thermal ablation depends on the composition of the concrete. For concretes made primarily of limestone aggregates, the gaseous decomposition products may carry away over 40 percent of the total initial mass. Highly basaltic concretes containing mostly SiO_2 (typical of German reactor construction) produce much less gas (10% or less of the initial mass) upon decomposition. The gas content of typical U.S. limestone/common-sand concretes is somewhere between these two extreme values. For example, in the case of limestone/common-sand concrete, approximately one-fourth of the original mass will become gaseous reaction products, primarily water vapor and carbon dioxide. As they bubble through the debris pool, these may then react with liquid metals to form H_2 and CO. The mass of unreacted water vapor will enter the containment atmosphere and may or may not condense, depending on prevailing thermal-hydraulic conditions.

The H_2, CO, and CO_2 are noncondensible and contribute directly to containment pressure loading. The contribution can be computed directly from the gas laws, the atmosphere temperature, and the containment free volume. Considerable data concerning the decomposition products of concrete exist. However, the prediction of the relative abundance and rates of generation of the various species of gas leaving the debris pool depend in large measure on the ability to model the chemical phenomena that are responsible for modifying the decomposition

BEST COPY AVAILABLE

911

gases after they leave the concrete. The chemical oxidation processes are particularly important for BWRs because of the high zirconium inventory in the core. Liquid zirconium is extremely active and its oxidation highly exothermic so that, during the reaction, debris temperature may be significantly elevated resulting in accentuated fission product release.

5.1.2.4 Contribution to Containment Overpressurization Resulting from Atmospheric Heating

As energy leaves the debris pool in the form of high-temperature gases, hot aerosols (a highly efficient mechanism for heating the atmosphere), and electromagnetic radiation, it must be absorbed by the surroundings. A quasi-steady-state equilibrium will be established between the heat flux from the pool, the atmosphere temperature, and the energy flux to available heat sinks. Structures in the line of sight of the pool are heated by radiation and contribute indirectly to elevating the containment atmosphere temperature. The rise in atmosphere temperature is accompanied by a corresponding increase in pressure loading of the containment. The magnitude of these effects depends on the power of the heat source, atmospheric composition, nature of available heat sinks, and the free volume of the containment.

5.1.2.5 Erosion of Concrete and Other Structures

Structural degradation in the vicinity of the debris pool may result from two mechanisms. Direct lateral thermal attack at the periphery of the debris pool may erode and weaken structural supports such as the reactor pedestal. For the Mark I BWR design, debris could come into contact with and penetrate the steel drywell liner resulting in early containment failure. After quasi-steady-state conditions are reached, the conservation of energy dictates that the total power must equal the sum of the heat flux involved in concrete ablation and that leaving the pool surface by convection and radiation. Both calculations and experiments have shown that the upward heat flux is significant and may degrade structures above the pool. The release of water vapor and CO_2 from unablated concrete can also be significant. Core-concrete aerosols and radiant energy could degrade engineered safety features such as fan coolers and filters. The quantification of these potential consequences again depends largely on the accuracy with which the computer codes being used can predict the direction in which the concrete attack occurs. While reduced downward attack lowers the probability of basemat penetration, energy conservation demands that it be accompanied by increased radial and/or upward heat fluxes. This conclusion carries the implication of increased lateral attack on the reactor support structures. An example of concern is the Mark III BWR containment design in which core debris is trapped within the reactor pedestal itself.

One pathway by which radioactive materials could reach the environment and pose a threat to the public is penetration of the concrete basemat. This mode of containment failure could result in contamination of ground water and/or the release of radioactive gases through the soil to the atmosphere. The composition of concrete varies widely; in general, it is comprised of four major components: (1) coarse aggregate, usually crushed rock or gravel, (2) fine aggregate, usually sand, (3) Portland cement, which binds the aggregates together, and (4) water. The net mass of concrete that can be disintegrated by the core debris is bounded by the total energy available integrated from the time of initiation of core-concrete interactions to the point where ablation ceases. For those plants with extensive cavity-floor surface available, the debris may spread over a large area with consequent reduced axial penetration. For plants in which the debris might become confined to a small area (such as the BWR Mark III design), downward ablation is augmented, and the potential for basemat penetration must be examined more carefully. In all cases, the possibility that the debris becomes quenched and/or coolable must also be considered. The ability to predict the rate and direction of attack by the core debris on the concrete cavity floor and surrounding structures is governed by the energy balance between the generated power and the upward, downward, and lateral heat losses. The relative directions in which concrete attack proceeds, i.e., downward versus lateral, is therefore important in assessing the potential for penetration of the basemat.

5.1.3 Core-Concrete-Interaction Analysis Codes--CORCON and VANESA

5.1.3.1 CORCON Code

The CORCON code (Ref. 5.1) has been developed by the NRC at Sandia National Laboratories as a best-estimate computational tool to calculate the physical and thermodynamic variables needed to characterize the progression of high-temperature core debris as it erodes concrete in the reactor cavity. From an assumed initial axisymmetric "crucible," the change of cavity shape is tracked as the ablation front advances in time. As the decomposition products of the concrete enter the debris pool, chemical interactions are taken into account. Mass and energy are conserved and the temperature profile of the system is followed. The composition and release rates of gases leaving the pool are computed. Radiative and convective heat fluxes from the surface of the debris pool to these surroundings or to an overlying water pool are calculated. These output variables computed by CORCON provide the data needed to characterize Items 2-5 listed in Table 5.1. CORCON MOD2, which includes improved interfacial heat transfer models, the effects of crust formation, and the influence of an overlying water pool, was released in October 1984 and has been incorporated in the NRC Source Term Code Package.

The CORCON code does not model any of the core-degradation processes that precede vessel failure. However, the stand-alone version does include a set of "base case" assumptions so that the code can be operated in the absence of detailed in-vessel calculations. These default assumptions are automatically invoked unless overridden by the user. The initial core debris is specified in terms of the mass composition of the pre-accident intact core, e.g., total kg of UO_2, Zr, etc. The fission product inventory is derived from a particular application of the ORIGEN burnup code referred to as SANDIA/ORIGEN. This default fission product inventory is coupled to a table of retention factors in order to compute the initial fission product inventory in the debris pool after the core exits the vessel. For example, all the noble gases are assumed to leave the core prior to debris pool formation; 80 percent of the tellurium is assumed to accompany the core debris into the pool, etc. The user can readily accommodate the CORCON input data to any specific accident sequence by numerical adjustment of these default parameters. It should be emphasized that an untailored, base case CORCON run does not purport to represent the results of any particular accident sequence.

93

5.1.3.2 VANESA Code

The VANESA code (Ref. 5.2) (also developed by the NRC at Sandia) models the physical and chemical processes that occur when gas bubbles generated by the decomposition of concrete pass through the molten debris pool and break at the surface. Chemical processes are taken into account to compute the equilibrium conditions of all the vapor phases of fission products and other pool components within the bubbles. The vapor phases of fission products and other components of the pool equilibrate with the other gases trapped within the bubble and condense to form atmospheric aerosols when the bubble bursts at the pool surface. Other aerosols are generated as the bubble film fragments into fine droplets, which are also swept into the atmosphere by the evolving gases. These aerosols are characteristic of the bulk pool composition. These values provide the aerosol information needed to analyze the subsequent evolution of the ultimate radiological source term referred to in Item 1 of Table 5.1. VANESA derives the requisite pool composition, gas flow rates, and temperatures from CORCON. The code also incorporates a model for an overlying layer of water and computes the resulting aerosol decontamination factor. Written originally as a stand-alone model, VANESA has been linked to CORCON to form the CORCON/VANESA package.

5.1.4 Sources of Uncertainties Associated With Predictions of Core-Concrete-Interaction Consequences

There are five identifiable classes of uncertainties that combine to form the overall uncertainty to be associated with the code output predictions used to characterize the potential consequences of core-concrete interactions. These five classes of uncertainties are listed in Table 5.2.

Table 5.2 Sources of uncertainties associated with predictions of core-concrete-interaction consequences.

1. Model uncertainties in code
2. Computational uncertainties
3. Uncertainties in computational data base
4. Uncertainties from other codes
5. Uncertainties attributable to exercise of user options

5.1.4.1 Model Uncertainties in Codes

Although a concentrated effort is made to base the fundamental phenomenological equations on the best state-of-the-art technical knowledge available, e.g., physics, chemistry, and thermal hydraulics, in many cases, such knowledge is limited. Many of the physical regimes being modeled lie outside the realm of thoroughly understood physics and chemistry. Material properties such as viscosities, specific heats, and surface tensions are poorly known, or perhaps not measured at all at temperatures above 2,000°C. Previously performed and ongoing experimental studies continue to provide insights from which these model uncertainties can be reduced. Illustrative of this effect was the significant finding that the interfacial heat transfer models in the released version of CORCON MOD2 and in the corresponding German code WECHSL could not adequately

94

BEST COPY AVAILABLE

predict the relative axial and radial concrete ablation rates in the large-scale BETA experiments conducted at Kernforschungszentrum, Karlsruhe, Federal Republic of Germany. This observation identified one model in both codes that required improvement; significant progress has already been made in this respect. As further experimental data become available, it is to be expected that areas where other model improvements are needed will be identified. Estimates of the magnitude of such model uncertainties can be made through a combination of scientific judgment and carefully planned and executed sensitivity studies; the results of some of these efforts will be described in Section 5.2.

5.1.4.2 Computational Uncertainties

To obtain quantitative predictions from any computer program, the differential equations used to model the phenomena must be solved and evaluated in terms of the available input data and boundary and initial conditions. There is always the possibility that uncertainties or inadvertent errors in the numerical algorithms, machine roundoff, or approximations employed may contribute unsuspected errors to the computed output values. One safeguard against such defects is a well-disciplined program of verification and code testing. It is important to distinguish these computational sources of uncertainty from those attributable to the phenomenological models themselves.

5.1.4.3 Uncertainties in Computational Data Base

There are many parameters used in the phenomenological models and in the numerical solutions that may carry with them a high degree of uncertainty. Examples of such variables are to be found in material properties (especially at high temperatures) such as thermal conductivity, latent heats, and thermal emissivity. In principle, these quantities could be measured; one difficulty lies in the fact that in many cases where these natural functions remain unmeasured, there is virtually no way to reliably estimate the uncertainties that should be attached to them.

Another source of uncertainty that is unrelated to the accident sequence itself is traceable to the fact that (as-built) equipment frequently does not conform to the engineering design specifications. For example, without the benefit of a chemical analysis, there remains some uncertainty that the concrete used to construct a particular reactor cavity does in fact conform to the specifications prescribed to the contractor. A thoroughly audited quality assurance program serves to reduce this problem in some measure. On the other hand, the manufacturer of reactor fuel is carefully monitored as is the construction and assembly of most in-vessel components so that the composition and geometry of the intact, undegraded core probably carry little uncertainty.

5.1.4.4 Uncertainties from Other Codes

In general, the tools (CORCON and VANESA) used to analyze core-concrete interaction phenomena do not consider processes that occur prior to the establishment of a debris pool. Input must be obtained from other computer codes used to analyze all the antecedent in-vessel core disruption and vessel failure mechanisms. It must be emphasized that all these codes suffer from the same generic sources of uncertainty described in this section (Section 5.1.4). In many cases, the difficulties encountered in attempting to model the complex high-temperature chemical and physical phenomena, which characterize the core degradation, meltdown, and vessel failure, are even less tractable than those encountered in the core-concrete interaction modeling. Therefore, the principal contributor to the uncertainties associated with core-concrete interaction predictions is in many cases probably traceable to the uncertainties present in the input variables derived from the codes used to analyze the earlier stages of the accident sequence.

5.1.4.5 Uncertainties Attributable to Exercise of User Options

The designers of most computer codes provide a variety of input and control options to the user. It is, of course, expected that the user's choices will be restricted so that calculations will remain within the domain over which the code has been tested. However, often it cannot be ensured that the user will adhere to this expectation. Another contingency against which the code developer cannot provide a safeguard is the intentional modification of the basic models and/or solution methods by the user. Some of the user-available parameters are thermal emissivity, temperature of the pool surroundings, and ablation enthalpy. To conserve computer cost, the computational time step may be chosen to be long; the exercise of this option has, upon occasion, been seen to affect the computed output. Before any calculational results are accepted for use such as in regulatory decisionmaking, not only the codes themselves must be validated, but the methods by which the user obtained results should be documented and verified.

5.1.4.6 Assessment of Uncertainty Bands and Levels of Confidence

The principal purpose of this report is identification of the major sources of uncertainty needed to derive plausible uncertainty ranges to be associated with fission product release fractions and containment-loading parameters. Because of the extreme difficulty of determining statistically meaningful uncertainty values associated with prevessel failure parameters, as well as with certain other contributors to the overall uncertainty, it is necessary, in many cases, to incorporate judgmental estimates rather than relying on established statistical uncertainty propagation methods. As in the case of computing best-estimate code output calculations, the uncertainty bands are also highly dependent on the particular plant and accident scenario.

5.1.5 Subissues Affecting Uncertainties in Calculating Core-Concrete-Interaction Phenomena

Information required as input for CORCON and VANESA must be derived from plant specifications and output data from other accident analysis codes that treat the in-vessel phenomena. This information is listed in Table 5.3. Except for the first two items, concrete composition and cavity shape, the inputs listed must be derived from the in-vessel and melt progression codes (e.g., Ref. 5.3). These variables are therefore identified as subissues whose uncertainties are unavoidably introduced into and propagated through the core-concrete-interaction calculation. The data covered in Items 1 and 2 must be derived from specifications of the particular plant under analysis.

96

Table 5.3 Subissues--significant input variables for CORCON and VANESA.

1. Composition and material properties of the cavity concrete.
2. Initial geometric configuration of the cavity at the time of vessel failure.
3. Composition and mass of the core debris at the time core-concrete interaction is initiated.
4. Initial temperature of the debris.
5. Mass flow rate and temperature of additional debris if deposition spans a period of time.
6. Fission product inventory present in the debris at the time it enters the pool.

5.1.6 IDCOR Modeling

The ex-vessel source term analyses carried out by the Industry Degraded Core Rulemaking (IDCOR) program were done with the integrated systems analysis code MAAP (Modular Accident Analysis Programs) (Ref. 5.4). The core-concrete aspects of the analysis used the DECOMP model. In the MAAP analysis, convective and radiative heat release from the debris pool surface are coupled to natural circulation processes in the containment.

Also, unlike the CORCON code, the DECOMP model in MAAP is one-dimensional; it treats concrete ablation of the sidewalls of the cavity the same as horizontal surfaces. These two differences in mathematical approach preclude the expectation that computational results could ever be expected to be identical. There are other significant differences in the IDCOR approach:

1. It is assumed that, at the time of vessel failure, only a fraction of the original core mass exits the vessel; debris is assumed to continue to flow into the reactor cavity for a period of hours.
2. Debris is considered, in most cases, to be more widely dispersed than it is in the NRC studies.
3. In virtually all cases, a crust is assumed to exist on the surface of the debris.
4. The fission product release model in MAAP is less detailed than is the VANESA code.
5. In all cases where water exists above the core debris, the debris pool is deemed to become quenched.

For all the above considerations, it is evident that direct comparison of IDCOR results with the NRC predictions cannot readily be made.

5.2 Research Program on Molten Core-Concrete Interactions

The NRC research program on core-concrete interactions is comprised of two basic elements, an analytical component together with a corresponding experimental program. In the analytical effort, the necessary computer codes are developed and tested, while the experimental work is focused on developing the data base needed for validation and refinement of the codes. Some of the available experimental results, together with comparison with code predictions, are described in the following sections.

5.2.1 Sensitivity of Core-Concrete-Interaction Predictions to Modeling and Input Variables

Since there are uncertainties associated with the code input values, it is important to investigate the degree to which those uncertainties are propagated through the code and are reflected in the output predictions. A number of such studies have been made with the CORCON and VANESA codes; some of this work is described in this section.

5.2.1.1 Battelle Columbus Peach Bottom Sensitivity Study

A number of parameter variations were made at Battelle Columbus Laboratories (Ref. 5.5) to study the sensitivity of the Source Term Code Package predictions to user-controlled input values. The tests involve sensitivities referenced in Items 3 and 5 (uncertainties in the data base and in the exercise of user options) of Table 5.2. A draft report of this work, to be incorporated as Chapter 6 of the Peach Bottom report, was available to us for this analysis. The TB1/TB2 sequence was used in the Battelle Columbus sensitivity study. The report refers to five cases (computer runs) from which the sensitivity to variations in three user-controlled parameters was tested: cavity radius, thermal emissivity, and concrete ablation temperature.

Sensitivity of Fission Product Release Fractions to Initial Cavity Radius. The first comparison was intended to examine the calculational dependency to the user's choice of the effective diameter of the concrete cavity used in the CORCON calculation. As written, the CORCON code requires that the initial concrete cavity shape be axisymmetric (not necessarily cylindrical). In applying the code, the user must attempt to devise an initial cavity shape that is believed to best approximate the actual circumstances for the particular plant being modeled. In this calculation, an initial cylindrical shape was chosen since the interior of the Peach Bottom pedestal is in fact cylindrical. The two values of the cavity radius used in the sensitivity study were 5 m and 3 m. The value of 5 m used for the base case assumes that a portion of the core debris flows through the doorway from the cylindrical pedestal region and spreads out over part of the annular drywell floor between the outer pedestal wall and the steel drywell liner. In the sensitivity study, the alternative assumption made was that none of the debris escapes through the doorway, but instead remains confined in a cylindrical pool within the pedestal region. If we use the plant data provided, the following values can be computed:

pedestal inside radius	10.125 ft
pedestal outside radius	13.125 ft
drywell inside radius	22.85 ft

98

pedestal inside area	322	ft^2
drywell annulus area	1,098	ft^2

(The floor area of the doorway, 9 ft^2, through the pedestal wall is disregarded.)

The effect of the parameter change made in this case is to reduce the radius of the assumed virtual cavity used in the base case from 5 m to 3 m (the actual reactor pedestal inside radius). The effect of this change is to reduce the floor area of the initial cavity by a factor of approximately 2.8 with a corresponding increase in pool depth. At the same time, the area of the vertical surface of the pool is increased by a factor of 1.68. It should be mentioned that in both cases the effect of the two sumps in the pedestal floor has been disregarded.

The sensitivity being tested is the prediction of radionuclide release fractions. The fission products have been classified into groups having common chemical properties, each group being represented by but one element as defined in Table 5.4.

Table 5.4 Fission product groups used in sensitivity studies.

Group Name	Elements in Group
Xe	Xe + Kr
I	I + Br
Cs	Cs + Rb
Te	Te + Sb, Se
Sr	Sr
Ru	Ru + Rh, Pd, Mo, Tc
La	La + Zr, Nd, Eu, Nb, Pm, Pr, Sm, Y
Ce	Ce + Pu, Np
Ba	Ba

The data presented in Table 5.5 are derived from Table 6.3 of the Battelle Columbus sensitivity study. The fission product groups are listed in Column 1. Column 2 shows the in-vessel releases (fraction of original whole core inventory at shutdown). Columns 3 and 5 show the total release (in-vessel plus ex-vessel). To more readily observe the effect of changing the assumed cavity radius from 16.9 feet to 10.125 feet, the data are presented (Columns 4 and 6) in terms of ex-vessel fission product release fractions. The ratio column (Column 7) shows the relative effect of decreasing the assumed cavity radius of 16.9 feet to a value equal to the inside Peach Bottom pedestal radius of 10.125 feet. The numbers in Column 8 express the fractional percentage change from the base case. Note that in all cases the releases of refractory fission products are reduced, but that there is virtually no uniformity with respect to the different fission product groups. However, since there are but two data points in the study, caution should be exercised in attempting to draw general conclusions or in

Table 5.5 Sensitivity of ex-vessel fission product release predictions to debris pool radius (TB1/TB2 sequence, Mark 1 BWR containment).

(1)	(2)	(3)	(4)	(5)	(6)	(7)	(8)
Fission Product		R = 16.9 ft		R = 10.125 ft		Relative Change	
Group	In-Ves	Total	Ex-Ves	Total	Ex-Ves	(6)/(4)	% Change
I	0.89	1.0	0.11	1.0	0.11	1.0	0
Cs	0.88	1.0	0.12	1.0	0.12	1.0	0
Te	0.38	0.78	0.40	0.72	0.34	0.85	-15
Sr	0.0012	0.84	0.84	0.78	0.78	0.93	- 7
Ru	1.6×10^{-6}	2.9×10^{-6}	1.3×10^{-6}	2.3×10^{-6}	0.7×10^{-6}	0.54	-46
La	1.1×10^{-7}	0.059	0.059	0.024	0.024	0.41	-59
Ce	0.0	0.090	0.090	0.054	0.054	0.60	-40
Ba	0.022	0.62	0.598	0.60	0.58	0.97	- 3

extrapolating the results. The possible significance of the above results requires further interpretation. To do this, one needs further information, e.g., time-dependent plots of gas-sparging rates and pool temperatures.

Sensitivity to Debris Pool Surface Emissivity. The second user-controlled parameter tested was the radiative emissivity of the pool surface (see Table 5.6). The value of 0.5 used in the base case was increased to 0.9, i.e., D(emissivity) = 80%. Thermal radiation from the pool surface is known to be the principal cause of upward heat loss from the debris. An increase in emissivity would be expected to cause a lowering of the bulk pool temperature and a reduction in gas-sparging rate. The reduction in releases of the refractory fission products, seen in Columns 7 and 8, is consistent with this conclusion. Note again that, as with the variation in pool radius, there is a wide disparity in the degree to which the different fission product species are affected. The results reported in this case, i.e., sensitivity of fission product release predictions to pool surface emissivity, carry somewhat reduced confidence. Before these calculations were made, a number of other modifications were made within the code system itself. Although the authors indicated their conviction that the code changes should not have affected the calculated results, the circumstance violates the guideline for sensitivity studies in general that nothing should be changed except the parameter under test.

Sensitivity to Concrete Ablation Temperature. Another parameter whose value must be specified by the CORCON/VANESA user is the ablation temperature of the concrete. In point of fact, no particular concrete possesses a unique ablation temperature but rather decomposes over a range of temperatures. The Battelle Columbus study explored the sensitivity of CORCON/VANESA output for three values of this parameter. Two temperatures, 1,690 K and 1,875 K (corresponding to the solidus and liquidus temperatures of the Peach Bottom limestone concrete), one below and one above the base case value of 1,750 K, were used. The results of this test are shown in Table 5.7. Note that the releases of tellurium, strontium, and barium are relatively insensitive to the variations in the ablation

Table 5.6 Sensitivity of ex-vessel fission product release predictions to surface emissivity of debris pool (TB1/TB2 sequence, Mark I BWR containment).

(1)	(2)	(3)	(4)	(5)	(6)	(7)	(8)
Fission Product Group		E = 0.5		E = 0.9		Relative Change	
	In-Ves	Total	Ex-Ves	Total	Ex-Ves	(6)/(4)	% Change
I	0.89	1.0	0.11	1.0	0.11	1.0	0
Cs	0.88	1.0	0.12	1.0	0.12	1.0	0
Te	0.38	0.78	0.40	0.69	0.31	0.76	-23
Sr	0.0012	0.84	0.84	0.76	0.759	0.90	-10
Ru	1.6×10^{-7}	2.9×10^{-6}	1.3×10^{-6}	1.8×10^{-6}	0.2×10^{-6}	0.15	-85
La	1.1×10^{-7}	0.059	0.059	0.016	0.016	0.27	-73
Ce	0.0	0.090	0.090	0.033	0.033	0.37	-63
Ba	0.022	0.62	0.598	0.59	0.568	0.95	- 5

Table 5.7 Sensitivity of ex-vessel fission product release predictions to ablation temperature of concrete (TB1/TB2 sequence, Mark I BWR containment).

(1)	(2)	(3)	(4)	(5)	(6)	(7)	(8)	(9)	(10)
Fission Product Group		E=0.9, T=1,750 K		T = 1,690 K			T = 1,875 K		
	In-Ves	Total	Ex-Ves	Total	Ex-Ves	% Change	Total	Ex-Ves	% Change
I	0.89	1.0	0.11	1.0	0.11	0	1.0	0.11	0
Cs	0.88	1.0	0.12	1.0	0.12	0	1.0	0.12	0
Te	0.38	0.69	0.31	0.68	0.30	- 3	0.71	0.33	6
Sr	0.0012	0.76	0.759	0.73	0.729	- 4	0.81	0.809	7
Ru	1.6×10^{-6}	1.8×10^{-6}	0.2×10^{-6}	2.0×10^{-6}	0.4×10^{-6}	100	1.6×10^{-6}	0.0	-100
La	1.1×10^{-7}	0.016	0.016	0.015	0.015	- 6	0.027	0.027	69
Ce	0.0	0.033	0.033	0.028	0.028	-15	0.058	0.058	76
Ba	0.022	0.59	0.57	0.55	0.53	- 7	0.61	0.588	3

temperature parameter. On the other hand, the ruthenium, lanthanum, and cerium releases show greater sensitivity. This behavior probably reflects the wide disparity in activity coefficients of the various species as a function of temperature.

In summary, note that in all three sensitivity studies (Tables 5.5 through 5.7), there is a pronounced disparity between the release fractions for the various fission product groups relative to the imposed changes in the input variables. This dependence upon fission product species is also seen for the other two tests, emissivity and ablation temperature. Note also the seemingly anomalous behavior of the ruthenium group release sensitivity to the variation in concrete ablation temperature. Without the complete time-dependent plots of the complete calculations, further interpretation of these results cannot be justified.

5.2.1.2 Sandia Peach Bottom and Surry Sensitivity Studies

A study at Sandia National Laboratories (Ref. 5.6) was conducted to explore the sensitivity of CORCON MOD2 and VANESA fission product release predictions to variations in code input data derived from in-vessel analyses. The sensitivity of release for five fission product groups to variations in four significant input parameters was tested. Table 5.8 (reprinted from Table 1 of the referenced report) depicts the matrix of input data used in the study. The base case data were taken from the Battelle Columbus studies of the Peach Bottom and Surry plants. Tables 5.9 and 5.10 show the results calculated for the Peach Bottom and Surry plants, respectively. The accident sequence considered for the Peach Bottom plant was the AE scenario, while for the Surry plant the TMLB' case was used. The base case input data in Table 5.8 therefore reflect the best-estimate Battelle Columbus calculations used as initial conditions for the CORCON calculations.

Table 5.8 Parameter variations used in Peach Bottom and Surry uncertainty studies.

	Peach Bottom		Surry	
Parameter	Base	Variation	Base	Variation
Initial Temperature (K)	2,125	2,500	1,807	2,500
Vessel Failure Time (min)*	126	70	275	80
Zirconium Content (kg)**	41,070	6,550 58,950	6,690	14,823
Steel Content (kg)	87,420	21,970	42,557	12,000

*Time after shutdown at which the melt-concrete interaction begins.
**Mass of metallic zirconium in the melt does not include oxidized zirconium, which is also present in the melt.

Sensitivity to Initial Debris Temperature. As for all the input parameters being tested, the initial temperature of the debris depends strongly on the in-vessel aspects of the accident scenario. The base case values for both plants represent temperatures below the solidus of the oxidic components of the melt. The interactions with the concrete are therefore delayed until the pool temperature increases. The effect of assuming higher initial melt temperatures is to advance the time of release. The higher value of 2,500 K implies that interaction, and therefore fission product release, will begin at an earlier point in time. In both cases (Peach Bottom and Surry), the temperature will fall rapidly and

Table 5.9 Refractory fission product release for Peach Bottom plant (total release in % at 10 hours)--AE sequence.

Case	Te	Ba	Sr	La	Ce
Base	58.2	44.3	62.3	1.4	2.5
High Temperature	59.9	45.5	65.9	2.3	4.0
Early Time	57.3	43.6	61.6	1.5	2.6
Low Zirconium	52.4	5.4	10.0	0.6	0.6
High Zirconium	55.7	58.0	75.7	1.6	3.4
Low Steel	96.6	66.5	87.9	4.6	8.6
Maximum*	93.0	79.5	94.9	5.1	11.7

*Maximum case includes high initial melt temperature, early start of core-concrete interactions, high zirconium content, and low steel content. See Table 5.8 for specific values.

Table 5.10 Refractory fission product release for Surry plant (total release in % at 10 hours).

Case	Te	Ba	Sr	La	Ce
Base	9.3	5.8	8.6	0.05	0.1
High Temperature	15.6	8.6	15.5	0.5	0.7
Early Time	10.6	6.0	10.0	0.2	0.2
High Zirconium	7.0	8.5	13.6	0.06	0.2
Low Steel	23.3	9.6	13.3	0.05	0.1
Maximum*	29.1	24.3	40.0	1.1	2.3

*Maximum case includes high initial melt temperature, early start of core-concrete interactions, high zirconium content, and low steel content. See Table 5.8 for specific values.

approach a quasi-equilibrium level. The Peach Bottom concrete is of high limestone content, which has a higher ablation temperature than does the limestone/common-sand concrete in Surry. Therefore, the transient interaction time, in the case when high initial temperature is assumed, is greater for Surry than for Peach Bottom, i.e., the bulk temperature must fall approximately 200 K more in the Surry case before equilibrium is reached. This effect is reflected in the data in Tables 5.9 and 5.10. Note that the release rates for the Peach Bottom case are relatively insensitive to the initial temperature. Although for the Surry case the relative releases (high temperature versus base case) are greater than for Peach Bottom, only for the lanthanum and cerium groups does the influence seem to be significant.

Sensitivity to Time of Vessel Failure. For Peach Bottom, the computed fission product releases are virtually insensitive to the tested variations in time to vessel failure. For Surry, only the lanthanum and cerium fission product groups indicate significant dependence.

103

Sensitivity to Initial Metallic Zirconium Content. Estimates (calculated or otherwise) of the degree of prefailure in-vessel zirconium oxidation vary widely. The quantity of unoxidized zirconium present in the debris at the time of core-concrete interaction initiation is highly significant and uncertain. The release of refractory fission products is augmented by higher debris pool temperatures. Chemical reaction energy resulting from zirconium oxidation is expected to increase pool temperatures over those existing in cases with low zirconium content. Therefore, refractory fission product releases are expected to be sensitive to zirconium content in the debris and increase with it.

The BWR core at Peach Bottom contains significantly more zirconium than does the Surry core. Two variations of initial zirconium content were examined for the Peach Bottom plant, one below and one above the base case. As might be expected, except for tellurium, the fission product releases are all sensitive to the amount of unoxidized zirconium present. For the Surry plant, the fission product releases follow the same pattern as seen in the Peach Bottom calculations. Except for tellurium, all the releases increased with the zirconium content.

Sensitivity to Steel Content. In-pool chemistry as well as pool stratification are sensitive to the amount of steel in the debris. Since the amount of steel present depends on the mode of vessel penetration and failure, i.e., meltthrough via a control rod drive penetration versus massive lower-head failure, there is considerable uncertainty in the initial steel content of the melt. For both the Peach Bottom and Surry cases, massive lower-head failure was assumed in the base case. The sensitivity of fission product releases to more limited steel content was tested by reducing the initial steel inventory by a factor of three to four. The reduced amount of steel present in the melt has several effects. Vaporization of metallic fission product components increases with their concentration in the metallic phase of the debris. The increased release of tellurium for both Peach Bottom and Surry may reflect this effect. Reduced steel content in the liquid metal phase of the debris also enhances the zirconium-oxidation reaction. This has the effect of increasing pool temperatures, which also augments vaporization of all the fission product groups. From the nature of this study, it is not possible to apportion the responsibility for the overall increased fission product releases that accompany reduced steel content.

Sensitivity of Gas Generation Rates. A sensitivity study was carried out with the CORCON code to investigate the influence of the debris pool temperature and relative amounts of unoxidized zirconium and steel present in the debris at the time of vessel failure. The ranges of temperature and unoxidized metal bracket what are believed to be credible bounding initial conditions for the Peach Bottom accident scenarios. Table 5.11 shows the total amount of gas release for the four principal components (CO, CO_2, H_2, and H_2O) integrated over a 10-hour period.

In summary, no attempt is made here to submit an exhaustive explanation of the sensitivities seen in the Sandia study; the reader is referred to the original report (Ref. 5.6). However, a number of general observations may be of use. The bottom rows in Tables 5.9 and 5.10 indicate the highest possible releases that might be expected for the postulated input values used in the sensitivity studies. In all cases, the source terms for the Surry plant are significantly less than those calculated for the Peach Bottom plant, i.e., 2.3 to 11.7 for cerium and 40.0 to 94.9 for strontium. The other ratios lie between these

Table 5.11 Total amount of gas released for Peach Bottom.

Case	CORCON Input			Gas Release (in 100 kg) at 10 Hours			
	Temp (K)	Zr (kg)	Steel (kg)	CO	CO_2	H_2	H_2O
1	2,125	41,070	87,420	262	122	7.47	21.7
2	2,500	41,070	87,420	259	131	7.39	23.0
3*	2,125	41,070	87,420	256	135	7.34	23.5
4	2,125	6,550	87,420	165	122	4.28	25.2
5	2,125	58,950	87,420	297	109	8.63	18.2
6	2,125	41,070	21,970	258	138	7.08	26.5
7*	2,500	58,950	21,970	307	136	8.71	24.3

*For all cases except those with an asterisk (*), the melt-concrete interaction begins 126 minutes after shutdown. An asterisk indicates that the start time is 70 minutes.

extremes. This effect accentuates the impact of plant design upon the ex-vessel source term. In this case, the effect is probably primarily due to the difference in structural concrete. The limestone concrete in Peach Bottom has a much higher ablation temperature and gas evolution rate than does the siliceous concrete used in the Surry plant. The higher zirconium content of the Peach Bottom BWR core is also an important contributor to the effect.

Note that, of the four input parameters varied in the study, the unoxidized zirconium content of the debris has the greatest overall effect, while the source term values are relatively insensitive to initial melt temperature and/or the time of vessel failure. It can readily be seen that, in attempting to estimate uncertainties to be associated with ex-vessel source term predictions, the uncertainties that inherently accompany state-of-the-art in-vessel code predictions will, in many cases, dominate such uncertainty estimates.

5.2.1.3 Sensitivity of Mark I Drywell Failure Time to Concrete Composition and Initial Debris Temperature

Earlier containment analyses of the Mark I BWR concluded that the most likely failure would be from overpressurization of the drywell (gamma mode). The possibility of seal failure resulting from high drywell temperature was also recognized (leak before failure). During the Containment Load Working Group study, a third mode of potential failure was identified at Brookhaven National Laboratory, i.e., meltthrough of the steel drywell liner by molten debris.

In the typical Mark I configuration, the cylindrical cavity within the concrete reactor pedestal is connected by a doorway to the outer annular region of the drywell, which is bounded by a steel liner. Contact of molten debris with the steel could melt and penetrate the liner, creating a direct leakage path from the drywell to the reactor building. In the Brookhaven study (Ref. 5.7), the sensitivity of this failure mode was examined with respect to concrete composition and debris temperature.

In Table 5.12, some of the calculational results are shown. The input data were based on the assumption of a TQUV accident scenario (loss of all coolant injection at scram and failure of the automatic depressurization system) at the Browns Ferry nuclear power station. In all cases it was assumed that the core debris was spread uniformly over a circular concrete floor having a 6-meter radius and bounded at its perimeter by the 3-centimeter-thick steel drywell liner. The increased time-to-failure in the case of basaltic concrete illustrates the importance of concrete composition. The lower ablation temperature of the siliceous material accounts in part for the retardation in the liner meltthrough. The calculated times to drywell failure from overpressurization, high temperature, and liner failure are also compared in Table 5.12. These results were derived through application of the CORCON code in conjunction with MARCH 1.1B.

Table 5.12 Comparison of potential BWR Mark I failure mode times.

Percent Core	Concrete Type	Initial Debris Temp (K)	Liner Ablate (cm)	Liner Fail Time (min)	Drywell Time to Fail (min)		Max Drywell P & T (during 5 h)	
					P	T	P	T
80	B	1,775	0.1	**	950	**	65	411
		1,900	0.3	**				
		2,550	3.0	5.5	460	**	108	477
	L	1,775	3.0	47.4	500	329	88	533
		1,900	3.0	14.9				
		2,550	3.0	3.5	133	62	145	622
60	B	2,550	3.0	5.4				
	L	2,550	3.0	3.8				

Note: B = basalt, L = limestone.
P = pressure, T = temperature.
** = no meltthrough.

The importance of concrete composition is again demonstrated; the higher pressures associated with the two limestone cases reflect the higher gas generation associated with limestone decomposition. It is clear that if the accident proceeds so that high-temperature debris reaches the drywell boundary, penetration of the liner may become the dominant mode of containment failure. This conclusion does not depend on whether or not solid and liquid components of the debris become separated in the pedestal region. The liquid metal component contains a high zirconium content that, when in contact with the annular drywell floor, will react with concrete decomposition gases; the augmented release of chemical energy will continue to drive the reaction despite the fact that the bulk of the decay power source remains within the pedestal. These calculations provide one example of how direct thermal attack by molten core debris can cause failure of an engineered safety feature (steel drywell liner). The results also provide some insight into the sensitivity to relevant input variables, i.e., concrete composition and initial melt temperature.

5.2.2 Comparison of Code Predictions With Experimental Results

5.2.2.1 Comparison of CORCON/VANESA Calculations With Results From SWISS and TURC Tests

A series of experiments were conducted at Sandia to study concrete ablation, as well as gas and aerosol generation rates exhibited under one-dimensional conditions. Cylindrical crucibles of refractory materials were used so that attack was constrained to the downward axial mode on limestone/common-sand concrete plugs cast into the bottom of the crucibles. In the SWISS tests (Ref. 5.8), the temperature of the stainless steel charge was maintained by induction heating. The TURC test series (Refs. 5.9 and 5.10) were transient (no sustained heating) and used both stainless steel and UO_2-ZrO_2 charges. In SWISS-1, water was poured into the crucible approximately 35 minutes into the experiment, while in SWISS-2 water was added shortly after experiment initiation. These data are seen in Figures 5.1 and 5.2 and compared with CORCON predictions. The CORCON predictions, as well as the observed experimental behavior, indicate that the presence of water over the molten steel seems to have little or no effect on the concrete erosion rate. The fission product aerosol data obtained from the SWISS experiments are still being analyzed and are not yet available for this report.

The CORCON and VANESA codes were used at Brookhaven to make blind posttest code calculations that were compared with the experimental aerosol data obtained in the TURC1SS and TURC2 tests. It can be seen in Figures 5.3 and 5.4 that the code predictions are in good agreement with the data. A chemical analysis of the aerosols produced during the TURC1 test allowed comparison of the tellurium component with CORCON and VANESA calculations performed at Sandia. This comparison is shown in Figure 5.5. Note the agreement between the code predictions and the experimental data.

5.2.2.2 BETA Test Results

Molten core-concrete interactions have been under study for over 10 years at the Nuclear Research Center (Kernforschungszentrum, Karlsruhe) in the Federal Republic of Germany. During 1984-1986, a series of tests (Ref. 5.11) were conducted in the large-scale BETA facility designed and constructed for this purpose. Highly instrumented concrete crucibles measuring 1.1 m outer diameter and 3 m high were used. For most of the tests, the inside diameter of the crucible cavity measured 38 cm. Melts of steel prepared from iron-alumina thermites were teemed into the crucibles. Typical melts comprised approximately 300 kg of steel with an overlying layer of 150 kg of aluminum oxide. The crucibles are mounted in a high-powered induction coil capable of depositing up to 1.9 MW in the melt.

Since the German reactor containments are constructed primarily of siliceous concrete, the original test matrix called only for concretes of this composition. Through NRC's cooperative research agreement, it was possible to conduct three additional tests with concrete crucibles cast with concrete more prototypical of U.S. reactor plants, i.e., high-limestone concrete and limestone/common-sand

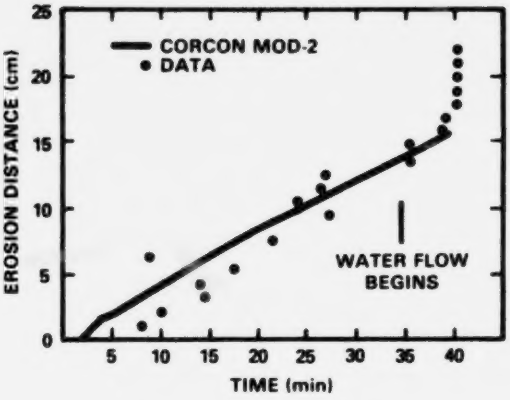

FIGURE 5.1 EROSION DATA TEST SWISS-1

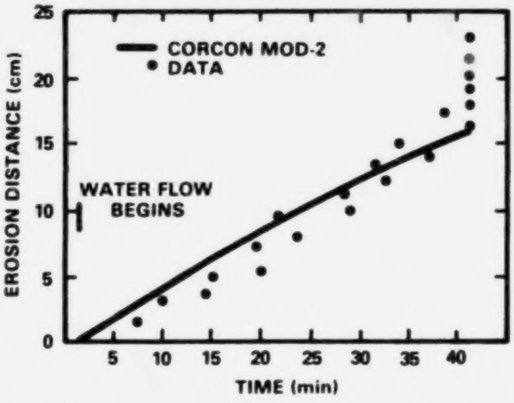

FIGURE 5.2 EROSION DATA TEST SWISS-2

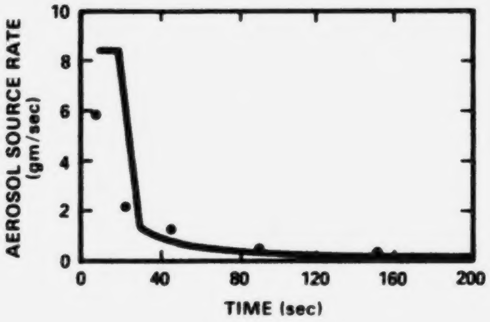

FIGURE 5.3
CORE CONCRETE INTERACTION TEST
TURC-ISS: AEROSOL SOURCE

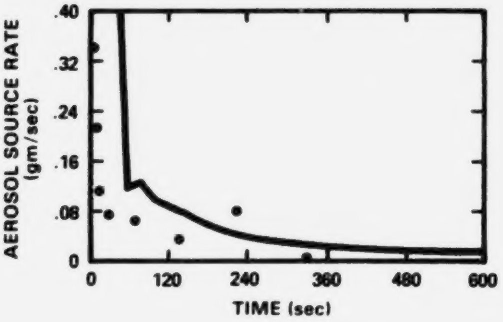

FIGURE 5.4
CORE CONCRETE INTERACTION TEST
TURC-2: AEROSOL SOURCE

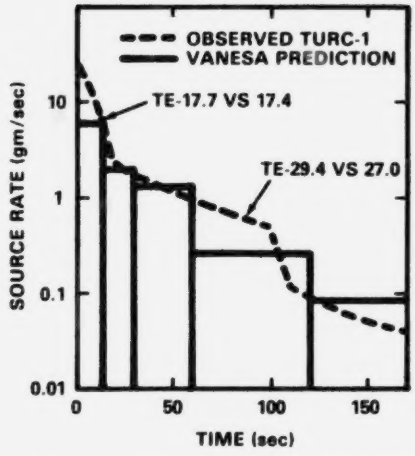

FIGURE 5.5 VANESA TE RELEASE PREDICTIONS

Figures 5.1 through 5.5

concrete. Throughout the experiment series, close liaison was maintained with the KfK scientific staff. These activities provided an opportunity to carry out both pretest and posttest calculations with the CORCON code for comparison with the experimental data. In parallel, the KfK analysts carried out corresponding calculations with their own core-concrete interaction code, WECHSL.

Schematic drawings of the BETA facility and the crucibles are shown in Figure 5.6. In addition to three acceptance tests (V0), 16 experiments were conducted with siliceous concrete and three with typical U.S. concrete crucibles. The designations V1 (high power) and V2 (lower power) correspond to the tests performed with German concrete; V3 represents the tests performed with U.S. concretes. Table 5.13 summarizes the significant features of the experiments.

After each test, the crucibles were sectioned vertically to expose the final configuration of the melt after the crucible had cooled. Figure 5.7 shows the results of one of the high-powered tests, V1.8 (1.9 MW), and Figure 5.8 shows the results of one of the low-powered tests, V2.3 (0.24 MW). A number of the most significant general observations drawn from the BETA test series are as follows:

- At high power levels, downward concrete ablation is accentuated relative to radial erosion. This observation led to a focused effort to modify the heat transfer correlations in CORCON.
- In all cases, a rapid fall in melt temperature followed teeming into the crucible. Measurements indicated that the final quasi-steady-state temperature rapidly approached a level somewhat above the freezing point of molten steel.
- In the lower-powered experiments, where interfacial crusts were assumed to form, gas sparging was not affected. It was concluded that the crusts remained permeable to gas flow.
- Aerosol generation was found to be significantly lower for the siliceous concrete relative to that observed in the tests with limestone concrete.
- In some of the tests, significant entrainment (emulsification) of the liquid metal into the oxidic component was observed, while in others stratification of the layers was evident. This observation, together with data obtained in a number of Sandia tests, demonstrates the futility of arguing as to whether or not the debris pool is stratified. Clearly, either configuration (or a mixture thereof) may exist.

The experiments using limestone/common-sand and high-limestone concretes were characterized by higher gas evolution rates (as might be expected) and higher aerosol generation. Analysis of the data obtained from the BETA test series is still under way at Sandia so that it would be premature to attempt to present final conclusions at this time.

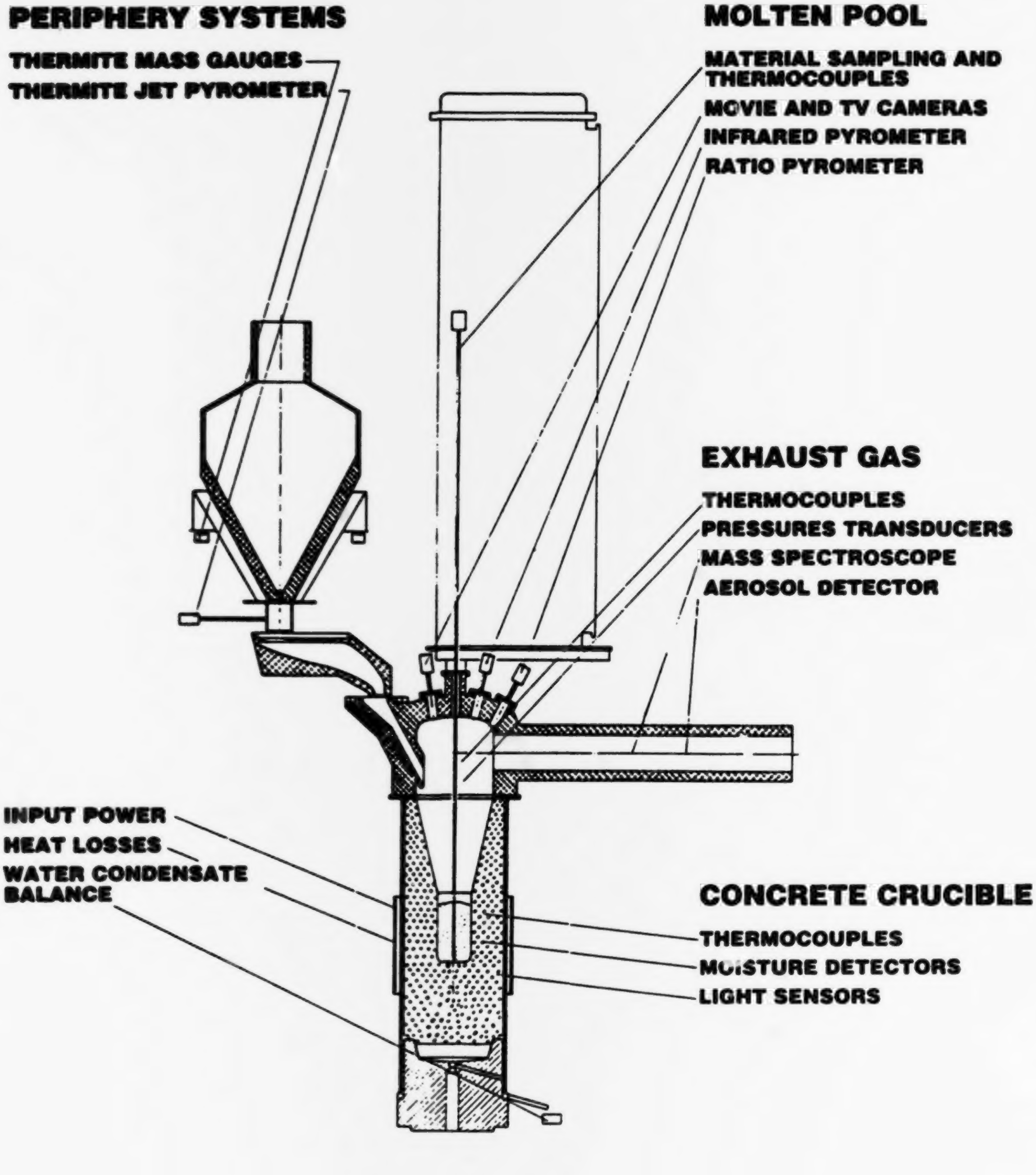
PERIPHERY SYSTEMS
THERMITE MASS GAUGES
THERMITE JET PYROMETER
MOLTEN POOL
MATERIAL SAMPLING AND THERMOCOUPLES
MOVIE AND TV CAMERAS
INFRARED PYROMETER
RATIO PYROMETER
EXHAUST GAS
THERMOCOUPLES
PRESSURES TRANSDUCERS
MASS SPECTROSCOPE
AEROSOL DETECTOR
INPUT POWER
HEAT LOSSES
WATER CONDENSATE BALANCE
CONCRETE CRUCIBLE
THERMOCOUPLES
MOISTURE DETECTORS
LIGHT SENSORS

Figure 5.6 BETA facility (Ref. 5.11).

110

BEST COPY AVAILABLE

Table 5.13 BETA experiment features.

Test	Melt	Power (kW)	Remarks
V0.1	Iron	0	) Test of
V0.1	Iron	400	) facility
V0.3	Iron + Oxide	1,700	)
V1.1	Iron	Pulsed	Pour failed
V1.2	Iron + Oxide	Pulsed	Lorentz-forces excluded
V1.3	Steel + Oxide	1,000	
V1.4	Steel	0	Transient
V1.5	Steel	450	
V1.6	Steel + Oxide	1,000	
V1.7	Steel + Oxide	1,700	
V1.8	Steel + Oxide	1,900	No dispersion (CaO)
V1.9	Steel + Oxide	400-200	CaO added
V2.1	Steel + Oxide	120-150	
V2.2	Steel + Oxide	50-90	CaO added
V2.3	Steel + Oxide	240	CaO added
V3.1	Steel + Oxide	1,700-2,500	US lime/comm sand, Heating from 0-66 s only
V3.2	Steel + Oxide	400->1,000	US limestone, 30 min heating
V3.3	Steel + Oxide	600- 200	US lime/comm sand, 60 min
V4.1	Steel + Oxide	1,000-300	600-mm dia crucible

5.2.2.3 Sustained Urania Reacting with Concrete (SURC) Tests (Ongoing)

In the SURC tests, prototypical reactor materials are used and allowed to interact with concrete under sustained heating conditions. The crucibles are highly instrumented so that concrete ablation, gas evolution, aerosol generation, etc., can be measured. This series of experiments is being initiated at the present time, and no results are yet available for incorporation in this report.

5.2.2.4 Experimental Characterization of Aerosol Generation and Properties from Core-Concrete Interactions--WITCH and GHOST Tests

The second series of tests currently under way at Sandia are referred to as the WITCH and GHOST tests. This work is aimed directly at the validation of the VANESA aerosol release model. Gas sparging through liquid pools is known to generate aerosols through two mechanisms:

1. When the bubbles break at the surface of the pool, fine droplets of the bulk material are swept away by the escaping gases; the WITCH tests are designed to investigate this phenomenon.

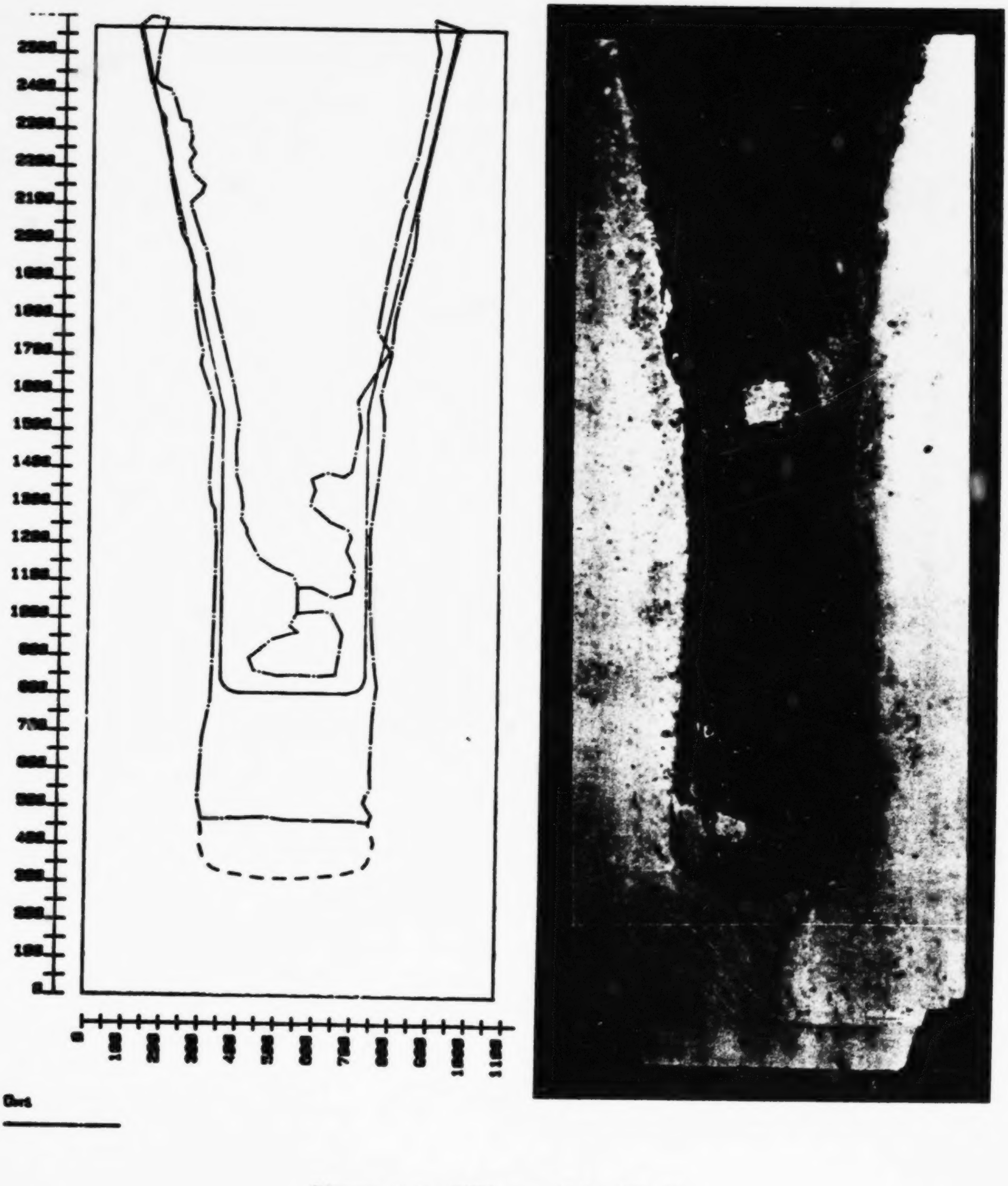
2500
2400
2300
2200
2100
2000
1900
1800
1700
1600
1500
1400
1300
1200
1100
1000
900
800
700
600
500
400
300
200
100
0
0
100
200
300
400
500
600
700
800
900
1000
1100
Dist

Figure 5.7 BETA crucible (V1.8).

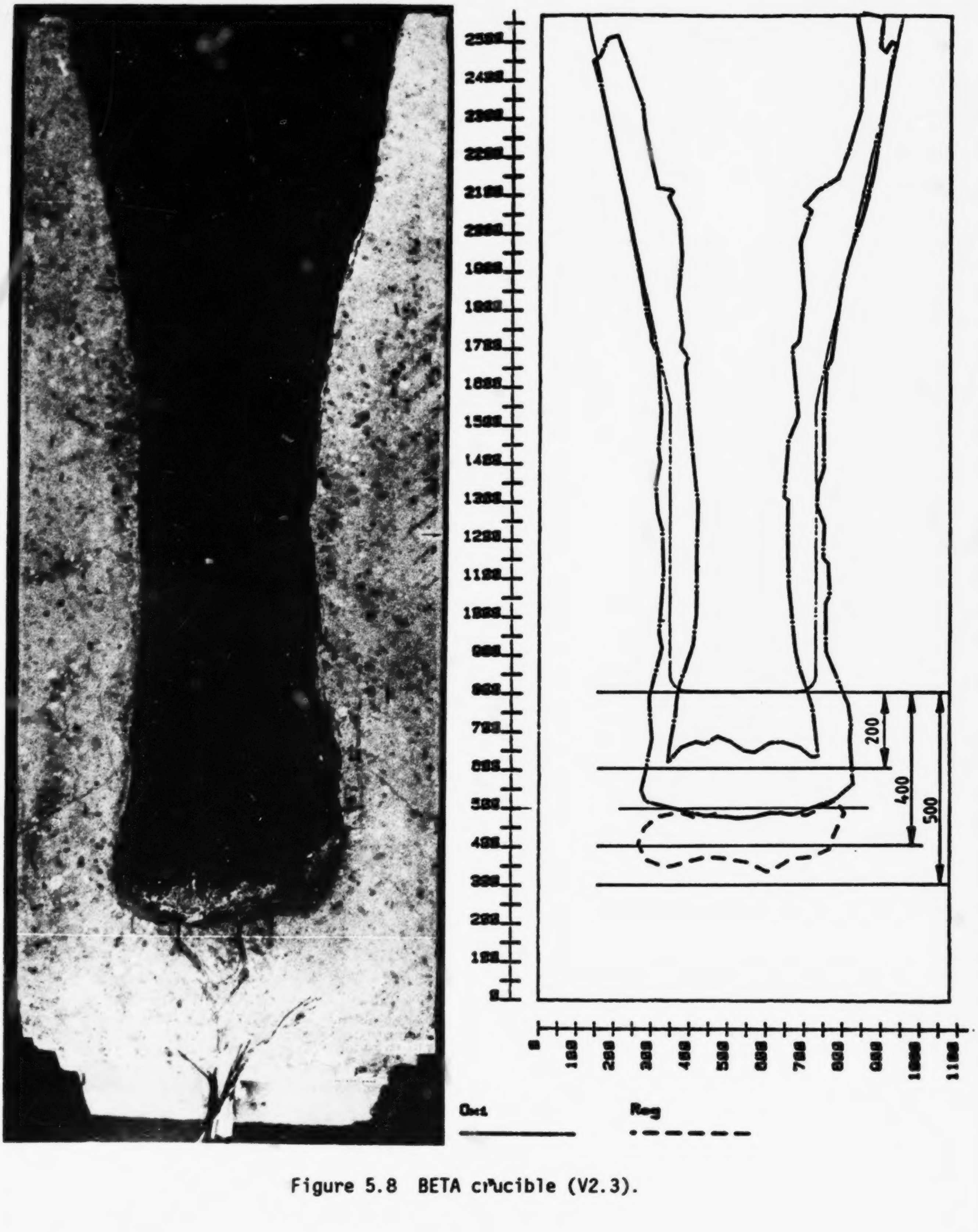

Figure 5.8 BETA crucible (V2.3).

2. Some of the vapors trapped within the bubbles condense into fine particles when the bubbles break. These condensation aerosols account for most of the fission product release from core debris. This condensation aerosol formation is the subject of the GHOST tests.

The apparatus to be used in the WITCH and GHOST experiments is near completion. Data are expected to become available in early 1987.

5.2.2.5 Special-Effects Tests on Thermal-Hydraulic Properties of Core-Concrete Interactions and Aerosol-Mitigation Behavior of Overlying Water Pools

The Brookhaven work falls into four general categories:

1. The study of mass entrainment between two layers of immiscible liquids through which gas sparging is taking place. It has been seen that the onset of mass entrainment requires a change in the modeling of heat transfer. Entrainment proved to be a serious problem at the BETA facility because electromagnetic coupling to the induction heating coil became lost as the steel pool became entrained into the oxidic layer.

2. The nature of heat transfer between layers within a stratified pool is important since it has a direct bearing on the nature of the source term calculations. The pool temperature is one of the most sensitive variables with respect to the VANESA condensation model.

3. In some cases, the decontamination of aerosols by pool scrubbing may be an important mitigating process. A study of this effect is currently in progress.

4. Along with the experimental and modeling activities, the Brookhaven staff has been intimately involved in a variety of code assessment and auditing activities as well as in a number of special study groups such as the Containment Load Working Group.

5.2.3 Conclusions and Recommendations of CSNI Specialist Meeting on Core-Concrete Interactions

A three-day conference sponsored by the Principal Working Group No. 4 of the Committee on the Safety of Nuclear Installations (CSNI) was held at the Electric Power Research Institute (EPRI) September 3-5, 1986. Sixty-five participants from nine countries attended the meeting: Canada, Federal Republic of Germany, Finland, France, Italy, Japan, United Kingdom, United States, and Switzerland. At the close of the meeting, the Programme Committee, together with the Session Chairpersons, prepared a summary of the principal conclusions developed during the technical sessions. The conclusions were classified into three general categories: (1) thermal-hydraulic aspects of molten core-concrete interactions (MCCI), (2) aerosol and radionuclide release aspects of MCCI, and (3) application of MCCI to specific nuclear plants. The timeliness of this conference with respect to the preparation of this report makes it appropriate to incorporate here a brief summary of the conclusions prepared by the meeting panel.

5.2.3.1 Thermal-Hydraulics Aspects of Molten Core-Concrete Interactions

1. The behavior of siliceous concrete is better understood than that of carbonate concrete.

2. The BETA experiments showed that the laminar gas film heat transfer models in CORCON and WECHSL underpredicted downward concrete erosion by liquid steel. The experiments showed lower quasi-steady-state melt temperatures than were predicted by the codes.

3. Both CORCON and WECHSL gas generation predictions for the BETA experiments were in satisfactory agreement with the experimental data. Gas composition analyses lend confidence to the code predictions regarding oxygen potential of the melt.

4. Early results of the SURC tests at Sandia (SURC 3) tend to reduce confidence in the CORCON predictions of the coking effect (which results from rapid oxidation of zirconium metal in the melt).

5. The importance of understanding the onset and phenomenon of interfacial mass entrainment between two stratified immiscible liquid layers was noted; separate-effect studies are ongoing.

6. Code improvement efforts should focus on more reliable predictions of (1) axial and radial concrete erosion (with respect to different concrete types), (2) core debris temperatures, (3) the distinction between behavior of metallic and oxidic melts interacting with concrete, (4) onset and properties of mass entrainment, and (5) nature and effects of crust formation and freezing.

7. Further experiments are needed to understand the influence of unoxidized zirconium in the metal phase on core debris chemistry and melt temperature.

8. The models for molten metal interacting with concrete seem to be reasonably adequate; on the contrary, the behavior of oxidic melts is virtually unstudied. It is important that the core-concrete-interaction research in this regard be pursued.

9. Knowledge concerning the uncertainty associated with model predictions and with the fundamental phenomenology involved in core-concrete interactions must be augmented.

10. Hot solid debris attack on concrete should be more thoroughly studied.

5.2.3.2 Aerosol and Radionuclide Release Aspects of Molten Core-Concrete Interactions

1. The core-concrete-interaction contribution to fission product release should be considered in the framework of containment loading and potential public risk consequences. These considerations are highly plant specific and intimately related to the potential for containment failure.

BEST COPY AVAILABLE

2. To provide more realistic (credible) fission product release predictions, the thermal-hydraulic aspects must be coupled to chemical equilibrium calculations.

3. To reduce the uncertainty in fission product release predictions, significant improvements must be made in the thermodynamic data base with respect to high-temperature chemical and material properties.

4. Further studies are needed to augment understanding of aerosol decontamination by water pools and/or surface crusts overlying core debris.

5. Further study of aerosol generation by hot solid debris attack on concrete is needed.

5.2.3.3 Application of Molten Core-Concrete Interaction to Specific Nuclear Plants

1. The effects of uncertainties in the prediction of containment loads and fission product releases must be taken into account.

2. Code predictions of the temperature history of core-concrete interactions are sensitive to initial and boundary conditions.

3. Containment loading was predicted to be sensitive to concrete composition and to assumptions about upward heat transfer.

4. The consequences of molten core-concrete interaction depend on (1) initial composition of debris, (2) initial temperature, (3) amount and rate of discharge from the reactor vessel, and (4) geometric configuration of debris in the reactor cavity.

5. Effects of the fluid-dynamic behavior of the corium layers (oxidic, metallic, and any overlying water) and potential instability effects must be assessed for possible inclusion in the codes.

6. Metallic Zircaloy oxidation can have important effects on the prediction of aerosol and radionuclide releases.

7. More attention should be focused on long-term phenomena: containment temperature, pressure, aerosol loading, steam content of containment atmosphere, containment basemat penetration, stabilization of the core debris in the ground and effects of delayed flooding on melt coolability, magnitude of melt-coolant interaction, and resuspension of radionuclides that may be present in the flooding water source.

8. The predictive codes should consider closer coupling between the debris-pool phenomena and the reactor cavity and the containment.

In addition to the foreign research reported and discussed at the meeting, the NRC staff and contractors reviewed much of the ongoing NRC-sponsored research. In Section 5.3, the consensus of the participants is reviewed in terms of the ongoing and planned NRC molten core-concrete-interaction research program.

5.3 NRC Molten Core-Concrete-Interaction Research Program and Technical Uncertainty Evaluation

5.3.1 Principal Sources of Uncertainty in Core-Concrete-Interaction Predictions

The phenomena that contribute to containment loading are primarily related to the thermal-hydraulic behavior of high-temperature core debris as it attacks concrete in the reactor cavity. Quantification of the radiological source term depends primarily on the debris pool chemistry and aerosol generation mechanisms. Although the containment-loading and radioactive aerosol release parameters have an interrelated impact on the ultimate risk, in this discussion, the two aspects of core-concrete interactions are considered separately for convenience. Tables 5.14 and 5.15 list the principal areas where further research is needed to reduce the uncertainties in source term and containment-loading predictions. The tables include recommendations gleened from the conclusions reached at the CSNI Specialist Meeting held in Palo Alto, California (see Section 5.2.3).

It is important to note that the phenomenological areas listed in Tables 5.14 and 5.15 are not equally relevant to all types of reactor plants. The question of zirconium oxidation, for example, is much more important for BWRs than for PWRs. The relationship of these areas of technical uncertainty identified in Tables 5.14 and 5.15 and the ongoing and planned NRC research program are discussed in the following section.

5.3.2 NRC Research Program on Molten Core-Concrete Interaction

The Office of Nuclear Regulatory Research has been conducting a research program in this area for a number of years. The emphasis on severe accident phenomenology was stimulated by the Three Mile Island accident. The current research program plan is discussed in the framework of two categories: (1) ongoing research programs presently in place (through FY 1987) and (2) programs planned for the near future intended to close recently identified gaps in the information needed to enable reduction of uncertainty bands associated with molten core-concrete-interaction code predictions. The current program is summarized in Table 5.16 while the planned research is described in Table 5.17.

Comparison of the program outlined in Table 5.16 with the research needs identified in Tables 5.14 and 5.15 shows that the current program is responsive to most of the items listed. In particular:

- The SURC program is addressing areas identified in Items 1, 3, and 7 of Table 5.14 and Items 1, 2, 3, 5, and 6 of Table 5.15.
- The WITCH and GHOST aerosol tests are concerned with Items 5 and 6 of Table 5.15.
- The hot solid/concrete experiments are concerned with Items 1 and 2 of Table 5.14 and Item 6 of Table 5.15.
- The thermal-hydraulic interfacial heat transfer and mass entrainment research involves Items 2, 4, and 5 of Table 5.14 and Items 2 and 3 of Table 5.15.

Table 5.14 Principal sources of uncertainties associated with thermal-hydraulic aspects of core-concrete-interaction phenomena.

---

1. Material properties and thermal-erosion characteristics of various types of concrete used in reactor construction.

2. Heat transfer correlations for corium-concrete and interlayer debris pool interfaces (in addition to concrete erosion, these factors largely control debris temperatures, which in turn impact fission product release).

3. Nature and magnitude of the "coking" effect associated with metallic zirconium oxidation (again, coking phenomena impact debris temperature).

4. Characterization of interlayer mass entrainment; better understanding of conditions that determine pool stratification versus heterogeneous mixing needed.

5. Debris-concrete heat transfer models vis-a-vis radial versus axial erosion rates for various concrete compositions and both metallic and oxidic melts.

6. Nature of surface crust formation and breakup as it affects debris coolability.

7. Characterization of hot solid debris attack on concrete needed to reduce uncertainty in long-term code predictions.

8. Influence of time-dependent mass addition to the debris pool.

9. Characterization of fluid-dynamic properties of core debris to enable modeling of debris spreading over the available cavity floor.

10. Detailed characterization of heat transfer from the debris pool to containment structures and atmosphere.

- The aerosol decontamination by water and/or porous crusts relates to Item 5 of Table 5.15.

Note that the research program currently in place is not responsive to Items 6, 8, 9, and 10 of Table 5.14 and Item 4 of Table 5.15. It will be seen, however, that the research plan under development includes all these items.

Note that activities encompassed by the research currently in place taken together with the planned projects shown in Table 5.17 comprise a research program that is responsive to all the technical areas (Tables 5.14 and 5.15) where significant uncertainties have been identified.

The following schedule of milestones has been established for the current research plan:

Table 5.15 Principal sources of uncertainties associated with fission product and aerosol release aspects of core-concrete-interaction phenomena.

1. Quantification of debris pool oxygen potential.
2. Time-dependent debris pool temperature profile.
3. Interactive coupling of chemical and thermal-hydraulic phenomena.
4. Data base of physical and chemical material properties (particularly activity coefficients of fission product species).
5. Characterization of aerosol decontamination by surface crusts and/or water pools overlying core debris.
6. Aerosol generation and transport accompanying hot solid debris attack on concrete.

Expected FY 1987 Milestones at Current Budget Level

- Program planned to study spreading behavior of high-temperature core debris for resolution of BWR Mark I drywell liner failure issue.
- Program to study surface crust formation and breakup caused by overlying water; determine influence on debris bed coolability; initiate program with feasibility study.
- Incorporate new information into CORCON MOD2.
- Conduct tests to determine the effects of boron carbide during molten core interactions with limestone and siliceous concretes.
- Compile a summary review of data on core debris-concrete interactions available for model validation.
- Complete the WITCH tests of aerosol generation by mechanical processes during core-concrete interaction. Issue report and recommendation of changes to VANESA.
- Complete the GHOST tests on aerosol generation by vapor-condensation processes during the core-concrete interaction. Issue report and recommend changes, if any, to VANESA.

Expected Milestones for FY 1988 and Beyond

- Complete integration of the CORCON MOD2 and VANESA codes into a single consolidated code. The CORCON/VANESA code package will perform the following analyses: (1) rate and direction of attack on structural concrete, (2) release rates and composition of vapor species from the core debris, i.e., water vapor and noncondensible and flammable gases,

Table 5.16 Current NRC research program on molten core-concrete interactions.

---

1. Experiments on prototypical reactor core materials interacting with concrete under conditions of sustained heating (SURC series).

   - Melts containing UO_2 fuel, stainless steel, zirconium (metallic and oxidic), boron carbide, and trace amounts of selected fission product elements are maintained at high temperatures by inductive heating within highly instrumented concrete crucibles. The data obtained provide information on melt-to-concrete heat transfer, influence of zirconium oxidation and B_4C chemistry on erosion phenomena, debris temperature, offgas composition, and fission product release.

   - Some tests will be conducted with water overlying the melt to study potential for quenching and/or aerosol decontamination.

   - Pretest and posttest calculations of all experiments conducted with CORCON and VANESA to provide code validation and guidance for model improvement.

2. Aerosol-generation experiments with metallic and oxidic melts conducted under conditions of sustained heating and controlled gas sparging (melts doped with fission product simulants).

   - WITCH series focuses on mechanical aerosol generation due to bubble film rupture.

   - GHOST series focuses on aerosol generation by vapor condensation.

   - Aerosol decontamination studied by addition of overlying water. These data are needed for VANESA validation and model improvement.

3. Concrete erosion by hot solid debris.

   - Study heat transfer by both metallic and oxidic materials to various types of concrete.

   - Study decomposition-gas evolution and aerosol generation.

   These data are needed to develop models for late-term accident conditions after debris solidification.

4. Experiments on interfacial heat transfer between layers of immiscible liquids with gas sparging.

   - These data derived from small-scale simulant experiments are essential for CORCON model development.

   - Study onset and nature of mass entrainment at accelerated gas-sparging rates.

   The metallic and oxidic components may be either stratified or emulsified (or somewhere between these two extremes). Understanding of mass entrainment is necessary for CORCON modeling.

Table 5.16 (continued)

5. Study of aerosol decontamination by water and/or porous crusts overlying core debris. Separate-effect tests needed to fill gaps in existing data base are conducted with highly controlled aerosol characterization, gas flow rates, and a wide range of thermal-hydraulic conditions of the water. To this time, the VANESA water-decontamination model has not shown acceptable agreement with available data. These experiments support and guide model improvement and validation.

6. Model refinement and code assessment constitute a significant aspect of the ongoing research program. As improvements are made, verified, and tested, they will be incorporated into the CORCON and VANESA elements of the NRC Source Term Code Package.

Table 5.17 Additional planned research.

1. Program to study surface crust formation and breakup caused by overlying water. Determine influence on debris bed coolability; initiate program with feasibility study.

2. Implementation and testing of the time-dependent mass addition subroutine in the CORCON code.

3. Program to characterize the fluid-dynamic properties of core debris to enable modeling of debris spreading over available cavity floor.

4. Program to study material properties and high-temperature erosion characteristics of different types of concrete as a function of material composition.

5. Special-effects program to measure fission product chemical properties and activity coefficients needed for VANESA model improvement.

(3) release of radiant and thermal energy from the debris pool to the containment, (4) characterize the radioactive and nonradioactive aerosol release to the containment atmosphere, (5) characterize the scrubbing (decontamination factor) effects of an overlying water layer, and (6) continue code predictions associated with the foregoing phenomena into the long-term accident phases due to continued concrete erosion by solid or partially frozen core debris.

- Conduct experimental program on aerosol decontamination by porous and/or solid crusts.

- As the experimental and theoretical data bases improve, refine the phenomenological models so that uncertainty can be reduced.

- Increased emphasis will be placed on the analysis of experimental data for the purpose of code validation (this effort is ongoing).

- The SURC series of experiments in which the interaction between prototypical core melt materials and concrete are tested under conditions of sustained induction heating will be completed in FY 1988.

- The experimental program on heat transfer phenomena at Brookhaven National Laboratory together with model development will continue in close coordination with the Sandia CORCON/VANESA development and validation work.

- In connection with the SURC experiments, an augmented effort to understand and model the zirconium-oxidation issue will continue. This is particularly important with respect to BWR safety because of the high zirconium inventory in the core.

- A research program will be completed on the study of debris-spreading phenomena and the influence on the BWR Mark I drywell liner failure issue and on release fraction for refractory fission products; issue draft report on the research and its implications for severe accident analysis.

- A research program will be conducted to resolve the question of whether or not surface crust formation and breakup may provide a mechanism by which debris beds may be rendered coolable.

- Continue to prepare and release periodic code update sets for CORCON/VANESA and maintain ongoing user support as needed.

- Continue to maintain close liaison and cooperation with Japan, the Federal Republic of Germany, and the United Kingdom where cooperative research and information exchange agreements have been established.

- Conduct experiments on boiling of water overlying immersible liquid pools.

5.3.3 Relationship Between Core-Concrete-Interaction Research Program and Expected Reduction in Code Prediction Uncertainties

In Section 5.3.1, the significant areas of uncertainty are identified in Tables 5.14 and 5.15. If the principal sources of uncertainty identified in Tables 5.14 and 5.15 are examined in terms of the five general categories of uncertainty sources listed in Table 5.2, it can be readily seen that virtually all the items subject to improvement through core-concrete-interaction research fall into the two categories: (1) uncertainties in the phenomemological models and (2) uncertainties in the computational data base. Reduction of predictive uncertainty implies increased precision as well as augmented confidence in the output. The former is derived through model improvement and the latter through code validation by a sufficiently broad experimental program to confirm the adequacy of the codes throughout the entire range of application demanded by severe accident conditions. Clearly, the experimental program serves both functions: (1) provides guidance for model refinement and (2) provides data against which accepted models can be tested.

122

Many of the items listed in Tables 5.14 and 5.15 are being addressed by the research program currently in place, while others are to be treated in the planned research programs. Areas having particularly high priority have been identified and are discussed below.

5.3.3.1 Heat Transfer Correlations

Considerable data exist concerning heat transfer phenomena involved in molten steel interactions with concrete. However, the adequacy of the CORCON models for truly prototypical reactor materials is virtually untested. The planned SURC tests directly address this problem. Preliminary transient tests with high-temperature oxidic melts showed that heat transfer to concrete was significantly inhibited by crust formation at the interface. The sustained heating feature of the SURC experiments will provide data to reduce this uncertainty. In any event, if the test results show that the CORCON models do not function correctly under these extreme conditions, the information will provide the knowledge needed for inproved model development.

5.3.3.2 Influence of Metallic Zirconium in Melt (Coking)

The rapid highly exothermic oxidation of metallic zirconium by concrete decomposition gases (H_2O and CO_2) was found to be the cause for what, at the time, seemed to be anomalies in the CORCON predictions of pool temperatures and gas flow rates, both of which sharply influence fission product release rates. The term "coking" was chosen to characterize the complete dissociation of CO_2 resulting in the presence of free carbon in the melt. The accuracy of this chemical scenario has not been confirmed or disaffirmed. The question is being addressed directly in the SURC program; in some of the experiments, metallic zirconium is added to the melt shortly after core-concrete interaction has been initiated.

5.3.3.3 Surface Crust Formation vis-a-vis Debris Coolability

In many accident scenarios, water is expected to overlie the debris pool. The SWISS tests indicated that the presence of overlying water had little effect on concrete attack. The first major uncertainty is the question of whether or not this result can be extrapolated to full-scale reactor cavity geometry. The second question is whether or not the presence of water will influence the debris pool temperature. This area of uncertainty is being given high priority because of the extremely high uncertainty identified with it.

5.3.3.4 Nature of Core Debris Spreading

To this time, most of the core-concrete-interaction research has focused on the quasi-steady-state phenomena contemplated by the CORCON and VANESA codes. The complicated transient processes involved in debris pool formation have not yet been adequately investigated. Identification at Brookhaven of the potential penetration of the BWR Mark I steel drywell liner brought the importance of the fluid-dynamic behavior of high-temperature debris into focus. The Oak Ridge National Laboratory evaluations of possible separation of the metallic and oxidic melt components also highlighted this question. To date, none of the experimental programs has directly addressed these questions. The planned program to study the fluid-dynamic properties of slurried melts is intended to answer these questions.

123

REFERENCES FOR CHAPTER 5

5.1 R. K. Cole, D. P. Kelly, and M. A. Ellis, "CORCON-MOD2: A Computer Program for Analysis of Molten-Core Concrete Interactions," Sandia National Laboratories, NUREG/CR-3920, SAND84-1246, October 1984.

5.2 D. A. Powers, J. E. Brockmann, and A. W. Shiver, "VANESA: A Mechanistic Model of Radionuclide Release and Aerosol Generation During Core Debris Interactions with Concrete," Sandia National Laboratories, NUREG/CR-4308, SAND85-1370, July 1986.

5.3 R. O. Wooton, P. Cybulskis, and S. F. Quayle, "MARCH2 (Meltdown Accident Response Characteristics) Code Description and User's Manual," Battelle Columbus Laboratories, NUREG/CR-3988, BMI-2115, September 1984.

5.4 IDCOR Technical Report 15.3, "Core-Concrete Interactions," September 1983.

5.5 R. S. Denning et al., "Radionuclide Release Calculations for Selected Severe Accident Scenarios," Battelle Columbus Laboratories, NUREG/CR-4624, Vols. 1-5, BMI-2139, July 1986.

5.6 D. R. Bradley and A. W. Shiver, "Uncertainty in the Ex-Vessel Source Term Caused by Uncertainty in In-Vessel Models," Sandia National Laboratories, SAND85-1664C, February 1986.

5.7 G. A. Greene, K. R. Perkins, and S. A. Hodge, "Mark I Containment Drywell: Impact of Core-Concrete Interactions on Containment Integrity and Failure of the Drywell Liner," International Symposium on Source Term Evaluation for Accident Conditions, IAEA-SM-281/36, October 1985.

5.8 R. E. Blose et al., "SWISS: Sustained Heated Metallic Melt Concrete Interaction with an Overlying Water Pool Experiment and Analysis," NUREG/CR-4727 (Draft), SAND85-1546, to be published.*

5.9 J. E. Gronager et al., "TURC1: Large Scale Metallic Melt-Concrete Interaction Experiments and Analysis," Sandia National Laboratories, NUREG/CR-4420, SAND85-0707, January 1986.

5.10 J. E. Gronager et al., "TURC2 and TURC3: Large Scale $UO_2/ZrO_2/Zr$ Melt-Concrete Interaction Experiments and Analysis," Sandia National Laboratories, NUREG/CR-4521, SAND86-0318, June 1986.

5.11 H. Alsmeyer et al., "BETA Experimental Results on Melt/Concrete Interactions: Silicate Concrete Behavior," Kernforschungszentrum Karlsruhe, Federal Republic of Germany, Proceedings of the CSNI Specialist Meeting on Molten Core Concrete Interactions (Palo Alto, CA), September 3-5, 1986, to be published.*

---

*Available in the NRC Public Document Room, 1717 H Street NW., Washington, DC.

BIBLIOGRAPHY

Brockmann, J. E., and F. Arellano, "WITCH/GHOST Program Plan," January 1986.

Brockmann, J. E., and F. Arellano, "WITCH Test Series I, Entrainment Release from Oxide Melts," Sandia Topical Report, June 1986.

Brockmann, J. E., and F. Arellano, "GHOST Test Series I - Vaporization Release from Steel Melts," Sandia Topical Report, June 1986.

Copus, E. R., and D. R. Bradley, "Interaction of Hot Solid Core Debris with Concrete," Sandia National Laboratories, NUREG/CR-4558, SAND85-1739, June 1986.

Greene, G. A., et al., "Audit Calculations of Ex-Vessel Fission Product and Aerosol Release to Containment for Selected Accident Sequences," BNL Technical Report, January 1985.

Perkins, K. R., G. A. Greene, and W. T. Pratt, "Containment Performance for Severe Accidents in BWRs with a Mark I Containment," BNL Technical Report, November 1984.

Perkins, K. R., G. A. Greene, and W. T. Pratt, "Containment Loading for Severe Accidents in BWRs with a Mark I Containment," BNL Technical Report, November 1984.

Yang, J. W., G. A. Greene, and W. T. Pratt, "Containment Loading for Severe Accidents in BWRs with a Mark II Containment," BNL Technical Report, June 1985.

6. HYDROGEN COMBUSTION

P. Worthington

6.1 Introduction

The major concern regarding hydrogen in LWRs is that the static or dynamic pressure loads from combustion may cause a breach of containment or that important safety-related equipment may be damaged because of either pressure loads or high temperatures. In order to assess the possible threats to containment and safety-related equipment and to understand the influence of hydrogen on reactor safety, knowledge of the following phenomena is required: (1) hydrogen transport and mixing, (2) ordinary deflagration, (3) flame acceleration and transition from deflagration to detonation (DDT), (4) detonations, (5) diffusion flames, (6) mitigation concepts, and (7) thermal and mechanical loads resulting from various combustion modes. The reactor safety concerns associated with this issue include (1) the probability and consequences of direct failure of containment from hydrogen deflagration, dynamic overpressurization due to accelerated flames or detonations, and breach of containment from penetration by combustion-generated missiles, (2) the survival and functioning of safety-related equipment exposed to hydrogen burns, and (3) the alteration of accident consequences by the changing state of fission products as a result of hydrogen combustion.

The objective of the NRC hydrogen research program is to develop an understanding of hydrogen sufficient to resolve the reactor safety issues related to containment integrity following hydrogen combustion. This understanding would be acquired by performing a sufficient number of small-, intermediate-, and large-scale experiments, developing guidelines and correlations, developing and validating phenomenological and empirical models, and incorporating hydrogen codes (models) in containment codes.

The uncertainty associated with quantifying the threat to containment from hydrogen burns is best realized by first quantifying the uncertainty for each of the seven combustion phenomena areas. Moreover, it is a coupling of these individual uncertainties that will lead to quantification of the threat posed to containment and safety-related equipment by hydrogen burns. For example, the understanding in the area of deflagration is very good. Quantitative predictive codes exist that have been assessed against experimental data with reasonable agreement. However, an understanding of conditions that will lead to transition from deflagration to detonation (DDT) or analytical tools to predict the consequences of DDT is not as good. Even though a qualitative picture of flame acceleration and DDT is emerging and phenomenological codes can make more accurate predictions, satisfactory comparison against experimental data has not yet been achieved.

The issue of hydrogen distribution and combustion is also a technical issue in Appendix J (see Section J.4) to draft NUREG-1150.

6.2 Description of Past, Present, and Future Research

The hydrogen research program had a twofold objective: (1) to quantify the threat to nuclear power plants (containment structure, safety equipment, and the primary system) posed by hydrogen combustion and (2) to disseminate information on hydrogen behavior and control. This program was comprised of both experimental and theoretical tasks to develop an adequate data base on hydrogen combustion phenomena. This data base will include information on all combustion modes, hydrogen combustion mitigation and preventive concepts, and thermal and mechanical loads.

Hydrogen behavior and control research deals with the pressure and temperature loads imposed on the containment and equipment by the accumulation and combustion of hydrogen during a severe accident. The severity of the hydrogen threat can depend strongly on the combustion mode(s) as well as the reactor and containment design. Therefore, experimental and theoretical efforts were planned to investigate each combustion mode. The front end of the combustion problem is the hydrogen transport and mixing. The concern regarding in-vessel hydrogen generation centers on the rate and quantity of hydrogen production and the hydrogen-steam mass and energy release rates from the reactor coolant system. These parameters strongly influence the flammability of the break flow and containment atmosphere and the magnitude, timing, and location of potential combustion mode(s). Hydrogen transport and mixing is important because it will influence the initial and boundary conditions for combustion and is closely coupled to the uncertainty in predicting the combustion mode, the mitigation scheme, and the resulting thermal and mechanical loads.

6.2.1 Deflagration

Deflagration is a form of combustion in which the flame moves at subsonic speed relative to the unburned gas. Unburned gas is heated to reaction temperature by thermal conduction and mass diffusion from the hot burned gas. Deflagration is a likely combustion mode in degraded core accidents. It is necessary to understand the nature of deflagrations in order to estimate the resulting containment pressure and temperature loads. In order to develop a data base on deflagration, experiments were performed at the Variable Geometry Experimental System (VGES), Fully Instrumented Test Site (FITS), and Nevada Test Site (NTS) facilities.

6.2.1.1 Deflagration Experiments in VGES Facility

Early in the program, over 100 tests were performed in 5-m^3 burn tanks at the VGES facilities at Sandia National Laboratories (Ref. 6.1). These tests were designed to examine the effects on hydrogen-air combustion by varying particular parameters: hydrogen concentration, igniter type, igniter location, precombustion gas motion, precombustion gas pressure, concentration of additional diluent gas (N_2, CO_2) and the presence of an aqueous foam, and the effects of hydrogen-air combustion on equipment and simulated equipment. The results of the VGES testing provided data covering a wide range of hydrogen combustion phenomena. Hydrogen burns in the VGES tank produced significant pressure rises at hydrogen concentrations above 4.75 percent. Measured flame propagation

BEST COPY AVAILABLE

velocities increased rapidly as the initial hydrogen concentrations were increased. Upward flame velocities were found to be larger than downward velocities. For the fans-off tests, combustion completeness was different for the upper and lower portions of the tank. The results obtained from combustion of hydrogen with reduced air quantities indicated that as the total amount of air decreases there is a slight decrease in pressure rise. The operation of fans during the testing had significant effects on the burn characteristics. Tests performed with the fans on showed increases in the burn velocity, pressure rise, peak pressure, and the mean pressure derivative and a decrease in the pressure rise time. For hydrogen concentrations below 8 percent, the fans-on test showed an increase in the burn completeness. However, for the tests with hydrogen concentrations above 8 percent, the primary effect of fans was to increase the chemical energy release rates. The effects of CO_2 addition on hydrogen-air combustion is to reduce the peak pressure, pressure rise, and burn velocity and to increase the time to peak pressure. At approximately 54 percent CO_2 it was observed that the hydrogen-air mixture would inert. For hydrogen-air mixtures with less than about 15 percent hydrogen, the addition of 620:1-expansion aqueous foam produced a reduction in the peak pressure and temperature. However, for mixtures with greater than 15 percent hydrogen, the combustion mode was an accelerated flame that resulted in damage to equipment inside the VGES tank (Ref. 6.2). The VGES testing provided data on the combustion of hydrogen-air mixtures under various conditions. These data were used to make preliminary assessments of the effects of hydrogen-air combustion on large systems. This data base was also used to develop analytical models to provide a first-order predictive capability.

6.2.1.2 Deflagration Experiments in FITS Facility

As an extension to the VGES-generated data base, 239 tests were performed in the FITS facility, which is a 5.6-m^3 burn tank with steam environment capability (Ref. 6.3). In this facility at Sandia, 119 hydrogen-air burns and 120 hydrogen-air-steam burns were performed to investigate the combustion characteristics and flammability limits of combustible atmospheres that might occur inside containment during a loss-of-coolant accident in a nuclear power reactor. The data collected included the transient pressure signatures, local measurements of the total and radiative heat flux, and thermocouple measurements that were used for flame-arrival time mapping. The pressure measurements were used to infer the global total and radiative peak heat flux and energy deposition (or thermal loading) due to postcombustion cooling of these gases.

For the FITS tests, pre-ignition temperatures ranged from 20°C to about 110°C. Results indicated that the overpressure due to combustion increases to a maximum at 30 percent hydrogen and then decreases with increasing hydrogen concentration. Steam was found to inhibit the combustion process, most notably at rich steam concentrations. As the steam content increased for a given hydrogen concentration, the peak pressure and burn completeness decreased. The global energy deposition was similar to the NTS results (FITS 5.6 m^3 versus NTS 2,048 m^3). However, the radiative fraction of the total energy deposition was approximately half that observed in the NTS tests. This comparison suggests that radiation is scale dependent. The discrepancies observed from current data can be largely attributed to differences in initial temperature and pressure and to vessel geometry. These differences are more pronounced in the lean region of the flammability curve. The current data for turbulent mixtures are

BEST COPY AVAILABLE

incomplete. These data for turbulent conditions are especially important in reactor safety analysis since sprays and fans may be operational at the time of ignition. The FITS tests indicated that hydrogen-air mixtures are completely inerted in the FITS vessel at 52 percent steam by volume. The complete flammability limit region has been curve fitted. The correlation developed using this fit will allow for the analyst to perform a calculation to determine the flammability of a mixture and the approximate time into the accident sequence when combustion might occur. Flammability limits for hydrogen and steam mixtures in turbulent and quiescent environments were measured to within an average of ± 7.5 percent and ± 2.2 percent hydrogen and steam, respectively.

Transient combustion pressurization data were collected using 141-1 precise sensors and XT-190 Kulite sensors. FITS pressure data indicated that cold wall hydrogen-air combustion is more severe than equivalent hot wall burns. The addition of steam appears to reduce the combustion severity when compared to the peak combustion pressure on a hydrogen-air basis. Steam reduces the severity of lean quiescent burns (fans off) and appears to act as a simple diluent similar to nitrogen (VGES results) in air for lean turbulent burns (fans on). Steam also reduces the combustion severity of rich hydrogen concentrations for both quiescent and turbulent conditions. However, steam appears to increase the duration of combustion as measured by the pressure rise time.

The heat transfer inside the FITS vessel includes both convection and radiation. The convective heat transfer is assumed to be the difference between the total and radiative heat transfer. Local heat transfer measurements were performed using the experimentally measured combustion-pressure transient to infer global heat transfer characteristics of the postcombustion cooling phase. The actual local conditions may be somewhat different from such global estimates, especially near the flammability limits where incomplete combustion occurs. However, for burns in which relatively complete combustion occurs, the inferred global heat transfer results are considered representative of the actual local phenomena. The FITS data showed that the partitioning of the early postcombustion heat transfer is affected by the concentration of steam in the volume, and the addition of relatively high steam concentrations reduces the early postcombustion heat transfer. The addition of steam slightly reduces the total energy deposition to the surroundings compared to equivalent hydrogen-air burns, while the addition of moderate quantities of steam generally increases the radiative heat transfer fraction during the cooling process. When large quantities of steam are added and the mixture becomes inert, convection is comparable to radiation during the cooling phase, and the gas emittance is proportional to the characteristic radiation length.

The FITS experiments extended the deflagration data base to provide a complete flammability map for the hydrogen-air-steam system for both turbulent and quiescent pre-ignition conditions. These data were used to develop a correlation that describes the entire flammability region. The data also provide useful reference points for benchmarking existing codes (e.g., HECTR) and newly developed computer codes for hydrogen-air-steam combustion characteristics and for containment response modeling. In addition, this data base will be used to reduce the uncertainty associated with the thermal response of safety-related equipment during combustion inside containment.

6.2.1.3 Large-Scale Hydrogen Combustion Tests at Nevada Test Site

In addition to the NRC program, the Electric Power Research Institute (EPRI) and others had extensive programs to investigate hydrogen combustion behavior in degraded core environments. EPRI was the primary contractor for the large-scale hydrogen combustion experiments at the Nevada Test Site (NTS) (Refs. 6.4 and 6.5). These large-scale tests were jointly sponsored by the EPRI, NRC, and six foreign governments. Prior to the NTS experiments, combustion studies had been performed in vessels ranging from bench-scale to about 18 m^3. NTS experiments were planned to extend the current combustion data base to extrapolate the results from small-scale tests to much larger reactor containment buildings. A spherical vessel with a diameter of 16 meters, a volume of 2,100 cubic meters, and a design pressure of 87 psig was used for all 40 NTS combustion experiments. The NTS test program had a threefold objective: (1) to provide a data base for validating codes for premixed combustion in a single compartment and to verify the existing small-scale data base, (2) to verify the effectiveness of the deliberate ignition approach to hydrogen control for a wide range of sources and environmental conditions, and (3) to measure equipment response during and after hydrogen combustion events. The test program included both premixed combustion tests and continuous injection (hydrogen) tests.

1. Premixed NTS Combustion Test

Emphasis was placed on lean mixture compositions. Earlier small-scale tests suggested that combustion behavior of lean mixtures is more difficult to predict than that of rich mixtures. Parametric studies for code validation and containment effects included hydrogen concentration (5%-13%), steam concentration (4%-40%), igniter location (bottom, center, top, with/without sprays), sprays and fans (on/off), and the number of igniters. The NTS experiments were able to readily simulate the combustion environment of Three Mile Island Unit 2 (TMI-2). Average flame speeds were less than 5.8 m/sec in the upward direction, and no tendency toward substantial flame acceleration or DDT was observed. Turbulence induced by sprays and fans produced elevated pressure ratios for the leanest mixture conditions. Pressure ratios were higher for elevated igniter locations than for quiescent bottom ignition tests. The time to peak pressure decreases with increasing hydrogen concentration and with enhanced turbulence. For the quiescent mixtures, higher initial steam content slows the burn despite the higher initial temperatures. Tests with fans on were intermediate between the quiescent and the sprays-on tests. At hydrogen concentrations greater than 10 volume percent, the time to peak pressure tended to converge irrespective of steam concentration and degree of turbulence. Burn completion ranged from 0 to 100 percent and was directly related to initial hydrogen concentrations. All burns at or above 7.7 volume percent hydrogen and up to 30 volume percent steam went to 100 percent completion regardless of turbulence level. In the test with 38.7 volume percent steam, the burn completion was 94 percent. For lean mixture conditions, turbulence promoted by fans and sprays appears to have affected the burn completion to a greater degree than ignition location. Top ignition under quiescent conditions resulted in very low burn completions because of quenching of the flame at the dome surface.

The NTS tests provided useful data to determine the effects of scale on combustion parameters such as peak pressure ratios, time to peak pressure, flame speeds, and burn completion. At large scale, the peak pressure ratios are higher and the pressure rise is slower. These effects are important in considering the pressure loads on containment structures during degraded core accident scenarios. This effect is important when determining equipment operability and thermal response data for assessing the performance of safety-related equipment during degraded core accidents in large containment volumes. When compared to a small-scale test, NTS data results suggest that combustion in a larger vessel will be more vigorous. Top ignition tests showed a rapid quenching of quiescent lean mixtures, and the introduction of turbulence promoted downward burning. Water sprays provided no adverse igniter cooling but did increase the burning rate and caused more rapid gas cooling. Based on NTS comparisons with small- and intermediate-scale tests, it is evident that vessel size and shape affect the combustion process at hydrogen concentrations of less than 8 volume percent. The vertical height from the igniter to the overhead surface where the flame quenching could occur may be an important effect. The surface-area-to-volume ratios are such that the small sphere would be expected to show a greater reduction in peak pressure due to heat transfer. For the intermediate-scale vessels, the overall fluid dynamics within the vessel may play a more significant role in the elongated, vertical cylinder vessels. Large-scale movement of gases in those geometries may sufficiently enhance the level of turbulence so as to account for higher pressure ratios than those measured at lean mixture conditions in the spherical test vessels with comparable volume. The increase in vessel volume from the NTS sphere to the TMI-2 vertical cylinder containment is about a factor of 27. The TMI-2 burn completion has been estimated at 85 percent. If the hydrogen concentration is accurate to within 0.7 volume percent, an extrapolation of the NTS burn completion data would be in good agreement.

Another effect of scale observed in the NTS experiments was the ability to sustain combustion in mixtures below the ignition limits previously defined by small-scale tests. The effect of steam addition on reducing pressure ratios and burn fractions was less dramatic than in smaller-scale tests.

2. NTS Continuous-Injection Tests

In the continuous-injection tests, there was continuous hydrogen and steam injection with pre-activitated igniters. The objectives of these tests were twofold: (1) to study the deliberate ignition approach to hydrogen control by visualization and measurement of combustion phenomena as well as the collection of data for validation of codes and equipment response and (2) to perform parametric studies for code validation and containment effects. Hydrogen-steam flow rates, ignition location, sprays and fans, and source geometry were varied. These continuous-injection tests suggested that fewer igniters are needed than previously believed and that the best location for igniters is in the upper half of the vessel (above hydrogen release point). Diffusion flames were observed at the source for low hydrogen-steam ratios, and instability in these diffusion flames increased almost linearly with an increase in pressure. Prior to these continuous-injection tests, it was expected that for a scenario in which there is continuous injection of hydrogen and steam, the favored mode of combustion would be deflagration and not diffusion flame burning. A deflagration was only achieved in one test when a very low flow rate was combined with water sprays and bottom ignition coupled with an intermediate Froude number. No ignition was observed when the source plume had a very low Froude number (0.002), the igniter was 1 meter below the source, and the atmosphere was quiescent.

The NTS continuous-injection tests extended the data base on hydrogen combustion phenomena. The source Froude number has a profound influence on the degree of mixing during the injection process. The various types of ignition behavior can be related to the Froude number and igniter location. The lack of multiple deflagrations and failure to ignite can be explained on this basis. As the source Froude numbers increase, the vessel contents become better mixed. Based on the NTS, Shepherd (Sandia) developed a model to accurately predict gas temperatures and pressures based on the assumption that wall-gas temperature differences reach a constant value after an initial transient and that total heat flux depends only on the fire power, vessel, and atmosphere heat capacities (Refs. 6.6 and 6.7).

6.2.1.4 Hydrogen Transport, Mixing, and Combustion Codes

1. HECTR 1.0 and 1.5

The HECTR (Hydrogen Event: Containment Transient Response) code is a reactor accident analysis tool designed to calculate the transport and combustion of hydrogen and the transient response of the containment. It is a major tool for predicting both local and global conditions during combustion sequences. HECTR is a lumped-parameter code and HECTR version 1.0 (Ref. 6.8) was developed from the data base generated from VGES, FITS, and other small-scale and intermediate-scale hydrogen combustion experiments. Models are included to calculate hydrogen combustion, radiative and convective heat transfer, and steam condensation or evaporation. The engineered safety features modeled in HECTR 1.0 are containment sprays, fans, ice condensers, sumps, suppression pools, and heat exchangers. HECTR 1.0 was successfully applied to analyzing the BWR Mark III and PWR ice condenser containments. HECTR version 1.5 contains significant improvements over 1.0 (Ref. 6.9).

HECTR 1.0 provided a first-order predictive capability, and as experimental data were made available updates were made to existing models, and new models were added to allow for calculations for all plant types (i.e., large, dry and subatmospheric PWRs) as well as for more severe core melt accidents. HECTR version 1.5 was released with the improvements provided in Table 6.1.

Before the large-scale experiments were performed at NTS, most of the existing data related to hydrogen combustion behavior was generated in bench-scale facilities and intermediate-scale vessels (Refs. 6.1 through 6.3 and 6.10). The HECTR code relies upon flame speeds, combustion completeness, ignition criteria, and propagation limits that were derived from the intermediate-scale experiments performed in the FITS and VGES. Since the combustion correlations determine the rate and amount of the energy release and time available for heat transfer, they strongly influence the calculated peak combustion pressure and temperature. The NTS experiments were performed to verify the data base established by the intermediate-scale tests and to validate the combustion models developed from these data (Ref. 6.4).

HECTR has been used to analyze the NTS large-scale hydrogen premixed combustion experiments (Ref. 6.11). When the HECTR combustion completeness correlation was developed, there was a very limited data base. Since the default flame speed correlation is based on VGES fans-on experiments, comparison to most of the NTS quiescent tests with the turbulence generated by the fans (VGES) resulted in a

Table 6.1 Capabilities of HECTR versions 1.0 and 1.5.

	Feature	Version 1.0	Version 1.5
1.	Natural Convection/Gas Transport	yes	yes
2.	Gas Treated	H_2O, H_2 O_2, N_2	H_2O, H_2, O_2, N_2,
3.	Implicit Numerics	yes	yes
4.	Intercompartment Fans	yes	yes
5.	Combustion	H_2	H_2 + CO
6.	Radiative Heat Transfer	from H_2O	from $H_2O + CO_2 + CO$
7.	Convective Heat Transfer	yes	yes
8.	Surface Conduction	yes	yes
9.	Containment Sprays	yes	yes
10.	Ice Condenser	1-D	2-D
11.	Sumps	yes	yes
12.	Mark III Suppression Pool	yes	yes
13.	Heat Exchanger	yes	yes
14.	Flexible Input of Source Gases	yes	yes
15.	Flexible Input of Energy Sources	no	yes
16.	Fan Cooler Model	no	yes
17.	Continuous Burning	no	yes
18.	Containment Leakage/Failure	no	yes

higher flame speed and burn time. Therefore, for the lean quiescent burn, the default correlations overpredicted the combustion completeness and flame speed, thus resulting in a higher peak gas pressure and temperature. A modified combustion completeness correlation was developed, and a similar effort to improve the algorithm used to predict flame speed and burn time is under way. Recalculations of the same NTS tests with the combustion completeness and burn time provided by EPRI show better agreement with the experimental data.

2. HMS-BURN Benchmarking Tool for HECTR

Since HECTR was being used as the major tool for reactor accident analyses (Refs. 6.12 through 6.16) for calculation of the transport and combustion of hydrogen, it was necessary to benchmark this code against a more detailed code. The HMS-BURN code (Hydrogen Migration and Mixing Studies--BURN model) (Ref. 6.17) was developed for benchmarking of HECTR. HMS-BURN solves time-dependent three-dimensional compressible Navier-Stokes equations with multiple species transport using a finite-difference approximation to the field equations. The chemical kinetics of hydrogen combustion is solved by a variant of the Implicit Continuous-fluid Eulerian (ICE) technique. In addition, a transport equation for the subgrid-scale turbulent kinetic energy density is solved to produce the time- and space-dependent transport coefficients.

HMS-BURN analyses have been performed on a Mark III-type containment where the formation of diffusion flames above the release areas in the suppression pool were established (Ref. 6.18). Transport calculations were also performed on a large PWR containment (Ref. 6.14) to determine hydrogen concentrations as a function of space and time. In cases where uniform mixing occurred, comparison to HECTR results showed good agreement. In a test in the FLAME facility where uniform mixing was not observed, HECTR showed poor agreement with HMS-BURN (Ref. 6.19).

3. HECTR-MAAP Standard Problem

In order to resolve differences between the NRC and the Industry Degraded Core Rulemaking (IDCOR) program on the hydrogen combustion issue, a standard problem was defined (Ref. 6.20) to compare hydrogen transport and combustion modeling between the HECTR and the MAAP (Modular Accident Analysis Program) codes. The important phenomena to be addressed included (1) natural circulation between the reactor cavity and lower compartment, (2) continuous in-cavity oxidation of combustible generation core-concrete interactions, and (3) incomplete burning in the lower and upper compartments. The problem selected was an S_2HF accident sequence in a PWR ice condenser containment. Because the objective was to compare hydrogen transport and combustion modeling between the HECTR and MAAP codes, the sources and initial conditions predicted by MAAP were used as input to HECTR. Since HECTR used the sources and initial conditions generated by the MAAP code, the HECTR results did not necessarily represent a best estimate of the pressure-temperature response of an ice condenser containment during an S_2HF accident.

The portion of the problem addressing incomplete burning in the lower and upper compartments is now completed (Refs. 6.21 and 6.22). The results of the HECTR analyses of the standard problem show that the calculated peak pressures using various compartment models are close to MAAP's prediction, provided ignition occurs at a hydrogen concentration below 7 percent. With the igniters working during the S_2HF accident, it is possible that combustion occurs at hydrogen concentrations below 7 percent. From the FITS tests (Ref. 6.3) at Sandia, combustion did occur at a hydrogen concentration of 5.5 percent with 30.4 percent steam concentration and the fans on. The probability of the flame at a point flashing back to the source location and burning as a diffusion flame was not considered. It is possible that this can happen, even though the first analysis showed that the flame may be unstable because of the high predicted steam-to-hydrogen-mixture ratio at the break. More work on diffusion flame stability is recommended to resolve this issue. Although the agreement of the peak combustion pressure between the HECTR and MAAP predictions is good, the discrepancy of the peak temperature is substantial. HECTR calculations were not in agreement with the MAAP prediction of a burn time on the order of 2 hours. Modeling differences that exist between HECTR and MAAP are particularly pronounced in multicompartment systems such as the ice condenser and Mark III containments. MAAP does not distinguish between flame ignition and flame propagation. Global burns in MAAP can never occur for mixtures greater than 7.3 percent hydrogen in air. Since essentially all containments can survive combustion under these conditions, MAAP never predicts any threat. MAAP does not allow for steam inerting. The incomplete burning modeled by MAAP is therefore considered nonconservative. Neither HECTR nor MAAP allows for the possibility of flame acceleration and detonation. Table 6.2 lists major differences in the combustion model of these two codes (Ref. 6.21).

Table 6.2 Modeling differences between HECTR and MAAP.

Combustion Model	HECTR	MAAP
Ignition Criterion	Depends on mixture concentration (user input; can be varied parametrically).	For global burn, uses flame speed criterion. For incomplete burn, check if burning velocity is greater than 1 cm/s.
Combustion Completeness	Calculates based on an empirical formula (a function of H_2 concentration).	Predicts a complete burn if flame temperature criterion is satisfied. For incomplete burn, uses an analytical formula (function of burning velocity, drag coefficient, igniter location).
Burn Time	Characteristic length divided by flame speed.	Regional radius divided by burning velocity for global burn. For incomplete burn, uses an analytical formula (function of burning velocity, drag coefficient, and density).
Flame Propagation	Upward, downward, horizontal propagations depend on H_2 concentration.	Upward propagation.

6.2.1.5 Deflagration Uncertainty

The likelihood and nature of deflagrations in reactor containments is strongly influenced by several parameters, namely, composition requirements for ignition, availability of ignition sources, completeness of burn, flame speed, and propagation between compartments (Refs. 6.1 through 6.4 and 6.11). In addition, combustion behavior is influenced by the effects of engineered safety features (fans, sprays), water fogs produced by steam condensation, carbon monoxide, and aerosols (Refs. 6.23 through 6.26). A number of research efforts by industry and foreign governments have been aimed at addressing the parameters affecting deflagration, and not all of these efforts are discussed in this chapter. A general understanding of those parameters that have a major impact on deflagrations has emerged over the years. For example, lower flammability limit values for hydrogen in air saturated with water vapor at room temperature and pressure were determined by Coward and Jones to be 4.1 percent hydrogen for upward propagation, 6.0 percent hydrogen for horizontal propagation, and 9.0 percent hydrogen for downward propagation (Ref. 6.27). These limits are still generally accepted. In reactor accidents, however, the condition inside containment prior to combustion may include elevated temperature, elevated pressure, and the presence of steam. Current research efforts have developed models and correlations to predict consequences of deflagration under reactor environments and scale.

Hydrogen deflagrations can be characterized as occurring at hydrogen concentration levels ranging from lean to rich. The hydrogen deflagration research completed to date provides a basis for assigning specific hydrogen concentration values to these levels. Combustion experiments performed at small, intermediate, and large scales with premixed hydrogen-air-steam mixtures confirms that hydrogen deflagrations will occur at hydrogen concentrations as low as approximately 5 percent. Combustion at this value is largely dependent on the presence of (1) ignition sources at elevations low enough in the containment/compartment to take advantage of upward flame propagation and (2) sufficient (although not quantitatively well-defined) convective mixing such as that provided by fans and sprays. The NTS tests suggest that turbulence induced by combustion initiated at low elevations in a compartment can be sufficient to promote significant combustion.

More recent experimental efforts provide additional confidence in our understanding of combustion behavior under expected plant conditions and have resulted in a reasonably complete data base at several scales for ignition limits, combustion completeness, flame speed, and burn pressure for hydrogen-steam-air mixtures. Theoretical relationships have been established to describe the effect on the various combustion parameters due to the operation of engineered safety features and the presence of water fogs. A lesser amount of information has been obtained concerning the effects of carbon monoxide and aerosols on the combustion behavior. However, a basic understanding of these effects also exists. Specifically, a correlation developed from data from the FITS facility has been shown to predict the lower flammability limits for hydrogen-air-carbon monoxide mixtures with reasonable accuracy (Ref. 6.3). Also, scoping tests have been performed by Sandia to address the effects of simulated aerosols on combustion (Ref. 6.24). These studies suggest that metallic aerosols significantly increase the vigor of the burns, while oxidic aerosols produce only minor changes in the burns. The effects of hydrogen combustion on fission product simulant aerosols was investigated (Ref. 6.28). These scoping tests provided qualitative insights into important sensitivities of the source term to the form of radioactive iodine in containment. Large amounts of elemental iodine in containment were produced when CsI/Al_2O_3 aerosol was exposed to hydrogen-air combustion. CONTAIN calculations suggest that sprays are effective in reducing both particulate and elemental iodine.

The uncertainty in the area of deflagration is closely coupled to the uncertainty in hydrogen transport and mixing. Both control volume and finite difference codes have been developed to address hydrogen transport, mixing, and deflagration. Significant progress has been made with HMS-BURN (finite difference) and HECTR (control volume). However, HECTR tends to overpredict the rate and degree of mixing. Some experiments imply that stratification and large gradients can form under certain conditions. There is a need for large-scale prototypical tests for validation of the transport and mixing models for both the finite difference and control volume codes.

The predictive capability of HECTR as an analytical tool for an assessment of the pressure and temperature resulting from deflagration is very good. Models and correlations developed from small-scale and intermediate-scale tests agree well with large-scale NTS results. Both developmental and maintenance work continues for HMS-BURN and HECTR. Models from the HECTR code are currently in CONTAIN, and improved correlations for HECTR models, as well as new HECTR models, will be incorporated in CONTAIN. Consideration is being given to incorporating three-dimensional models from HMS-BURN in a CONTAIN 3D version.

6.2.2 Accelerated Flames and Transition from Deflagration to Detonation

Flame acceleration occurs during the propagation of a flame around obstacles. The flame front is distorted by the obstacle establishing eddies or vortices that broaden the flame front and yield a high volumetric rate of heat generation; more air is entrained and hence the burning rate and the flame front velocity increase. Flame speeds can be increased from a few meters per second up to several hundred meters per second depending on the distance the flame is allowed to travel and the number of obstacles encountered. Turbulence induced by fans can also lead to flame acceleration if the requisite hydrogen concentration exists.

Over the past several years, Sandia has conducted research to better understand flame acceleration phenomena and to assess the parameters involved in the transition from deflagration to detonation. This effort included small-scale experimental work performed by Sandia's subcontractor (McGill University, Canada) (Refs. 6.29 through 6.31); analytical model development by Sandia-Livermore using the CONCHAS-SPRAY and VORTEX DYNAMICS codes (Refs. 6.32 and 6.33); and MINI-FLAME (Ref. 6.34) and FLAME (Refs. 6.22, 6.35, and 6.36) experiments at Sandia. The Sandia FLAME facility is an experimental structure designed to study accelerated flames and transition to detonation at large scale. The facility is a reinforced concrete channel with integral dimensions of approximately 6 feet in width, 8 feet in height, and 100 feet in length. The top of the channel is comprised of steel plates that can be removed to provide vent areas ranging from 0 to 50 percent.

The first series of tests conducted in FLAME investigated the effects of the venting in an obstacle-free channel. In these tests, top vent areas of 0, 13, and 50 percent were considered with hydrogen concentration ranging from 12 to 30 percent. Measurements included flame speeds down the channel, overpressures, and the occurrence or absence of DDT. Significant flame acceleration or DDT was not observed in any tests with 50 percent top venting regardless of hydrogen concentration. For tests with either no top venting or 13 percent top venting, DDT occurred when the hydrogen concentration exceeded 24 percent.

FLAME Test Series II investigated the effect of obstacles on flame acceleration. The presence of obstacles greatly reduced the threshold for DDT. DDT has been observed for conditions of 20.0 percent hydrogen, with 50 percent venting and with the presence of obstacles simulating ice condenser upper-plenum air-handling units in the FLAME channel. DDT was also observed at 15 percent hydrogen and 0 percent venting in the presence of simple obstacles. The effect of scale on DDT was assessed by duplicating the conditions of the tests performed in FLAME in the mini-FLAME facility (1/12 FLAME).

137

Research performed to date to address the matter of flame acceleration and DDT has led to an improved understanding of the conditions required for these phenomena to occur. Results of tests indicate that significant flame acceleration can occur at hydrogen concentration in excess of 13 to 15 percent if the mixture is confined. Approximately 13 percent venting appears to support flame acceleration, and venting in excess of 13 percent tends to significantly reduce the likelihood of DDT. The presence of obstacles, however, may alter the relationship between vent area and requisite hydrogen concentration for flame acceleration and DDT.

The two important observations from the FLAME Series I and II, mini-FLAME, and McGill tests are (1) vents can act like obstacles for sensitive mixtures, and (2) obstacles can negate the effect of very large venting for sufficiently sensitive mixtures. The intensity of the combustion depends on the competition between turbulency-enhanced burning and pressure relief through venting.

In conjunction with the McGill work, the CONCHAS-SPRAY code was modified by Sandia-Livermore to analytically model flame acceleration phenomena. The objectives of this effort were (1) to provide a predictive capability for flame acceleration, (2) to provide analysis for interpretation of experimental observation, and (3) to investigate scaling laws. CONCHAS-SPRAY was compared with small-scale experiments at McGill University and with large-scale FLAME tests at Sandia. At present, CONCHAS-SPRAY models underpredict flame acceleration pressures and flame speeds by a factor of two. Further development on CONCHAS-SPRAY is needed but has been terminated.

The uncertainty associated with flame acceleration and DDT is closely coupled to detonation and will be factored into the detonation uncertainty.

6.2.3 Detonation

Hydrogen detonations involve the reaction of hydrogen through the supersonic propagation of a burning zone or combustion wave. The pressure loads developed are essentially dynamic loads. For certain containment designs and accident sequences, hydrogen transport calculations indicate that detonable mixtures can be formed in limited regions of containment. Detonation of this hydrogen can potentially threaten containment integrity and equipment survivability.

The possible modes of initiation of detonation include direct ignition (Ref. 6.37), ignition by a hot jet of combustion products (Ref. 6.38), and DDT (Ref. 6.36). Because very powerful ignition sources are not expected to be present in an accident, most accident scenarios assign a very low probability to the detonation mode. However, given our improved understanding of DDT, this may no longer be a valid assumption.

Major questions regarding detonation of a flammable mixture include (1) whether the mixture is detonable for the particular geometry under consideration and (2) whether the ignition source is of a sufficient energy level to directly initiate a detonation. Substantive research (Ref. 6.39) has been performed by Sandia and McGill, in conjunction with the work on flame acceleration, to address these questions. This research was directed toward establishing a relationship between the characteristic detonation cell size and the geometric confinement and gas mixture conditions required to support a detonation.

The Heated Detonation Tube (HDT) (Refs. 6.39 through 6.41) facility at Sandia was constructed to allow a more detailed study of the effects of initial temperature, pressure, and diluent gas concentration on the fuel-air requirements for detonations. In contrast to the small tube diameters (on the order of several inches) used in earlier detonation tests, the HDT is approximately 17 inches in diameter and 43 feet long and is capable of operating above 100°C. The capability to operate at elevated temperatures permits testing with superheated steam as one of the constituent gases.

Direct measurements of detonation cell size from smoked foil records and pressure records were performed in hydrogen-air, hydrogen-air-carbon dioxide, and hydrogen-air-steam mixtures over a wide range of mixture compositions and initial conditions. Testing performed in the HDT has achieved several objectives. First, the testing has confirmed a previously established relationship between detonation cell size and hydrogen concentrations in hydrogen-air mixtures. Results indicate that, for hydrogen-air mixtures at room temperature and atmospheric pressure, the detonation cell size ranges from approximately 0.6 inch for a stoichiometric mixture to approximately 2 feet for a mixture with 15 percent hydrogen. The curve is quite steep at lean mixtures and cell size increases rapidly for concentrations below 15 percent hydrogen (Ref. 6.42).

The effects of diluent gases such as steam and carbon dioxide (CO_2) on the detonability of hydrogen-air mixtures has been addressed in HDT tests. The data show that relatively small additions of diluents can significantly reduce the detonability of a hydrogen-air mixture. The addition of 5, 10, and 15 percent CO_2 increased the cell size by factors of 1.5, 2.8, and 12.8, respectively, at stoichiometry. The HDT tests have also confirmed the effect of mixture temperature and steam concentration on the required hydrogen concentration and cell size for detonation. The results confirm that these two effects have opposing effects. Higher initial temperatures were found to decrease the cell size; for a 100°C increase, a factor of three decrease in cell size was observed at stoichiometry, with a somewhat smaller reduction observed at leaner hydrogen concentrations. Higher steam concentrations were found to increase the cell size; the addition of 10, 20, and 30 percent steam resulted in increases in cell size by factors of 6, 30, and 60, respectively, at stoichiometry. The effects of steam dilution are partially offset by the decrease in cell size due to the higher initial temperature and pressure in the steam tests. The available information suggests that for a mixture containing about 10 percent steam at saturation temperature, the lower detonability limit would be at least 13 percent hydrogen. In a recent HDT test, a 12.5 percent hydrogen-air-steam mixture was detonable (at 20°C).* The HDT tests provide evidence that the presence of steam or carbon dioxide in a combustible mixture, even in relatively small amounts, significantly increases cell size and reduces the likelihood of detonations.

6.2.4 Uncertainty in DDT and Detonation

A model has been developed by Shepherd (Ref. 6.43) at Sandia (2ND model) for the purpose of applying HDT test results directly to containment conditions, e.g., pressures and temperatures, for hydrogen-air mixtures with steam and carbon dioxide diluents. For containment conditions, Shepherd's model yields a detonability limit envelope for hydrogen-air-steam mixtures that approaches that for the flammability limit and mixtures with a hydrogen concentration as low as about 10 percent predicted to be detonable. However, there are uncertainties in the model. The model predicts existing data to within only a factor of four and does not account for the beneficial effects of suspended water (droplets and vapor) in suppressing detonations. Additional uncertainty is introduced in extrapolation to larger scales and reactor conditions of temperature and pressure. When Shepherd's model is extrapolated to high temperatures, it is predicted that increasing temperature will have the effect of sensitizing off-stoichiometric hydrogen-air mixtures. It is also predicted that at elevated temperatures steam loses its inerting effect and behaves as a sensitizer. Extensive high-temperature combustion research is needed to adequately reduce the uncertainty in the detonation model. Hence, the uncertainty in whether a mixture is detonable can be large at borderline hydrogen concentrations.

---

*Note added in proof: In a more recent test at 100°C, the lowest concentration of hydrogen that allowed a detonation to propagate was 11.5 percent.

The uncertainty regarding the detonability of lean mixtures is offset by the fact that the critical initiation energy increases dramatically as hydrogen concentration decreases and cell size increases (Ref. 6.44). Critical initiation energy varies with the cube of cell size. Initiation energy increases significantly with the presence of steam and water sprays. It should be noted, however, that geometry and degree of containment can influence detonability and act to decrease the energy requirements. For example, a detonation of a 13.5 percent hydrogen mixture was directly initiated in the HDT facility using 80 g tetryl. Nevertheless, energy sources of this magnitude are considered extremely unlikely to exist in containments.

Deflagration is a likely mode of combustion in degraded core accidents. Since it cannot be ruled out that deflagration will occur and, given the complexity of the reactor geometry and the uncertainty in mixing models and the potential for locally high hydrogen concentrations, this ordinary deflagration could lead to flame acceleration followed by DDT. Based on McGill, mini-FLAME, FLAME, and international research efforts, a data base now exists on flame acceleration, DDT, and detonations. A qualitative picture of flame acceleration and DDTs has now emerged. Phenomenological codes are improving, but all developmental work has stopped. Large-scale experiments are needed for different geometries and obstacle configuration. Flame acceleration and transition from deflagration is possible under certain conditions. In order to adequately quantify the threat posed by detonation, work needs to continue in this area to quantify the uncertainty associated with DDT and to have in place a predictive tool for flame acceleration and DDT.

Both experimental and theoretical work on flame acceleration and DDT is completed. The Shepherd 2ND model has been used to address detonation for a large, dry PWR (Ref. 6.45). If the 2ND model is to be used to interpolate and extrapolate detonation data to reactor environment and scale, theoretical work, coupled with high-temperature combustion experiments, needs to continue on this model to further reduce the uncertainty.

Review of Hydrogen Combustion Research by National Academy of Sciences

The Committee on Hydrogen Combustion was formed in 1985 and was composed of seven experts in the areas of nuclear reactor safety, physics, gas dynamics, combustion, chemical kinetics, and hazard analysis. These experts were asked to perform an independent assessment of the technical issues related to the behavior and control of hydrogen generated in severe accidents and to determine the degree to which current knowledge may support regulatory decisionmaking. In recent years a great deal of safety-related hydrogen combustion research has been carried out at different scales, and various geometries and computer codes have been developed based on these experimental results. Because of the importance of this work, the committee was asked to assess (1) the ability to scale up and to interpolate and extrapolate data from experimental scale to actual plant conditions and (2) to assess whether all important areas of research have been adequately addressed.

The committee concluded (Ref. 6.46) that the current research program on hydrogen combustion had properly covered most technical aspects in this area and that an extensive large-scale experimental program is not needed. However, the committee did recommend some further work. Among its recommendations are the following:

- To further reduce uncertainties in hydrogen release, transport, mixing, and combustion models by comparison with large-scale experimental results and to incorporate some zone and field modeling efforts into existing codes.

- To develop methods for improving the reliability of igniter systems during station blackout scenarios and continue to develop catalytic igniter systems.

- To reduce uncertainties in diffusion flame and subsonic premixed flame phenomena (flame acceleration and DDT) through planned experiments.

- To reduce uncertainties associated with the likelihood of failure of subatmospheric containment under detonation loads through more detailed analysis.

- To reduce uncertainties associated with the possibility of detonation for large, dry containments having fan coolers through more detailed analysis.

- To form a new review panel to provide a critical assessment of modeling techniques currently being developed or used in the area of hydrogen transport and combustion.

Current funding is not available to adequately address these concerns.

REFERENCES FOR CHAPTER 6

6.1 W. B. Benedick et al., "Combustion of Hydrogen: Air Mixtures in the VGES Cylindrical Tank," Sandia National Laboratories, NUREG/CR-3273, SAND83-1022, July 1984.

6.2 M. R. Baer et al., "Hydrogen Combustion in Aqueous Foams," Sandia National Laboratories, NUREG/CR-2865, SAND82-0917, November 1982.

6.3 B. W. Marshall, "Hydrogen:Air:Steam Flammability Limits and Combustion Characteristics in the FITS Vessel," Sandia National Laboratories, NUREG/CR-3468, SAND84-0383, December 1986.

6.4 L. B. Thompson et al., "Large-Scale Hydrogen Combustion Experiments," EPRI Report NP-3878, in press.*

6.5 J. A. Achenbach et al., "Large-Scale Hydrogen Burn Equipment Experiments," EPRI Report NP-4354, December 1985.

6.6 J. E. Shepherd, "Analysis of Diffusion Flame Tests," Sandia National Laboratories, to be published.*

6.7 J. E. Shepherd, "Hydrogen-Steam Jet-Flame Facility and Experiments," Sandia National Laboratories, NUREG/CR-3638, SAND84-0060, July 1985.

6.8 A. L. Camp et al., "HECTR Version 1.0 User's Manual," Sandia National Laboratories, NUREG/CR-3913, SAND84-1522, April 1985.

6.9 S. E. Dingman et al., "HECTR Version 1.5 User's Manual," Sandia National Laboratories, NUREG/CR-4507, SAND86-0101, April 1986.

6.10 R. Torok et al., "Hydrogen Combustion and Control Studies in Intermediate Scale," EPRI Report NP-2953, June 1983.

6.11 C. C. Wong, "HECTR Analyses of Large-Scale Pre-Mixed Hydrogen Combustion Experiments," Proceedings of the International ANS/ENS Topical Meeting on Thermal Reactor Safety (San Diego, CA), American Nuclear Society, Vol. 2, Section XI.4, February 1986.

6.12 A. L. Camp, Sandia, letter to J. Telford, USNRC, "Consensus Summary for Standard Problem 6 of the Containment Loads Working Group," dated June 5, 1984.*

6.13 A. L. Camp et al., "MARCH-HECTR Analysis of Selected Accidents in an Ice-Condenser Containment," Sandia National Laboratories, NUREG/CR-3912, SAND83-0501, January 1985.

6.14 D. B. King and A. C. Peterson, "Hydrogen Transport in a Large Dry PWR Containment During Selected Arrested Accident Sequences," Sandia National Laboratories, NUREG/CR-4599, to be published.*

---

*Available in the NRC Public Document Room, 1717 H Street NW., Washington, DC.

6.15 J. C. Cummings et al., "Review of the Grand Gulf Hydrogen Igniter System," Sandia National Laboratories, NUREG/CR-2530, SAND82-0218, March 1983.

6.16 C. C. Wong, Sandia, letter to P. Worthington, USNRC, "Hydrogen Production and Combustion-Induced Loading of the Large-Dry and Subatmospheric PWR Containments," dated May 23, 1986.*

6.17 J. R. Travis, "HMS: A Computer Program for Transient, Three-Dimensional Mixing Gases," Los Alamos National Laboratory, NUREG/CR-4020, LA-10267-MS, February 1985.

6.18 J. R. Travis, "Hydrogen Diffusion Flames in a Mark III Containment," Joint ANS/ASME Conference on Design, Construction, and Operation of Nuclear Plants (Portland, OR), Supplement 1 to Vol. 46, p. 136, August 5-8, 1984.

6.19 J. R. Travis, "HMS Development and Assessment," Hydrogen Mid-Year Review, Silver Spring, MD, April 22, 1986.*

6.20 M. Plys, Fauske and Associates, Inc., letter to C. C. Wong, Sandia, dated October 1985.*

6.21 C. C. Wong, Sandia, letter to P. Worthington and R. Palla, USNRC, "A Standard Problem for HECTR-MAAP Comparison, Part I-Incompleted Burning," dated March 13, 1987.*

6.22 M. Berman et al., "Recent Results in Hydrogen Research," Proceedings of the U. S. Nuclear Regulatory Commission Fourteenth Water Reactor Safety Information Meeting (Gaithersburg, MD), October 27-31, 1986, NUREG/CP-0082, Vol. 6, February 1987.

6.23 K. D. Marx, "Air Currents Driven by Sprays in Reactor Containment Buildings," Sandia National Laboratories, NUREG/CR-4102, SAND84-8258, May 1986.

6.24 L. S. Nelson et al., "The Effects of Reactor Core-Simulant Aerosols on Hydrogen/Air Combustion," Sandia National Laboratories, SAND85-1577, to be published.*

6.25 L. S. Nelson et al., "The Behavior of Resistively Heated Hydrogen Igniters During Operation of Water Sprays in Containment," Sandia National Laboratories, NUREG/CR-4193, SAND85-0360, in preparation.*

6.26 L. S. Nelson et al., "Influence of 100- and 200-Micron Water Droplets on Lean Hydrogen Deflagrations," Sandia National Laboratories, NUREG/CR-4796, SAND85-2643, to be published.*

6.27 H. F. Coward and G. W. Jones, "Limits of Flammability of Gases and Vapors," Bureau of Mines, U.S. Department of Interior, Bulletin 503, 1952.

---

*Available in the NRC Public Document Room, 1717 H Street NW., Washington, DC.

143

6.28 G. D. Valdez, "CONTAIN Code Calculations of the Effects on the Source Term of CsI to I_2 Conversion Due to Severe Hydrogen Burns," Sandia National Laboratories, NUREG/CR-4499, SAND86-7108, October 1986.

6.29 R. Knystautas et al., "Transmission of a Flame from a Rough to a Smooth-Walled Tube," Proceedings of the Tenth International Colloquium on Dynamics of Explosive and Reactive Systems (Berkeley, CA), Vol. 106, pp. 37-52, August 1985.

6.30 J. H. Lee et al, "High Speed Turbulent Deflagrations and Transition to Detonation in Hydrogen-Air Mixtures," Comb. Flame 56, pp. 227-229, 1984.

6.31 J. H. Lee et al., "Turbulent Flame Acceleration: Mechanisms and Computer Modeling," McGill University, Sandia Report SAND83-8655, August 1983.

6.32 W. T. Ashurst and P. K. Barr, "Discrete Vortex Simulation of Flame Acceleration Due to Obstacles-Generated Flow," Sandia National Laboratories, SAND82-8724, September 1982.

6.33 K. P. Barr, "Simulation of Flame Propagation Through Vorticity Regions Using the Discrete Vortex Method," Sandia National Laboratories, NUREG/CR-3835, SAND84-8715, September 1984.

6.34 K. D. Marx, "Modeling of Flame Acceleration and Transition to Detonation," Hydrogen Mid-Year Review, Silver Spring, MD, April 21, 1986.*

6.35 M. P. Sherman, "The Effect of Transverse Venting on Flame Acceleration and Transition to Detonation in a Large Channel," Dynamics of Explosions, Vol. 106, pp. 66-89, 1986.

6.36 M. P. Sherman, "FLAME Experimental Program," Hydrogen Mid-Year Review, Silver Spring, MD, April 21, 1986.*

6.37 J. H. Lee et al., "Photochemical Initiation of Gaseous Detonation," Acta Astronautics 5, pp. 971-978, 1978.

6.38 R. Knystautus et al., "Direct Ignition of Spherical Detonation by a Hot Turbulent Gas Jet," Seventeenth Symposium (International) on Combustion, pp. 1235-1245, 1978.

6.39 M. Berman, "A Critical Review of Recent Large-Scale Experiments on Hydrogen-Air Detonations," Proceedings of 23rd ASME/AICHE/ANS National Heat Transfer Conference (Denver, CO), American Nuclear Society, p. 316, August 1985.

6.40 S. R. Tieszen et al., "Detonability of Hydrogen-Air-Diluent Mixtures," Sandia National Laboratories, SAND85-1263, to be published.*

6.41 S. R. Tiezen, "Heated Detonation Tube Experiments," Hydrogen Mid-Year Review, Silver Spring, MD, April 21, 1986.*

---

*Available in the NRC Public Document Room, 1717 H Street NW., Washington, DC.

6.42 S. R. Tieszen et al., "Detonation Cell Size Measurements in H_2O-Air-H_2O Mixtures," AIAA Progress in Aeronautics and Astronautics Series, Vol. 106, p. 205, 1986.

6.43 J. E. Shepherd, "Chemical Kinetics of Hydrogen-Air Diluent Detonations," Proceedings of the Tenth International Colloquium on Dynamics of Explosive and Reactive Systems (Berkeley, CA), Vol. 106, pp. 263-293, August 1985.

6.44 W. B. Benedick et al., "Critical Charge for Direct Initiation of Detonation in Gaseous Fuel-Air Mixtures," Proceedings of the Tenth International Colloquium on Dynamics of Explosive and Reactive Systems (Berkeley, CA), Vol. 106, pp. 181-202, August 1985.

6.45 M. P. Sherman and M. Berman, "The Possibility of Local Detonations During Degraded-Core Accidents in the Bellefonte Nuclear Power Plant," Sandia National Laboratories, NUREG/CR-4803, SAND86-1180, January 1987.

6.46 National Research Council, "Technical Aspects of Hydrogen Control and Combustion in Severe Light-Water Reactor Accidents," report prepared by Committee on Hydrogen Combustion, Energy Engineering Board, Commission on Engineering and Technical Systems, Academy Press, Washington, DC, 1987.

7. IODINE CHEMICAL FORM

L. K. Chan

7.1 Introduction

The low release of iodine from the Three Mile Island plant during the 1979 accident suggested to some that a possible explanation might be the formation of a low-volatility iodide compound, namely cesium iodide (CsI), and that it was transported as such within the plant instead of molecular iodine as previously assumed. Thermodynamic analyses conducted for NUREG-0772 (Ref. 7.1) showed the formation of CsI during transport in the reactor coolant system (RCS) but its formation was not favored in the reactor core. However, the analyses considered only the effects of parameters known, at the time of the study, to affect the chemical form of iodine. Since the publication of NUREG-0772, additional experimental evidence, although preliminary and in some cases not reproducible, indicates that other factors may also affect CsI stability in the RCS and containment.

If iodine is transported through the RCS as CsI, a significant fraction could be retained by aerosol deposition or condensation because of its lower volatility. Iodine release to the containment is therefore reduced. If the containment fails early, precluding the containment mitigation processes, RCS retention becomes more significant. Volatile iodides are vapor species and are more readily transported in the RCS. Although they are reactive with metal surface constituents such as nickel, they also readily react with aerosol materials such as silver. The aerolized silver iodine can escape the RCS, depending on the efficiency of aerosol trapping, whereas the nickelous iodide cannot unless it is revaporized.

Iodine retention in containment is more complicated. Particulate iodide such as CsI may not be as efficiently retained as some forms of volatile iodine species. The latter are chemically active and sometimes can be more efficiently retained than aerosols that undergo removal by settling alone. An example of these volatile iodide species is molecular iodine (I_2). I_2 is easily retained by suppression pools (Ref. 7.2), sprays (Ref. 7.3), and ice condensers (Ref. 7.4). It is also attracted to wet containment walls and other surfaces (Ref. 7.5). On the other hand, organic iodides are more difficult to trap. However, calculations based on the present state of technology indicate that organic iodides are minor species, although the uncertainties associated with these predictions are large (Ref. 7.5).

If CsI were stable and were extensively retained in the RCS, it would be susceptible to revaporization later in the accident. CsI revaporized from the RCS would enter the containment when mitigative processes are less potent. If the containment fails at this time, the net result of CsI stability is to create a late source of iodine.

This issue, therefore, is what are the chemical forms of iodine in the RCS and containment, and what are their relative quantities over the range of severe

146

accident conditions. The issue is expected to affect all types of plants and accident sequences and is also a technical issue in draft NUREG-1150 (see Section J.9 of Appendix J to NUREG-1150) (Ref. 7.6).

7.2 Description of Past, Present, and Future Research

Factors affecting the chemical form of iodine in the RCS include, but are not limited to, the following: temperature, hydrogen-to-steam ratio, cesium-to-iodine ratio, boron compounds, and perhaps other factors such as radiation. Except for boron compounds and radiation, the effects of these parameters on iodine speciation are well known and documented. It was concluded based on those known effects that, under most of the severe accident conditions in the RCS and assuming that there are no other factors involved, CsI is the thermodynamically favored species. Recent studies indicated that the assumption of "no other factors involved" may be invalid and that the concept that CsI is the dominant chemical form of iodine may be jeopardized.

7.2.1 Past Research

7.2.1.1 Iodine Chemical Forms in Reactor Coolant System

One of the pertinent findings related to this issue came from the Sandia National Laboratories separate-effect experiments to study the transport behavior of CsI in the RCS (Ref. 7.7). Results from experiments conducted in the absence of radiation showed that CsI is stable in the presence of stainless steel surfaces and steam for temperatures up to 1,300 K. Scoping experiments conducted in a low-level radiation field, however, indicated a significant decomposition of CsI with most of the cesium held up on the steel surfaces of the experimental apparatus and iodine collected downstream in the condensate tank. Volatile iodides, in particular hydrogen iodide (HI), are believed to have been generated. These results were not reproduced in a subsequent test (see discussion below).

The effect of radiation on CsI stability was reviewed in a meeting in December 1985 at Argonne National Laboratory (Ref. 7.8) (and in a second meeting in July 1986 at the Atomic Energy of Canada Limited at Whiteshell (Ref. 7.9)). At the Argonne meeting, a recommendation was made that the Sandia radiation experiments should be repeated at another independent facility to confirm the current experimental finding. The Electric Power Research Institute (EPRI) is sponsoring such a program at the Atomic Energy of Canada at Whiteshell. The first test in the program, which is to repeat the Sandia radiation experiment, was scheduled for January 1987.

Sandia has also repeated their radiation experiments (Ref. 7.10). In the new test, which lasted for 12 hours, the radiation field was raised and lowered twice for a duration of 3 hours each. In other words, the experiment was run without the field for the first 3 hours and during Hours 6 through 9. During Hours 3 through 6 and 9 through 12, the experiment was run with the field on. All other conditions were kept the same as in the previous radiation experiments.

The new Sandia radiation experiment resulted in some unexpected observations. While previous experiments suggested that CsI was stable in the absence of radiation and unstable with radiation, the present results showed that it was unstable regardless of whether the field was present. The cesium-to-iodine ratio in the condensate tank decreased steadily from about 0.78 at the beginning of the experiment to 0.62 at the end of 12 hours. Cesium was retained on the metal surfaces as previously observed.

Although the Whiteshell radiation experiments have not yet been run, experiments in the absence of radiation were conducted (Ref. 7.9). Experimental conditions in the Whiteshell tests were similar to those in the Sandia tests without radiation, except for some differences in the size and type of materials used for the apparatus. Results from the Whiteshell experiments showed that the cesium-to-iodine ratio in the condensate varied from 0.87 to 0.91 during most of the 8-hour run for the test with the acid-washed surface (the one Sandia used but was abandoned because of concern over trichloroethylene). For the test with an acetone-rinsed surface, the cesium-to-iodine ratio in the condensate ranged from 0.93 to 0.97. The cesium-to-iodine ratio with the acid-washed surface indicated a slightly higher extent of CsI decomposition. It is unclear whether chloride residue from the hydrochloric acid wash is assisting in the decomposition of CsI. Results from a recent diagnostic experiment at Sandia showed opposite trends in chloride concentration and CsI instability during the test, i.e., CsI instability was high when chloride concentration was low. However, Sandia pointed out that the effect cannot be dismissed until further evidence is obtained.

The latest Sandia results, the Whiteshell results without radiation, and the Oak Ridge National Laboratory parametric study (see below) were reviewed in a second meeting held in July 1986 at the Atomic Energy of Canada Limited at Whiteshell. The meeting was sponsored by the joint EPRI-NRC Steering Committee, whose charter is to review the Sandia and Whiteshell work. The committee consists of consultants and NRC and EPRI contractors and staff. The following recommendations were made by the committee in the July meeting:

1. Sandia should identify and control the variable(s) that was causing the decomposition of CsI.

2. Sandia and Whiteshell should work together to provide a common basis for result comparison. That is, both laboratories should standardize cleaning procedures, analysis methods, etc.

3. Analytical work such as the Oak Ridge parametric study should be emphasized to provide assessment of the impact of the iodine chemical form issue on source terms.

The committee also concluded that the effect of radiation on CsI stability is unclear from the known experimental results and that the effect needs to be investigated, in particular at higher levels of radiation.

Conflicting results on CsI instability were also obtained in other experimental programs sponsored by NRC and EPRI. Deposition samples from NRC-sponsored fission product release programs at Oak Ridge and the Power Burst Facility (PBF) supported the formation of CsI (Ref. 7.11). Analysis of the samples collected in the laboratory-scale furnace in the Oak Ridge experiments indicated that cesium and nearly all iodine were deposited at the same location at 500°C on the deposition tube as would be expected for CsI. Analysis of the deposition samples collected above the core from the PBF Severe Fuel Damage Test 1-3 showed the presence of at least one CsI particle. The PBF samples also showed the co-deposition of cesium and iodine similar to that observed in the Oak Ridge

148

experiments. Aerosol samples collected in the EPRI-sponsored Source Term Experiment Program (STEP) at the TREAT reactor indicated a majority of the iodine aerosols found were associated with cesium. However, iodine in the absence of cesium was also detected on nickel wire samples (Ref. 7.12).

The presence of boron carbide (B_4C) or borated coolant in the reactor vessel also affects CsI stability. Separate-effect experiments at Sandia and Winfrith (United Kingdom) showed that B_4C can be oxidized by steam to form boric oxide and boric acid, which later react with CsI to form cesium metaborates and HI (Refs. 7.13 and 7.14). Borated coolant may be evaporated to form boric acid during coolant boiloff. However, for the case of B_4C oxidation, in the environment of the core where the quantity of steam is limited and the oxidation of Zircaloy is thermodynamically more favorable, it is uncertain whether boric oxide or boric acid will be formed in quantities significant enough to affect CsI chemistry. Furthermore, boric oxide or boric acid formed in steam-rich regions of the core may not survive the reducing conditions present in the RCS in most severe accident sequences. Experiments conducted at Karlsruhe's Niels facility resulted in negligible oxidation of B_4C when steam was fed into the bundle.* It is noted, however, that there are several tons of borated coolant available from the waters of a PWR, and, if a very small fraction of this borate is present in the RCS, it could affect the behavior of cesium iodide and cesium hydroxide (CsOH). Based on this discussion, it can be concluded that the uncertainty in this area lies in the rate of generation of boron compounds in PWR and BWR cores and the stability of these compounds in the RCS.

Although they seem to be in disarray, the above results can be partially pieced together with the following explanation. At sufficiently high temperatures, the exchange reaction with steam and CsI occurs:

$$CsI + H_2O \text{ ----- } CsOH + HI \qquad (1)$$

The extent to which reaction (1) occurs is dependent on the absolute pressure, the oxygen potential, and the temperature of the gas phase. Entrapment of the cesium-bearing product of reaction to form a compound more stable than CsOH will also enhance reaction. For instance, boron compounds can react with CsOH to form cesium borates, thus pushing reaction (1) toward the right. In addition to boron, Sandia noted that silica impurities in steel can capture CsOH to form cesium silicates (Ref. 7.15). The observed CsI decomposition in the Sandia radiation experiments can be explained as the result of thermal processes in which the cesium-bearing product of reaction reacted with the oxide surfaces on stainless steel. The same explanation was proposed by analysts from the Battelle Columbus Laboratories in the July review meeting to explain the extent of decomposition observed in the Whiteshell scoping tests without radiation (Ref. 7.9).

Following the July meeting, Battelle Columbus conducted a small-scale experiment to confirm the Sandia and Whiteshell observations.** The experiment simulated the Sandia and Whiteshell conditions such as CsI concentration and temperature.

---

*Information was obtained from S. Hogan, KfK, in July 1986.

**Information was obtained from C. Alexander, Battelle Columbus Laboratories, in October 1986.

However, the test was performed in a batch-type reactor (instead of the flow reactors used in the Sandia and Whiteshell tests). The extent of CsI decomposition and the formation of HI were measured as functions of time using an online mass spectrometer. Results obtained in this experiment indicated that CsI was decomposed to form HI until the stainless steel surface was saturated with a cesium-oxygen compound. The CsI-to-HI ratio was increased from 10exp(-3) to 10exp(5) from the beginning of the test to the end of the test.

Battelle Columbus further performed a calculation using the above experimental results to examine the effect of CsOH on CsI stability in the presence of stainless steel and steam.* Input conditions for the calculation were:

Temperature: 1,300 K
Pressure: 100 ATM
H_2/H_2O ratio: 7
CsOH concentration: 0.1 mole
CsI concentration: 0.015 mole

Data on the equilibrium deposition of CsOH on stainless steel surfaces were obtained from the above experiment. The calculation also considered the entrapment of cesium-bearing species by boron compounds. The input value for the ratio of boric acid to CsOH and CsI was approximately 20. Results of the analysis showed a complete dissociation of CsI to form HI and the total retention of CsOH by the stainless steel. There was essentially no cesium borate present at the end of the calculation, indicating a lack of interaction between the cesium-bearing species and the boron compounds. It should be noted that these results were obtained from an equilibrium calculation and the latter was conducted at one set of severe accident conditions. The Battelle Columbus experiments were especially designed to evaluate the total range of reactivity of CsI with steam in the presence of stainless steel and were not kinetic in nature as were the Whiteshell and Sandia experiments.

The process of thermal decomposition followed by entrapment of one of the products of decomposition has not been reconciled with some experimental observations. It has not been tested against the earlier Sandia test and the Winfrith CsI experiments where CsI was found to be stable and against the Oak Ridge fission product release tests and the in-pile PBF experiments where cesium and iodine were found to be co-located. Nor has it explained the EPRI STEP results where a majority of the iodine aerosols collected were associated with cesium. A possible explanation could be that the environmental conditions that existed at the sample locations during the sampling period in the release tests may not favor the formation of separate cesium and iodine species or the surface entrapment of CsOH, or that the experimental conditions in the transport tests do not favor the proposed mechanism. As discussed earlier, the formation of separate cesium and iodine species depends on the temperature, pressure, and the H_2-H_2O ratio. Surface entrapment of CsOH depends on the rate of CsOH transport, surface microstructure, and the availability of reactive surface constituents. A detailed kinetic analysis of the sampling conditions in the various experiments cited is necessary to resolve the inconsistency.

---

*Information was obtained from C. Alexander, Battelle Columbus Laboratories, in October 1986.

150

7.2.1.2 Iodine Chemical Forms in Containment

The potential for the formation of volatile iodides in the containment has been known for some time but was not applied to any analytical study prior to that for NUREG-0956 (Ref. 7.11) because of insufficient data for model development. Compared to the determination for the RCS, formation of volatile iodides in the containment is less controversial.

Volatile iodides can be formed from CsI if it escapes the RCS. When CsI is dissolved in water, such as in the containment sump, it dissociates to form a cesium ion and an iodide ion. The iodide ion in solution may be converted to volatile iodine (I_2) or to methyl iodide (CH_3I). Those volatile forms may subsequently be revaporized, depending on the conditions in the sump. The volatility of iodine species from aqueous solutions has been studied extensively in the past in the absence of radiation. Oak Ridge National Laboratory has been investigating the effect of radiation on iodine volatility (Ref. 7.16). They found that for an aqueous solution at pH 6.0, the ratio of iodine concentration in the aqueous phase and that in the gas phase was greater than 10 exp(5) without radiation. With one megarad of gamma radiation, the ratio decreased to less than 10 exp(3). At pH 9.0, the effect of radiation on the ratio of aqueous iodides and volatile iodides was not apparent. The same study also showed that methane bubbled through an iodide solution with one megarad radiation was found to result in organic iodide formation. In a similar test without radiation, a negligible conversion was obtained. The situation may be relevant in a BWR suppression pool where methane from B_4C conversion is transported through the pool, which contains various dissolved iodine species. When silver aerosols were added to the above experiments with radiation (Ref. 7.16), iodine volatility was decreased because of the formation of insoluble silver iodide.

CsI also decomposes during hydrogen combustion in the containment. In a scoping study at Sandia National Laboratories (Ref. 7.17), the behavior of CsI aerosols at various hydrogen concentrations was studied at the Variable Geometry Experimental Series (VGES) chamber. Results from tests with 30 volume percent of hydrogen in air (stoichiometric composition) showed that as much as 75 percent of the input CsI was converted. Most of the dissociated iodine was found to be I_2. The extent of CsI decomposition was decreased with decreasing hydrogen concentration.

Although less than 1 percent of the bundle inventory of iodine during the sampling period was present in the containment vessel, airborne samples were collected, with a radioiodine species sampler to distinguish the chemical forms of iodine, in the containment vessel during the LOFT LP-FP-2 test (Ref. 7.9). The filters were analyzed by gamma ray spectroscopy and found to contain I-131, I-132, I-133, and I-135 as molecular iodine (I_2), methyl iodide (CH_3I), and hypoiodius acid (HOI). These fission products and others originated from leakage from the LOFT primary system and blowdown suppression tank into the containment. Samples were collected for several days following the test.

All these studies resulted in an alteration of the initial iodine chemical forms. In the studies of iodide behavior in water pools without silver and in hydrogen burns, iodine volatility was increased. In the case where silver was present in the aqueous solution, the altered species resulted in decreased volatility.

The above experimental results have been incorporated into the TRENDS (Transport and Retention of Nuclides in Dominant Sequences) code. The code was developed in the NRC Severe Accident Sequence Analysis program at Oak Ridge and contains correlations that describe the various transport processes for gaseous iodine species in the containment. Three types of iodine transport are considered. Convective transfer between control volumes and within each control volume is allowed, and changes in phases and chemical forms may occur. Models for the following iodine species in the phases indicated are included: I_2 (gas, aerosol, liquid, surfaces, deposited aerosol), CH_3I (gas, liquid, painted surface), CsI or I (gas, aerosol, liquid, surfaces, deposited aerosol), HI (gas, liquid, steel surface, deposited aerosol), and AgI (precipitate).

Much of the input data for the TRENDS code is output from other codes (e.g., temperatures, flow rates, aerosol behavior parameters); the validity of any TRENDS calculation is obviously dependent on the accuracy of such data. In situations where data were incomplete, approximations had to be made. For example, it was assumed that the concentration of iodate in aqueous solutions is small at severe accident conditions and that iodate conversion to I_2 can be neglected. One of the comments received during the July review meeting was that this assumption may be incorrect. Also, constants for the rate of deposition of HI and I_2 onto aerosols were approximated because of a lack of data. These assumptions and approximations need to be experimentally verified. Finally, equations describing the interconversions between species and phases were obtained in some cases from literature, but mainly from the experiments described above. These experiments were tailored to the specific conditions for the parametric calculations (see below). Additional experiments are needed to generalize the models so that they can be applied to a wide range of severe accident conditions.

Another process that belongs to the subject of containment iodine behavior and on which information is currently lacking is the behavior of decayed Te-132 in the containment (and RCS). Te-132 may be present in the containment (and RCS) in many chemical forms. The fate of the I-132 generated needs to be evaluated, experimentally and/or analytically.

7.2.1.3 Impact of Iodine Chemical Forms on Source Terms

While recognizing its insufficiencies, the TRENDS code was used in a sensitivity study to evaluate the impact of RCS volatile iodide formation on the environmental release of iodine. Before embarking on a discussion of the sensitivity study, a literature survey is given to present past work related to this study.

Previous analyses were conducted to estimate the release of iodine from the plant assuming that iodine was in the form of either CsI or elemental iodine. But the assumptions used in the analyses may be inadequate based on the present state of technology. The BMI-2104 study conducted calculations for five plants, and many sequences were based on the assumption that all the iodine was in the form of CsI. Although consideration was given to RCS retention, containment processes for potential volatile iodide formation were not included. For the Surry TMLB' sequence, significant RCS retention was predicted, and the plant release for iodine was 7 percent (Ref. 7.18). The Reactor Safety Study conducted similar analyses but assumed that all iodine was in the form of I_2. In that study, RCS retention was ignored but containment removal of I_2 was considered. Results for a sequence comparable to Surry TMLB' indicated that the

152

environmental release of iodine was a factor of 10 higher than BMI-2104 (Ref. 7.19). For other plants and sequences, the relative environmental release of iodine will probably be different.

Calculations were also made to estimate the impact of volatile iodide formation on the effectiveness of engineered safety features. The SPARC code was used to study the attenuation of molecular iodine in suppression pools (Ref. 7.2). The conditions used were from the Peach Bottom TC1 sequence (anticipated transient without scram but with hot suppression pool). Kinetic analyses, which assume that the rate of I_2 scrubbing is controlled by gas-phase mass transfer resistance, and equilibrium analyses with time-resolved partition coefficients were conducted. The effect of HI formation in the RCS and organic iodide formation in the suppression pool were not considered. Results showed that all I_2 decontamination factors for the TC1 sequence were greater than 10,000. This indicates that suppression pools provide effective scrubbing for molecular iodine. If HI is formed in the RCS and passes through the suppression pool, the decontamination factor for iodine (I from HI) will be lower (but will probably remain large) as a result of increased pool acidity due to HI. Similarly, if organic iodide were generated in the pool, its volatile nature will decrease the overall decontamination factor for iodine. The Oak Ridge parametric study concentrates on estimating the effectiveness of suppression pools and ice beds in retaining HI and CH_3I.

The ICEDF code was similarly used to investigate the retention of elemental iodine and CH_3I in ice condensers (Ref. 7.4). The conditions used were from the TML-gamma accident sequence (transient sequence with loss of core cooling). Assuming that all the iodine is in volatile forms and that there is about 50 percent of the initial ice inventory left in the ice condenser at the beginning of the calculation, the decontamination factors calculated for I_2 and CH_3I are 7.1 x 10 exp(9) and 1.4, respectively. For the case of no CsOH coming out from the RCS because of the reactions to form cesium silicates, borates, molybdates, and tellurides, etc., the decontamination factor for CH_3I remains the same but that for I_2 decreases to 7.0.

The analytical results indicated that if CH_3I is formed, it will remain gaseous as it passes through the ice condenser. The Oak Ridge study (Ref. 7.14), which is based on experimental models, shows that the formation of organic iodide is small, even for BWR reactors where methane can be generated from the decomposition of boron carbide. Methane is a key ingredient in the formation of methyl iodide. For I_2 and HI, since it is likely that some CsOH will leave the RCS, their retention in ice beds will probably be large.

As mentioned above, experiments at the Sandia VGES facility showed that in a near stoichiometric hydrogen burn, 75 percent of the input CsI aerosols was decomposed to form molecular iodine (Ref. 7.17). To assess the impact of this effect on the environmental release of iodine, the CONTAIN code was used (Ref. 7.3). The analysis was conducted for the Surry TMLB' and TML accident sequences. Both sequences are similar except that the TML sequence allows for the operation of containment sprays. The containment was assumed to have failed immediately after the hydrogen burn in both sequences. For this analysis, it was assumed parametrically that 75 percent of the CsI aerosols suspended in the containment at the time of the burn was converted to I_2. The analytical results indicated that, for the TMLB' sequence and the TML sequence with containment sprays failed after the hydrogen burn, the effect of CsI decomposition was to increase the release of iodine from containment by a factor of three. It should be noted that chemical phenomena affecting the behavior of volatile iodides in the containment are not modeled in CONTAIN so that the numerical results may be overestimated. In addition, if CsI is decomposed in the RCS, hydrogen burn may not have any effect on the chemical form of iodine, although iodine release from containment may be increased if hydrogen combustion fails the containment.

The most valuable piece of information from the CONTAIN study is the assessment of the effect of containment sprays on the retention of volatile and particulate iodides. The sequence calculated was the Surry TML sequence with the containment sprays operating, even after the hydrogen burn. The assumptions used were the same as those in the above calculations. Results of the analysis showed that, for the case of 75 percent conversion of CsI to I_2, the presence of containment sprays decreased the iodine release from containment by a factor of 40. For the case of no CsI conversion, the effect of sprays was to decrease the iodine release fraction by a factor of nine. If containment sprays are available, the effect of CsI decomposition on severe accident source terms is predicted to be small.

To update the Reactor Safety Study and the BMI-2104 study, a sensitivity analysis was conducted for NUREG-0956. The calculations were performed by Oak Ridge National Laboratory using the TRENDS code. The following plants and sequences were analyzed:

Plant: Surry   Accident Sequence: TMLB'-delta (no rainout)*
TMLB'-delta (rainout)**
TMLB'-epsilon†

Plant: Peach Bottom   Accident Sequence: TC-gamma††

Results of this study are provided in Table 7.1. The TMLB' rainout case will not be presented here but was discussed in Reference 7.5. The phenomenon of rainout in containment is no longer believed to be technically justified. The calculation was conducted because, at the time it was done, a position on rainout was not established.

Table 7.1 Atmospheric release of iodine aerosols and vapors (percent of core inventory).

		Base Case	Case 1	Case 2	Case 3
Surry:	TMLB'-delta	19	21	54	51
	TMLB'-epsilon	0.3	0.3	0.5	6.2
Peach Bottom:	TC-gamma	1.3	2.0	--	6.5

---

*Station blackout with early containment failure and without steam condensation at containment failure.

**Station blackout with early containment failure and with steam condensation at containment failure.

†Station blackout with late containment failure.

††Anticipated transient without scram, with core melt preceding containment overpressure failure.

154

The base case is the actual BMI-2104 value. Case 1 is the same as the BMI-2104 case except that containment and suppression pool chemistries are taken into consideration. In both the base case and Case 1, the chemical form of iodine entering containment is assumed to be CsI. Case 2 assumes that 80 percent of the iodine is HI and 20 percent is CsI. Case 3 corresponds to the case of 100 percent HI formation in the RCS and, in addition, no CsOH enters the containment sump or suppression pool. The release numbers given above are the sum of both aerosol and gaseous iodine release. Except for Case 3, the release of gaseous iodine species is usually orders of magnitude smaller than the release of iodine deposited on aerosols.

Relative to the base case, the Case 1 results indicate that containment or suppression pool iodine chemistry does not make much difference in the environmental release of iodine. The Peach Bottom results for all cases may not reflect the true effect of the suppression pool in volatile iodide removal since the decontamination factor for HI was assumed to be the same as CsI. Increasing the level of volatile iodide formation in the RCS to 80 percent (Case 2) results in approximately a factor of two increase in iodine release for both Surry sequences. Comparing results of Cases 2 and 3, the decrease in pH due to the absence of CsOH in the containment sump or suppression pool increases iodine release by about an order of magnitude but only for the TMLB'-epsilon sequence. In the delta sequence, the containment is breached at the same time that iodine enters from the RCS. Thus, most of the atmospheric release occurs before processes such as deposition onto surfaces or aerosol settling become important. This is the reason that there is little difference in the amounts released in Cases 2 and 3. Surface absorption of volatile iodine occurred in the delayed containment failure case (TMLB'-epsilon). It should be noted that in the calculations the coefficient for the rate of deposition of iodine on containment surfaces was assumed to be fixed at some constant value and that the containment wall surface areas were overestimated. The calculations are being rerun with more accurate values for containment surface area and for improved models for natural convection mass transfer coefficients.

Further review of the Surry results indicates that containment failure time dominates iodine release. The effect of RCS volatile iodide generation is less important although it increases the overall release of iodine. Quantitatively speaking, release from the delta sequence is about two orders of magnitude higher than release from the epsilon sequence, whereas release due to the formation of volatile iodides (Case 2 versus Case 1) has only risen twofold. For delayed containment failure accidents, the alkalinity of the sump water controls the ultimate release of iodine.

For the Peach Bottom TC-gamma sequence, the suppression pool pH seems to be a major factor in iodine release. The original objective of this calculation is to estimate the effectiveness of the suppression pool in scrubbing volatile iodides. This objective has not yet been met since it was assumed in the analysis that the decontamination factor for HI is the same as that for CsI. That assumption has now been corrected and the reanalysis of the Peach Bottom TC-gamma sequence is in progress.

In applying the results of this study, one should remember that the TRENDS code is still being improved and has not yet been validated. Furthermore, the calculations were conducted for a limited number of accident sequences and plants. As recommended by the EPRI-NRC Steering Committee in the July meeting, the analytical study should be expanded to include other accident sequences and plants so that generalizations can be made as to the importance of volatile iodide formation.

7.2.2 Present Research (FY 1987)

The chemical form of iodine in the RCS and containment affects the release of iodine and cesium from the plant. Both topics are being pursued in parallel. The work will provide a timely response to the recommendations made by the Steering Committee in the July meeting.

For iodine chemical form in the RCS, the committee recommended that Sandia should identify and control the variables that were causing CsI decomposition. A process consisting of the thermal decomposition of CsI to form CsOH in steam, followed by entrapment of the CsOH by the stainless steel surface, was proposed to explain CsI decomposition with and without low-level radiation. The process was supported by results from the Battelle Columbus separate-effect experiments. Further confirmation will be obtained in the Whiteshell program where experiments with low-level radiation are planned.

The process of thermal dissociation followed by surface capture, however, has not been shown to apply to the deposition behavior of cesium and iodine observed in fission product release experiments at Oak Ridge, PBF, and TREAT. It also has not been applied to the Winfrith results from separate-effect transport experiments with CsI. The reason could be attributed to the conditions at the sampling locations in the release experiments. These conditions may not favor either the formation of separate cesium and iodine species or the deposition of CsOH on stainless steel surfaces. Experimental conditions in the Winfrith experiments also may not favor the decomposition of CsI. To test the proposed CsI decomposition theory with the cited experimental results, an analytical model based on the proposed process needs to be established. Subsequently, a kinetic analysis can be conducted to examine the various experimental situations cited. This work will be done by Sandia.

Experimental work is also planned for this issue. The Whiteshell experiments without radiation and the recent Sandia diagnostic experiments with CsI showed that the effect of an acid-washed surface on CsOH capture cannot be excluded. Chloride left behind on the stainless steel surface from hydrochloric acid rinses may be assisting the surface retention of CsOH. Other factors such as the extent of surface oxidation or the availability of silica for reaction with CsOH, and mass transfer limitations, from the bulk gas to the stainless steel surface or through the oxide layers on the surface, will also affect CsOH entrapment. These factors will be explored at Sandia. If they are found to be important, functional dependencies will be obtained. Additionally, the effect of excess CsOH--a condition typically present in severe reactor accidents--on CsI stability needs to be kinetically validated, although the Battelle Columbus equilibrium calculation indicated that the presence of 10-to-1 molar ratio of CsOH to CsI did not affect CsI decomposition.

Further fission product release experiments at higher temperatures are needed in the Oak Ridge program. Current information from this program on iodine speciation and quantities released was obtained at or below 2,400 K. Data at more severe fuel damage conditions are needed to provide a data base to estimate concentrations of iodine species and other fission products and actinide species in the RCS. These concentrations can have a significant impact on the course of reactions and rates of reactions in the RCS. The Oak Ridge experiments are currently planned for temperatures up to 2,700 K. The final PBF experiment, SFD 1-4, was completed in FY 1985. Additional analysis and interpretation of PBF data are also being completed. The in-pile experiments at NRU are designed to investigate in-vessel hydrogen generation during fuel degradation but will also provide confirmatory data on the chemical form of iodine to the PBF and TREAT observations.

As for the effect of boron compounds on CsI stability, the quantity and stability of oxidized boron compounds in the reactor core and the RCS as a function of time and under various severe accident conditions are needed. The rate of boric oxide or boric acid generation in the reactor core may be obtained as follows. For a BWR core with B_4C control rods, the severe fuel damage experiment in the in-pile Annular Core Research Reactor (ACRR), the DF-4 test, will confirm the German data on the extent of B_4C oxidation or the rate of boric oxide and boric acid generation. For a PWR core, the rate of evaporation of borated coolant may be estimated based on the noncongruent vaporization of boric acid-water solutions. To examine the behavior of boron compounds at transport conditions in the RCS, in particular under hydrogen-rich conditions, an analytical study is planned at Battelle Columbus. Calculations will be conducted not only at severe accident conditions predicted with the Source Term Code Package, but also at experimental conditions employed in the Sandia and Winfrith experiments. The latter is desirable in order to validate the analytical models used in the calculations.

For iodine chemical form in the containment, the Steering Committee recommended that the Oak Ridge sensitivity study should be expanded to obtain a general perspective on the importance of the iodine chemical form issue on source terms. Further calculations with the TRENDS code are being planned for other accident sequences and plants. But prior to the conduct of these calculations, the TRENDS code needs to be improved, in particular in the following areas. The mass transfer correlations used for the transport of volatile iodides to the containment walls--a process that is critical in containment iodine transport in PWR plants--needs to be reexamined and validated. A model of the chemical interactions of iodate in aqueous solution should be added to TRENDS. Models for the rate of deposition of HI and I_2 onto aerosols may need to be modified. In addition, adsorption isotherm data are needed for these species on a variety of aerosols. These improvements and others not mentioned here need to be made. Some can be made promptly, while others depend on the availability of experimental results (see below). When TRENDS improvement activities are completed, a reassessment of the calculations presented above will be made. The reassessment will include PWR as well as BWR plants, since a model for the scrubbing of volatile iodides in suppression pools, in addition to that for particulate iodides, was added. Subsequently, the study will be expanded to include other plants and accident sequences. Sequences with hydrogen burns should be examined mechanistically and in conjunction with other chemical processes occurring in the containment. Other plants of interest include BWR plants with Mark II and Mark III containments. PWR plants with large, dry containments such as Zion are also of interest.

As mentioned above, some models in TRENDS need to be experimentally supported. In the absence of experimental data at the time of the sensitivity study, assumptions and approximations were made to the models in TRENDS. These assumptions and approximations presently need experimental verification. Additionally, other models in TRENDS were based on results from experiments tailored for the specific conditions present in the sensitivity calculations. The experiments should continue to address other conditions so that the models can be applied over a wide range of severe accident conditions. All these experiments are presently in progress at Oak Ridge National Laboratory.

7.2.3 Future Research (FY 1988 and beyond)

Although confirmation will be provided from the Whiteshell experiments, low-level radiation does not seem to affect CsI stability. The effect of high-level radiation, however, is uncertain, as pointed out in the July review meeting. As recommended by the participants in that meeting, an experimental investigation is needed to determine the effect of high-level radiation--typical of that encountered in the RCS during severe accidents--on fission product chemistry. If further discussions show this to be the case, high-level radiation experiments will be conducted, as discussed below. For a start, experiments at dose rates of about 10 exp(4) rad/min are currently planned at Whiteshell. The NRC-sponsored work at Sandia will explore the possibilities of conducting experiments at dose rates of about 10 exp(5) rad/min. This dose rate is about two orders of magnitude higher than that used in previous Sandia radiation experiments. The high-radiation dose experiments should show the susceptibility of CsI to decompose radiolytically. Additionally, HI freed by decomposition may be retained on RCS surfaces by reaction with materials such as silver or nickel to form metal iodides. Metal coupons consisting of these metals can be placed in the reaction tube to determine such HI retention mechanisms. The radiation experiments should also include other parametric variations such as the cesium-to-iodine ratio and other volatile fission products. These separate-effect experiments will be supported by the continued examination of cesium and iodine behavior in integral tests such as the Oak Ridge release experiments, the PBF tests, the EPRI STEP experiments at TREAT, and future tests at NRU.

For iodine chemistry research in the containment, future research should focus mainly on multieffect experiments to validate the TRENDS code. These experiments do not need to be large scale, but they should be integral in nature to demonstrate chemical phenomena omitted in TRENDS. The experiments should simulate severe accident conditions in the containment where all critical processes affecting iodine transport or retention should be included.

A process that may affect iodine release from the plant is the decay of Te-132 to I-132. Te-132 in particulate forms may liberate volatile I-132 when it decays. This may contribute to the volatile iodide concentration in the containment. Analytical and/or experimental work is being planned to determine the chemical form of iodine generated from the decay of various forms of Te-132. The research is also applicable to RCS conditions where a late source of iodine from tellurium decay may be possible and may escape the failed reactor vessel

158

into the containment. One approach to this problem is to assume that stable iodine compounds are formed that are similar to the original tellurium compounds and to conduct a thermodynamic analysis of the resulting iodine compounds to determine their stability. The case of Te-132 decayed into gaseous I-132 has been studied (Ref. 7.20). Results showed that iodine release was increased by a factor of five for the Browns Ferry station blackout accident sequence.

7.3 Technical Uncertainty Evaluation

Uncertainties in the chemistry of iodine and cesium in the RCS and the chemistry of iodine in the containment contribute to the overall uncertainty in the iodine chemical form issue. Research is being planned in both areas and specific details are described below. Specific tasks, including schedules, are summarized in Table 7.2.

Table 7.2 Tasks and schedules.

Task Title	Completion Date
RCS Iodine Chemical Form	
Sandia analytical study	March 1987
Sandia exploratory experiments	September 1987
Sandia radiation experiments	September 1988
Oak Ridge release experiments	September 1989
PBF data analysis	September 1987
Battelle Columbus study on boron compound effect	March 1987
Containment Iodine Chemical Form	
Oak Ridge iodine experiments	June 1987
Oak Ridge TRENDS calculations	September 1987
Oak Ridge tellurium decay experiments	September 1988
TRENDS validation	--

7.3.1 RCS Iodine Chemical Form (1987)

Following one of the recommendations made by the EPRI-NRC committee to find the cause for CsI dissociation, a mechanism was proposed whereby CsI thermally decomposes in steam to form CsOH, which subsequently reacts with the stainless steel surface. The mechanism, however, has not been tested against conditions other than those used in the Sandia and Whiteshell experiments. Results obtained in experimental programs conducted at Oak Ridge, PBF, TREAT, and Winfrith indicated that either CsI was formed or it was stable. It could be that the conditions in these experiments do not favor either the formation of separate cesium and iodine species or the deposition of CsOH on steel surfaces. Analytical evidence is being obtained at Sandia by:

159

- Developing a kinetic model based on the proposed mechanism of volatile iodide formation, and conducting an analytical study using this model at conditions that existed in the cited experiments or near the sampling locations in the cited experiments.

The task is expected to be completed by March 1987.

Experimentally, tests are planned to explore the effects of various factors on the surface retention of CsOH. One factor that may have an effect is the chloride residue from surface rinses with hydrochloric acid. Other factors such as the extent of surface oxidation, excess CsOH, and mass transfer processes involving surface structures also may affect CsOH entrapment. These factors will be examined at Sandia by:

- Conducting experiments to determine the importance and subsequently the functional dependencies of the various parameters on the surface capture of CsOH.

Task completion is expected by the end of FY 1987.

The Oak Ridge fission product release experiments and the in-pile PBF experiments have been providing information concerning the chemical form and rates of release of iodine. The information is limited to temperatures at or below 2,400 K. Data are needed on iodine chemical form at higher temperatures or at conditions of more severe fuel damage. The Oak Ridge experiments will be extended to 2,700 K. The last PBF experiment has been completed but data analysis and interpretation will continue. Briefly,

- For FY 1987, conduct three Oak Ridge high-temperature fission product release tests. (The remaining five tests are to be conducted in FY 1988 and FY 1989.)

- Analyze and interpret fission product behavior for PBF tests 1-3 and 1-4.

Both tasks are expected to be finished by the end of FY 1987.

The dispute in the issue of boron compound effect on CsI stability lies in the quantities and stability of oxidized boron compounds in the reactor core and RCS. The rate of boron compound generation in a BWR core with B_4C control rods can be confirmed in the in-pile ACRR DF-4 experiment; the rate for a PWR core with borated coolant may be estimated. Equilibrium analyses, and possibly kinetic analyses, of the stability of the boron compounds after formation for a wide range of H_2-H_2O ratios are planned at Battelle Columbus. Conditions of the analyses will be extracted from the Source Term Code Package predictions published in NUREG/CR-4624 (Ref. 7.21) and from the Winfrith and Sandia separate-effect experiments on this subject. The latter will provide validation to the models used for the study.

- Conduct the ACRR DF-4 experiment at Sandia.

160

- Perform estimates on boron compound generation in a PWR core, and perform analysis to study the stability of these compounds in the RCS under various severe accident conditions, including those used in laboratory experiments.

The first test is included under the issue of in-vessel core melt progression, since the test is intended to study fuel degradation behavior with B_4C control rods. The second task will be completed by March 1987.

7.3.2 Containment Iodine Chemical Form (1987)

Another suggestion made in the July meeting was to emphasize the Oak Ridge parametric study and to use the results from this study for closure of the iodine chemical form issue. At present, only limited plants and accident sequences have been analyzed, and the conclusions are plant- and sequence-specific. The present study is being expanded so that perspectives can be obtained for a broad spectrum of plants and accident sequences. But prior to the conduct of these additional calculations, models in the TRENDS code for processes that contribute most to the environmental release of iodine need to be improved. Experiments are being conducted also at Oak Ridge to provide the necessary data for the improvements.

- Conduct experiments to provide data for model improvements in TRENDS.

- Improve TRENDS models with new data, reassess existing calculations with the improved TRENDS code, and expand calculations to include other plants and accident sequences.

The first task will be completed by June 1987 and the second task by the end of FY 1987.

7.3.3 RCS Iodine Chemical Form (1988 and Beyond)

The EPRI-NRC committee also recommended at the July meeting that the radiation experiments should be conducted at higher levels such as those relevant to severe accident conditions in the RCS. Sandia will thus explore the possibilities of:

- Conducting radiation experiments at dose rates of approximately 10 exp(5) rad/min.

Oak Ridge will continue to provide experimental data on the chemical form of iodine at severe fuel damage conditions.

- Conduct the remaining five fission product release experiments.

Experiments at NRU and ACRR will also provide data on this issue. As with the DF-4 experiment, these experiments will be noted under the topic of in-vessel core melt progression.

The Oak Ridge tests will be finished by the end of FY 1989.

7.3.4 Containment Iodine Chemical Form (1988 and Beyond)

For FY 1988 and FY 1989, containment iodine research will focus mainly on the validation of the TRENDS code. Integral experiments, not necessarily large scale, will be carried out to determine chemical phenomena and synergistic effects not modeled in TRENDS. The task has not been delegated, but its objective has been identified and it is:

- To conduct multieffect experiments to validate the TRENDS code. The experimental conditions should simulate those in the containment during severe accidents.

The schedule for this task has not been determined.

Additionally, analyses and/or experiments are planned to determine the fate of I-132 formed from the decay of Te-132. If volatile iodides are formed, iodine source terms may be affected. Oak Ridge will:

- Conduct thermodynamic analyses and experiments to determine the chemical and physical form of I-132 formed by the decay of the various forms of Te-132.

The task is expected to be completed by the end of FY 1988.

REFERENCES FOR CHAPTER 7

7.1 U.S. Nuclear Regulatory Commission (USNRC), "Technical Bases for Estimating Fission Product Behavior During LWR Accidents," NUREG-0772, June 1981.

7.2 P. C. Owczarski, Pacific Northwest Laboratories (PNL), letters to J. Mitchell, USNRC, dated December 13, 1985, and January 15, 1986.*

7.3 G. D. Valdez and D. C. Williams, "CONTAIN Code Calculations for the Effects on the Source Term of CsI to I_2 Conversion Due to Severe Hydrogen Burns," Proceedings of American Chemical Society Symposium on Chemical Phenomena Associated With Radioactivity Releases During Severe Nuclear Plant Accidents (Anaheim, CA), NUREG/CP-0078, to be published.*

7.4 P. C. Owczarski, PNL, letter to L. Chan, USNRC, dated April 14, 1986.*

7.5 E. C. Beahm et al., "Calculations of Iodine Source Terms in Support of NUREG-0956," Oak Ridge Technical Letter Report, ORNL/NRC/LTR-86/17, July 1986.

7.6 USNRC, "Reactor Risk Reference Document," NUREG-1150, Vol. 3, Draft Report for Comment, February 1987.

7.7 R. M. Elrick and D. A. Powers, "Effects of Ionizing Radiation on the Transport Chemistry of Cesium Iodide," Proceedings of the Specialists' Workshop on Iodine Chemistry in Reactor Safety (Harwell, England), United Kingdom Atomic Energy Authority, AERE R 11974, p. 291, January 1986.

7.8 L. Chan and C. Ryder, USNRC, memo to M. Silberberg, USNRC, Subject: Summary of the Meeting on the Effect of Ionizing Radiation on the Stability of Cesium Iodide, dated January 10, 1986.*

7.9 R. Ritzman, EPRI, and L. Chan, USNRC, "Summary of the Joint EPRI-NRC Meeting to Review the Status of Work on Cesium Iodide Stability in Severe Accident Environments," September 18, 1986.*

7.10 R. M. Elrick, "Experiment Plan for Continued Study of Cesium Iodide Stability Including a Review of Previous Results," draft report for review, July 1986.*

7.11 M. Silberberg et al., "Reassessment of the Technical Bases for Estimating Source Terms," NUREG-0956, July 1986.

7.12 J. K. Fink et al., "Chemical Characteristics of Material Released During Source Term Experiments Project (STEP) In-Pile Tests: Part II," Proceedings of American Chemical Society Symposium on Chemical Phenomena Associated With Radioactivity Releases During Severe Nuclear Plant Accidents (Anaheim, CA), to be published.*

---

*Available in the NRC Public Document Room, 1717 H Street NW., Washington, DC.

7.13 R. M. Elrick and R. A. Sallach, "Fission Product Chemistry in the Primary System," Proceedings of the International Meeting on Light Water Reactor Severe Accident Evaluation (Cambridge, MA), American Nuclear Society, Vol. I, p. 4.6-1, August 1983.

7.14 B. R. Bowsher et al., "The Interaction of Cesium Iodide with Boric Acid Under Severe Reactor Accident Conditions," Proceedings of American Chemical Society Symposium on Chemical Phenomena Associated with Radioactivity Releases During Severe Nuclear Plant Accidents (Anaheim, CA), NUREG/CP-0078, to be published.*

7.15 R. M. Elrick et al., "Reaction Between Some Cesium-Iodine Compounds and the Reactor Materials 304 Stainless Steel, Inconel 600 and Silver," Vol. I, Cesium Hydroxide Reactions, Sandia National Laboratories, NUREG/CR-3197, Vol. 1, SAND83-0395, June 1985.

7.16 E. C. Beahm et al., "Chemistry and Transport of Iodine in Containment," Proceedings of a Symposium on Source Term Evaluation for Accident Conditions (Columbus, OH), October 28-November 1, 1985, IAEA report, March 1986.

7.17 L. S. Nelson et al., "The Behavior of Reactor Core-Simulant Aerosols During Hydrogen/Air Combustion," Proceedings of the U.S. Nuclear Regulatory Commission Thirteenth Water Reactor Safety Research Information Meeting (Gaithersburg, MD), NUREG/CP-0072, Vol. 6, p. 371, February 1986.

7.18 J. A. Gieseke et al., "Radionuclide Release Under Specific LWR Accident Conditions," PWR Large Dry Containment Design (Surry Plant Recalculations), Battelle Columbus Laboratories, BMI-2104, Vol. V, July 1984.

7.19 USNRC, "Reactor Safety Study--An Assessment of Accident Risks in U.S. Commercial Nuclear Power Plants," WASH-1400 (NUREG-75/014), October 1975.

7.20 C. F. Weber et al., "Tellurium Precursor Effect on Iodine Transport in a BWR Accident," Trans. Amer. Nucl. Soc., Vol. 49, p. 257, June 1985.

7.21 R. S. Denning et al., "Radionuclide Release Calculations for Selected Severe Accident Scenarios," Battelle Columbus Laboratories, NUREG/CR-4624, Vols. 1-5, BMI-2139, July 1986.

---

*Available in the NRC Public Document Room, 1717 H Street NW., Washington, DC.

8. FISSION PRODUCT REVAPORIZATION

L. K. Chan

8.1 Introduction

One of the major developmental advances in severe accident analysis since the Reactor Safety Study relates to the accounting for radionuclide retention in the reactor coolant system (RCS). The retention is predicted to occur as materials released during core heatup and degradation are transported through the RCS to the "break" (broken pipe, relief valve, etc.). For accidents involving relatively long RCS-transit times (e.g., station blackout in PWRs), the fraction of released material predicted to remain in the RCS can be large. For example, calculations for the Surry station blackout sequence in BMI-2104 (Ref. 8.1) showed retention of approximately 80 percent of the cesium and iodine species.

A process that can potentially counteract this RCS retention is the revaporization of radionuclides. Since the decay heat associated with the radionuclides of concern will, to some extent, be transferred to the RCS structures where they reside, the potential exists for the structures to be sufficiently heated to result in revaporization of the material. This process can thus affect both magnitude and timing of radioactive releases. The issue of fission product revaporization is also a technical issue in Section J.8 of Appendix J to NUREG-1150 (Ref. 8.2).

The importance of this issue lies in the timing of fission product revaporization. For early containment failure accidents, the radioactivity release is high. The additional activity associated with the revaporized fission products is not expected to dramatically increase the overall release. For delayed containment failure accidents, the consequences associated with fission product revaporization are more noticeable and increasingly significant if the timing of revaporization is delayed. If fission products revaporize early, i.e., near the time of vessel failure, the revaporized materials will enter the containment and interact with a concentrated source of aerosols coming off the core-concrete interaction. The result is some mitigation of the revaporization process. If fission products revaporize slowly and the process continues into the later part of the accident when the containment aerosol concentration is low, retention of the revaporized fission products is more difficult. The consequence may be a larger source term for the volatiles. From the standpoint of revaporization chemistry, the case of slow and continuous revaporization seems more likely, as discussed below.

Factors affecting fission product revaporization are post-vessel-failure thermal hydraulics, heat loss through vessel and pipe walls, and revaporization chemistry. The accident conditions relevant to this issue range from those present immediately after vessel failure to those present after containment failure. Prior to vessel failure, fission products that revaporize can recondense on

165

cooler surfaces in the RCS. Also, the containment processes would likely mitigate them effectively, provided the containment has not failed. If the containment fails early, the consequence would be as described previously in this section. Few computer codes have the capability of predicting flow velocities in the reactor vessel after vessel failure. Consequently, considerable attention is given to the discussion of post-vessel-failure flow conditions, as indicated below.

Conditions that are prerequisites to fission product revaporization are:

1. A significant deposited fission product source in the RCS for revaporization, namely, extensive RCS retention during the early part of the accident.

   Sequences that were predicted to have significant retention are the station blackout, ATWS, and TW sequences, the small-break LOCA sequences for PWRs and BWRs, and the PWR interfacing LOCA sequence. A small extent of RCS retention was estimated for the large-break LOCA sequences in the BMI-2104 study. The latter sequences are therefore less likely candidates for fission product revaporization.

2. Reasonable flow inside the vessel after vessel failure to carry revaporized fission products to the containment.

   Sequences that are believed to have significant flows inside the vessel after vessel failure are the LOCA-type sequences. TMLB' or other similar sequences were assumed to result in RCS failure at the bottom head of the vessel. The RCS failure location in high-pressure sequences is currently a technical issue under RCS natural circulation. The resulting single opening in the vessel is believed to sustain minimal convection inside the vessel. Openings in the RCS piping and the reactor vessel for LOCA-type sequences cause a "chimney" effect, which results in significant flows inside the vessel after vessel failure. Induced LOCAs, which are defined by the failure of an RCS component prior to vessel failure, could have the chimney effect. However, analysis conducted so far indicates little fission product retention for this type of sequence because of the high RCS temperatures (see discussion below).

To summarize, the prime candidates for fission product revaporization in the RCS are the small-break LOCAs and the PWR interfacing LOCA sequences. Of these two, the latter is less consequential since the revaporized fission products may not leave the RCS or the emergency core cooling system piping to increase the environmental source term of iodine. The long transport path and large temperature gradient from one end of the transport path to the other in the containment bypass sequence would merely result in the revaporized fission products moving downstream to be recondensed.

A related issue that should be treated here is the decay of Te-132 to I-132. Te-132 deposited in-vessel will decay continuously into I-132, which may be released to the containment. The result may be a late source of I-132. Information to model the consequence of Te-132 decay needs to be established.

As for the low-volatility radionuclides, their potential for revaporization also needs to be considered. Following vessel breach, air from the containment may be drawn through the RCS. The resulting oxidizing environment may cause the revaporization of the low-volatility materials. For instance, deposited ruthenium and molybdenum may be converted to their respective oxides: RuO_2 and MoO_3, which are more volatile than the metals. Metal tellurides such as those discussed above may also be oxidized and vaporized as tellurium oxides (TeO, TeO_2, or $TeO(OH)_2$).

Finally, deposits on RCS surfaces that are formed by condensation of radionuclide species may form non-ideal mixtures that can depress the vapor pressures of the deposited materials. Unreacted cesium hydroxide (CsOH) and cesium iodide (CsI) may form such a mixture when they coexist on structural surfaces. If CsI and CsOH are present in the mixture in a one-to-nine ratio, the vapor pressure of CsI over this mixture would be depressed significantly. The vapor pressure of CsOH would differ only slightly from that of pure CsOH.

Incorrect assumptions concerning the revaporizing species will result in the incorrect predictions of the timing of revaporization. High vapor pressure species would revaporize early. Early revaporization will cause little additional consequence since there are natural mitigation processes to reduce this source term. Additionally, if the containment fails early, the source term is so large that any augmentation due to fission product revaporization would be no more than noticeable. But the consequence for delayed revaporization may be large and may be erroneously dismissed because of incorrect revaporization chemistry.

It is possible that the stable fission product compounds formed by chemical reaction may not revaporize to any significant extent for temperatures up to and near the melting point of stainless steel. Although it may contribute to a late source of radioactivity, the release of deposited fission products after structural material melting is an unknown because of the lack of information on the behavior of the molten structures after vessel meltthrough.

8.2 Description of Past, Present, and Future Research

8.2.1 Past Research

The amount of fission products revaporized depends on the structural surface temperature. The latter is increasing as a result of the decay of deposited radionuclides. However, heat losses through insulated and uninsulated components of the reactor vessel and the RCS could reduce this temperature. Heat loss through uninsulated piping is generally not modeled in system analyses. However, the models currently in RELAP5 (and other thermal-hydraulic codes) can be used and are adequate to treat this effect. Heat loss through insulated piping is not treated in these codes, however. The Industry Degraded Core Rulemaking (IDCOR) program claims that revaporization is unimportant in large, dry PWRs because heat loss through vessel and pipe walls prevents the RCS surfaces from heating up sufficiently for fission product revaporization. They believe that the insulation materials will deteriorate and lose their function at the high temperatures of a severe accident. An independent confirmation of the IDCOR finding is needed.

167

The chemical forms of the deposited radionuclides affect the vapor pressures of the radionuclides and therefore the source during revaporization. At present, the chemical forms of most fission products adopted for analytical calculations are based on assumptions. Iodine is assumed to be in the form of CsI regardless of changes in the environmental conditions with time and location. Similarly, the remaining cesium not associated with CsI is assumed to be in the form of CsOH. Tellurium transport is also simplistically modeled and is based mainly on the properties of elemental tellurium. Other nonvolatile radionuclides such as molybdenum and ruthenium are lumped together under the general term "aerosols." The potential for revaporization of these materials has been neglected.

The chemical form of iodine is currently another area of uncertainty that is being investigated (Ref. 8.2). In that issue, the assumption that iodine is solely in the form of CsI is being challenged. Evidence from various experimental programs indicates that volatile iodides can be formed under severe accident conditions. Gaseous iodides such as molecular iodine (I_2) or hydrogen iodide (HI) may react with control rod aerosols to form silver iodide (AgI) or with structural surfaces to form nickel iodide (NiI_2) in the RCS.

These materials would exhibit revaporization properties different from those of CsI and consequently need to be considered in the revaporization of iodine compounds.

Besides CsI and CsOH, cesium may form cesium molybdates in the reactor core, as evidenced from the in-pile experiments at TREAT (Ref. 8.3). Additionally, results from laboratory experiments showed that cesium may not stay as CsI and CsOH during transport (Refs. 8.4 and 8.5). The consequence of CsI dissociation has been discussed above. CsOH was found to react with structural surface constituents to form cesium silicates, phosphates, aluminates, manganates, or other more complex compounds. Cesium as either the hydroxide or iodide can also react with condensed or suspended boric acids or boric oxide to form cesium borates. These various forms of cesium exert vapor pressures much different from that of CsOH.

Similarly, some tellurium may be released from the reactor core as tin telluride. In the RCS, elemental tellurium may react with control rod aerosols to form silver telluride or cadmium telluride. Elemental tellurium can be efficiently retained on RCS surfaces by reaction to form nickel telluride. Both tin and silver tellurides can form aerosols and are subjected to less efficient physical retention processes. Consequently, the formation of tin or silver tellurides would affect the amount of tellurium deposited and the source for the subsequent revaporization process. Additionally, deposited tin and silver tellurides may exert different vapor pressures from that of nickel telluride.

Stone and Webster conducted an analysis to assess the extent of revaporization in BWRs for a TW sequence and an AD (large-break LOCA with vapor suppression failure) sequence (Ref. 8.6). In the AD sequence in which the extent of RCS retention was predicted by Stone and Webster to be 75 percent, the fraction of fission products revaporized was estimated to be approximately 68 percent of the core inventory, or 90 percent of the deposited fission products, after 15 hours into the accident. It is noted that the 75 percent RCS retention

calculated by Stone and Webster for a large-break sequence is high compared to the 19 percent calculated by Battelle Columbus. The number is more compatible with that of the S_2D sequence for a PWR in BMI-2104. For the TW sequence, Stone and Webster reported an unspecified but small extent of revaporization. In the Stone and Webster analysis, the thermal-hydraulic code used was the THREED-RCS code, which was derived from the RELAP-4 code Mod 5, but details of the THREED calculation have not been reviewed by experts in this area. The same cannot be said about the Stone and Webster treatment of fission product chemistry. In their calculation, the volatile fission products were lumped together as "fissium." The latter had the mass and decay power of the combined iodine, cesium, and tellurium deposited in the RCS and the vapor pressure of CsI.

IDCOR included revaporization in their source term calculations for Peach Bottom (Ref. 8.7) and Grand Gulf (Ref. 8.8) and a sensitivity analysis on the extent of revaporization as a function of fission product vapor pressure for the Peach Bottom TQUV sequence (Ref. 8.9). For transient-type sequences, namely, TQUV, TQW, and TC for Grand Gulf and TW, TC, and TQVW for Peach Bottom, the extent of fission product revaporization calculated by IDCOR ranged from approximately 40 percent of the core inventory of CsI for Grand Gulf TQW to nearly 100 percent for Peach Bottom TQVW. For LOCA-type sequences for Grand Gulf (AE) and Peach Bottom (S_1E), 8 and 47 percent, respectively, of the initial CsI inventory were predicted to have revaporized. These numbers are in contradiction with the Stone and Webster finding that the chimney effect in LOCA-type sequences would cause a larger extent of fission product revaporization than found in transient-type sequences. For the NRC/IDCOR technical issue on RCS natural circulation, IDCOR first assumed flow directions and subsequently estimated the flow magnitudes. If the same approach is used in their revaporization calculations, the treatment of the issue is inaccurate.

The sensitivity study conducted by IDCOR for the Peach Bottom TQUV sequence indicated that, when the vapor pressure was reduced to 0.01 of the nominal vapor pressure used in previous calculations, a smaller (about 30 percent) but continuous fission product revaporization was predicted. The calculations considered heat loss through insulated and uninsulated portions of the reactor coolant system. Two conclusions can be drawn from the IDCOR calculations: (1) despite heat loss through insulated and uninsulated pipings, fission product revaporization still occurs, and (2) lower fission product vapor pressures will result in slow and continuous revaporization. The latter supports NRC's initial thoughts on the importance of chemistry with regard to fission product revaporization.

The NRC Severe Accident Sequence Analysis (SASA) program at Sandia National Laboratories has analyzed the issue of revaporization for the TMLB' sequence for Bellefonte (Ref. 8.10). The New York Power Authority version of the CORSOR-MERGE-TRAPMELT code was used in the analysis in conjunction with MARCON and other codes. For the TMLB' sequence with containment failure due to leakage at the time of vessel failure, results showed that 21 percent of the core inventory of CsI (18 percent for CsOH) was revaporized. The calculations were carried up to 7 hours after the initiation of the accident. This is much shorter than the computation time used in the Stone and Webster analysis (greater than 15 hours) or the IDCOR analysis (greater than 50 hours). If longer time is allowed for this analysis, the extent of revaporization could be higher. On the other hand, the calculations were carried out assuming no natural convection in the reactor vessel prior to vessel failure. In the presence of natural convection, the extent of fission product revaporization is expected to be lower because of higher RCS gas and surface temperatures and therefore less fission product deposition on surfaces. In the New York Power Authority suite of codes, post-vessel-failure thermal hydraulics in the vessel was crudely modeled, and the revaporization chemistry was based only on the vapor pressures of pure CsI and CsOH.

In addition to the TMLB' sequence, the SASA program has also analyzed a pump seal LOCA sequence. Calculations with the same suite of codes indicated high RCS gas and structural temperatures that resulted in large CsI and CsOH releases to the containment (93 percent for CsI and 77 percent for CsOH). It is likely that, for induced LOCAs in general, the extent of RCS retention for CsI and CsOH is small. However, if CsI and CsOH are converted to less volatile species, the extent of RCS retention would be higher and this type of sequence may need to be considered.

Comparing the SASA TMLB' calculations with the Stone and Webster TW analysis, there seems to be a disagreement between the two sets of results. The Stone and Webster calculations resulted in negligible revaporization for a BWR transient sequence, while the SASA calculations showed approximately 20 percent revaporization for a PWR transient sequence. Different conditions in the two plant types, accidents or otherwise, may be responsible, but differences in modeling and assumptions used in both analyses may also contribute to the different observations. A detailed review of both works is necessary to resolve the disagreement.

The NRC Source Term Code Package has fully coupled fission product transport and thermal-hydraulic analyses, but, in the absence of information on post-vessel-failure core conditions, it does not include any in-vessel thermal-hydraulic and natural circulation effects after vessel meltthrough. It also does not model detailed chemical interactions between fission products and other species. Nevertheless, an empirical assessment of this issue with the TRAP-MELT/MERGE part of the code package was conducted (Ref. 8.11). The calculations were made for the Surry TMLB' sequence where the flow path for fission product transport in the RCS was assumed to be the same prior to and after vessel failure. That flow path started from the core and went through the hot leg, the surge line, and the pressurizer to the containment. It was also assumed that a constant flow rate was sustained in the RCS after vessel failure. Results of the analysis showed that fission products revaporizing from the hotter surfaces were subsequently recondensed on cooler regions of the RCS. The net effect was a negligible amount of fission products entering the containment as a result of revaporization. The results are a direct consequence of the long flow path assumed for the transport of the revaporized fission products. The longer the flow path, the larger the surface area at cooler temperatures and the higher the probability for the recondensation of the vaporized fission products. The flow path for fission product transport depends on the location of RCS failure. For high-pressure sequences like the TMLB' sequence, RCS failure location is currently part of the technical issue on RCS natural circulation. The staff position on that issue favors an induced

LOCA at the hot leg over a pump seal LOCA or a steam generator tube rupture. If that is the case, the flow path for the transport of the revaporized fission product is shorter, and the mentioned results may have underestimated the importance of the fission product revaporization issue, at least for the Surry TMLB' accident sequence.

A separate-effect analysis to determine the effect of chemistry on fission product revaporization was conducted with the TRAP-MELT code at EG&G (Ref. 8.12). The analysis is not yet completed since only one chemical process was modeled and incorporated into the EG&G version of TRAP-MELT. That process was the non-ideal interaction between condensed CsI and CsOH. When CsI and CsOH condense on structural surfaces, some of these compounds may react with the surface constituents to form stable compounds, while the rest remain on the surface to form a non-ideal mixture. If CsI and CsOH are present on the surface in a one-to-nine ratio, the interaction would have a significant impact on CsI revaporization since it will be the minor constituent with a small activity coefficient in the liquid mixture. As a continuation to this study, additional chemistry models, for example, on reactions to form other species, are being incorporated in the TRAP-MELT code (see Section 8.2.2). The chemistry models are being supplied by Sandia.

The EG&G analysis was performed with assumed flow path and temperatures that remained the same throughout the calculation. The structural surface temperature and gas temperature in the control volume were assumed to be the same at 1,000 K. Calculations were also carried out for the case when the gas temperature was lowered to 408 K. A range of flow velocities (0.1 to 10 m/s), which was believed to be relevant to post-vessel-failure conditions in the vessel, was used. Conditions at the high (10 m/s) and low (0.1 m/s) end of the flow regime are assumed to be applicable to LOCA and transient sequences, respectively, since LOCA sequences have the chimney effect and are more likely to have higher flows. All other conditions were adopted from the BMI-2104 results for the Surry TMLB' sequence, in particular, results at the time of vessel failure. To test the sensitivity of fission product revaporization to chemistry, runs were made by turning the chemistry models on and off while keeping other conditions constant.

Results from the EG&G analysis indicated that in the absence of the CsI-CsOH interaction, and at a velocity of 1 meter per second and gas and surface temperatures of 1,000 K, the extent of CsI revaporization after 5 minutes of computation time was 0.15 of the surface inventory of CsI and that of CsOH was 0.18. Values for fission product inventories were taken from the BMI-2104 estimates for the Surry plant. When the chemistry model for the CsI-CsOH interaction in the TRAP-MELT code was turned on, the extent of CsI and CsOH revaporization was 7.7 x 10(-4) and 0.15 of the surface inventory of each species, respectively. Compared to the case of no CsI-CsOH interaction, the fractions of CsI and CsOH revaporized were decreased by factors of 200 and 1.2, respectively. As expected, the impact on CsI revaporization is more significant.

The results cited above for the cases with and without chemistry were obtained from a computation time of 5 minutes. When the calculations were extended to 54 minutes, the rates of CsI and CsOH revaporization for the case with the chemistry model turned on were changed. The rates of revaporization for CsI

171

and CsOH during the first 5 minutes of calculation were 2.0 x 10(-6) and 1.9 x 10(-3) kilogram per second, respectively. When the computation time was extended to 54 minutes, the CsI and CsOH rates were changed to 2.9 x 10(-6) and 8.3 x 10(-4) kilogram per second, respectively. At the end of the 54-minute calculation, about 70 percent of the deposited CsOH was vaporized while only about 1 percent of the CsI was transported to the gas phase. The CsI-CsOH ratio during this time increased from 0.20 to 0.64. The increase in the CsI-CsOH ratio can be attributed to the fact that the vapor pressure of CsI is reduced more than that of CsOH at the start of revaporization when CsI is the minority species. This effect is decreased with increasing time because the concentration and vapor pressure of CsI increase toward their steady-state values where the ratio of the rates of evaporization of the species equals the ratio of the surface concentrations. As a result, a majority of the CsI will be revaporizing at a later time. The analysis clearly demonstrates a case of delayed revaporization caused by revaporization chemistry.

For delayed containment failure accidents for the Surry plant, the iodine source terms to the atmosphere were predicted to be on the order of 10(-4) or 10(-5) of core inventory (Ref. 8.1). In general, up to 80 percent of the volatile fission products was calculated to be deposited in the RCS (Ref. 8.1). If a majority of the deposited CsI revaporizes at a later time when natural mitigation processes in the containment are inefficient, the iodine source term for delayed containment failure accidents could be significantly higher than 10(-4) or 10(-5) of the core inventory.

To determine the effect of the temperature gradient from the surface to the bulk gas on fission product revaporization, a calculation was conducted by lowering the gas temperature from 1,000 K to 408 K, while keeping the surface temperature the same at 1,000 K. Results of the analysis showed an increase by only a factor of about 1.2 (that is, a 20 percent increase) in the fractions of CsI and CsOH revaporized when the gas temperature increases from 408 to 1,000 K. In this case, the surface-to-gas temperature gradient seems to be less important than revaporization chemistry. Additional calculations were also conducted to determine the sensitivity of fission product revaporization to flow velocity. Increasing and decreasing the velocity from 1 to 10 meters per second and from 1 to 0.1 meter per second, respectively, changed the revaporization source term by less than a factor of nine. In most cases, the magnitude of change was about a factor of five or six. In the absence of important chemical interactions, mass transfer limitation dominates CsOH revaporization. It is also an important factor in CsI revaporization although the interaction between condensed CsI and CsOH has a larger impact on the revaporization of these species.

In another study, Powers and Bieniarz examined the effect of various chemical forms of cesium on cesium revaporization (Ref. 8.13). The analysis was performed with the New York Power Authority suite of codes. The code was modified to incorporate the chemistry of (1) cesium reaction with silica to form cesium silicate on the stainless steel surface, (2) cesium revaporizing as pure cesium borate, and (3) cesium revaporizing from a mixture of 10 mole percent cesium borate and 90 mole percent boric oxide. Other conditions used in the analysis were not reported. Results of the analysis showed that, for Case 1, the CsOH not reacted with the surface revaporized rapidly after vessel failure. The cesium that reacted to form cesium silicate did not revaporize. For Case 2, cesium borate revaporization was found to be slow but continuous. For Case 3, there was negligible cesium revaporization throughout the 2-hour calculation. All three cases resulted in different conclusions. Yet they could be present at the same time in the RCS during a severe accident. If one or more of these cases, or others not reported here, were excluded from revaporization analyses, large errors could be included in the calculated results.

8.2.2 Present Research (FY 1987)

The issue of fission product revaporization consists of two subissues, namely, post-vessel-failure thermal hydraulics (including heat loss through insulated surfaces) and revaporization chemistry. Because of the difference in the nature of these subissues, they will be treated separately.

8.2.2.1 Post-Vessel-Failure Thermal Hydraulics

Flow and mass transport information in the RCS after vessel breach is necessary to predict the transport of the revaporized fission products from the RCS to the containment. Flow conditions after the vessel has failed are controlled by natural convection. Treatment of natural circulation to date is mainly empirical, particularly when applied to post-vessel-failure conditions. Past studies by IDCOR, Sandia, and Battelle on fission product revaporization had to assume flow patterns prior to estimating the magnitudes of the flow velocities. Stone and Webster may have treated the subject mechanistically, but details of their work were not published. For these reasons, a task was established at EG&G to perform mechanistic calculations with the RELAP5 code. This will be an independent calculation without chemistry models. A separate chemistry calculation is planned and will use, as boundary conditions, the flow velocities and surface temperatures estimated from the RELAP5 calculations.

One disadvantage of these separate calculations is that feedback between thermal hydraulics and chemistry is absent. As fission products are transported from the surface to the gas phase, the heat source associated with the decay of the deposited fission products becomes smaller. This can affect structural surface temperatures and magnitudes and patterns of natural convection flow. Subsequently, revaporization source terms can be affected. Feedback between thermal hydraulics and chemistry is desirable. A combined calculation with RELAP5 and TRAP-MELT is possible since the linkage between the two codes was made, but this calculation is postponed to FY 1988 pending further indications from the results of the separate-effect analyses.

Another factor that may affect post-vessel-failure thermal hydraulics but which has not been considered extensively in past studies is heat loss through insulated and uninsulated parts of the pressure vessel and RCS piping. The temperatures of the structural surfaces in the RCS and consequently the rate of fission product revaporization will be affected by these heat losses. IDCOR predicted that structural surfaces in large, dry PWRs will not heat up enough to revaporize the deposited fission products because of heat loss through surfaces with deteriorated insulation. Effort should be expended to confirm the IDCOR finding by

1. Reviewing the IDCOR heat loss models,

173

2. Developing a best-estimate model based on manufacturers' data on the insulation materials used in nuclear power plants, and

3. Incorporating the models in thermal-hydraulic codes for subsequent analysis of this issue.

8.2.2.2 Revaporization Chemistry

A review of past literature on fission product revaporization indicated that fission product chemistry was incompletely modeled and consequently the chemical forms of deposited fission products, their vapor pressures, and the timing of revaporization may have been incorrectly predicted. The work necessary to predict the chemical forms of deposited radionuclides has been initiated. Post-test examination of deposition surfaces in the Power Burst Facility tests, the Electric Power Research Institute source term experiments at TREAT, and surfaces in the TMI-2 reactor are being used to identify possible forms that could be adopted by deposited radionuclides. These data are being supplemented by information on possible chemical forms of deposited fission products from laboratory studies. Additional data of this type may be obtained from the forthcoming NRU tests and the Annular Core Research Reactor source term experiments.

Analytically, a task has been identified at Sandia to develop chemistry models to predict the chemical forms of deposited radionuclides. The models are based on calculated and published thermodynamic data. It is understood that there is substantial uncertainty associated with this data base and that experimental verification of these data is needed. The chemistry models include models for non-ideal mixtures believed to be formed by various deposited radionuclides, models for cesium reactions in the gas phase and on structural surfaces, and models for tellurium behavior in the RCS. The decay of Te-132 into I-132 and the oxidation of deposited nonvolatile radionuclides after vessel breach will be modeled in FY 1988 as part of future work. The models developed at Sandia will be incorporated in the EG&G version of the TRAP-MELT code.

Following the completion of TRAP-MELT improvements by EG&G, preliminary analysis will be conducted to determine the effect of improved chemistry on the timing and rates of fission product revaporization. The calculations will be conducted in a manner described for the EG&G work in Section 8.2.1. Boundary conditions such as flow velocities and surface temperatures will be obtained in a separate analysis using RELAP5. Since delayed revaporization is more important, the calculations will be extended beyond the 54 minutes used in the previous analysis. The rates of revaporization as a function of time will be determined, and the results at several hours after vessel meltthrough will be reviewed to determine the potential impact of revaporization chemistry on severe accident source terms for delayed containment failure accidents. If the potential impact on source terms is great, an integrated analysis with the RELAP/TRAP-MELT code package will be conducted in FY 1988.

8.2.3 Future Research (FY 1988 and beyond)

If fission product revaporization occurs at later times at significant rates based on the separate-effect thermal-hydraulic and chemistry calculations, the next step toward the resolution of this issue is to obtain an accurate analysis of the impact of delayed revaporization on source terms. This can be accomplished partly by an integrated analysis using the RELAP/TRAP-MELT code package.

The use of the code package will enable feedback between thermal hydraulics and chemistry and will provide a better estimate of the timing of revaporization. To estimate the impact on source terms, that is, the effectiveness of various containment processes on the mitigation of the revaporized fission products, a code capable of analyzing radionuclide behavior in the containment is needed. The CONTAIN code has been selected and is currently in operation at EG&G. CONTAIN, however, concentrates on the behavior of radionuclide aerosols in the containment. It may be found that the behavior of radionuclide gases is also important. In this case, the TRENDS code needs to be coupled to the CONTAIN code. The coupling is currently planned for FY 1987 as part of the scoping of work at Sandia and the Oak Ridge National Laboratory.

The conditions for the integrated analysis will be chosen as follows. As a minimum, two plant types and two accident sequences for each plant type should be considered in the integrated analysis. This constitutes a total of four calculations. The plant types should be a PWR and a BWR, preferably Surry and Peach Bottom, respectively. The accident sequences should be a transient sequence and a small-break LOCA sequence with a chimney effect. These two sequences should be able to provide bounding values for flow and mass transport conditions in the vessel after vessel failure. Both sequences also have high RCS retention prior to vessel failure--a prerequisite for fission product revaporization. Delayed containment failure modes such as, but not limited to, basemat meltthrough should be considered. If necessary, additional calculations covering other sequences and plants can be conducted.

On revaporization chemistry, models need to be developed for the revaporization of nonvolatile radionuclides due to oxidation in the air and the generation of I-132 due to the decay of deposited Te-132. Furthermore, as noted earlier, the thermodynamic data base used to develop the chemistry models is uncertain. To reduce the uncertainty in this data base and to validate the models, separate-effect experiments are planned at Battelle Columbus. The Battelle Columbus experiments will provide data on speciation and vapor pressures in the gas phase. Multieffect experiments may also be necessary to validate the various kinetic limitations to fission product revaporization and to identify other factors that may affect revaporization.

8.3 Technical Uncertainty Evaluation

The uncertainties in post-vessel-failure thermal hydraulics and fission product chemistry contribute to the overall uncertainty in the issue of fission product revaporization. To approach this issue, research on both areas is conducted in parallel. Specific details of both areas of research, including schedules, are given below and summarized in Table 8.1. The current program ends in FY 1988, but more time is needed to complete the experimental work (see Section 8.3.4).

8.3.1 Thermal Hydraulics (FY 1987)

IDCOR claims that, in large, dry PWRs, heat loss through deteriorated insulation on RCS components will prevent heatup of structural surfaces and consequently fission product revaporization. To provide an independent confirmation of the IDCOR finding, a task was established at EG&G. Specific objectives of this task are:

Table 8.1 Tasks and schedules.

Task Title	Completion Date
1. Thermal Hydraulics	
Heat loss calculations	December 1986
Flow analysis	June 1987
2. Revaporization Chemistry	
Model development	December 1986
Model incorporation	June 1987
Revaporization calculations	September 1987
3. Integrated Analysis	September 1988
4. Experimental Validation	
Separate-effect experiments	September 1988
Multieffect experiments	September 1990

- To search the literature for heat loss data on the typical insulation materials used in nuclear power plants.
- To perform sensitivity calculations to assess the effect of heat loss through insulation on structural surface temperatures.

The task was scheduled for completion by December 1986.

Past studies based mainly on an empirical approach to natural circulation indicate a need for a mechanistic analysis to confirm the flow and mass transport conditions in the vessel after vessel breach. The work is to be carried out at EG&G. The calculations will consider heat loss through insulated surfaces and will provide initial and boundary conditions for the separate-effect chemistry analysis. The specific task objective is:

- To perform scoping calculations to determine magnitudes of flow rates, velocities, and surface temperatures.

This task is scheduled to be completed by June 1987.

8.3.2 Revaporization Chemistry (FY 1987)

The fission product chemistry models currently present in TRAP-MELT and other fission product behavior codes are inadequate to treat the problem of revaporization. As a result, radionuclides were found to revaporize early, and the impact on severe accident source term was incorrectly estimated. Accurate predictions of the chemical forms of deposited radionuclides are necessary to estimate the vapor pressures and the times at which the radionuclides revaporize. A task was established at Sandia:

- To develop gas-phase and surface chemistry models, based on thermodynamic data, to predict the chemical forms of deposited iodine, cesium, and tellurium.

All models will be delivered to EG&G and will then be coded and added to the EG&G version of the TRAP-MELT code. The improved TRAP-MELT code will subsequently be used in a separate-effect analysis to assess the effect of chemistry on the timing of fission product revaporization. Conditions for the calculations will include the flow data obtained in the separate-effect thermal-hydraulic analysis. The specific tasks for EG&G are:

- To incorporate the chemistry models developed at Sandia in the TRAP-MELT code.

- To perform independent revaporization calculations using the improved TRAP-MELT code and the boundary conditions provided by the RELAP5 analysis.

TRAP-MELT improvement activities should be completed by June 1987, and the revaporization calculations should be completed by September 1987.

8.3.3 Integrated Analysis (FY 1988)

The separate analyses conducted for the thermal-hydraulic and chemistry study do not consider feedback between thermal-hydraulic results and chemistry results. One example of feedback that needs to be considered is surface temperature. As fission products vaporize from the surface into the gas phase, the heat source associated with the decay of deposited fission products becomes smaller, and the surface heatup decreases. This information needs to be fed back into the thermal-hydraulic analysis so that a new surface temperature can be estimated for subsequent revaporization calculations. The result is a more accurate estimate of the timing of revaporization. Additionally, an estimate is needed on the effect of revaporization on severe accident source terms for delayed containment failure accidents. The CONTAIN code will be used for this calculation. EG&G will:

- Conduct integrated analyses with the RELAP/TRAP-MELT code package and the CONTAIN code to estimate the timing of revaporization and the corresponding impact on source terms.

The calculation should be conducted for a PWR and a BWR plant. For each plant selected, a transient and a small-break LOCA sequence should be used as conditions for the study. Task completion is expected by September 1988.

8.3.4 Experimental Validation

As discussed earlier, there are large uncertainties associated with the thermodynamic data base used for the development of the chemistry models. Experimental verification of the data base is needed and is planned at Battelle Columbus. Gas-phase interactions and surface interactions, including non-ideal interactions in liquid mixtures, will be considered. The experiments will provide data on the chemical forms of radionuclides and their characteristic vapor pressures. Activity coefficients in the liquid mixtures can then be calculated using the experimentally obtained vapor pressure data. In the Battelle Columbus program, multieffect experiments are also being considered to verify the integrated analyses on fission product revaporization. The specific task order for Battelle Columbus is:

- To conduct separate-effect experiments to verify the thermodynamic data base used for model development.
- To conduct multieffect experiments to verify the experimental predictions on fission product revaporization.

The separate-effect experiments are scheduled to be completed by September 1988. The multieffect experiments are expected to be finished by September 1990.

REFERENCES FOR CHAPTER 8

8.1 J. A. Gieseke et al., "Radionuclide Release Under Specific LWR Accident Conditions," PWR Large Dry Containment Design (Surry Plant Recalculations), Battelle Columbus Laboratories, BMI-2104, Vol. V, July 1984.

8.2 U.S. Nuclear Regulatory Commission (USNRC), "Reactor Risk Reference Document," NUREG-1150, Vol. 3, Draft Report for Comment, February 1987.

8.3 J. K. Fink et al., "Chemical Characteristics of Materials Released During Source Term Experiments Project (STEP) In-Pile Tests: Part II," Proceedings of American Chemical Society Symposium on Chemical Phenomena Associated With Radioactivity Releases During Severe Nuclear Plant Accidents (Anaheim, CA), NUREG/CP-0078, to be published.*

8.4 M. Silberberg et al., "Reassessment of the Technical Bases for Estimating Source Terms," NUREG-0956, July 1986.

8.5 R. M. Elrick et al., "Reaction Between Some Cesium-Iodine Compounds and the Reactor Materials 304 Stainless Steel, Inconel 600 and Silver," Vol. I: Cesium Hydroxide Reactions, Sandia National Laboratories, NUREG/CR-3197, Vol. 1, SAND83-0395, June 1985.

8.6 M. Donahue et al., "Analysis of Retention/Revaporization in a BWR Mark II Power Plant," Proceedings of an International Symposium on Source Term Evaluation for Accident Conditions (Columbus, OH), International Atomic Energy Agency, STI/PUB/700, p. 279, March 1986.

8.7 Technology for Energy Corporation, "Peach Bottom Atomic Power Station--Integrated Containment Analysis," IDCOR Program Technical Report 23.1, November 1984.

8.8 Technology for Energy Corporation, "Grand Gulf Nuclear Station--Integrated Containment Analysis," IDCOR Program Technical Report 23.1, November 1984.

8.9 Fauske and Associates, Inc., "IDCOR Technical Report 85.2: Technical Support for Issue Resolution," Atomic Industrial Forum, July 1985.

8.10 R. D. Gasser, P. P. Bieniarz, and J. L. Tills, "Analysis of Station Blackout Accidents for the Bellefonte Pressurized Water Reactor," Sandia National Laboratories, NUREG/CR-4563, SAND86-0576, September 1986.

8.11 H. Jordan and M. Leonard, "Fission Product Revaporization in the Reactor Coolant System," Proceedings of an International Symposium on Source Term Evaluation for Accident Conditions (Columbus, OH), International Atomic Energy Agency, STI/PUB/700, p. 227, March 1986.

8.12 D. Hagrman, "Analysis of Retention/Revaporization in a Large Pressurized Water Reactor," letter report to NRC dated August 4, 1986.*

---

*Available in the NRC Public Document Room, 1717 H Street NW., Washington DC.

8.13 D. A. Powers and P. Bieniarz, "Influence of Chemical Form on Cesium Revaporization from the Reactor Coolant System," Proceedings of American Chemical Society Symposium on Chemical Phenomena Associated With Radioactivity Release During Severe Nuclear Plant Accidents (Anaheim, CA), NUREG/CP-0078, to be published.*

---

*Available in the NRC Public Document Room, 1717 H Street NW., Washington DC.

NRC FORM 335
(2-84)
NRCM 1102
3201, 3202

U.S. NUCLEAR REGULATORY COMMISSION

BIBLIOGRAPHIC DATA SHEET

SEE INSTRUCTIONS ON THE REVERSE

1 REPORT NUMBER *(Assigned by TIDC, add Vol. No., if any)*
NUREG-1265

2 TITLE AND SUBTITLE
Uncertainty Papers on Severe Accident Source Terms

3 LEAVE BLANK

4 DATE REPORT COMPLETED

MONTH	YEAR
April	1987

5 AUTHOR(S)

6 DATE REPORT ISSUED

MONTH	YEAR
May	1987

7 PERFORMING ORGANIZATION NAME AND MAILING ADDRESS *(Include Zip Code)*
Office of Nuclear Regulatory Research
U.S. Nuclear Regulatory Commission
Washington, D.C. 20555

8 PROJECT/TASK/WORK UNIT NUMBER

9 FIN OR GRANT NUMBER

10 SPONSORING ORGANIZATION NAME AND MAILING ADDRESS *(Include Zip Code)*
Same as 7, above.

11a TYPE OF REPORT
Technical

b PERIOD COVERED *(Inclusive dates)*

12 SUPPLEMENTARY NOTES

13 ABSTRACT *(200 words or less)*

An assessment of the severe accident source term technology was recently published by the NRC in NUREG-0956. State-of-the-art methods described in NUREG-0956 are now being used in risk assessments and as the basis for implementing the NRC's Severe Accident Policy Statement and its Safety Goal. Notwithstanding major advances in source term technology resulting from recent severe accident research programs, NUREG-0956 identified eight technical areas where uncertainties remain large and where our near-term research efforts should be focused. Individual programs within the severe accident research program are being adjusted to address these eight areas of uncertainty with a concentrated effort. To plan for these program changes, NRC research program managers have reviewed the nature of the uncertainties in their respective subject areas and prepared background papers. These background papers (or uncertainty papers) are presented in this report.

14 DOCUMENT ANALYSIS - a KEYWORDS/DESCRIPTORS
Source Terms
Severe Accidents
Fission Products

b IDENTIFIERS/OPEN-ENDED TERMS

15 AVAILABILITY STATEMENT
Unlimited

16 SECURITY CLASSIFICATION
(This page)
Unclassified
(This report)
Unclassified

17 NUMBER OF PAGES

18 PRICE

*U.S. GOVERNMENT PRINTING OFFICE:1987-181-682:60094

181

BEST COPY AVAILABLE